Permeability and Pore Structure of Hardened Cement Paste and Mortar.

NyameÃŒ?, B. K

PERMEABILITY AND PORE STRUCTURE OF HARDENED CEMENT PASTE AND MORTAR

A thesis submitted to the University of London
for the degree of
Doctor of Philosophy

by
BENJAMIN KWAME NYAME

University of London Kings College
Faculty of Engineering
Department of Civil Engineering

SEPTEMBER 1979

TITLE OF THESIS: Permeability and Pore Structure of Hardened Cement Paste and Mortar.

AUTHOR: BENJAMIN KWAME NYAME.

ABSTRACT

Permeability of hardened cement paste (hcp) was studied in relation to the modes of change in pore structure due to hydration and water/cement (w/c) ratio. The effects of the addition of aggregate to hcp on permeability of mortars were studied in this thesis.

The saturated permeability was measured by a steady-state method which takes advantage of the hydrostatic pressure in sealing truncated conical disc specimens at pressures up to 2000 psi. Complementary measurements of the pore size distributions by mercury porosimetry, total porosities by helium comparison pycnometry and the evaporable water contents at 105°C were made to characterise the pore structure of hardened cement paste and mortars. The purpose was to identify the most appropriate variable(s) of the structure of hcp and mortars that relate(s) to permeability.

It was found that although the permeability of hcp increases with increasing total porosity, permeability is a multivalued function of total porosity and depends on whether the change in porosity derives from changes in water/cement ratio or times of hydration. It was possible to identify, from the pore size distributions, a primary continuous pore radius, which is thought to correspond to the maximum spacing between the weakest links in the bonds of cement hydration products. It was found that permeability of hardened cement paste was closely and uniquely related to the primary continuous pore radius irrespective of whether the mode of change in pore structure results from differences in water/cement ratio or times of hydration.

The measurements of permeability of mortars prepared with both normal and lightweight aggregates indicated no substantial differences in permeability for the two types of aggregate inclusions in the pastes. It was found that the addition of aggregates of lower total porosity than the paste to the pastes reduce the total porosity of mortars but increase permeability as the volume concentration of the aggregate increases.

Suggestions for future work include further measurements of the effect of aggregate additions to pastes at different levels of paste porosity on permeability. Measurements to elucidate the fundamental relationship between the primary continuous pore radius and compressive strengths and elastic constants of hardened cement paste, and their relationships with the nature of the cement hydration products.

To my father, Emmanuel

my mother, Sarah.

ACKNOWLEDGEMENTS

The stages from the conception of a piece of research to its completion not only require the devotion of the researcher but, more important, the suitable guidance of an experienced researcher, hence I am indebted to Dr. J.M. Illston for providing such guidance.

The contributions from the teaching,research and technical staff at Kings College, London are also gratefully acknowledged.

My sincere thanks to the staff at the School of Engineering at Hatfield Polytechnic who, in various ways, assisted during the second stage of this work. In particular,the assistance from Mr. Harmer, Mr. D. Oxley and the technical staff of the Civil Engineering Division at Hatfield - Polytechnic is appreciated.

My thanks to Dr. H.G. Midgley, Mr. S. Sabri, and Dr. B. El-Jazairi for many fruitful discussions on this work. Special thanks to Dr. H.G. Midgley for making the electron micrographs presented in chapter 1 available, and Mr. J. Rice for assisting with the photographs.

I am indebted to Mrs. Margaret Butler for typing this thesis at times when she could otherwise have been engaged.

LIST OF CONTENTS

* * * * * * * * * * * * * * * * * *

* * * * * * * * * * * *

* * * * * * * * *

* * * *

* *

*

INTRODUCTION

The advances in current practices of concrete technologists have been mainly achieved by a great deal of accumulated experience of the suitable choice of mix design parameters that have been tested and known to 'work'. It is well accepted that the full utilisation and exploitation of any material requires much more knowledge about its basic structure in relation to its properties.

The pioneers in studying the relationships between the structure and properties of hardened cement paste were Powers and Brownyard[9], whose extensive investigations provided the background upon which much future research into the nature of, particularly, the hardened cement paste phase of concrete were to be based. At a recent conference at the University of Sheffield[25,37], the need to interrelate structure and properties of hardened cement paste was reassessed. The need to provide the means for a full physical, chemical and mathematical description of hardened cement paste, and concrete remains essential.

Permeability is known to be one of the most important properties of concrete that indicates the durability of the material, nevertheless, studies on permeability has not acquired the same prestige as its other properties.

The present investigation deals with the relationships between permeability of hardened cement paste and mortars and their pore structures, from a fundamental level of direct measurements. An important concept of analysis introduced in the present study pertains to <u>modes of change</u> in pore structure. The approach here has been to consider not only the direct relationship the parameters of pore structure bear on permeability but also to consider the mode of change in pore structure. It is believed that, in this way, several processes that are likely to affect pore structure can be categorised into modes of change. For instance, it was possible to deduce from the test results, that the mode of change associated with aggregate inclusions produces an unexpected relationship between total porosity and permeability, in that a reduction in porosity <u>did not</u> produce a corresponding reduction in the measured permeability.

As a further example, it is known that the mode of change in pore structure due to air-entrainment, increases[101,102] porosity but reduces permeability. These two examples illustrate the importance of recognising not only the pore structure but also the mode of change in pore structure in relation to permeability.

The present investigation therefore deals with the relationships between pore structure and permeability as influenced by three basic modes of change in pore structure, namely, hydration, w/c ratio, and aggregate inclusions in paste.

In chapter 1, a review is presented on the researches previously performed on permeability and pore structure of hardened cement pastes and concrete. A brief survey of some theoretical approaches for the relationships between pore structure and permeability is made. Methods for determining both permeability and pore structure are reviewed. It was concluded that direct measurements to study the relationship between pore structure and permeability of the composite material necessitates the recognition of the three basic modes of change already mentioned.

In chapter 2, a description of the apparatus used, the procedures adopted, and the test results to justify the procedures adopted are given.

In chapter 3, the results of the experiments are presented, and the relationships between the measured pore structure parameters and permeability sought by a process of elimination of basic and fundamental variables of pore structure. The purpose was to identify the most efficient and reliable basic parameter in relation to permeability.

Chapter 4 presents a discussion of the results in greater depth, interpretations are made and functional relationships for the measured parameters deduced, and an alternative concept of pore continuity introduced.

The conclusions are drawn in chapter 5, together with practical implications of the findings in this thesis and suggestions for future work.

CHAPTER 1

A REVIEW OF THE PREVIOUS WORK ON PORE STRUCTURE/PERMEABILITY RELATIONSHIPS WITH PARTICULAR REFERENCE TO HARDENED CEMENT PASTE AND CONCRETE

Introduction.

The review consists of three seperate but interrrelated sections.

The pore structure section first outlines the means of describing pore structure in general. Pore structure of hardened cement pastes is described in two stages - the capillary pore structure and the pore structure of the hydration products.
Methods of determining pore structure are reviewed.

Next, permeability and diffusion coefficients are defined. The methods for measuring these coefficients for concretes are outlined, and the relationships previously obtained summarised.

The final section briefly reviews the theories on pore structure and permeability.

It is the purpose of the review to outline the researches on the fundamental relationships between pore structure and permeability of hardened cement pastes, mortars and concretes and to bring out the reasons for the fundamental approach in the study presented in this thesis.

1.1 Pore structure

1.1.1 General description and classification

Broadly, pore space is that which exists between the matrix of solid phases of a porous material. In the particular case of hardened cement paste, a large proportion of the solid phase consists of calcium silicate hydrates (C-S-H gel) which exhibits various degrees of physical and chemical bonding forces with water within the paste matrix. The extent to which water contributes to the rigid structure of the pastes is shown by its reversible and irreversible drying shrinkage properties[1,2]. A distinct separation of the actual solid phases of hcp from the fluid phase, therefore, involves a thorough understanding of the structure of, particularly, the C-S-H gel, and consequently, present definitions of pore structure and its measurement remain arbitrary and depend very strongly on current concepts of the structure of the C-S-H gel.

In relation to the flow of fluids, useful classifications of pore space are based on size, interconnectivity, the magnitudes of the fluid-solid interaction forces and the morphology of the pore space.

On the basis of pore size, Dubinnin[3] classifies pores from the peculiarities of sorption methods of pore structure analysis. For the hypothetical cylindrical pore model, this classification defines pore radii (r) as: macropores $r > 1000$ A, mesopores $16\ A \leqslant r \leqslant 1000\ A$ and micropores $r < 16$ A. On the basis of fluid-solid interaction forces[4], voids are pore spaces within which the fluid behaviour and properties are negligibly affected by the bounding solid phases. In capillaries, the behaviour of the fluid is affected but its properties are not, whereas force spaces are so small that both the fluid behaviour and properties are altered by the strong fluid-solid interaction forces. The pore structure of cement gel can be considered to represent force spaces and therefore contribute negligibly to permeability. The complexity and variety of pore shapes inevitably makes it necessary to adopt simple hypothetical model pore geometries to describe the pore size. Often, either cylindrical, slit-like or spherical pores are assumed. In this work, a cylindrical pore model of hcp is assumed because of the simplicity it affords in pore structure analysis by mercury intrusion porosimetry. This choice was not influenced by the unconvincing deduction made[5] and reiterated[7] that 'if the pore shape is unknown, the best idealisation is the cylindrical pore model' and is a 'fortunate choice'.

Karnaukov[8] describes pore morphology by differentiating between corposcular and spongy systems. Corposcular pore systems result from the imperfect packing of the solid phases, whereas spongy systems refer to the channels and cavities within the solid phases. This very important description may perhaps be compared with Powers'[9] division of hardened cement paste into an aggregation of gel pores and capillary pores. The description also[8] defines pore size from a globular model in terms of pore throat diameters and the number of contact points of globules in plane sections through a porous system and it provides a very useful possibility of disseminating pore structure information from electron micrographs. A further advantage of this description is that it suggests a two-stage pore continuity - corposcular pore continuity and spongy pore continuity. The concept of pore continuity is most essential in relation to saturated permeability and is therefore indispensible and very worthwhile classification in the context of this work.

Provided suitable pore shape models are adopted, the pore size distribution relates the expected fractional pore volume to characteristic pore sizes within the material.

Pore size distributions may be described by gross or averaging parameters such as

porosity (ε) ; ratio of total pore volume to bulk volume or weight of material.

specific surface area (S); total external surface area of solids per bulk volume or weight of solids.

hydraulic radii (r_h); ratio of pore volume to surface area of bounding solids.

tortuosity(C) ; ratio of actual flow path length of fluid particles to the length of the porous material. This factor is believed[11] to allow for the discrepancies between actual pore geometry and the hypothetical straight cylindrical model.

These averaging parameters do not necessarily provide all the detailed features of hcp pore structure, but together, they are useful for describing the flow of water in hardened cement pastes.

For the purposes of describing pore structure in this work Table 1.1 is presented to show approximate equivalence of possible terms to be used.

TABLE 1.1 Pore structure descriptions

size[3]	morphology[8]	hardened cement paste[9]	fluid/solid forces[4]
macropores	corposcular	capillary pores	voids
mesopores			capillaries
micropores	spongy	gel pores/interlayer spaces	force spaces

1.1.2 Pore structure of hardened cement pastes

Powers and Brownyard[9] were first to apply the *BET theory[12], at its early conception, to water vapour sorption isotherms of hardened cement pastes. They found that the surface areas of fully hydrated pastes were of the order of 180 - 220 m^2/g of dry pastes (0.5μmHg at 23°C), and within 10% agreement were independent of the type of cement. The surface areas of hydrating pastes were also proportional to the non-evaporable water contents of the pastes, (non evaporable at a vapour pressure of 0.5μ and 23°C, as above), The amounts of water adsorbed by the pastes in the vapour pressure range of approximately 0.45 to 1.0, (which is indicative of the onset of capillary condensation of Type II isotherms[39]) were proportional to the initial water/cement ratios. These very important evidences, together with others, led to the following deductions of the pore structure of hardened cement pastes[13], relevant to this work.

(1) The same products of hydration are being formed and with such high surface areas, most of the products are colloidal particles - i.e. at least one dimension between 10^{-9} and 10^{-6} meters.

(2) The hydration products have characteristic porosity (approx 26% by volume), characteristic pores (gel pores of order 18 - 20 A diameter) and occupy about twice the volume of the original reactants.

(3) Pore space of hardened cement paste consists of gel pores within 'cement gel' and capillary space originating from the initial water filled space. Hydration increases the volume of 'cement gel' and reduces that of capillary pores without much (less than 0.3%) change in the overall volume of the hardened paste.

(4) Capillary space may be rendered discontinuous by the growth of 'cement gel' if the initial w/c ratio is less than 0.7[26]. Full hydration completely eliminates all capillary space if the initial w/c ratio is less than 0.38[26].

* BET = Brunauer, Emmett and Teller

With these four basic deductions, a model of the pore structure of hardened cement pastes was formulated, and with this model, computations of total and capillary porosities have been made[13-16], using the initial w/c ratios, degree of hydration and densities of the hydration products and unhydrated cement. Porosities calculated from the 'Powers model', or otherwise, have been related to mechanical properties such as elastic modulus [1,20], basic creep[21], compressive strengths to a limited extent[17-19] and most important of all permeability[22-24]. These correlations have effectively demonstrated the importance of this single material property in assessing the engineering properties of hardened cement pastes. Illston[25] recently stressed the unexploited potential advantages of characterising concrete materials by porosity in everyday technology, but with some reservations of other variables such as age and cement type that represent microstructural rearrangements on the structure. He emphasised the importance of incorporating such evidence without too great an increase in algebraic complication for the practicing engineer.

1.1.2.1 The capillary pore structure

The model of pore structure of hcp developed by Powers and Brownyard[9] suggests that there are basically two types of pore space. The capillary pore system originates from the initial water-filled space of the fresh paste, and being orders of magnitude larger than the gel pore system is held to be mainly responsible for permeability of the pastes[22,23]. Powers, Copeland and Mann[26], considered from test data on permeability of pastes that if the assumption is made that the flow through hcp is similar to that though a granular body where the resistance to flow is determined by the viscous drag on the particles forming the body, then a semi-empirical equation, to be described later, was found to fit the data for mature pastes containing no alkali. Conclusions regarding the continuity or lack of continuity of the capillary system were made for other specimens by studying the conformity of the data to the equation deduced from viscous drag concepts. On this basis, the following estimates, shown in Table 1.2, were made for the curing times required for the continuous capillary pore structure to become blocked by cement gel to produce capillary cavities.

TABLE 1.2 Estimates of curing times required for the capillary pore system to become blocked by cement gel/ref. 26/

w/c ratio	Time required
0.40	3 days
0.45	7 days
0.50	14 days
0.60	6 months
0.70	1 year
>0.70	Impossible

From a physical point of view, discontinuity of the capillary pore system due to hydration is beneficial in reducing permeability as fluids must flow through 'gel pores' of much smaller size and higher resistance to flow. In small pores, however, hydration reactions stop either due to insufficient water for the reaction or limited space for the growth of the products[9,23]. Total discontinuity of the capillary system is therefore probably never possible.

Diamond[40] critically compared sorption and mercury porosimetry methods of pore structure analysis and concluded that mercury intrusion is relatively more efficient in assessing the distributions of the large pore structure of hardened pastes.

On the all important question of pore continuity in relation to permeability, Winslow and Diamond[28] examined the distributions of pore sizes in hcps of different w/c ratios and degrees of hydration using mercury porosimetry. They found that the pore volume unintruded by mercury at a pressure of 15000 psi was much less than 28% by volume of the pastes and that the pore volume between 100 and 1000A is substantial at all ages. They also combined their tests with direct examination of fracture surfaces of hcp and concluded from their observations that 'most of the volume in cement paste is neither capillary nor gel porosity per se, but consists of spaces between particulate hydration products, supplemented by pores in spongy hydration products'. Whilst accepting that their findings did not completely agree in quantitative terms with the model of Powers, their conclusions could be qualitatively compared with the Powers' model if the 'space between particulate hydration products' are likened to the 'capillary pores' and the 'pores in spongy hydration products' compared with the 'gel pores'. Auskern and Horn[29] took issue with the conclusions of Winslow and Diamond and showed that if the assumption is made that the gel porosity is the unintruded pore volume at a maximum mercury pressure of 50000 psi, a fair agreement between the experimental results and the Powers' model calculation is found.

The most important observation from the work of Winslow and Diamond[28], however, is the identification of the 'threshold diameter'. They made a series of carefully conducted tests to assist in interpreting this all-important pore structure parameter. Their findings are summarised below.

(1) Very little mercury intrusion occurs above the threshold diameter and the greatest proportion of intrusion commences at the threshold diameter.

(2) Fracture surfaces of samples tested at pressures just below and above the threshold diameter and examined under a microscope showed that for intrusion.

  (a) just below the threshold diameter many regions on the surface had little evidence of mercury penetration

  (b) just above the threshold diameter showed droplets of exuding mercury uniformly spaced over all the regions of the fracture surface.

(3) At or near the threshold diameter, the rate of mercury penetration was slow compared with the rate of intrusion for coarser pores, and the bulk of the pore space in pores smaller than the threshold diameter.

(4) The threshold diameter decreases steadily with age and tends to a steady value after 7 days. It is also larger for higher w/c ratio pastes.

The variation of the threshold diameter with age is illustrated in Fig 1.1 taken from the paper of Winslow and Diamond[28]. They interpreted the threshold diameter to correspond to the minimum diameter of pores which are geometrically continuous throughout all regions of the hydrated cement paste and in essence provided a very important means of directly determining continuous pore sizes. Other investigators[32,82] have since noted and confirmed this useful pore structure parameter but no attempt has, to the author's knowledge, been made to relate it to other physical properties of hardened cement pastes in the manner that efforts have been made for capillary porosity.

Most investigators of pore structure by mercury intrusion prefer to present their results in terms of the cumulative pore size distributions. From this type of plot it is difficult to locate precisely the position of the threshold pore diameter as described by Winslow and Diamond[28]. Diamond and Dolch[30] showed that it is possible to estimate the value of the threshold diameter or the maximum pore radius by a trial and error technique of fitting its position in such a manner that the whole of the cumulative pore size distribution function can be fitted to a modified logarithmic-normal distribution function of the form similar to those used for particle size distributions given by

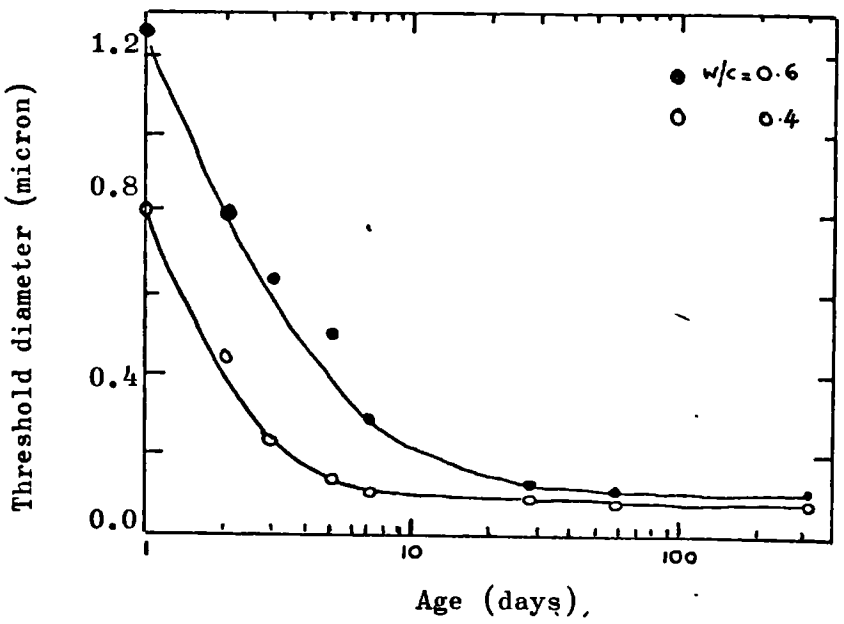

Fig. 1.1 : Threshold diameter as a function of age of hcp/ref.28/

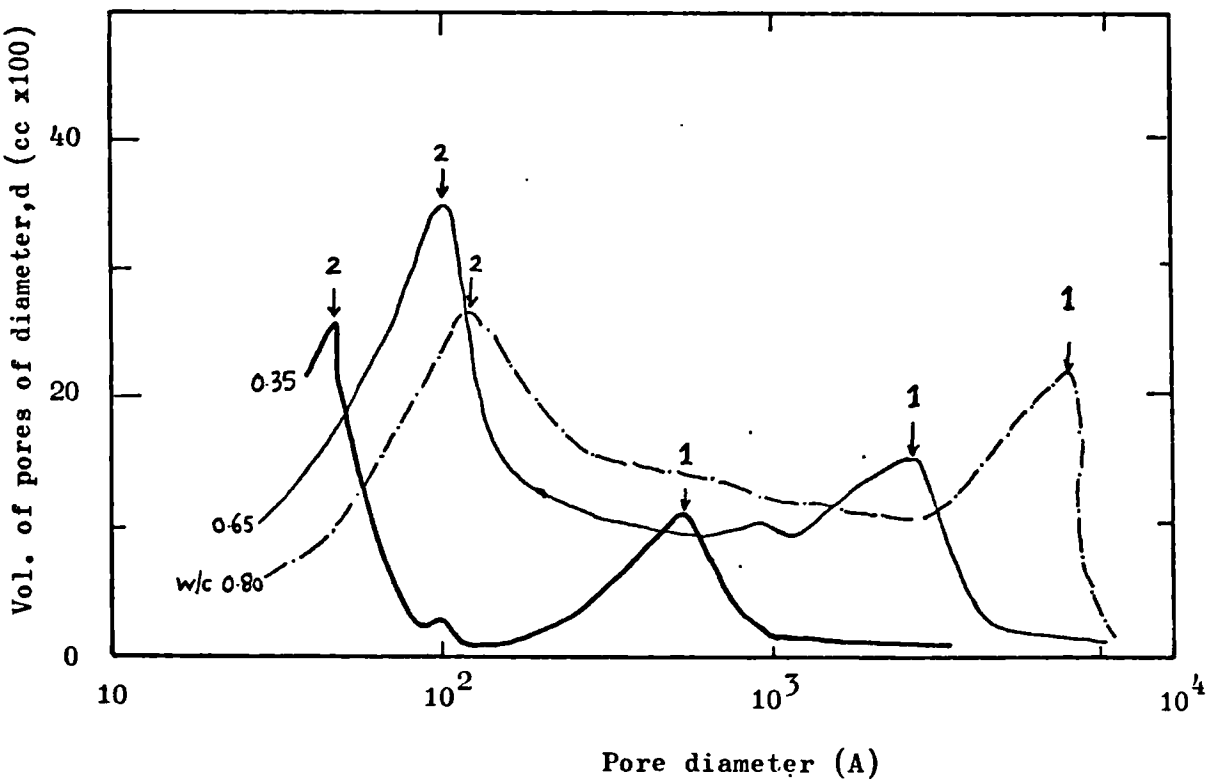

Fig 1.2 : Mercury intrusion pore size distribution of hcp cured for 11 years /ref. 33/

$$P(M) = 50 - 50 \text{ erf } \left(\frac{\ln M^*/\bar{M}^*}{\sqrt{2} \ln \sigma}\right) \qquad (1.1)$$

where $P(M)$ = percentage pore volume in diameters larger than M

$M^* = M_\infty M / M_\infty - M$

M_∞ = the maximum pore radius located by trial and error

$\bar{M}^*$ = the mean of the distribution of the modified pore size M^*

σ = the geometric standard deviation of the distribution of the modified pore size M^*

$$\text{erf}(x) = \frac{2}{\sqrt{\pi}} \int_0^x e^{-\lambda^2} \, d\lambda$$

The main postulate of this description is that it is the modified pore size parameter M^* which is normally distributed rather than the actual pore size M. On the basis of the success of fit of the equation to the pore size distributions of hardened cement pastes, they concluded that the pore structure of the pastes belong to a single distribution and therefore there is no evidence of a separate class of gel pores. They also noted and documented the variation of the maximum pore size and found it to decay with age to sensibly constant values at approximately 2 months.

Fig 1.2 is taken from data cited by Verbeck[33] of differential pore volume distributions of hcps hydrated for 11 years. It demonstrates qualitatively the essential peaks (marked (1)) in the large pore diameter classes which indicate the existence of 'threshold diameters' even at such long curing periods. It also shows the dependence of the parameter on w/c ratio; i.e. larger values are associated with higher w/c ratios. Using the interpretation of Winslow and Diamond[28] for the threshold diameter, it can be concluded from Fig 1.2 that the estimates for the curing times for the capillary pore system to become blocked by cement gel indicated by Table 1.2 are unsubstantiated.

Fig 1.2 also shows other distinct peaks marked (2) on the distributions in the region of approximately 100 A. Danyushevski et al[24,34] have identified these features of the pore structure of the pastes. They tentatively called these 'intermediate pores'. They found that the 100 A pattern or peaks were strongly dependent on the hydration conditions and were particularly well defined for specimens cured at 77°C. As a result of examination of fracture surfaces of the pastes using scanning electron microscopes, they suggested that the pores in the 100A region form the space mesh within the larger hydration products such as tobermorite and calcium hydrosulphoaluminates (ettringite).

For the purposes of assessing permeability, however, it is sufficient to note the very vivid analogy of the pore structure of hardened cement paste drawn by Winslow and Diamond as[28]

> '..constituting a geometrical system analogous in some respect to a finely branched river system, with relatively large pores intruded at the threshold diameter corresponding to the major rivers flowing through a geographical region and the rest of the pores corresponding to local branch streams'

*Electron micrographs taken by Midgley and Pettifer[35] of fracture surfaces of pastes at two extreme w/c ratios (0.25 and 1.0) shown in Plates 1.1 and 1.2 indicate the large differences in porosities and capillary pore channels associated with the differences in w/c ratios. It can be seen on the micrograph of the 0.25 w/c ratio that the original unhydrated cement grain is surrounded by a highly dense region of hydrated material forming the reaction rim. This dense part is clearly not crossed by the path of the crack, whilst the more porous regions between adjacent grains is crossed by the crack. The porous regions between adjacent grains perhaps correspond to the threshold diameter from mercury intrusion and if this is the case, then it might be inferred that the threshold diameter provides a measure of the maximum spacing between the weakest links in the bonds between products of hydration, hence it is to be expected that the threshold diameter must be closely related to the strengths of the pastes as well as permeability. There is therefore the need to define this parameter from pore size distributions by mercury intrusion in order to relate it to the properties of the pastes. This is attempted in this investigation.

1.1.2.2 Pore structure of cement gel

The colloidal nature of the cement hydration products would indicate that the flow of water in the pores within the products is negligible in comparison with the flow in the capillary space, hence the detailed pore structure of cement gel would be relatively unimportant in relation to permeability. Historically[9], cement gel was thought to have a characteristic porosity of 26% by volume and characteristic pore sizes. This description of the pore structure of the gel were mainly based on experimental results of Powers and Brownyard[9] who found that the water vapour adsorption isotherms of pastes of differing w/c ratios when plotted as the amount of water adsorbed per unit monolayer capacity as a function of relative vapour pressure gave essentially isotherms corresponding to the Type II of the Brunauer classification[39]. They found that with this type of plot , hardened cement pastes of differing w/c ratios and degrees of hydration produced isotherms which were indistinguishable from each other below about 0.45 relative vapour pressure.

* The author is indebted to Dr. H G Midgley for making the micrographs available.

Plate 1.1 : Replica surface of set portland cement paste (w/c = 0.25) x 2350 /ref 35/

Plate 1.2 : Replica surface of set portland cement paste (w/c = 1.00) x 2700/ref 35/

In addition, a limiting isotherm was closely approached by mature pastes of different types of cement.

This isotherm, called the cement gel isotherm, was believed to be a characteristic of the gel. The porosity of the gel was assumed to correspond to a capacity for evaporable water equal to three times the monolayer capacity - a value obtained by extrapolation of the cement gel isotherm to a relative vapour pressure of 1.00. Later studies[27] of the pore structure of hcp by nitrogen and water vapour sorption indicated that the minimum gel water content could be as low as 2.46 times the weight of water necessary to cover the gel surfaces with a monolayer of adsorbed water. It was shown from the pore size distributions that the pore system could be classified into smaller (S-pore) and larger (L-pore) systems but not gel pores and capillary pores of equal sizes. It was concluded that

(1) There is a wide range of pore sizes in hcp
(2) The hydraulic radius of the S-pore system increases with increasing w/c ratio
(3) The hydraulic radius of the L-pore system also increases with increasing w/c ratio.

With the development of electron microscopy and X-ray diffraction methods of study a greater deal of direct information for the structure of hardened cement paste is being accumulated. It is found that the main component of cement gel is calcium silicate hydrate (C-S-H gel) which is not a compound of uniform stoichiometric composition but a series of hydrates of varying composition[36,37,41]. The composition is found to be influenced by the conditions of hydration (eg w/c ratio, temperature and impurities) and because of the difficulty in distinguishing between water which is chemisorbed and that which is physically sorbed, no clear definition of total porosity of hcp has been agreed on. The methods of estimating porosity, which invariably involve drying are likely to affect the chemical composition, morphology and hence the pore structure of the pastes and it is difficult to specify the drying conditions which do not affect the hydrate structure.

Midgley[36] presented a review of the microstructure of hcp and described three main possible morphologies of the calcium silicate hydrate as (a) fibrous (b) plate-like (c) crumpled foils - usually found in synthetic preparations or possibly at high w/c ratios[35]. It was concluded that the microstructure of hcp consists of[36] hexagonal plates of calcium hydroxide, calcium aluminate hydrates, and needles of ettringite within the mass of the gel and in the water-filled spaces.

The solid phases were considered to be set in a matrix of calcium silicate hydrate gel of either the fibrous or plate-like form together with small spherulitic growths of calcium hydroxide[36].

Diamond[37] classified the C-S-H gel particles found from electron microscopic investigations into four main types, and made a clear distinction between the 'inner product' and the 'outer product'

Type 1 C-S-H gel - fibrous particles that are usually found radiating outward from the cement grains at early ages.
order 0.5 - 2 microns in length
less than 0.2 micron across
Nature: extensive and dendritic branching, partly rolled at outer ends, flexible and sometimes hollow tubes.

Type II C-S-H gel -reticular network
Elongated particles similar to type 1 in dimensions and generally branch to form a three dimensional interconnected reticular network.

Type III C-S-H gel-equant grain
Small flattened particles about 0.3 micron across.

Type IV C-S-H gel- inner product (reaction rim)
dimpled appearance with closely packed pores or particles.

It is supposed that for hcp, all or some of the above types of C-S-H gel would form a rigid network together with any other hydration products present and in the main (as Plate 1.1 suggests) the overall stability of the structure with respect to external loading may be determined by the links of the products between adjacent cement grains.
Midgley and Pettifer[35] studied the effect of water/cement ratio on the morphology of hydration products formed and concluded that for high w/c ratios, and therefore sufficient space, both the fibrous and the crumpled foil forms of C-S-H gel are formed. This in terms of pore structure would indicate that the porosity of the gel could vary with w/c ratio, and similarly the average widths of the gel pores.

Various models for the structure of the C-S-H gel have been postulated. The structure is thought to be closely related to a layered natural mineral, tobermorite[38]. The main controversy on the structure of relevance to pore structure and permeability pertains to the correct measure of the porosity and surface area of the ultimate structure. In the Feldman model[42-44], it is contended that during water vapour sorption measurements, a substantial part of chemisorbed interlayer water enters and leaves the spaces between the layers of the C-S-H gel even in the vapour pressure range (0.07 - 0.33), where the BET surface areas are calculated, therefore the surface areas and porosities obtained from water vapour sorption are invalid, because they include interlayer surfaces and pore volumes which are essentially part of the structure of the gel. It is suggested that the pore volumes and surfaces from nitrogen sorption are at least approximately correct because in this case only the external surfaces of the gel particles are measured.

Brunauer and coworkers[46] agree that water is probably lost from the hydrate sheets during first drying but once the material is D-dried, it is no longer capable of reincorporating water into the sheets (this view has been withdrawn[7]) and so the BET surface areas calculated on adsorption are valid, because negligible amounts of chemisorbed water is reincorporated in the hydrate structure. It is held[46] that the surface areas and porosities measured by nitrogen adsorption are inappropriate because of limited accessibility of nitrogen molecules into fixed-dimension ink-bottle pores. This is considered to be due to

(1) The larger nitrogen molecule in comparison with the water molecule.

(2) Lower thermal energy of the nitrogen molecule in comparison with the water molecule because of the differences in temperature at which the experiments are carried out (-179°C compared with 22°C for water)

These factors are considered to hinder the diffusion of the nitrogen molecules into pore constrictions. It is considered that since the process by which the nitrogen molecule can penetrate the pores is an activated diffusion process, if sufficient time is allowed for equilibrium to be reached at each vapour pressure, penetration of nitrogen molecules may be possible.

Since the flow of water is likely to be almost wholly carried by the capillary pore system, the foregoing differences in the views on the pore structure of hcp are unlikely to be relevant in this work.

1.1.3 Methods for determining pore structure

The complete description of pore structure requires the measurements of the distributions of pore sizes, shapes, volumes and surfaces over the entire range of pore size spectrum within a porous solid. The distributions of the large (capillary) pores in hardened cement paste have been successfully achieved by use of mercury porosimetry[28-32]. Sorption methods tend to be more efficient for the smaller pores (less than 500 A diameter)[40]. The helium comparison pycnometer does not give information on pore sizes but it has been applied mainly to study the collapse or re-expansion of interlayer spaces within the calcium silicate hydrates of hydrated cement paste[50-52,55]. Reviews of other methods not often applied to cement pastes are given elsewhere[53,54].

1.1.3.1 Sorption methods.

The amounts of adsorbate lost or gained with changes in relative gas pressure at constant temperature can be measured to enable estimates of pore size distributions and surface areas of the solid phases of a porous solid to be made. Treatments of the BET theory for multimolecular adsorption can be found in references 39 and 56. The theory enables estimates of surface areas to be made, and rests on the assumption that the adsorbate must be held by physical attraction forces to the surfaces of the solid phases. Complications for surface area estimates could arise in the case of hydrates, as in cement paste, due to dehydration and rehydration in the range of vapour pressures when water is used as the adsorbate [42-44,58,46]. Evidences obtained from an independent basis of measurement using low angle x-ray methods, however, indicate that the surface areas from water-vapour sorption are not invalidated because of rehydration and dehydration of the hydrates[6]. If the proximity of the solid phases tend to the order of magnitude of the size of the adsorbate molecule, Dubbinnin and others[68-71] point out that the BET theory modelled as successive layer by layer coverage of the adsorbed molecule on the surface of the solid phases tends to depart from the real behaviour of the molecules, hence the theory can no longer be applied to estimate surface area and the whole concept of surface area loses its significance.
The pore size distributions from sorption isotherms can be estimated by applying the Kelvin equation for condensation in capillaries, thus[39]

$$r_c = - \frac{2 \gamma V \cos \theta}{RT \ \ln(P/p_o)} \qquad - (1.2)$$

where r_c = radius of cylindrical core
V = molar volume of adsorbate in liquid form
γ = surface tension of adsorbate in liquid form.
T = temperature (^oK)
R = gas constant
θ = contact angle between liquid and pore wall
P/P_o = relative gas pressure.

The pore radius given by equation 1.2 is in fact that part of the pore which is not covered by adsorbed molecular layers, therefore corrections for the thickness of the adsorbed film need be made to obtain the true pore radius. The estimates of the thickness of the adsorbed film as a function of relative pressure on non-porous specimens are used to correct for this effect[39]. t-curves suitable for the analysis of hardened cement pastes by water vapour sorption are given in reference 64. A choice in the assumption of any pore shape for analysis of pore sizes distributions can be made if the approaches proposed by Brunauer and co-workers[65-67] are used. In these analyses, the hydraulic radius of the core is deduced instead of the pore radius, The core is that part of the pore which fills up by capillary condensation or remains empty after evaporation. Pore properties can be deduced from the data on the core if any pore shape model is assumed. Other computational procedures for estimating pore size distributions have been formulated.[59-63]

1.1.3.2 Mercury porosimetry

The basic principle of mercury porosimetry for the analysis of pore structure is that a non-wetting fluid (i.e with contact angle greater than 90^o) penetrates pores only if the resistance to wetting due to the surface tension of the fluid can be overcome by the applied pressure. Hence,[39]

$$p = \frac{-2\gamma \cos \theta}{r} \qquad (1\text{-}3)$$

r = radius of cylindrical pore
γ = surface tension of fluid
θ = contact angle between solid surface and fluid surface
p = absolute pressure

This method is described further in chapter 2. Measurements of contact angles of oven-dried specimens of hardened cement pastes were found to be 117^o [28], and the angle tends to vary with drying conditions. It is interesting that it is generally considered that the contact angle may vary with the applied pressure but recently it has been shown[18] that for relatively hard materials such as porous alumina this is not the case.

1.1.3.3 Helium pycnometer

This method employs the gas laws to determine solid volumes by displacement principles and is outlined in chapter 2. It has found much success for studying the collapse and re-expansion of interlayer spaces due to penetration and withdrawal of interlayer hydrate water [42,43] but is susceptible to questionable interpretations [75,76].

1.1.4 Summary

The review so far indicates that for permeability, it is necessary to recognise the threshold diameter obtained from mercury intrusion measurements[28] as an important pore structure variable. There is a need to assess the applicability of the helium pycnometer to evaluate the definition of total porosity which may not include interlayer pore volumes as part of the pore system. It is also necessary to recognise the effect of w/c ratio and hydration on the pore structure of hcp, and in particular, on the threshold diameter.

1.2 Permeability definitions and measurements

Gradients of moisture contents, hydrostatic pressure, stress, temperature and concentration of chemicals disturb the states of equilibrium of the fluids in a porous material and this results in flow of the fluids to restore equilibrium. In principle, if the state of the fluid, i.e. density, local velocities and temperature are assumed to be continuous functions of space and time, it is possible to apply the equations of continuity, conservation of momentum and a suitable relationship between stress and deformation of the fluid to obtain full d fferential equations describing the motion of the fluid[77,78]. The solution of such differential equations require that the boundary conditions of the fluid and solid phases of the material are specified, and in the case of porous materials this constitutes an intractable task, therefore, empirical laws generally suffice for the relationships between the gradients and the fluid flux.

1.2.1 Darcy's law

Darcy's empirical law relates the hydraulic gradient to the steady state rate of flow of fluids in a saturated porous material. It defines permeability, simply, as the velocity of fluid per unit hydraulic gradient as in

$$Q = K A \frac{dh}{dx} \qquad (1.4)$$

where K = coefficient of permeability (m/s)

Q = steady state volumetric flow rate (m^3/s)

A = cross-sectional area of porous sample (m^2)

$\frac{dh}{dx}$ = hydraulic gradient across sample in the direction of flow (dimensionless)

Permeability as defined by equation 1.4 is an index of the resistance of the material to flow of fluids and it depends on both the structure of the material and the properties of the fluid, provided no other gradients apart from the hydraulic gradients are responsible for the flow. The flow must also be laminar and the resistance to flow due to viscous drag[11]. Carman[11] suggests that the rate of flow is inversely proportional to the viscosity of the flowing fluid and therefore a specific permeability coefficient, K_o, may be defined which depends only on the structure of the porous material but not on the properties of the flowing fluid, thus

$$Q = K_o \frac{A\rho g}{\mu} \frac{dh}{dx} \qquad (1.5)$$

where P = density of fluid (kg/m^3)

g = acceleration due to gravity (m/s^2)

μ = absolute viscosity (Ns/m^2)

K_o = specific permeability (m^2)

and $Q, A, \frac{dh}{dx}$ are as previously defined.

There are indications[79] that the viscosity of fluids in microporous materials with high surface areas may be higher in the smaller pores than in the larger pores because of strong physical forces of attraction emanating from the solid surfaces. The uncertainty of such fluid property change of water in hardened cement paste excludes the use of this later definition of permeability and the former is therefore adopted in this work.

The limitations and conditions necessary for Darcy's simple law to be valid have been extensively discussed elsewhere[4]. In very broad terms, deviations from Darcy's law are found to occur due to[4]

(a) High flow velocities with Reynolds number greater than limiting reported ranges of 0.1 to 75, but this type of deviation is unlikely to be relevant for the flow in hardened cement pastes.

(b) Molecular effects due to very high forces of attraction between the fluid and the surfaces of the solids in small flow channels. This type is most probably highly relevant for hardened cement pastes but it is certainly not easily established as the material continuously changes it structure during any steady state permeability measurements.

(c) Osmotic effects; Powers emphasises deviations from Darcy's law due to osmotic pressures caused by differences in calcium hydroxide concentrations in hardened cement pastes[22,92] for measurements made at low hydraulic gradients (approx. 1,000)

Various other modifications and improvements on Darcy's simple law have been proposed and reviewed[4] but their use to describe the flow of water in hardened cement pastes and concretes is severely limited by the fact that the measurement techniques used for permeability of these materials are far from being sophisticated enough to provide the basic experimental data necessary for providing the confidence in their use.

1.2.2 Fick's laws

Fick's empirical laws relate diffusion coefficients to concentration gradients for unsaturated and non-steady state flows. The first for one dimensional flow is given by[78]

$$J_x = -D_x \frac{dc}{dx} \qquad (1.6)$$

where, J_x = flux of fluid in a direction x and at position x
D_x = diffusion coefficient at position x
$\frac{dc}{dx}$ = concentration gradient at position x

The second law relates the rate of change of concentration gradients through the principle of conservation of mass and by assuming that the diffusion coefficient is independent of position, it can be shown that[78] the second law is given by

$$\frac{dc}{dt} = D_x \frac{d^2c}{dx^2} \qquad (1.7)$$

Murata[83] employed Fick's laws in the studies of penetration of water into concretes and derived a relationship between diffusion coefficients and steady state permeability of concrete. In studies of capillary rise, Valenta[84] essentially applied the same law to predict permeability from the rates of capillary elevation of sealed specimens. The interrelations between non-steady state diffusion coefficients and steady state permeability coefficients remain essentially empirical for concretes but provide useful indices for the capacity of the material to absorb or admit flow on a relative basis.

1.2.3 Methods for measuring permeability of concrete

Owing to the difficulties of setting up experimental apparatus to measure permeability of concrete in a manner that strictly conforms to the requirements of Darcy's law, several previous workers[85-91] have measured the 'permeability' of concrete by employing non-steady state test methods. In many cases, the inflow rates of water into unsaturated specimens were determined and used as a measure of permeability. Typically, Washa[91] expressed permeability as the inflow rate (10^6 gals/sq ft/hr) for the 40-50 hour interval from the beginning of a test under constant pressure. Other investigators[87-89] neglected capillary heads in very low pressure tests on unsaturated specimens but calculated permeability coefficients using Darcy's law from the results. In many of these comparative tests, it was possible to study the effects of various parameters on permeability but quantitative comparisons of the results could not be made. This section outlines the methods that have been employed in the past for permeability measurements for concrete in two distinct categories of direct and indirect methods.

The emphasis is placed on the experimental difficulties and the relative merits of the test methods.

1.2.3.1 Direct methods

Direct methods require the measurements of steady state inflow or outflow or both. Powers and others[9,22,92], and Ruettgers and others[93] notably used steady state permeability techniques. Due to the very low rates of flow possible in hardened cement pastes, steady state flows are difficult to establish and are only closely approched, often requiring long periods of testing. Powers and others[92] reported the order of 14 days to attain steady state flows at imposed hydraulic gradients of approximately 1000. The necessary long periods under pressure means that the specimens continuously hydrate and alter the pore structure, hence the permeability of the test samples. It has been suggested[94] that exact steady state flows cannot be possible until complete hydration is achieved. It has nevertheless been possible to obtain measures of permeability of early age specimens using disc specimens and reasonably high pressures[24,92]. By far the most essential requisite of steady state measurements is the elimination of leaks around specimens. Apparatus has been described[92,95,96] which offer means of avoiding leaks but perhaps the use of tapered specimens by Powers and others[92] is most effective in overcoming this most important problem.

1.2.3.2 Absorption rate methods

Permeability can be compared on a relative basis by studying the rates at which partially dried concretes absorb water[97-100]. Rates of absorption, however, depend very much on the moisture contents of the samples and this represents the greatest problem of maintaining standard and reproducible drying conditions for the tests.

Levitt[98,99] developed a test procedure involving the measurement of the amount of water absorbed by the surface of concrete under a fixed hydrostatic head of 200 mm in specified times of 10 minutes and 24 hours. This low head test is generally that experienced by the conditions of driving rain and is therefore appropriate as a test to indicate the permeability and hence the durability of the surface of concrete. However, it is generally known that the surface properties of concrete is often quite different from the bulk due to excess cement content and variable packing of the aggregates on the surface. The permeability or durability indicated by this test procedure may therefore not provide the complete picture of the state of the material or its soundness.

Figg[100] developed a simple method which requires a hole to be drilled perpendicular to the surface of in-situ concrete, thus improving on the major

disadvantage of Levitt's test procedure. The small hole(5.5 mm diameter by 30 mm deep) is plugged with catalysed siliconc rubber and allowed to set in-situ, thus providing a rubber bung through which a hypodermic needle can be inserted to protrude below the plug. The apparatus is then connected to the hypodermic needle through a three-way tap by plastic tubing. For the air permeability method, the test cavity is first evacuated to 15 kN/m^2 by a hand pump. The pump is then isolated and the time required for the pressure in the cavity to rise to 20 kN/m^2 as indicated by an aftached closed end manometer is used to indicate permeability. The water permeability is measured by filling the test cavity with water from a syringe. The time required for the meniscus in an attached horizontal capillary tube to travel a fixed distance is used as a measure of the water permeability. The greatest advantage of this method is that it is claimed to be relatively quick and also non-destructive in that the small hole drilled is automatically sealed by the test procedure. Figg[100] showed that with this method,good correllations could be obtained for w/c ratios,compressive strength,ultrasonic pulse velocity measurements and the indicated permeabilities. It was also claimed that the method of drilling did not affect the reliability of the indicated permeability. The major problem was found with the effect of moisture contents and it was suggested that a miniaturised microwave moisture meter be developed to measure the moisture contents prior to testing to correct for this effect.

Pihlajavaara and Parroll[97] adopted Figg's method to study the correlations between permeability and compressive strengths of concrete. The effects of size of aggregates and moisture contents on the indicated permeabilities were also studied. It was found that the water absorption tests were not suitable for moist concretes although the air permeability method seemed to yield reasonable results even for moist concretes. It was observed that permeability tends to be greater the larger the aggregate size. It was found that both the air and water permeability methods could be adequately used for oven dried specimens and the correlations between compressive strengths and permeability was clearly higher strengths for lower permeability but with rather large scatter at high strengths. Very poor correlations were found for permeability and the mix proportions of the concrete in contrast to that reported by Figg[100]. It was concluded - 'no final and detailed conclusions can be made and the usefulness of the method remains still a more or less open question'. This main conclusion was based on the rather large scatter of the results which was quite correctly attributed to the cracks caused by the drilling procedure of the method as well as the unrepresentatively small size of the test cavity in relation to the test samples. The most important contribution from the

tests conducted by Pihlajavaara and Parroll[97] is the recognition of the fact that permeability is largely influenced by cracks in concrete. It is proposed[81] that deteriorated concrete with internal cracking such as converted high alumina concrete structural members could be effectively identified using the simple method developed by Figg.

1.2.3.3 Penetration methods

Penetration test methods for estimating permeability of concretes depend on applying Fick's laws to the motion of the saturated front of the fluid under an applied hydrostatic pressure[83,101].

Tyler and Erlin[101] proposed a simple method for measuring penetration which effectively avoids the all important problem of sealing the test sample for leaks around the specimen. The test specimens were subjected to an equal all-round hydrostatic pressure up to 5000 psi thus avoiding sealing. In the tests, both the quantity of inflow, the rate of inflow and the depth of penetration were measured at suitable time intervals. It was assumed in the computation of permeability using Darcy's equation, that

(1) the moisture distribution is uniform throughout the specimens at the start of the tests.

(2) the water penetrates uniformly from all the faces of the cylindrical specimens

(3) the flow is parallel from both the curved surface and the ends of the specimens

(4) penetrated regions are completely saturated.

The effects of compressibility of the specimens at high pressures, any capillary attraction, and the back pressure developed from the compressed air within the specimens were all neglected. In applying Darcy's equation to the nature of the flow, two seperate forms of estimating the hydraulic gradient and the area of the specimens conducting the flow were ingeniously introduced for short and long term penetration. For short term penetration(less than 24 hr), the area used was simply the curved surface area of the test specimen, whereas for longer periods, the average of the curved surface area and that of the unsaturated inner concentric cylinder was used. The hydraulic gradient was found from the ratio of the applied head to that of the length of the flow path. The length of the flow path was suitably defined to vary with the penetration as

$$l = \frac{q(t)}{Q} \cdot (\text{Volume of cylindrical specimen})$$

where,

l = length of flow path

$q(t)$ = cumulative inflow at time t

Q = total inflow at complete saturation.

This neat and simple way of accounting for the variable hydraulic gradient in an unsaturated flow problem was successfully used to calculate the permeability coefficient for concretes and was found to agree with tests conducted by direct steady state methods. Since its introduction,however, this method appears not to have been adopted but it is a potentially effective method which avoids the all important problem of leaks in steady state methods. It suffers again from the point of view of maintaining standard moisture contents as with all non-saturated tests.

Murata[83] measured the average depths of penetration of water in sealed specimens by employing a range of hydrostatic pressures up to 20 kg/cm^2, for periods up to 48 hours. The specimens were dried at room temperature for fixed periods up to 10 days prior to penetration tests. The penetration data was analysed by employing Fick's law. It was shown that if the volume of fluid penetrating the specimen is assumed to cause a volumetric expansion, then the analogy between Darcy's law and Fick's first law could be used to relate diffusion coefficient and permeability coefficient by

$$D = \left(\frac{K\,E}{d_w} \right)^{\frac{1}{2}} \qquad (1.9)$$

where,

D = diffusion coefficient (cm^2/s)

K = permeability coefficient (cm/s)

E = compressibility of saturated concrete(g/cm^2)

d_w = density of water (g/cm^3)

The compressibility,E, was calculated from the initial modulus of elasticity and Poisson's ratio for concrete. The test method was used to study the effects of hydration and air entrainment on permeability and it was found that air-entrainment reduces permeability except at low w/c ratios. The interrelations between compressibility(hence, elastic modulus and Poisson's ratio), diffusion coefficient and permeability coefficient found by Murata is a substantial contribution in the correlation of properties, but many more tests are necessary to obtain confidence in the relationship.

An attractive method of studying the permeation of water into concrete by studying the changes in the electical resistance of probes embedded in the test specimens has been proposed by Bracs and others[102]. Low heads of water were used and the reduction in the local resistance between pairs of embedded electrodes were measured at frequent intervals. This enables both the rates of permeation and the relative changes in the moisture contents at different sections within the material to be monitored. The authors found it a useful tool for classifying the quality of concretes by use of the initial speeds of permeation.

Valenta[84] proposed a simple means of measuring the capillary rise of specimens sealed from the ambient conditions with a polyester coating. Fick's law was applied to the movement of the liquid front and the driving force assumed to be due to a constant capillary attraction. The permeability coefficient could then be related to the apparent velocity of the liquid front by

$$\frac{dx}{dt} = K \left(\frac{h_o - x}{x} \right) \qquad (1.10)$$

where,

K = coefficient of permeability (m/s)

$\frac{dx}{dt}$ = apparent rate of rise of liquid front (m/s)

h_o = capillary attraction head (m)

x = elevation of liquid front (m)

The solution of the above equation is given by

$$t = \frac{h_o}{K} \left(\ln \frac{h_o}{h_o - x} - \frac{x}{h_o} \right) \qquad (1.11)$$

which can be shown on expansion of the logarithmic term and neglecting the higher order terms of x/h_o to simplify to

$$t = x^2/2Kh_o \qquad (1.12)$$

It is suggested that at least two determinations of the elevation,x, as a function of time,t, required for the elevation,x, could provide the data for estimating the permeability coefficient of the material as well as the capillary attraction head. With this type of test it is again essential to maintain suitably uniform moisture contents through the test samples.

1.2.4 Permeability of hardened cement paste and concrete

The long term durability of concrete structures depends on,among other factors, the resistance concrete offers to the ingress of potentially deleterious fluids. One of the indices of such resistance is the permeability of concrete and as such ought to contribute to the specification for the durability in the design of concrete mixes. Strength may be correlated to permeability[96,97,100] and it may be possible to specify strength and suppose that permeability is

also automatically specified, but it is quite possible to have concretes of of the same compressive strengths but widely different permeabilities[96,97]. This nature of variability can be expected in that the strength of the material depends not only on the internal pore structure of the concrete, as is the case for permeability,but also on the nature and strength of the solid phases formed as a result of hydration. The information on permeability of concrete or constituents of concrete have been very limited mainly because of the relative difficulties associated with its measurement and its limited exploitation in design specifications. This section presents the available information previously found from measurements and attempts to rationalise the causes of the variations previously found, where possible.

1.2.4.1 Effects of water/cement ratio and hydration

Water/cement ratios mainly control the initial porosity of pastes and much of the data obtained from both direct and indirect measurements of permeability generally confirm that permeability increases with increasing w/c ratio[83,85-94]. Hydration is known to produce cement gel of greater specific volume than the initial reactants hence reducing the volume of the capillary pore system and thus causing marked reductions in permeability[92,93]. Fig 1.4 illustrates the relative changes in permeability due to hydration with respect to the 28 day permeability values obtained from the literature. It can be seen that the greatest effect of hydration occurs up to 28 days, and it appears that the effect of hydration is independent of the composition of the concrete. It will be necessary to monitor both the effects of hydration and w/c ratio on the internal pore structure and its relationship with the variables of the pore structure of pastes.

1.2.4.2 Effects of treatments and aggregates

Moist, steam and air curing reduce permeability of concretes[87,89,104,105] and it has been found that moist curing is the most effective in reducing permeability and air curing is the least effective.

Air entrainment has been found to reduce permeability[101,102] and although this could be associated with improved workability, it is quite significant to note that this type of treatment increases the total porosity.

An increase in the fineness of cement is found to be beneficial in reducing permeability because of increased degrees and rates of hydration[85,87,92].

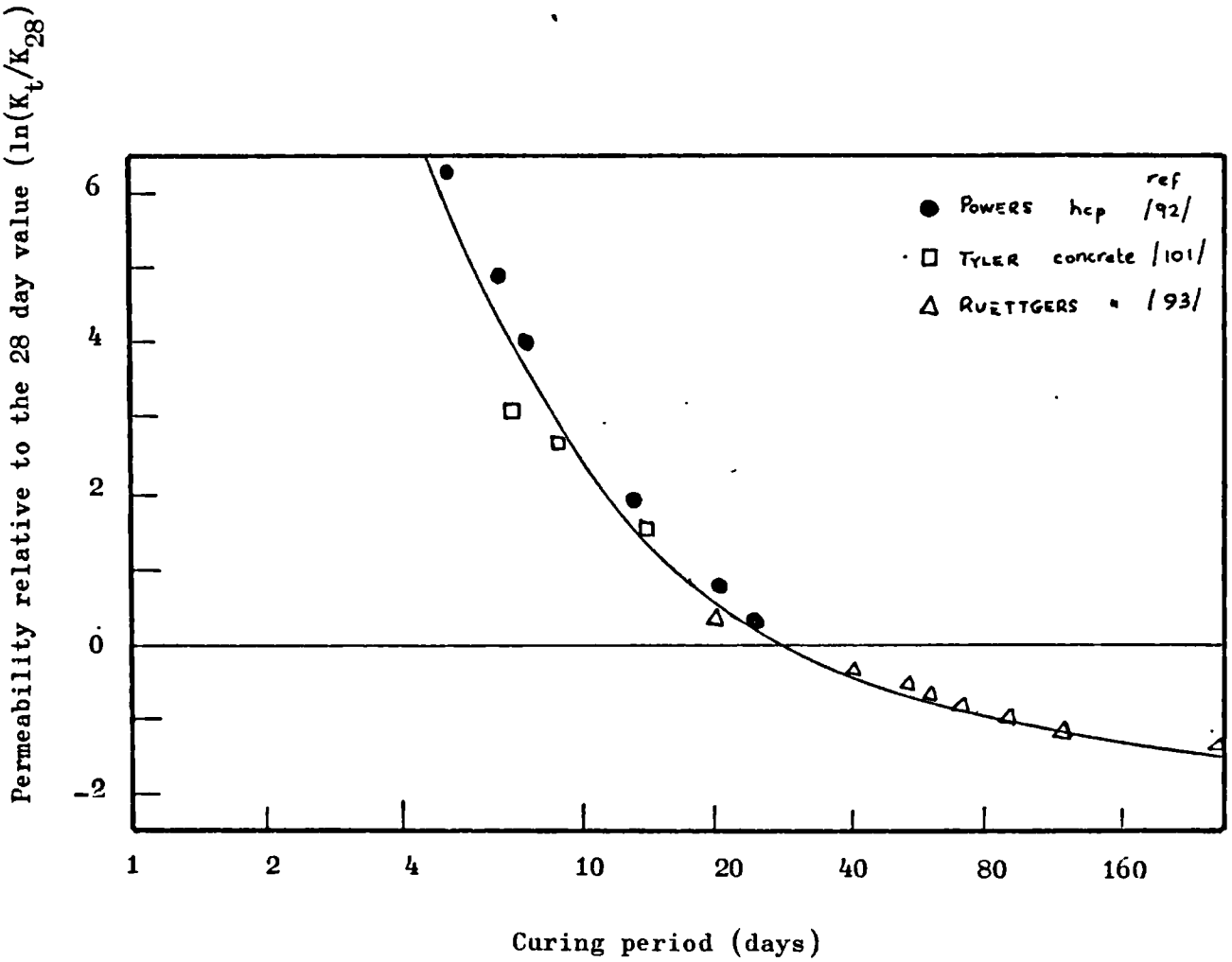

Fig. 1.4: Relative changes in permeability due to hydration compiled from the data in the literature.

Polymer impregnation is perhaps the most effective means of reducing permeability[107] although large scale impregnation is at present not economically feasible.
Superplasticised concrete is found to be less permeable than ordinary concrete of similar mix proportions[96] and again this could be explained in terms of an improvement in the workability that results from the addition of super-plasticisers.

A very limited amount of work has been done on the effects of grading of aggregates on permeability. The addition of aggregates to cement paste is construed to cause a reduction in the number of flow channels per unit gross cross-sectional area and to lengthen the flow paths which may be considered to reduce permeability[102]. However, the formation of fissures around the aggregate particles may be considered to increase permeability[102]. This mode of permeability variation is of great importance in the present investigation.

Permeation studies indicate that improved permeability results from using smaller maximum aggregate size[90,83,102] and although this could be associated with the ability of the aggregates to pack more effeciently in the paste matrix hence reducing the interconnectivity of the pore system systematic appreciation of the mode of packing of aggregates has not been tested experimentally.
Crude oil permeability studies of concrete[96] indicated that the optimum fine to total aggregate ratios for reduced permeability of concrete of w/c ratio of 0.6 was between 40-55%; this would indicate that a grading that ensured approximately the same amount of fines as coarse aggregate would result in low permeability. It was found that[96] aggregate gradings corresponding to zones 2 and 3 of BS 882, 1965 produce concretes of lower permeability than zones 1 and 4.

Alternative studies of the effects of aggregates has been achieved by considering the volume concentration. Fig 1.5 taken from reference 86 indicates that permeability increases with increasing volume concentration, irrespective of the grading of the aggregates. It is not possible to deduce the manner of increase in permeability with increasing volume concentration unless changes in the internal pore structure are linked with the changes in permeability; a subject of interest in this thesis.

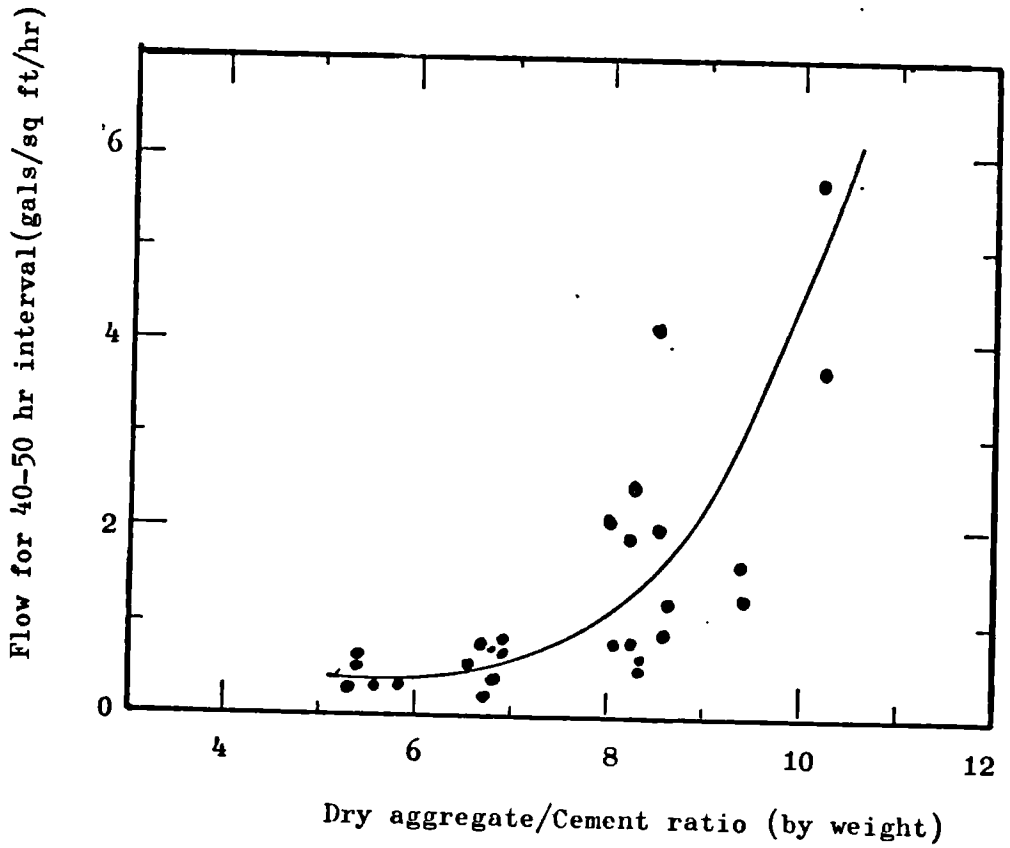

Fig. 1.5 : Effect of aggregate volume concentration on permeability/ref.86/

1.2.4.3 Studies on pore structure and permeability of hardened cement pastes and concretes

In the previous section, an outline of the effects of treatments and the inclusion of aggregates in the hcp phase on permeability were summarised. To obtain a full appreciation of these effects on permeability, it is necessary to link the studies with the changes in the pore structure resulting from methods of preparation or added ingredients.

Powers et al[22] deduced a semi-empirical equation for the relationship between permeability and the pore structure of mature hcp based on viscous drag theories and showed that

$$K_1 = \frac{1.36\ 10^{-10}}{v(T_c)} \quad \frac{(1-c)}{c} \exp\ (1242/T + 0.7)c/1-c) \quad \cdot \qquad (1.13)$$

where $v(T_c)$ = viscosity of fluid at a temperature of T_c ^{o}C (poise)
c = volume concentration of particles
T = absolute temperature (deg K)
K_1 = permeability coefficient (cm/s)

The link to porosity is made by assuming[13] $c = 1 - p_c$ where p_c is the capillary porosity of the pastes. In later studies[26] the above equation was used to deduce capillary continuity or discontinuity of pastes of different states of hydration by considering the lack of fit of permeability data to the equation. Experimental data cited by Verbeck[33] and very approximately shown in Fig 1.6, however, suggested that pastes of different capillary porosities covering the fresh state to pastes cured for 242 days fit the same equation deduced for mature pastes.
This suggests that

(1) either the concepts of capillary continuity deduced from considerations of lack of fit to equation 1.13 are in error
(2) or that capillary porosity is a singled-valued function of permeability of hardened cement pastes.

More tests are therefore needed here to establish the relationship between porosity and permeability of hcp.

Robson[109] extensively tested hcps, mortars and concretes for permeability and although no measurements of porosities were made, he noted and attempted to explain the apparently large scatter of his results. A hypothesis was put forward for the flow of water in hcps and concretes which states that

> ' The flow through any specimen is the sum of a small integral number of nearly equal flows'.

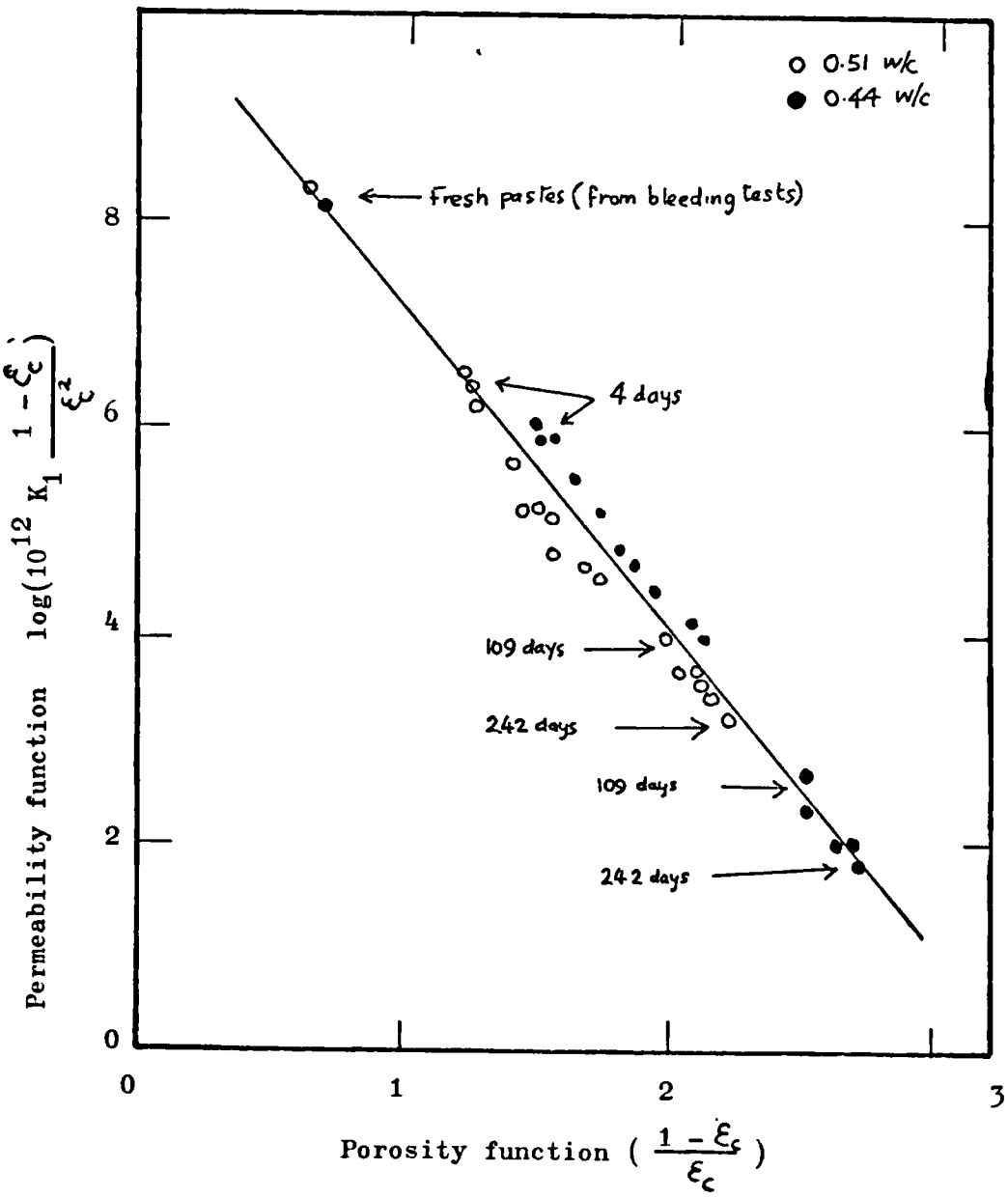

FIG. 1.6 Relationship between capillary porosity and permeability of hardened cement paste /ref. 33/

On this postulate, it was considered that the flow could be characterised by a 'unit pore flow' which can be deduced from the measured output flow rates through specimens as follows;

$$\bar{q} = \frac{\text{Sum of observed flow rates}}{\text{Sum of a sequence of guessed number of pores}} \qquad (1.14)$$

where $\bar{q}$ = unit pore flow

and

$$R = q_i - m\,\bar{q} \qquad (1.15)$$

where m = superficial pore density

R = remainder

q_i = observed flow rates (ordered by magnitude)

The superficial pore density was deduced by repeatedly dividing the observed flow rates by a sequence of integers until a set of numbers close to integers could be found. Robson showed that with this method of analysis, the remainder terms conformed to a normal distribution function and the unit pore flows varied in a reasonable manner with w/c ratio and times of hydration. The variation of the unit pore flow with curing time and water/cement ratio is shown in fig 1.7 taken from Robson's paper. This rather interesting and highly original statistical method of analysis was described at the time to belong to a new field of statistics requiring subjective means of solution. Robson's conclusion was that permeability is not a function of total porosity but reflects the chance of occurrence of paths of linked pores.

This conclusion was based on very sophisticated philosophical arguments, Interestingly, at the discussions following Robson's paper, Pihlajavaara suggested the possibility of positively identifying the unit pore by mercury intrusion porosimetry but at the time it was thought not possible to determine effectively the porosity to the flow of water by this method. Although Robson's hypothesis has been slightly too difficult to put into practice the main contribution from his work is the postulate that the total pore space need not contribute to the flow but that the flow could be akin to that through interconnected or linked flow paths or possibly cracks.

This suggestion poses special problems as to the measurement of the effective or ineffective flow pore space in hcps. Hancox[111] used a method based on measuring the electrical resistivity of the fluids in saturated and partially saturated ordinary and high alumina cement pastes to determine the effective porosity for the conduction of fluids and found that the pore space limiting flow was independent of time of hydration and could be related to the porosity of the sample by

$$F = \xi^{3.4} \qquad (1.16)$$

where,

F = fractional cross sectional area of pastes limiting flow

ξ = total porosity of sample

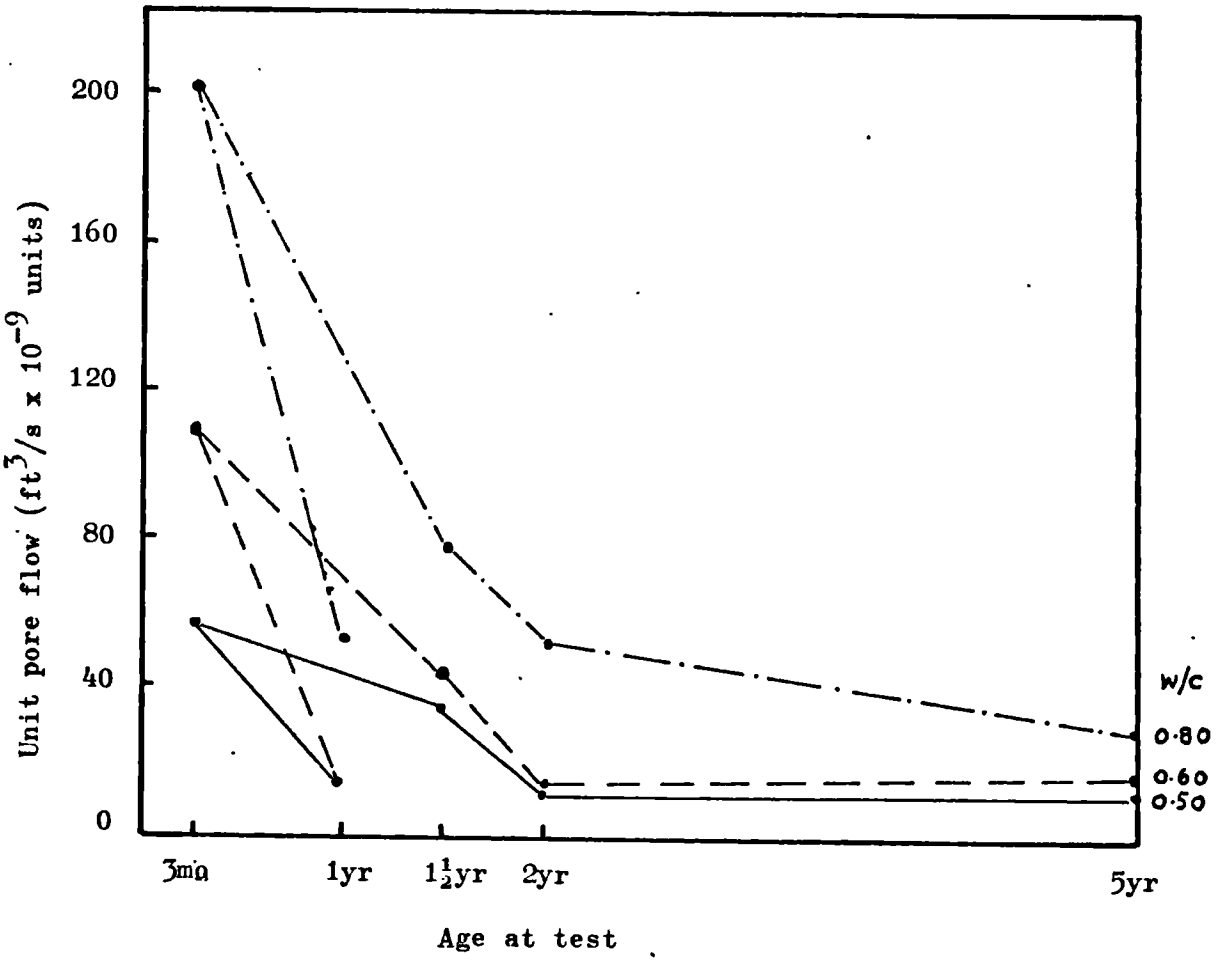

Fig. 1.7: Unit pore flows for concretes /ref 109/

1.2.5 Summary

The data cited by Verbeck[33] suggest that porosity and permeability are uniquely related irrespective of time of hydration quite in contrast with the fact that Powers and others[26] found it convenient to deduce capillary continuity or lack of it from the lack of fit of the data to equation 1.13 derived for mature pastes only. The philosophy of Robson[109] tends to indicate that permeability is not directly related to porosity, whereas Hancox[111] suggests that the ineffective flow space is related to porosity but not dependent on time of hydration. There is a need for further tests to elucidate the porosity-permeability relationship resulting from differences in w/c ratio and times of hydration.

The outline of the available test methods indicate that a steady state technique must be used, therefore the main concern here is that an adequate sealing technique must be found and must be simple. Darcy's law would appear to be adequate for analysing the flow, and there is a need to attempt to eliminate the causes of scatter of results.

1.3. Interrelationships between pore structure and permeability

Studies on the relationships between the pore structure of a porous material and its permeability have been pursued extensively from theoretical points of view and by use of models to represent the porous medium. With as many models as experimental data on pore structure and permeability, this section is not intended to be exhaustive. Extensive reviews of many of the models are given elsewhere[4,77,78,110]. Detailed derivations of equations will not be attempted, the purpose here is to present what the author considers to be useful possibilities of relating pore structure data of hcp and mortars to measured permeabilities.

1.3.1 Models based on Hagen-Poisseiulle's equation

Time honored models of pore structure based on a bundle of straight or tortuous cylindrical capillaries predict permeability by employing the Hagen-Poisseiulles's equation[4] for the flow of fluids in a cylindrical capillary which is given by

$$Q = \frac{\pi r^4}{8\eta} \frac{dp}{dx} \qquad (1.17)$$

where Q = volumetric flow rate

r = radius of capillary

$\frac{dp}{dx}$ = pressure gradient along capillary

η = viscosity of fluid

If the porous medium is replaced by a bundle of n capillaries of different radii, and average radius $\bar{r}$, it can be deduced[4] that permeability, K, is given by

$$K = A \varepsilon \bar{r}^{-2} \qquad (1.18)$$

where ε = porosity of material

A = constant related to tortuosity

$\bar{r}$ = average pore radius

In terms of a pore size distribution function M*(r), the average pore radius r^{-2} may be defined such that

$$K = A \int_0^{r_\infty} r^2 M^*(r)\, dr \qquad (1.19)$$

where M*(r) = differential pore size distribution function such that

$$\int_0^{r_\infty} M^*(r)\, dr = \varepsilon \qquad (1.20)$$

and r_∞ = maximum pore radius in material

ε = total porosity

In a variant of the straight cylindrical model (fig 1.8a)where the pores can be considered as serially lined up with constrictions (fig 1.8b), it could be derived that[4]

$$\frac{1}{K} = \frac{A}{\varepsilon}\left[\int_0^{r_\infty} r^2 M^*(r)\, dr\right]^2 \int_0^{r} \frac{M^*(r)}{r^6}\, dr \qquad (1.21)$$

With these two basic models, a description of the relationship between the pore size distributions, porosity and permeability can be made and any inherent assumptions involved in assuming regular geometries can be absorbed by the tortuosity factors. Many more networks of these two basic models have been proposed and reviewed[100]. The infinite number of combinations possible no doubt allows for many modifications which may be more complex than obtaining the data directly from measurements. A further drawback with most of the above models is that it is often implicitly assumed that an increase in total porosity would necessarily imply an increase in permeability.

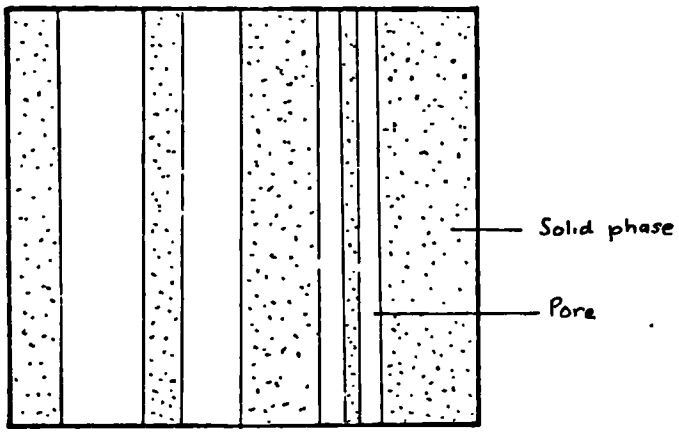

Fig. 1.8a Parallel connected capillaric model of porous media

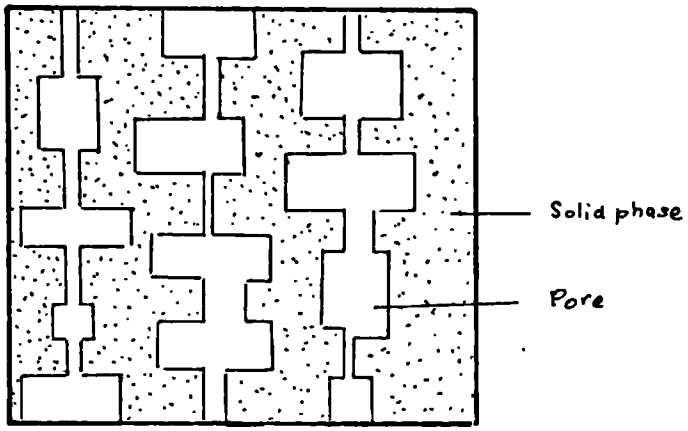

Fig 1.8b Serial connected capillaric model of porous media

1.3.2 Hydraulic radius theories

The hydraulic radius of a porous system is the ratio of pore volume to the surface area of the solid boundaries. This ratio can be visualised as relating the volumetric output flow rate to the resistance due to viscous forces counteracting the flow. Hydraulic radius theories apply to completely interconnected, randomly distributed pores which are reasonably uniform in size[4,78]. A basic expression for permeability in terms of hydraulic radius, r_h, is given by[4]

$$K = C\, r_h^2 \quad f(\varepsilon) \qquad (1.22)$$

where $f(\varepsilon)$ = a porosity function for permeability

C = a dimensionless constant accounting for tortuosity

r_h = hydraulic radius

In the well known Kozeny-Carman theory[11], a porosity function may be derived such that

$$K = C \frac{\varepsilon}{(1-\varepsilon)^2} \quad \frac{\varepsilon^2}{S_o^2} \qquad (1.23)$$

where S_o = surface of solids exposed to fluid per unit volume of solids

C = a constant related to tortuosity

Childs and others[112] propose that hydraulic radius theories fail to describe the permeability of materials whose structure consist of many fissures which contribute negligibly to total porosity and specific surface area and yet dominate permeability. It is possible that hardened cement pastes and concretes may be regarded as belonging to the group of materials not easily described by hydraulic radius theories because of

(1) Robson's suggestions on the unit pore flow index instead of permeability[109]

(2) Powers and others[22] found discrepancies between the Kozeny-Carman theory and experimental data for the permeability of hcp.

1.3.3 Viscous drag theories

Viscous drag theories of permeability consider the porous medium as an assemblage of particles of various shapes. The drag on each particle due to the motion of the fluid relative to the stationary particles may be deduced by employing mainly Stokes law or other modifications of it[113]. For materials such as hcp, the effects of particle interactions on the drag forces due to the smallness of the interparticle spacings are not negligible. Powers and others[22] were able to allow for the effects of particle interactions by studying the rates of fall of tapioca in oil in studies of the permeability relationships with particle sizes of the hydration products of hcp. It was possible to obtain estimates of particle sizes in agreement with those obtained from electron microscopy. This indicates that viscous drag theoretical considerations could be at least more appropriate than hydraulic radius theories for hcp.

1.3.4 General summary of the review

To obtain a greater understanding of the relationships between the pore structure and permeability it is necessary to recognise first the various ways in which the pore structure of concrete or components of concrete may change either with the

(1) methods of preparation
or (2) mix ingredients
or (3) subsequent treatments.

and to relate these modes of change to variations in permeability from direct measurements. The measurements may then be compared with some of the more general theories on the relationships between pore structure and permeability. The three most essential modes of change of pore structure recognised and to be investigated in relation to permeability in this thesis are

(1) initial water/cement ratio
(2) hydration
(3) aggregate inclusions

It is the purpose here to identify the most appropriate definitions of the pore structure parameters that relate to these basic modes of change in relation to permeability.

CHAPTER 2

EXPERIMENTAL APPARATUS AND PROCEDURES

The purpose of the experiments is outlined in this chapter. A description of the design of the apparatus for permeability measurements is given. The apparatus used for the measurements of the structure of hardened cement pastes and mortars is described. The chapter also includes an exposition of some test results to assess the reliability of the measurements made.

2.1 Purpose of Experiments

The experiments were planned to obtain accurate measurements of steady state water permeability of hardened cement pastes as influenced by changes in water/cement ratios and hydration. These measurements were to be made over a wide range of hydrostatic pressures and the corresponding hydraulic gradients.

The measurements of permeability were to be related to measurements of pore size distributions, porosities and other variables of the pore structure of hardened cement paste, with the prime intention of identifying the most appropriate definition(s) of the structure of hardened cement paste that relate(s) to permeability.

The steady state permeabilities of mortars prepared with both normal and lightweight sand particles were to be measured to elucidate the effect of the inclusion of aggregates of different porosities and pore structures in the hardened cement paste phase on steady state permeability.

The overall objective was, therefore, to study three principally different ways of changing the pore structure of a composite i.e.

1. initial w/c
2. hydration
3. aggregate

and to relate these modes of change to saturated permeability of the composite.

2.2. Variables

A summary of the ranges of variables used in the investigation is given below.

Hardened cement pastes:

w/c ratio	0.23 - 1.00
hydration	3 days-20 months

Mortars:

aggregates	normal, density = 2.50 g/cc
	lightweight 1.59 g/cc
	particle sizes - 2400 + 150micron
w/c ratio	0.47

Applied hydrostatic pressures up to 2000 psi.

2.3 Preparation of test samples

Samples were prepared from ordinary portland cement D25 with compositional details given in Appendix 2.1. Mixing and casting was done at approximately 22° C in a temperature controlled laboratory. A standard amount of 1 kg of cement and the required amount of distilled water were weighed to an accuracy of 0.1 g. Mixing was done in a Hobart type CE mixer. The standard procedure adopted for each batch was to mix for 4 minutes, and remix 10 minutes later for a further minute. The mixture was covered with damp cloth during the rest period to minimise evaporation losses. The double mixing procedure was adopted to prevent false set and it allows comparisons to be made with results of previous and on-going investigations done within the research group.

The mixture was transferred and sealed in glass containers. The glass containers were then rolled on the electric roller shown in Plate 2.1 at approximately $\frac{1}{2}$ rev/minute for 4 hours. This rolling procedure was to minimise settlement at the time of casting as it produced a reasonably stiff paste. It was found necessary to roll samples with w/c greater than 0.71 for an additional two hours in order to achieve a reasonably stiff paste.

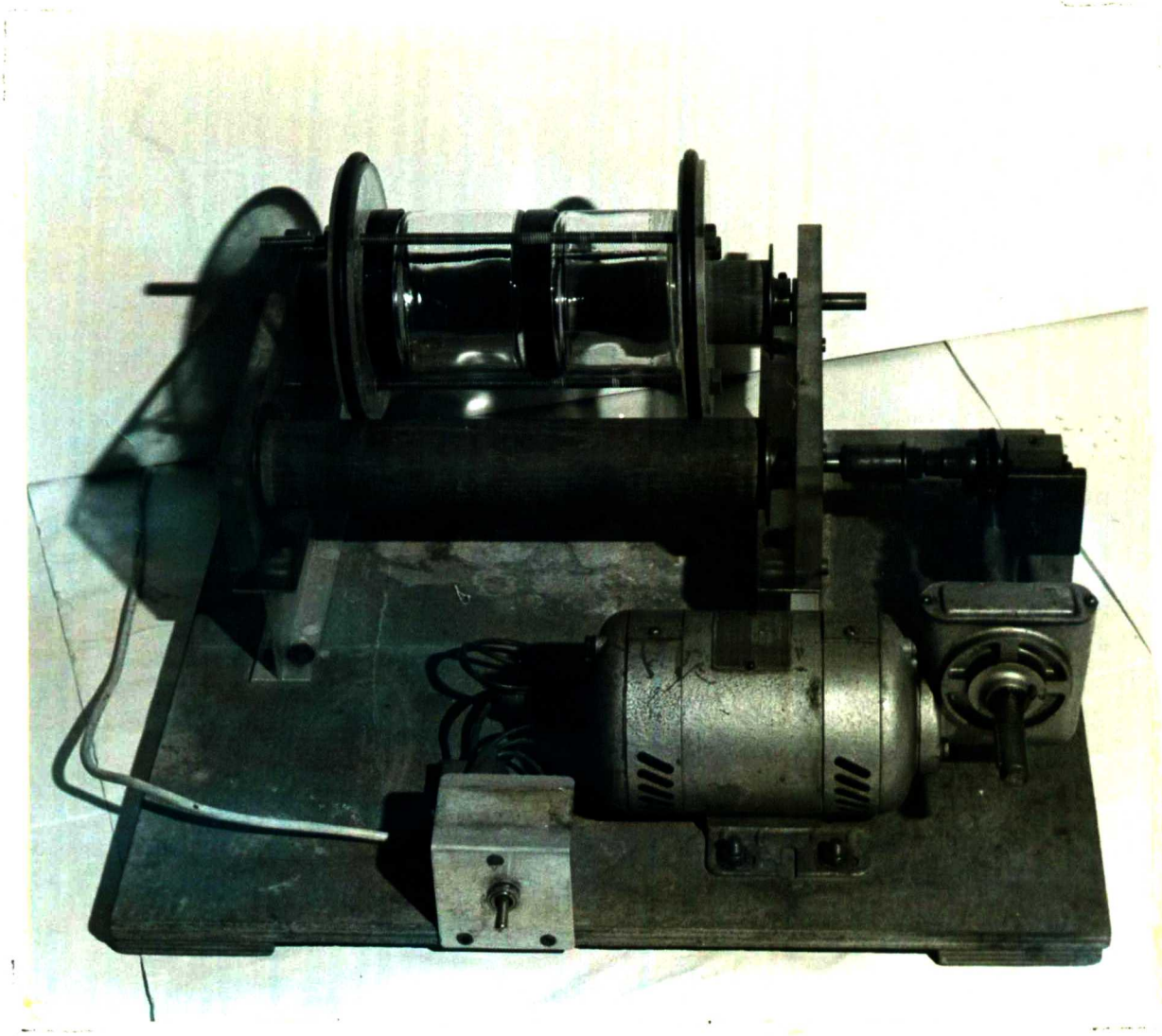

Plate 2.1: Electric roller used to roll fresh paste to minimise settlement prior to casting hardened cement paste samples.

Casting was done in the moulds shown on Plate 2.2 designed to mould truncated conical specimens (70mm long, 20mm - 30mm diameters). The shape of the moulds was to provide a means of sealing the specimens in the permeameters as will be described later. The mixture was cast into the moulds in two layers while being gently vibrated on the shaker shown in Plate 2.2. The period of vibration was standardised to 5 - minutes after the moulds have been completely filled. For pastes with w/c ratios of 0.23, however, compaction by means of a tamping rod was made in conjunction with vibration. Twelve specimens were cast in each batch in the manner described.

The moulds were covered with damp tissue paper and placed over water in a humid plastic container. The plastic container was covered with a polythene sheet to maintain a reasonably high humidity at the initial setting of the pastes. The samples were demoulded at approximately 14 hours after casting. To facilitate easy demoulding, the inner surfaces of the moulds were lightly oiled prior to casting each batch of samples. The specimens were continously cured in distilled water in sealed bottles for periods up to 20 months prior to measurements of steady state water permeability. Mortars were prepared in a similar manner as described but sufficiently stiff to make the rolling procedure unnecessary as also found with the 0.23 w/c ratio pastes.

In reference 92, the truncated conical specimens were found to provide an adequate means of sealing the permeability specimens. The shape was produced by tapering cylindrical specimens in a lathe. In this investigation, it was thought necessary to eliminate the tapering process by casting the shape directly using the moulds as described. This approach although simpler had some minor disadvantages in that it was later found that porosity gradients tend to develop in the direction of casting particularly for pastes with high water/cement ratio. The gradients in porosity are considered to be partly due to settlement and partly due to the shape of the mould. The shape favours a type of horizontal compaction from the taper which is superimposed on the vertical compaction due to the vibration procedure described. Typical variations in the evaporable water contents at 105°C for the high water/cement ratio pastes are shown in Fig 2.1.

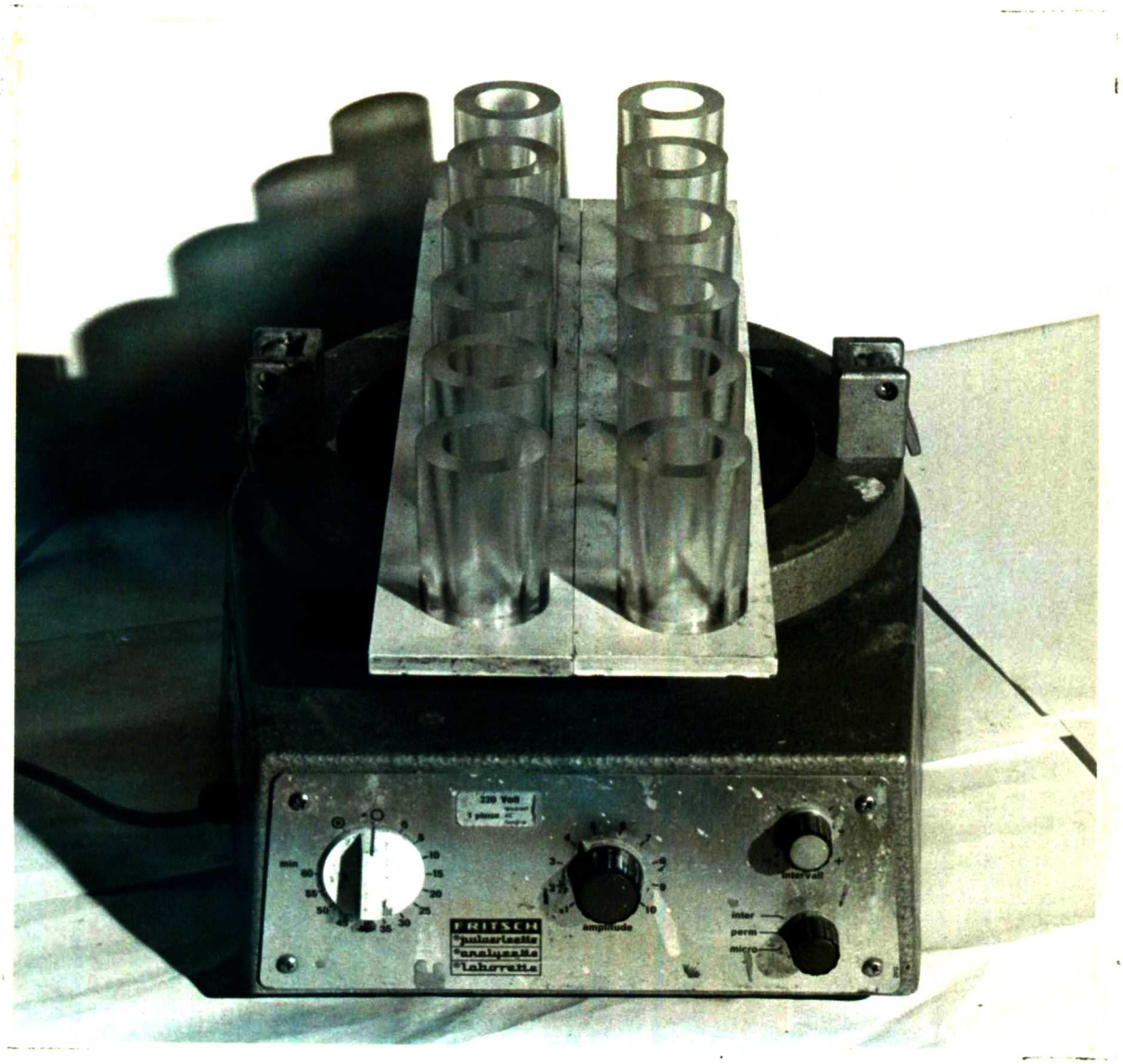

Plate 2.2: Truncated conical shaped moulds used for casting permeability test samples shown placed on the shaker used for compacting the pastes.

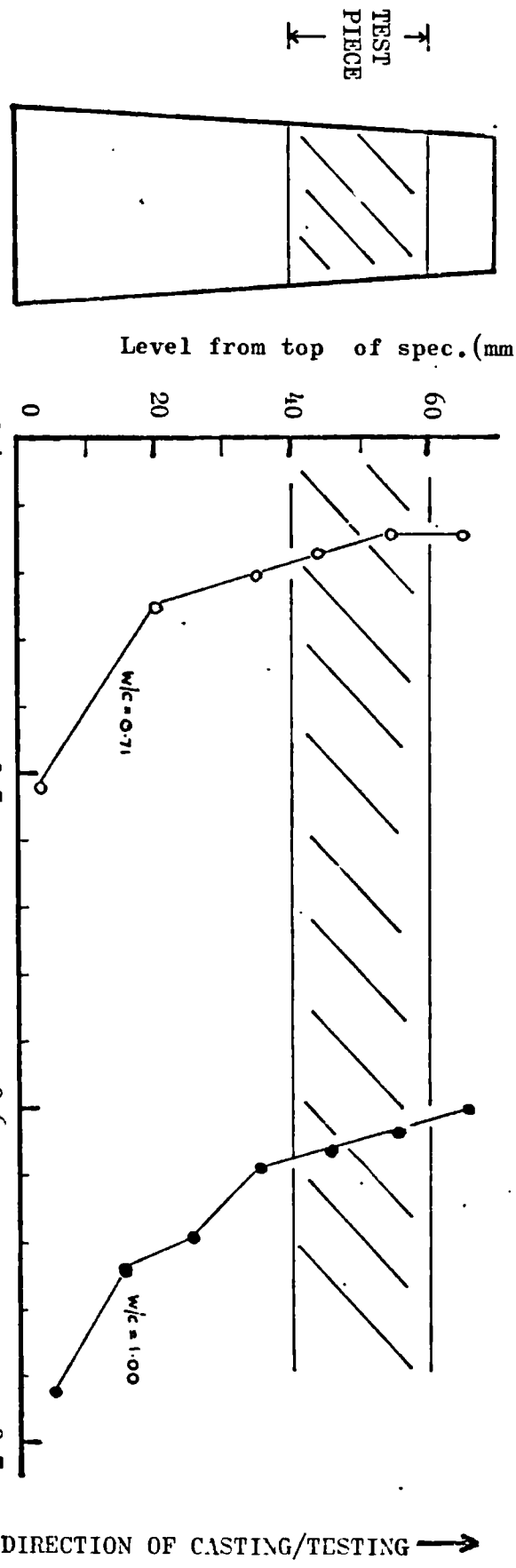

Fig. 2.1: Typical variations of total porosity along the lengths of high w/c ratio pastes caused by the combined effects of the taper of the mould and settlement.

Samples for steady state permeability measurements were cut from the whole piece as shown in Fig 2.1 using a diamond saw and ensuring that the samples were kept continously wet throughout the cutting process, by dripping water from a vertical reservoir on to the specimen. The lower 10mm piece as shown in Fig 2.1 was always discarded and the middle portion cut to between 10mm and 20mm thick was used for the measurements. It can be seen from the typical porosity variations along the specimens shown in Fig 2.1 that this middle portion could be regarded as being of reasonably uniform porosity. Much of the differences in the porosity of the specimens appear to occur for the top 35mm of the cast specimens. It was not found necessary to measure the porosity variations along the 20mm test samples. The faces of the test samples were ground parallel to each other. The size of the test piece resulted from a long experience on the sealing of permeability specimens. It was also a result of obtaining measurable outflow rates through the specimens after successful sealing was achieved and will be described in section 2.4.1.

2.4 Apparatus for steady state permeability measurements

The main requirements for the design of the system for measuring steady state saturated permeability were as follows.

(1) Seal specimens in high-pressure permeameters to avoid leak around specimens.
(2) Provide a source of constant hydrostatic pressures up to 2000 psi and to maintain the pressures over periods extending to at least 4 weeks without interruption.
(3) An accurate means of measuring particularly low output flow rates (order 0.1 cc/hr) through at least six specimens simultaneously.

The means of achieving the above requirements are described below.

2.4.1 Permeameters and sealing technique

The detailed design drawings of the permeameters used are given in Appendix 2.1. The essential features for achieving the seal on the test specimens are that the inner-section of the pressure cells was tapered in the same way, at 5 in 70, as the shape of the specimens. This enabled a silicone rubber sealing jacket to be axially compressed on to the side of the specimen as the specimen and its sealing jacket are forced up the cell under an applied hydrostatic pressure.
A photograph of the assembly is shown on Plate 2.3 to illustrate the mode of assembly of the pressure cell in the permeameter and the manner of locating the specimen in the pressure cell. Six $\frac{1}{4}$ inch bolts and the two neoprene sealing rings were found to be adequate for holding the high hydrostatic pressures of 2000 psi safely. It was essential to ensure that all the six bolts were tightened evenly. The sealing rings had to be correctly and centrally located in the recess on the plates (labelled A and C on plate 2.3) as failure to maintain this simple precaution resulted in fairly dramatic failures of the sealing rings.

The literature on the sealing of permeability specimens, in the writer's opinion, often failed to provide adequate accounts of the means and the success of achieving sealed specimens - a matter of great practical importance for permeability measurements. Here, an account is given of the nature of the type of experimental problems associated with providing adequate sealing.

It was thought that good bonding between the silicone rubber and the specimen would imply good sealing. As a result of this thought, the curved surfaces of the specimens were coated with two or three layers of a silicone primer supplied by Ceiba Geigy. The coating was allowed to harden for approximately 20 minutes prior to casting the specimen in the mould as will be described later. An excellent bond was always achieved but on assembling the permeameters on the pressure lines, it was found that the hydrostatic pressure acting on the samples and the sealing jacket caused differential movement between the specimen and the silicone rubber jacket resulting in loss of bond. The resulting rough mating surfaces could therefore not seal. Nevertheless with this method of sealing, it was possible to seal some of the specimens.

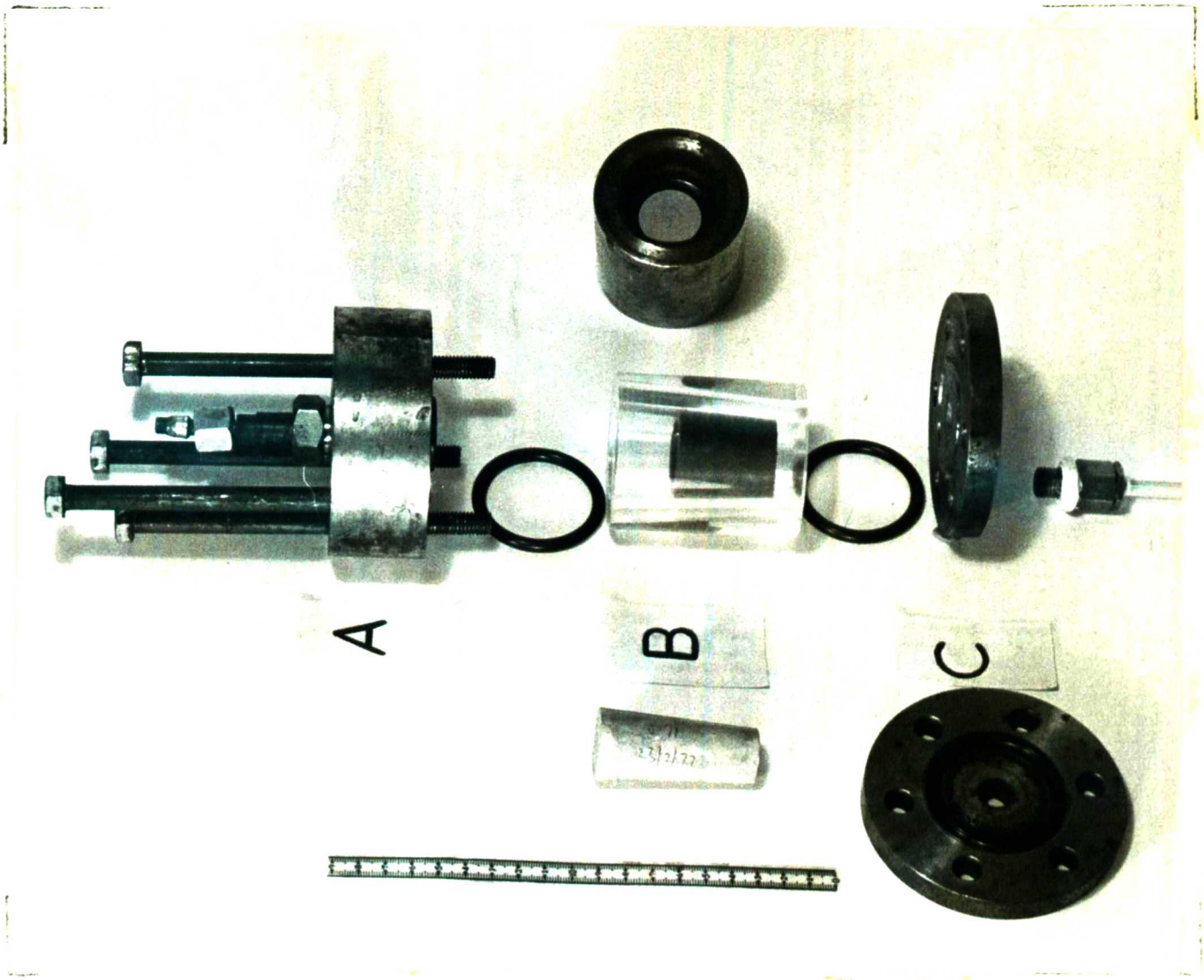

Plate 2.3: Assembly of the components of the high pressure permeameter showing a typical full length test sample and the mode of fitting sample in the permeameter (B).

However, with the specimens initially 60 mm long, it was found that for the sealed specimens, considerable periods of over 4 weeks was necessary to obtain any measurable flow rates even at the imposed hydrostatic pressure of 2000 psi. The sensitivity of the system for measuring output flow rates is described in Section 2.4.3. This evidence was therefore used to modify the sealing technique and to reduce the length of the test sample to 10 - 20 mm as previously described.

The technique finally used was to produce the silicone sealing jackets separately using the pressure cells as moulds and dummy specimens cast to the truncated conical shape. This enabled smooth mating surfaces to be cast for the sealing jackets. Liquid silicoset rubber (Type 101, ICI Ltd/Ceiba - Geigy Ltd.) was catalysed with a type B curing agent. The mixture was thoroughly stirred for at least five minutes. Specially manufactured perspex base caps with recess for locating the samples centrally were inserted in the pressure cells prior to being partially filled with the catalysed silicoset rubber. Any entrapped air bubbles were gently vibrated from the liquid rubber prior to inserting the dummy specimen into the rubber and locating the smaller end face of the specimen into the recess in the perspex base cap. The hardened rubber sealing jackets were stripped from the dummy specimen after 24 hours and stored for later use.

To effect the seal, the hardened rubber was cut to the same length as the test sample but at a depth along the whole of the rubber mould which ensured that the inner diameters of the sealing jacket was at least 3 mm less than the end diameters of the test sample. This allowed the sealing jacket to be initially tightly fitted onto the test sample prior to being forced in the direction of taper of the pressure cell as shown in plate 2.3 (label B). The space in the cell was filled with deaired water before the permeameter was assembled. This was to ensure that no air was to be trapped within the permeameter when the hydrostatic pressure is applied on the test sample. On final assembly of the permeameter, any trapped air would be expelled and could be seen by the excess water being expelled by downward motion of the centre spigot shown in Appendix 2.1 (drawing nos. H/6 & H/4).

In some cases it was necessary to drive the centre spigot further down to eliminate any further air that may have been trapped, but often by suitably filling the space completely it was possible to avoid any air bubbles within the pressure cell.

The most critical stage of the sealing method involved the admission of water under pressure into the permeameters. To take full advantage of the pressure in assisting the sealing, the klinger valves on the test bed (see plates 2.4 and Fig 2.2) were opened and quickly closed repeatedly hence ensuring that no sudden and large pressure drops occurs on the system as a whole - an extremely necessary precaution if other samples have already been installed on the system. Large and sudden pressure drops tend to destroy the seal on the specimens. This procedure was also effective in that it allows the specimens and the sealing jackets sufficient time to move slowly and evenly further up the pressure cells thus improving the seal as a result of gentle and gradual axial compression of the sealing jacket onto the curved surface of the test specimen. A further, and indispensable, advantage of this sealing method is that it enables several trials to be made with the same specimen but using different sealing jackets if one failed to achieve a seal on previous trials. The most important evidence obtained with regard to the effectiveness of the sealing technique was found with the 0.23 w/c ratio pastes. No flow rates could be detected at an applied pressure of 2000 psi for most of the samples until at least seven days under pressure. With this evidence and from the consistency of the results to be presented in Chapter 3, it was concluded that the sealing technique was more than adequate.

2.4.2 Constant hydrostatic pressure

A commercial miniaturised air-driven hydraulic pump with a stainless steel pumping section suitable for water applications was used to provide the hydrostatic pressure. A general view of the pump and the permeability test bed is shown on Plate 2.4. The pump, a Haskel model MS 21, has a nominal air-drive piston area to plunger area ratio of 21. It was therefore possible to control the hydraulic pressure of the measuring system up to 2000 psi by setting the compressed air line supply pressure up to 100 psi.

Plate 2.4: View of the Haskel miniaturised pump and the hydraulic accumulators for controlling pressure.

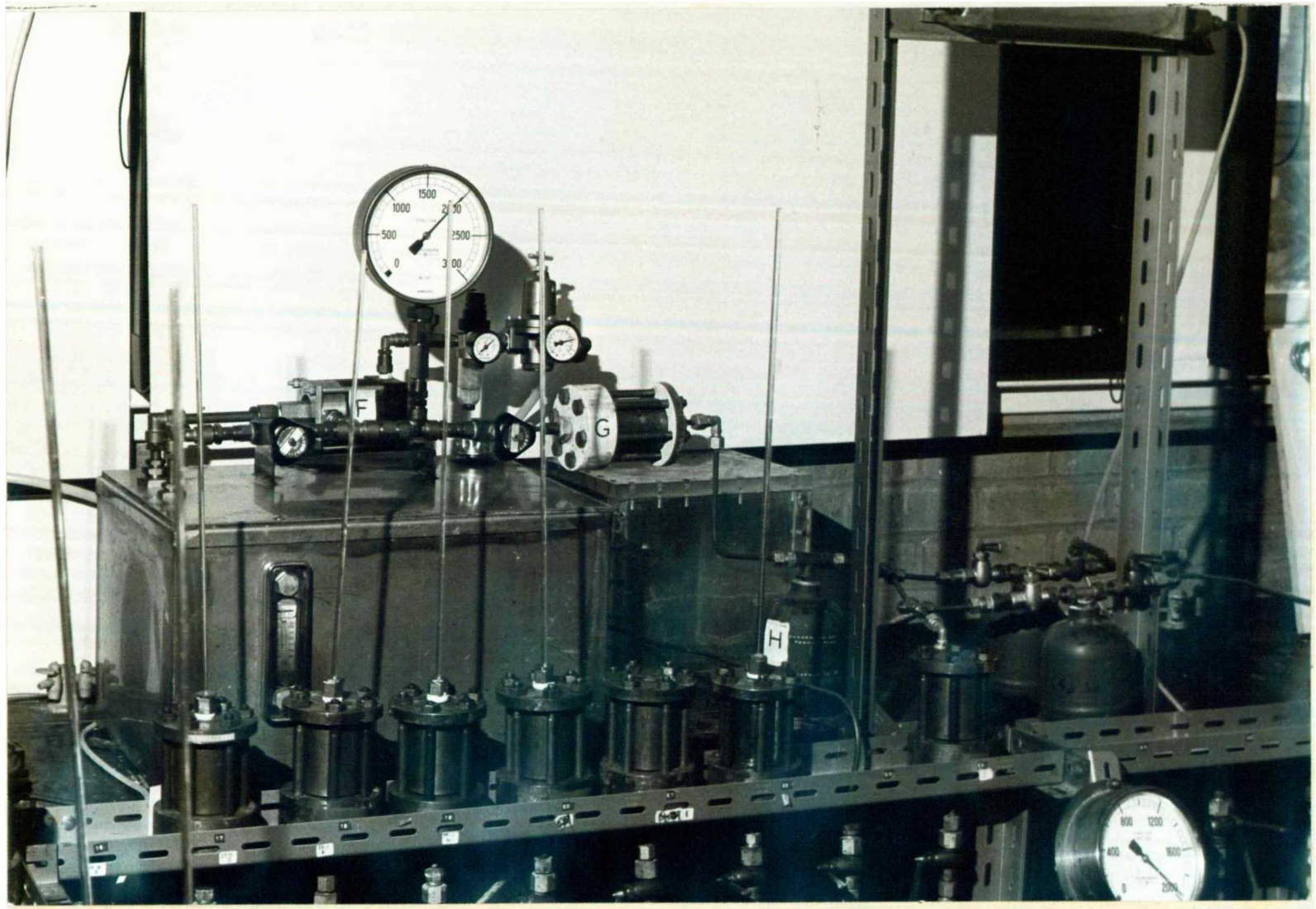

The pump is designed [80] to cease pumping automatically when the preset regulated maximum hydraulic pressure is reached, and to resume pumping when the line pressure falls below a narrow range. In actual application, this narrow range was found to be approximately 80 psi for pressures greater than about 1200 psi and about 40 psi for pressures below 1200 psi. This represents a variation of the mean line pressures of $\pm$ 4% and $\pm$ 8% respectively. The frequency of the pump cycles depends on the flow rates through the specimens and for tests performed at pressures below 250 psi, it was necessary to control the pressure manually.

The cycling action tended to produce sudden pressure variations on the measuring circuit, hence it was decided to include three hydraulic accumulators precharged to 80,250, and 700 psi respectively and connected in parallel to enable the appropriate accumulator to be connected on the line depending on the desired line pressure. The hydraulic circuit is shown on Fig.2.2. The minimum burst pressure of the accumulators is three times the precharge pressure, therefore, the range of pressures up to 2000 psi could be used with the appropriate connection. The set of accumulators (shown G on plate 2.4) were connected in series with a very porous piece of mortar (w/c 0.47, sand:cement 4:1) installed in a permeameter (F on plate 2.4) which further smoothened out the effects of pump pulsations on the line and was also an effective pseudo-needlevalve. The function of the piece of mortar could possibly be further extended to maintain a constant pressure on the line based on the following considerations. If the pressure control circuit and the test bed circuits (see Fig 2.2) are assumed to be analogous to a hydraulic system consisting of a pipe with a fixed conductivity feeding a given amount of fluid per unit time into a reservoir (the accumulators) which is in turn drained in a controlled manner by the test specimens, then it should be possible to select the piece of mortar (with respect to length and permeability) in a manner to ensure that either a constant hydrostatic head can be maintained on the test bed, or only a small fraction of the change in pressure on the hydraulic pressure production circuit is transmitted to the measuring circuit.

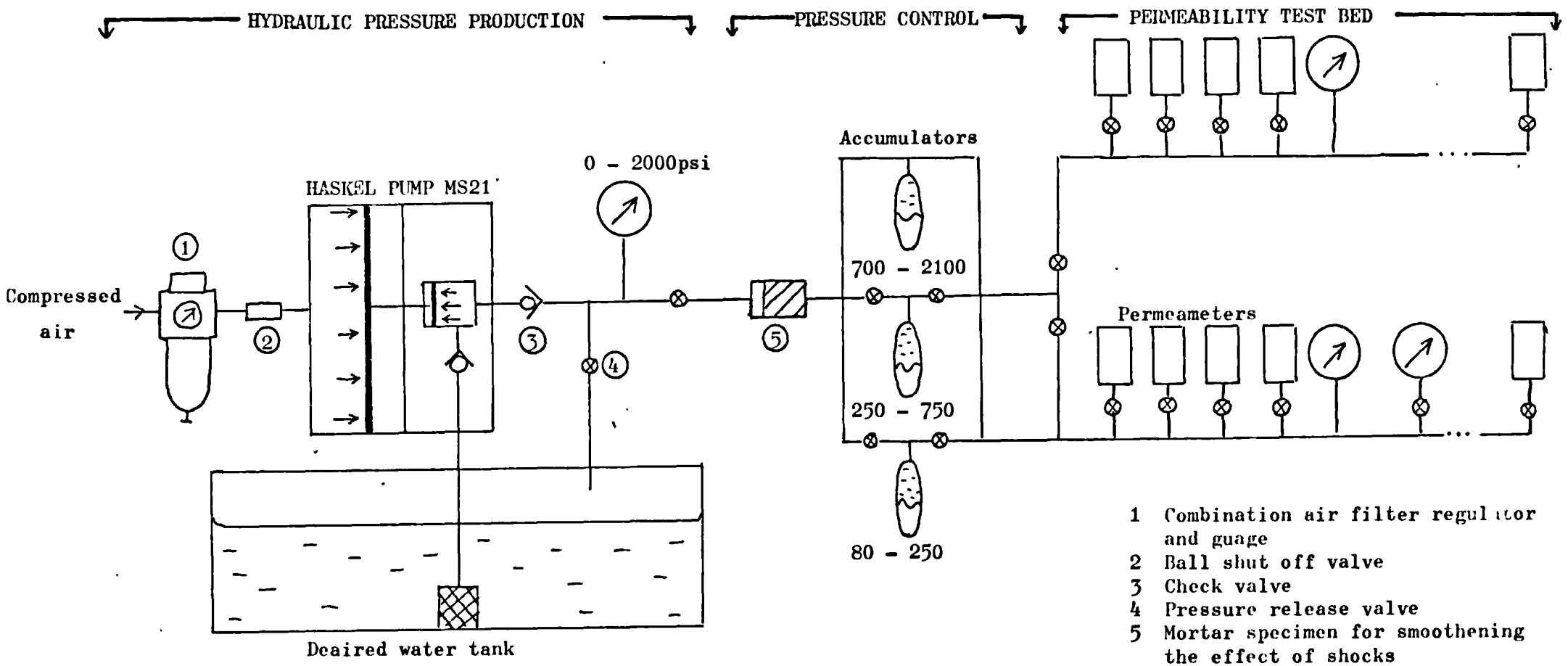

Fig 2.2: Hydraulic Circuit for Permeability Measurements

The pump suction was connected to a ten-gallon capacity stainless steel tank which was kept filled with deaired water and used throughout the investigation. Some earlier tests made with ordinary water which had not been deaired, however, showed no significant differences in the permeability values obtained from the measurements, in comparison with those obtained from later tests using deaired water.

The test bed consisted of a rigidly assembled 'handy angle' L-framed structure shown on plate 2.5. The frame was rigidly bolted to the floor to minimise errors in the measurements of the level of the water meniscus which were likely to be caused by vibrations and other disturbances. Although the supports for the cathetometers were adequately rigid, an extra precaution was taken during the measurement by avoiding resting elbows on the fixed bench which was likely to cause very small errors due to the minor sagging of the bench top.

Thirty hydraulic pressure supply points were built with $\frac{1}{4}$ inch bore copper tubing and brass klinger valves (AB10). The hydrostatic pressures on the lines were measured by a 12 inch Bourdon test gauge. Two ordinary Bourdon gauges were connected on the line (see fig 2.2.) to provide a check. A constant level pressure device illustrated on plate 2.5 was used for the steady state tests conducted at pressures in range 1 (as described in section 2.6.1)

2.4.3 Output flow rate measurements

The change in the level of the water meniscus in capillary tubes of different internal diameters were measured to an accuracy of 0.001 cm by means of cathetometers. The cathetometers were placed on a rigidly built bench as shown on plate 2.5 and were sufficiently free from vibrations. Time intervals were measured to an accuracy of 0.1 seconds with a Cassio electronic stop watch with time lap measurement facility. It was possible to measure a maximum of six different flow rates through a set of six samples per day.

Plate 2.5: The general view of the permeability test bed and the system for output flow measurements.

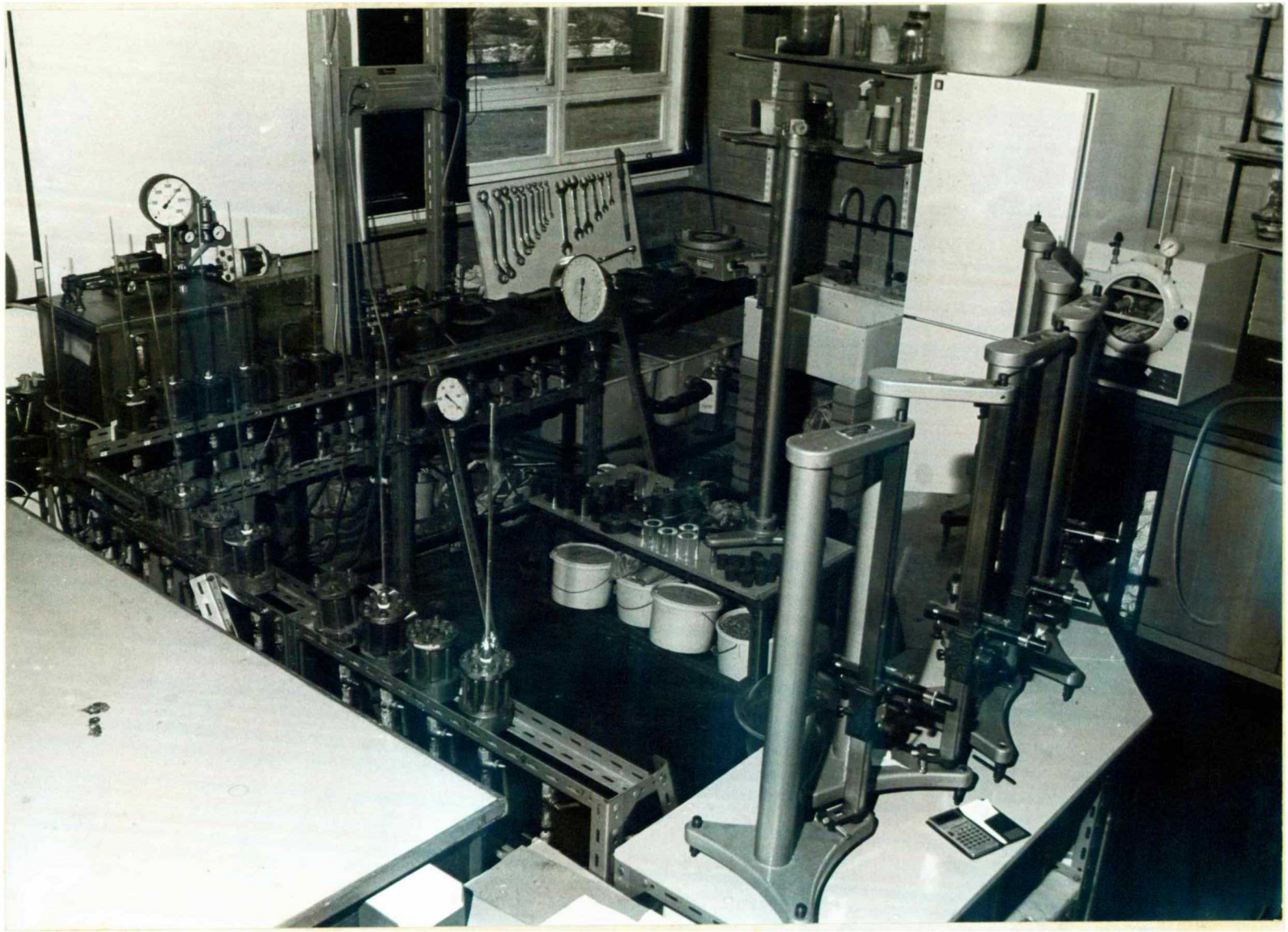

The frequency of measurement varied from 15 minutes to approximately 4 hours, depending on the permeability of the samples. It was also possible to calculate the flow rates during each measurement hence establish steady flow rates during the measurements. The criterion for steady flow rates used in the present investigation is described in section 2.6.1.

2.5. Apparatus for pore structure measurements

Measurements of pore size distributions, hydraulic radii, and surface areas were made with mercury intrusion porosimetry. The total porosities were determined from the evaporable water contents at 105°C and complemented by the helium comparison pycnometer. The following sections briefly describe the equipment used.

2.5.1 Mercury Porosimeter

A commercial Carlo Erba Series 200 porosimeter with a date reduction unit attachment was used. The principle of the porosimeter has been outlined in section 1.1.3.2 and the means of analysing the data will be given later.
The porosimeter comprises of a system for generating and measuring pressure, a means of detecting the level of mercury in a glass dilatometer plotting the data for the relationship between pressure and the amount of mercury penetrating into the sample.
A schematic representation of the circuit for the porosimeter is given in Fig 2.6, and the instrument is illustrated on plate 2.6 where the separate filling device to be described later, can be seen on the right of the instrument housing. The data reduction unit can be seen on top of the instrument.

The pressure on the mercury in the dilatometer is transferred by ethyl alcohol which is drained from the reservoir to fill the autoclave prior to a run. The pressure on the alcohol is produced by the small piston of a 1:100 pressure intensifier whose large piston is actuated by oil drawn from a reservoir by a low pressure pump. The design of the autoclave ensures that an equal all-round hydrostatic pressure is transmitted by the alcohol to the glass dilotometer hence enabling pressures up to 2000 kg/cm^2 to be reached without breaking the dilotometer. The pressure in the autoclave is measured by a pressure transducer whose output is fed to both the data reduction unit and a chart recorder.

The measurement of the amount of mercury penetrating a sample in the dilatometer is achieved by means of electrical contact between the level of mercury and a metalic probe which is driven by a synchronous motor to establish electrical contact at each pressure increment.

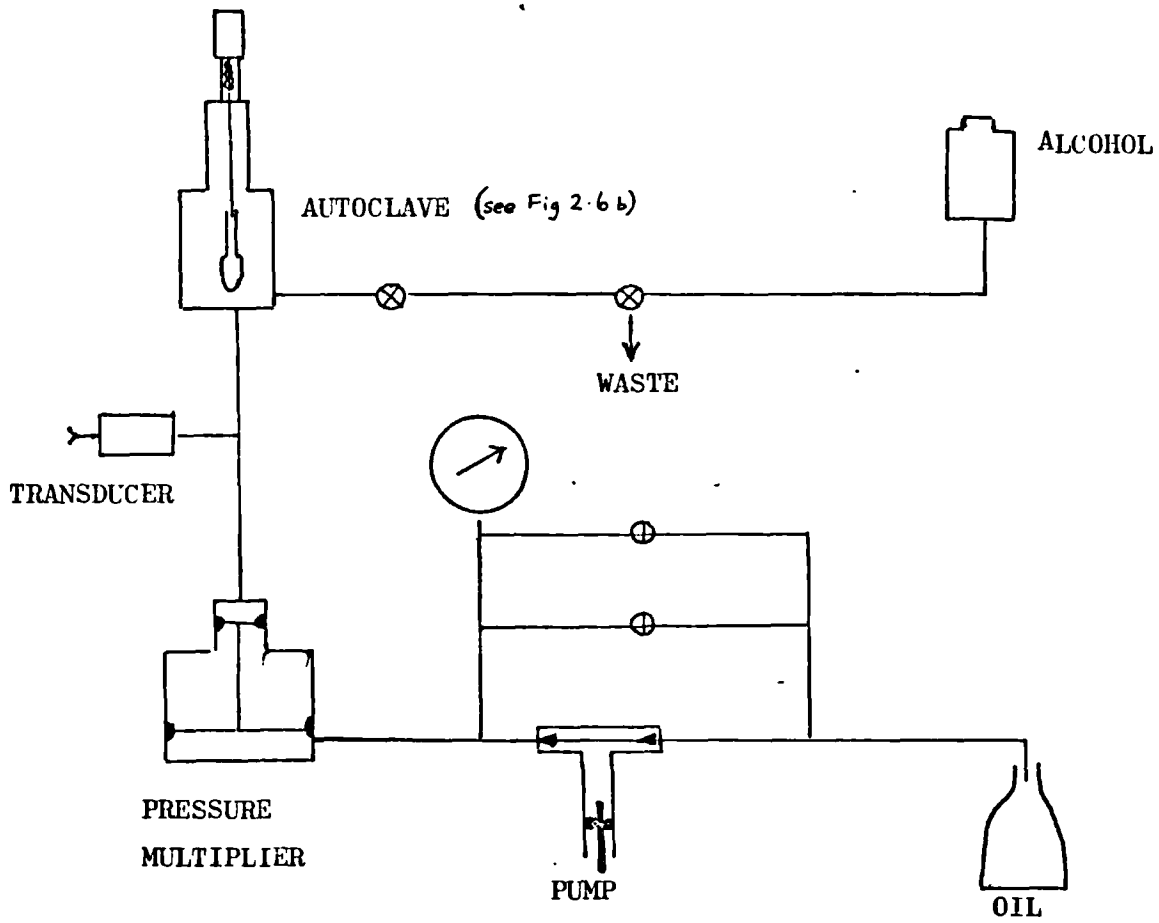

Fig 2.6: Simplified circuit for the mercury porosimeter

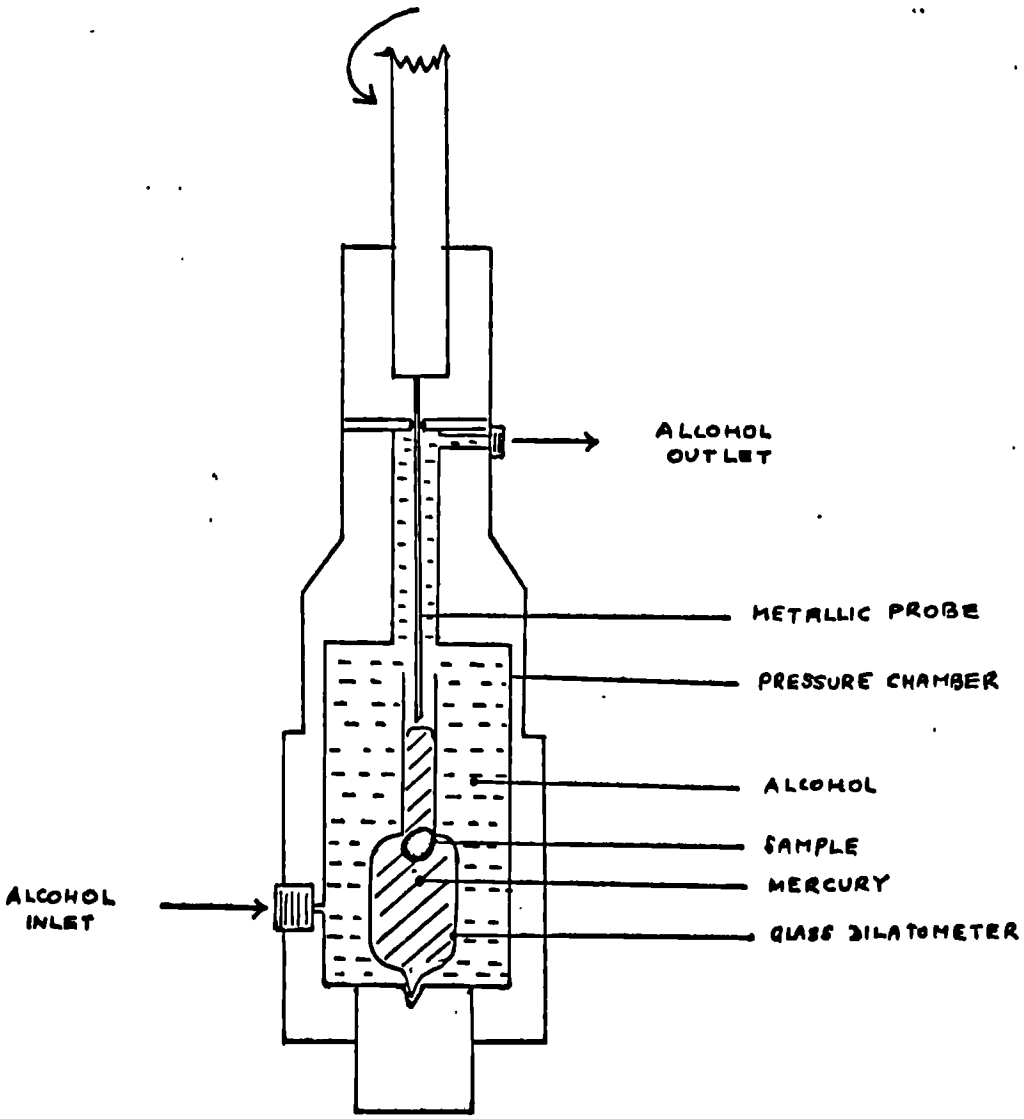

Fig 2.6b: Detailed sketch of the autoclave system of the mercury porosimeter.

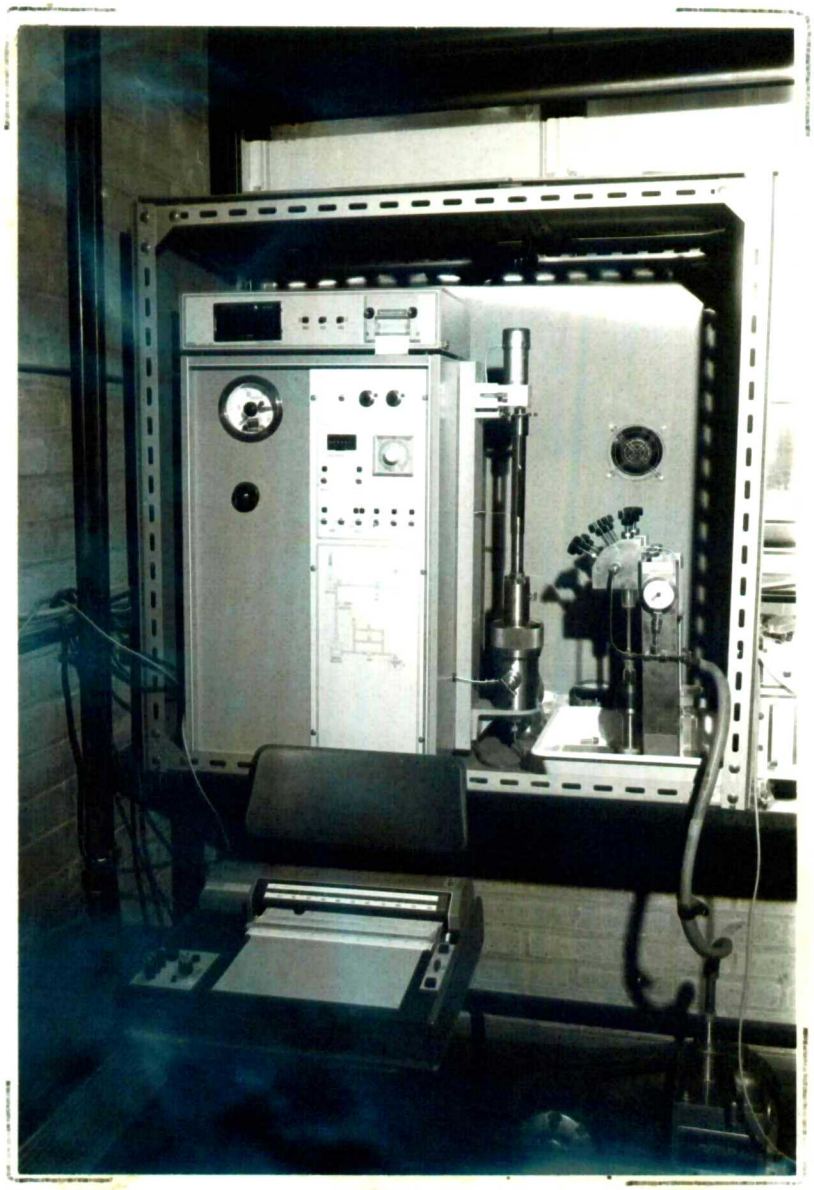

Plate 2.6: A Photograph of the Carlo Erba Series 200 Mercury porosimeter.

A ten-groove cam on the shaft of the motor operates a micro-switch thus providing a pulse per 0.1 mm probe travel. The pulses are fed to the data reduction unit and chart recorder for printing and plotting. The glass dilatometer used consists of a sample holder and a stem which is calibrated to have a constant diameter of 3mm. The constant section provides a means of directly calculating the volume of mercury intruded for any given probe travel.

Degassing of the sample prior to pore size distribution determination is achieved by use of the filling device shown on plate 2.6. It consists of three shut-off valves linked to a vacuum pump, a mercury reservoir and the atmosphere, through a tube which may be linked to the stem of the dilatometer. The dilatometer head may be sealed to a gasket on the filling device by means of a spring loaded support, as illustrated on plate 2.6. The filling device was used to evacuate the samples and fill the dilatometer with mercury while under vacuum.

2.5.2 Helium Comparison pycnometer

The helium pycnometer can be used to determine the volume of solids by helium displacement. A photograph of the helium pycnometer is shown on plate 2.7, and a schematic representation of the system is given in fig 2.7. Essentially, the apparatus consists of two isolatable cylinders whose volumes can be varied by means of movable pistons with handwheel attachments. The cylinders can be isolated by means of a coupling valve. The reference cylinder is provided with two stop positions such that the volume of gas contained within it can be doubled or halved for any complete piston sweep between the two stop positions. The measuring cylinder is designed to incorporate a sample cup and the sample. The travel of the measuring cylinder piston is reproduced on a digital counter designed to indicate the solid volume directly in cubic centimetres. The principle will be explained later. The pressure of the gas in the cylinders can be balanced with respect of each other by means of a sensitive diaphragm linking the cylinders whose deflection is amplified by a differential pressure indicator located at the front of the instrument. The zero or null pressure differential indication may be found by means of a parallx mirror mounted behind the pointer of the differential pressure indicator.

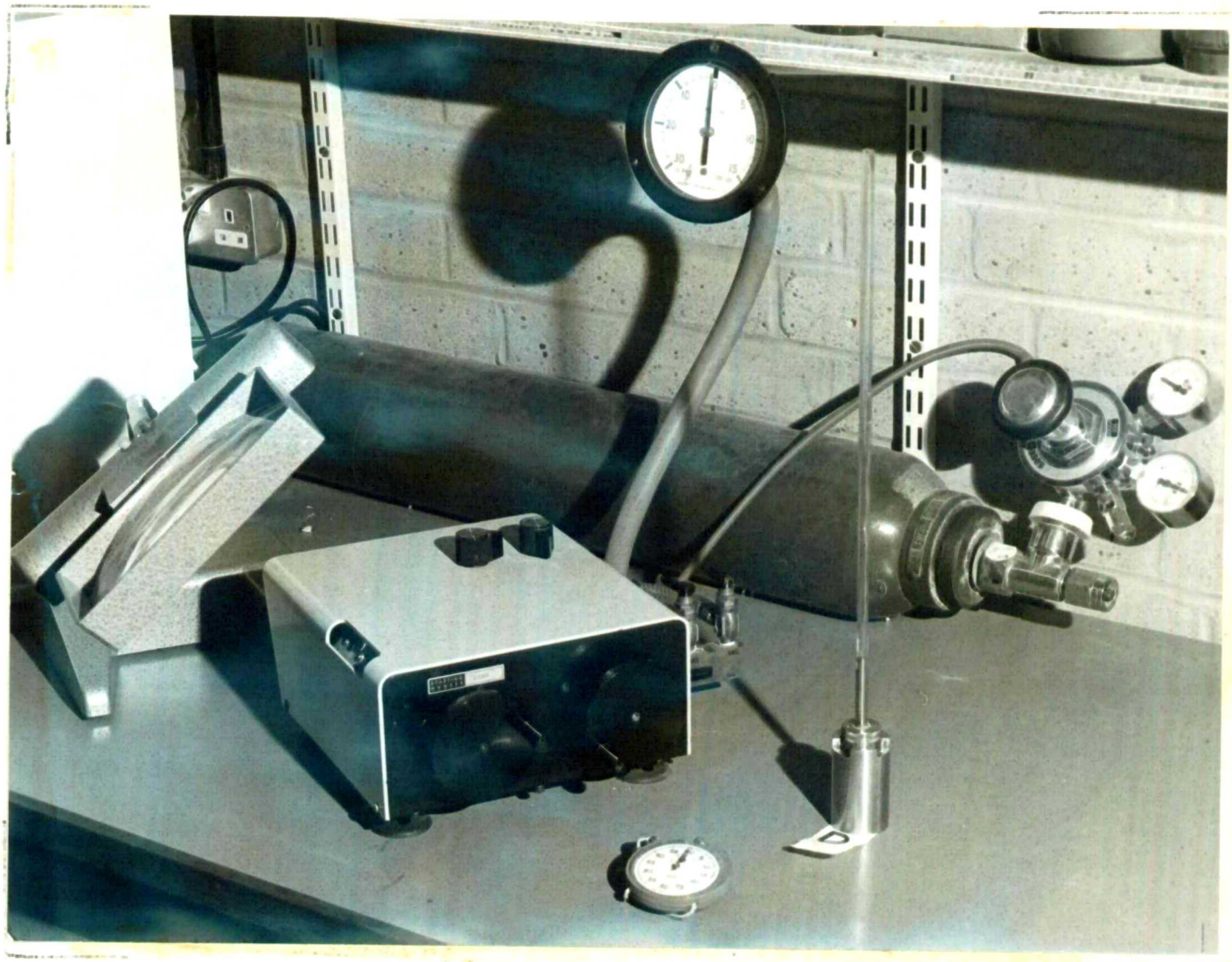

Plate 2.7: A view of the helium comparison pycnometer and accessories

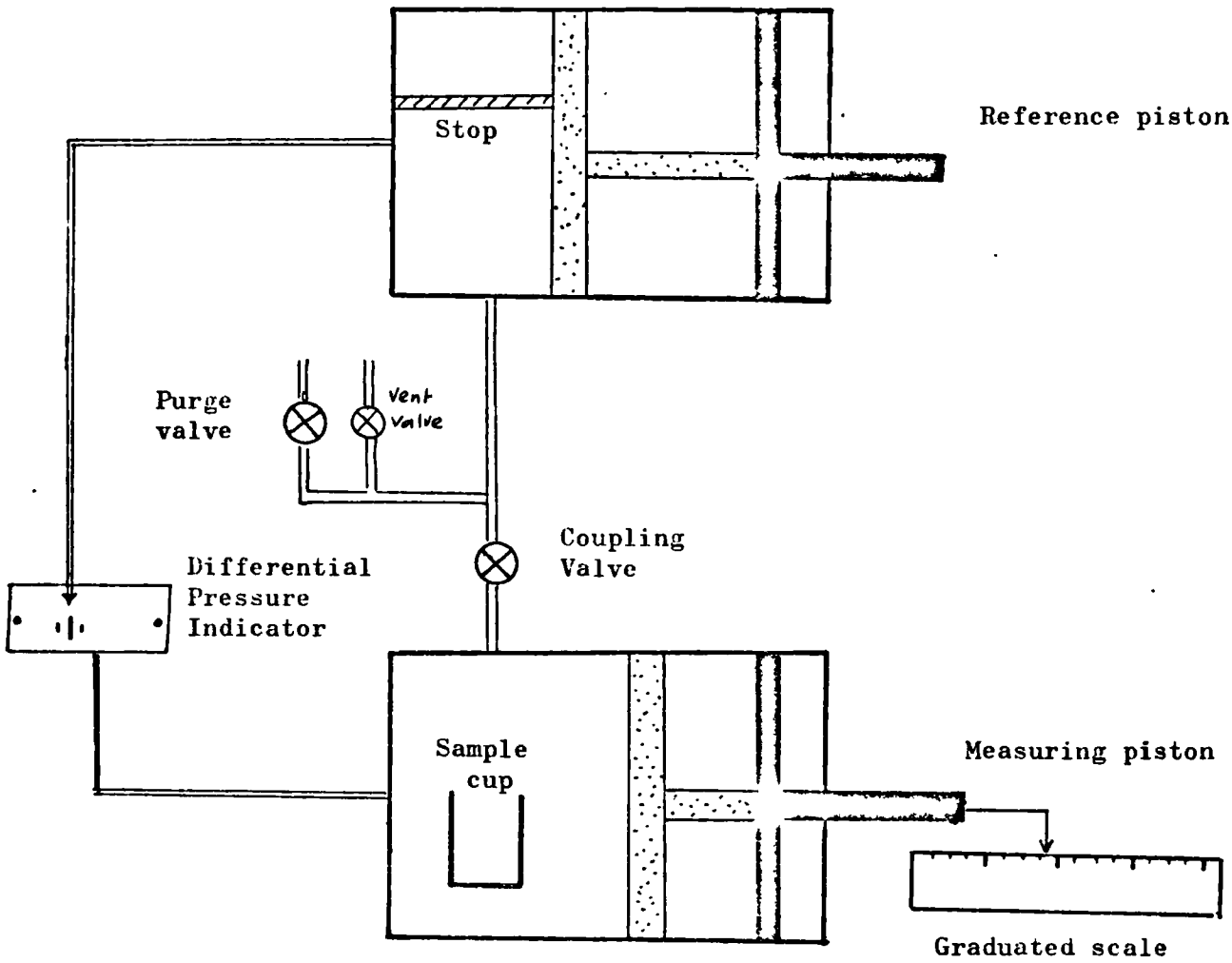

Fig 2.7: Schematic representation of the Helium Comparison Pycnometer

The instrument is equipped with a purging facility which enables the two cylinders to be evacuated prior to being filled with helium. In the present investigation, the vent valve was connected to a pressure gauge shown on plate 2.7 to enable a definite measure of the pressure of the gas admitted into the system to be made, and checked to be one atmosphere before commencing the compression stage to be described later. This was a result of previous trial runs which indicated that substantial loss of reproducibility is found if the alternative approach of venting the system for a specific time was used. The differences in readings were mainly attributed to initial deviations of the gas pressure from atmospheric pressure.

A schematic representation of the principle of solid volume measurement is given in Fig 2.8. The pressures within the cylinders are changed from an initial value, P_1, to a final value P_2. The piston positions are therefore changed from x_o to x_1 for the reference cylinder, x_2 to x_3 for the measuring cylinder containing no sample, and x_2 to x_4 for the measuring cylinder containing a sample of volume V_s of solid material. At constant temperature and for slow compression, the ideal gas law gives the following relationships between the gas pressures and volumes for the states 1,2 and 3 shown on fig 2.8.

For 1 $$P_1 A_r x_o = P_2 A_r x_1 \qquad (2.4)$$

2 $$P_1 A_s x_2 = P_2 A_s x_3 \qquad (2.5)$$

3 $$P_1 (A_s x_2 - V_s) = P_2 (A_s x_4 - V_s) \qquad (2.6)$$

Where A_r and A_s = sectional areas of the reference and measuring cylinders respectively.

V_s = volume of solid material of sample

Subtracting equation 2.6 from 2.5 and rearranging gives the volume of the sample V_s as

$$V_s = (x_3 - x_4) P_2 A_s / (P_1 - P_2) \qquad (2.7)$$

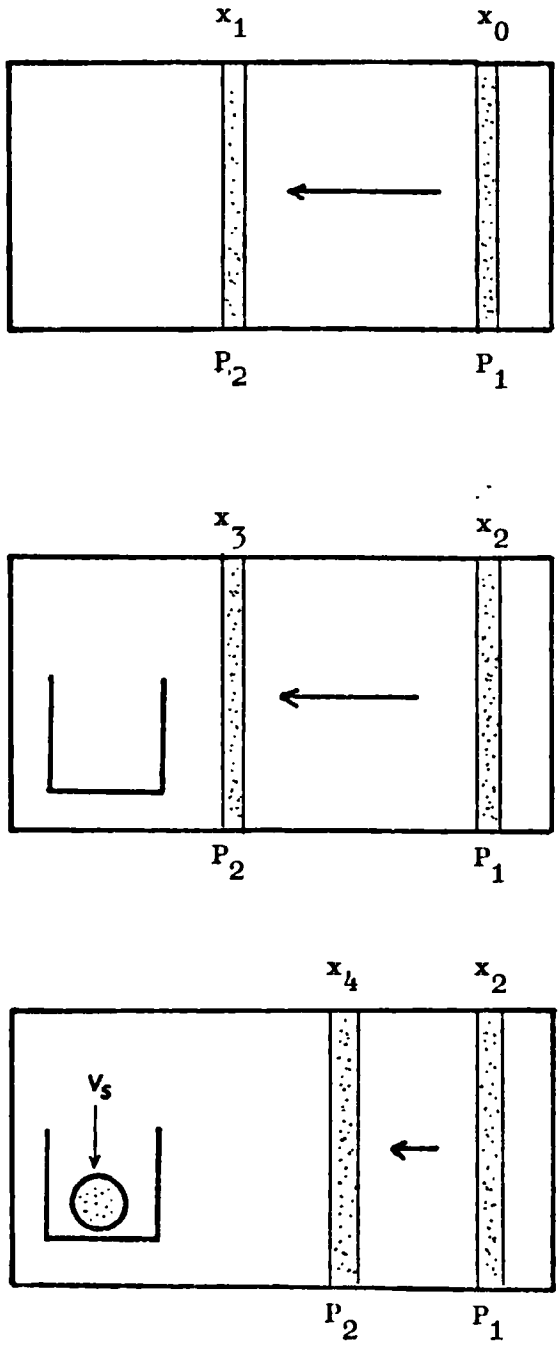

Fig 2.8: An illustration of the principle of solid volume measurement employed by the helium comparison pycnometer.

It can be seen that the volume of the solids of a sample can be found by calibrating the system for zero solid volume indication (x_3) and using standard starting and final pressures, P_1 and P_2 respectively. In this case the volume of solids can be seen to be directly proportional to the piston position at balance (x_4).

The validity of the derivations presented rests on the system being leak free, which in actual operation was found not to be the case. As a result of this, great care is essential in interpreting the results of the pressure changes in either of the cylinders over long periods when the gases in both cylinders are compressed. If a porous solid is used instead of a non-porous solid, the compressed gas may exhibit some delay in filling the pores of the evacuated sample depending on the extent of which the pores are interconnected, presumably the permeability of the material to helium, the surface area exposed to helium and possibly the moisture content of the material.

A series of tests performed on samples of different moisture contents to enable an assessment of the suitable condition required for the measurement of total porosity of hardened cement paste will be described in section 2.6.4. In further results to be presented in Chapter 3, the inflow of helium into pastes of potentially different permeabilities will be shown.

2.6. Experimental Procedures

The purpose of this section is to describe the procedures adopted in the measurements of both the properties and the state of the materials of relevance in this work. To achieve such an objective, it has been necessary to include results of tests which were conducted to establish the basis of the procedures adopted.

2.6.1 Saturated permeability measurements

The test samples were sealed in the permeameters in the manner described in section 2.4.1.

The wide range of permeability values obtained in this work could only be obtained by applying a wide range of pressures and using capillary flow tubes with diameters varying from 0.5mm to 10mm. Since time of hydration was an important variable in this investigation, it became necessary to standardise the time for measuring output flow rates in order to minimise the effects of changes in flow rates caused by hydration during the measurements. A further complication arose from the disolution of soluble hydration products in the flowing water and again by use of rigid steady state flow citeria it was possible to minimise any errors due to different rates of disolution.
The preliminary tests carried out on early and mature age specimens to elucidate the effects of imposed hydrostatic pressure and hydration on the attainment of steady state flow rates are described below.

For the early age samples, pastes of medium w/c ratios (0.59 - at 7 days) were used. Pressure increments were applied at approximately 2 hourly intervals, starting at 140 psi. In the course of the two hours, measurements were made an hour after the pressure increment had been applied to obtain output flow velocities in each of the four samples used. The mean flow rate obtained at each pressure step was used in computing the saturated permeability coefficients. The results are presented in table 2.1a. and illustrated in fig 2.9a. The pressure increments were applied to a maximum of 1620 psi and the whole test lasted for 12 hours. The pressure was maintained at 1620-psi for a further 8 hours before taking further readings of flow rates.

The ratio of permeability coefficient at any given pressure (or time under pressure) to the starting pressure (140 psi) are also given in table 2.1a. It can be seen that during the 12 hours under test, a reduction in permeability of approximately 70% of the initial values were found for the four specimens.

TABLE 2.1a Effects of pressure and hydration on permeability of early age specimens (w/c = 0.59, 7 days initial curing)

		1	2	3	4	5	6	7	8
Time under pressure(hr)		0-2	2-4	4-6	6-8	8-10	10-12	12-20	
Pressure(ps		140	180	222	340	715	1620	1620	
sample		Permeability 10^{-10} m/s							K20h/K12h
1		1.76	1.69	1.64	1.55	1.49	1.26	0.92	
	K_p/K_{140}	1	0.96	0.94	0.88	0.85	0.72	0.52	0.73
2		2.19	2.29	2.22	2.05	1.82	1.52	1.27	-
	K_p/K_{140}	1	1.05	1.01	0.94	0.83	0.69	0.58	0.84
3		1.85	1.74	1.64	1.52	1.40	1.18	0.86	-
	K_p/K_{140}	1	0.94	0.89	0.82	0.76	0.64	0.47	0.73
4		1.94	1.86	1.97	1.64	1.44	1.20	0.93	-
	K_p/K_{140}	1	0.96	0.92	0.85	0.74	0.62	0.48	0.78

The reduction in permeability with time under pressure is also found to approximate to an exponential decay curve (fig 2.9a). For the further 8 hours at the maximum applied pressure, the reduction in permeability for all the four specimens is of the order of 50% of the initial values, and approximately 75% of the values at 12 hours (column 8, table 2.1a). The output flow rates were found to be steady to within two significant figures during the hourly measurements. Tests carried out on 0.23 w/c ratio pastes also cured for 7 days in water during the same period as the above tests produced no measurable output flow rates at all stages of the pressure increments. These results therefore led to the following conclusions.

(1) neither a fixed standard pressure could be used for all the test samples.

(2) Nor a whole range of pressures applied on each specimen to deduce permeability because of the impracticality of obtaining reasonable flow rates at different pressure steps in reasonable time to avoid the effects of hydration on the specimens to be tested at early age.

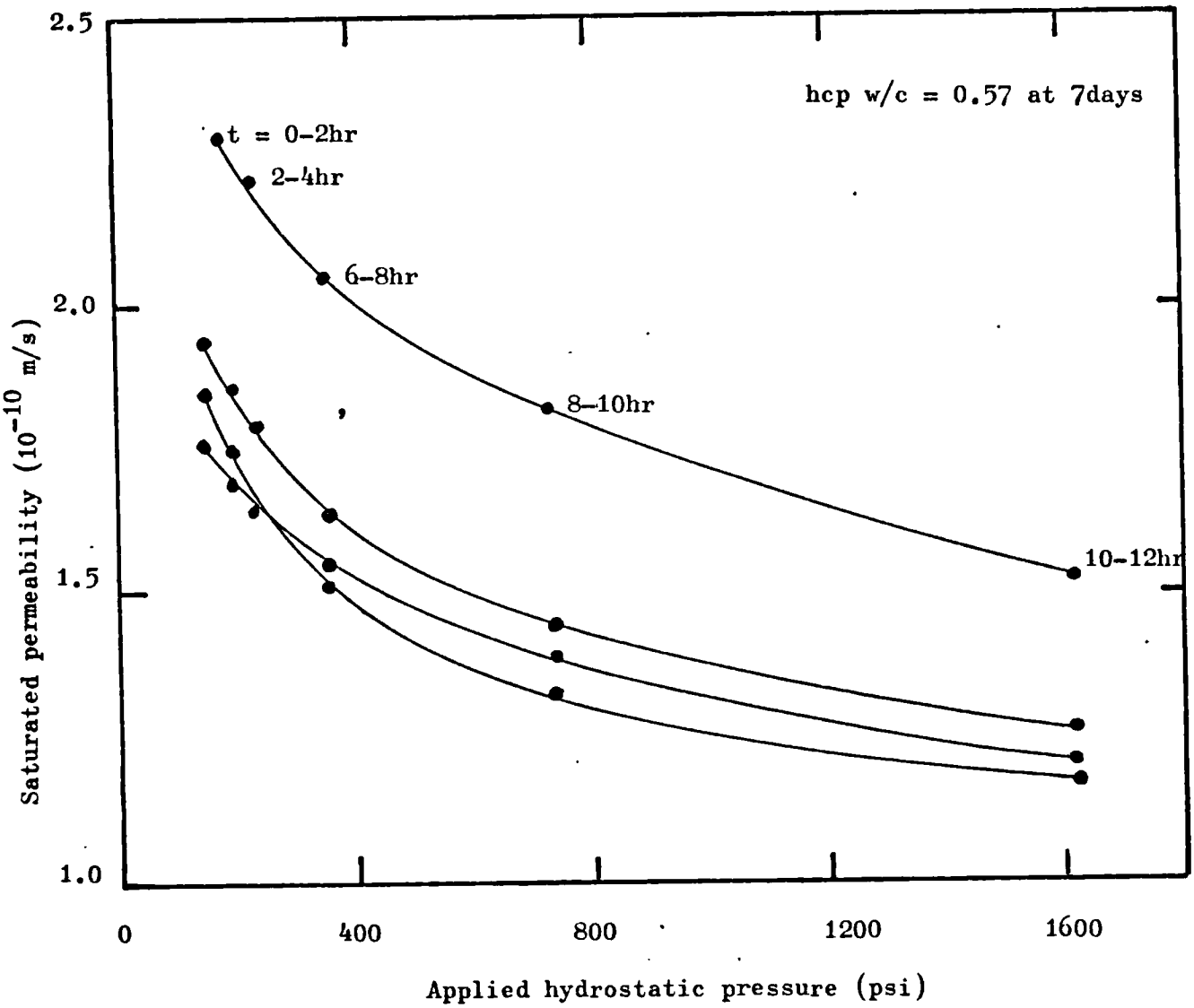

Fig. 2.9a: Changes in permeability of hardened cement paste samples with applied pressures and times under pressure.

For the mature samples 0.65 w/c ratio pastes cured in water for 21 days followed by conditioning at 90% relative humidity for 9 months were used. The relationship between the applied pressure and the permeability coefficients computed in the manner described previously are given in table 2.1b and illustrated in fig 2.9b. The steady state flow rates were measured in the course of a day when the pressure increments had been applied and maintained for at least 12 hours in this case. It was not possible to simulate the tests done for early age samples exactly because the flow rates were not sufficiently high to enable the readings to be made in a period of only 2 hours as before. It can be seen from fig 2.9b that permeability reduces with increased pressure or time under pressure. Attempts at decreasing the pressure in steps produced leaks around the specimens, thus it was not possible to establish whether the reduction in permeability at higher pressure was due to hydration, clogging of the pores, or due to the increased pressure. It should be interesting to mention here that because of the technique of sealing the specimens in the permeameter, it is possible to place the samples in a state of longitudinal compression superimposed on a radial compression which could possibly tend to reduce the effective flow channels within the specimens, hence reduce permeability with increasing pressure. A much more practically likely cause of the reduced permeability could be attributed to improved seal on the specimens at high pressures, but the fact that 0.23 w/c ratio pastes cured for 21-days and tested simultaneously produced no measurable output flow rates throughout the variations in pressure refute this possibility. The most essential deductions from the test on the mature pastes were as follows.

(1) The seal on the specimens is effective for monotonically increasing applied pressure steps.

(2) Permeability decreases with either increasing pressure steps.

or (3) Time under pressure (hydration)

or (4) Clogging of the pores.

To standardise the tests, therefore, it was necessary to ensure that the applied pressure is sufficient to produce measurable outflow rates in a given time under pressure. The compressive strengths of the pastes are also variable, which implied that if the applied pressure is too great, the specimens of lower strengths would fail under pressure in the permeameters - (this was actually observed in practice). The compromise finally used was to select four ranges of pressure for the measurements as stated in table 2.2a.

TABLE 2.1b Effect of pressure and hydration on permeability of mature specimens (w/c = 0.65, 21 days in water, 9 mths at 90%RH)

Time under pressure(dys)	1	2	3	4	5
Pressure(psi)	190	490	1025	1485	1910
Sample	Permeability 10^{-11} m/s				
1	3.06	2.47	2.10	2.24	1.81
K_p/K_{490}	1.24	1	0.85	0.91	0.73
2	-	9.32	8.38	8.22	7,40
K_p/K_{490}	-	1	0.90	0.88	0.79
3	1.92	1.98	1.45	-	1.36
K_p/K_{490}	0.97	1	0.73	-	0.69

TABLE 2.2a Range of applied pressures for steady state Permeability tests

Range	Applied pressure (psi)
1	2 - 25
2	90 - 250
3	800 - 1000
4	1700 - 2000

Specimens were tested in the ranges given in table 2.2b depending on w/c ratio and times of hydration.

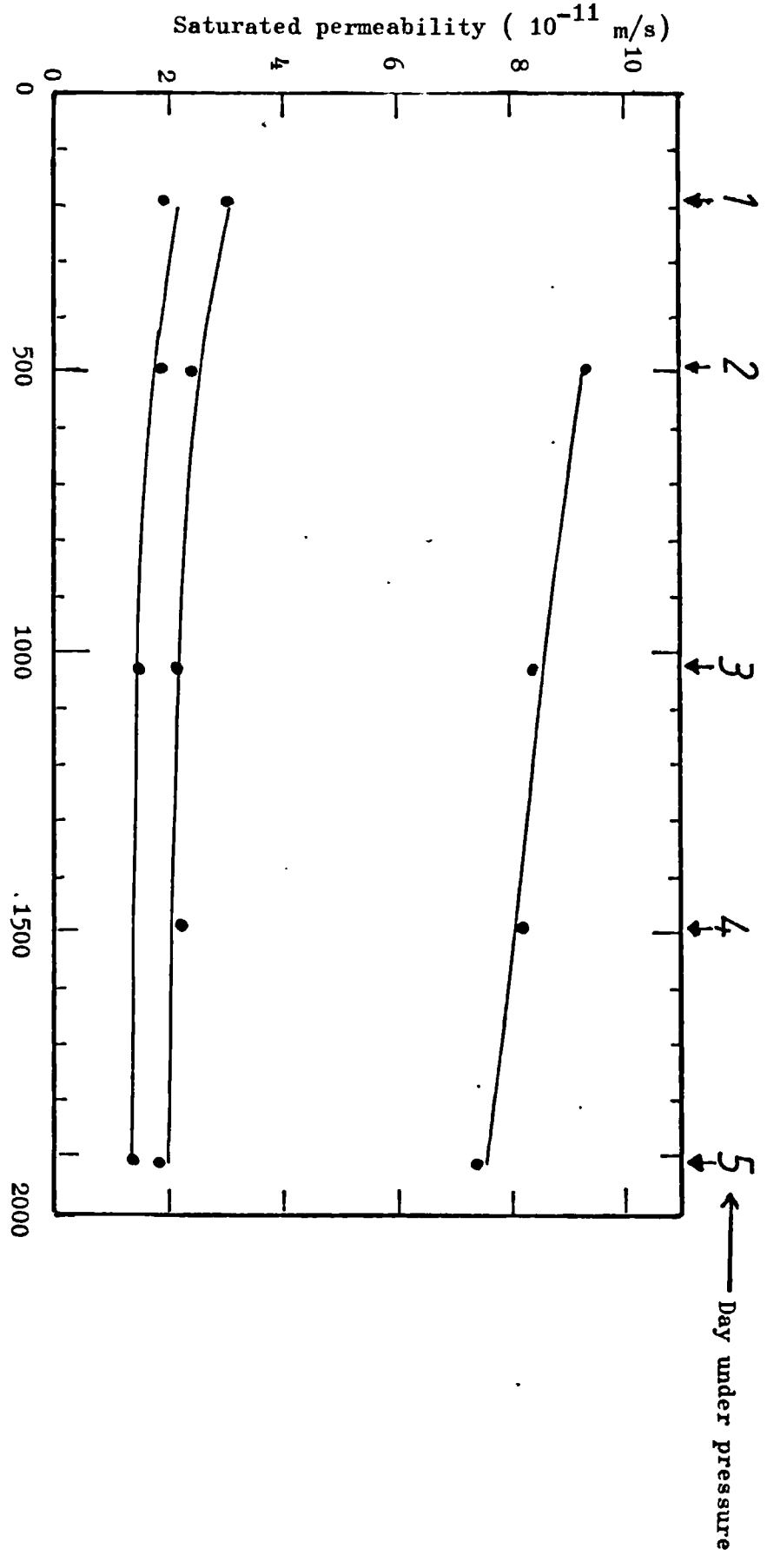

Fig 2.9b: Effect of applied pressure and time under pressure on permeability of hcp (w/c 0.65 21days cure)

TABLE 2.2b Ranges of applied pressures for test specimens

Time of hydration (days)	3	7	28	10m	20m
w/c	Range of applied pressure				
0.23	4	4	4	4	4
0.47	3	3/4	4	4	4
0.59	2	3	4	4	4
0.71	2	2	3/4	4	4
0.83	-	2	3/4	-	-
1.00	1	2	2	3	-

All mortar specimens were tested in range 4.
For samples designated 3 and 7 days, test samples were mounted on the 2nd and 6th days respectively. The measurements were made for output flow rates on the 3rd and 7th days respectively. For all other specimens, the samples were mounted on the actual specified day and maintained under pressure for a further 7 days to ensure that flow was occurring. Measurements of the actual flow rates were made from the seventh day till the output flow rates could be found to be steady to within two significant figures at the least. This would normally require a series of one to eight readings per sample per day for at least five days for most specimens. If steady state flow rates could not be found within this period, the test was discontinued because it was considered that the effects of specimen hydration would affect any later steady flow rates likely to be measured. In many cases, however, the lack of steady flow rates could be attributed to inadequate sealing of the specimens in the permeameters.

The reason for the initial seven day exposure of specimens to pressure prior to measurements is that is was found that during this period, either no flow rates could be measured for some samples or that the flow rates obtained were generally not sufficiently close to being steady.

Output flow rates were measured as described in section 2.4.3, and it was necessary to select the appropriate capillary flow tube to ensure that the rates of change in the level of the water meniscus did not exceed 1.5 cm/min. This value was found to be the maximum rate which could be reasonably measured. In most cases, however, the rate of change in the level of the meniscus in the 0.5 mm diameter capillary was less than 1 mm/min. Values of the order of $\simeq$ 1 μm/min were found for the lower w/c ratio pastes (less than 0.47) at range 4 applied pressure for samples which were only 10mm thick.

2.6.2 Measurements of pore size distributions and total porosities

The actual samples tested for steady state permeability as described in sections 2.3 and 2.6.1 were broken into fragements of approximately 1 gram with sharp blows from an archeological hammer at the conclusion of the permeability tests. The minute and fine particles of hardened cement paste on the fragments were washed off in a beaker of water. The fragments were surface dried with damp tissue paper, quickly weighed to an accuracy of 0.01g and dried in an oven at 105°C to constant weight. The drying period normally took at least 3 days.

The evaporable water contents, expressed as gram of water per gram of dry paste was determined from the measurements of weight loss on drying at 105°C. The dry densities of the batch of samples were determined from the apparent volume measured to 0.1cc accuracy using a mercury displacement volumeter shown on plate 2.7 (marked D). The total porosity was calculated from equation 2.8.

$$\varepsilon = W_{105}\, \rho_a\, \rho_w \qquad (2.8)$$

where

W_{105} = weight loss at 105°C (g/g dry paste)

ε = total porosity (cc/cc)

ρ_a = apparent dry density (g/cc)

ρ_w = density of water (1.0g/cc)

For the measurements of the pore size distributions of the pastes, a fragment from the batch between 0.5 - 2.0g was selected and weighed to an accuracy of 0.01g. The weighed fragment was then placed in a dilatometer, mounted on the filling device and evacuated for a minimum of 30 minutes using a speedivac single stage high vacuum pump. At the conclusion of the evacuation, the dilatometer was filled with mercury while under vacuum. It was found that air bubbles trapped in the tube linking the mercury reservoir to the dilatometer tended to be drawn by suction into the dilatometer at the initial stage of opening the mercury release valve on the filling device. To overcome this source of error, it was necessary to admit the mercury into the dilatometer in two stages. First, a few drops of mercury were admitted into the dilatometer until a slight kick of the pointer of the vacuum gauge could be observed, which indicated the release of the trapped air into the dilatometer. The mercury release valve was then closed and the dilatometer evacuated for a further five minutes before the final filling was done. The dilatometer was placed in the autoclave of the porosimeter, appropriately assembled, filled with alcohol and completely sealed for the start of the run. The digital voltmeter and the strip chart recorder were zeroed and calibrated to read the full scale pressure of 2000 kg/cm^2 before each run. The printing and plotting of the pressure-volume data is done automatically and each run required approximately 90 mins. to complete depending on the porosity of the sample and the delay timer setting.

It was necessary to correct for the compressibility of the mercury. A blank run performed without a sample in the 3mm bore dilatometer showed that the change in the volume of mercury was, to reasonable limits, directly proportional to the applied pressure and could be approximated by equation 2.9.

$$h_{Hg} = 0.0024\ P \qquad (2.9)$$

where

P = applied pressure (kg/cm^2)

h_{Hg} = correction for mercury compressibility (mm)

Equation 2.9 was used throughout the analysis of the pore size distributions to be described in section 2.8.2.

2.6.3 Helium flow procedure for measuring porosity

The porosity measurements made with the helium comparison pycnometer were to supplement the values obtained from drying at 105°C and were not intended to estimate the degree of collapse or reopening of interlayer spaces as the method has been applied in other investigations[50-52].

A weighed amount of the fragments described in the previous section of between 10 - 20g were placed in the sample cup and clamped into the sample compartment. Before clamping, the reference piston was brought to its far stop while the measuring cylinder piston was moved to indicate the instrument starting volume (105.5cc) on the digital readout. With the coupling and purge valves open, both cylinders were evacuated for 30 minutes. Helium was then admitted slowly into the cylinders until the pressure gauge connected to the vent valve indicated one atmosphere. The purge valve was closed after 10 secs was allowed for the gas within the cylinders to equilibriate to one atmosphere. The coupling valve was closed after 20 secs thus isolating the two cylinders.

The gas in both cylinders was then slowly and simultaneously compressed by rotating the handwheels, while maintaining the differential pressure indicator on the scale - a precaution necessary to avoid damage to the sensitive diaphragm. The compression was completed with the reference piston at its final stop position representing a swept volume of half the initial gas volume. The gas pressure in the reference cylinder was thus doubled to two atmospheres. At the conclusion of the compression, which takes about one minute, the measuring handwheel was rotated to bring the differential pressure indicator to the null position hence balancing the pressures in both cylinders at two atmospheres. The reading taken immediately after this first balance was used as the instantaneous solid volume of the sample, and is recorded within 30 secs after the balance. Prolonged exposure of the sample to helium results in the drift of the indicator due to the flow of helium into the sample, or leak of helium to the atmosphere or both. At suitable time intervals when significant changes in the position of the differential pressure indicator could be observed, the measuring handwheel was used to rebalance the pressures until the indicated solid volume approaches less than 0.01 cc/hr or begins to increase, which was not an unusual occurrence particularly after an overnight exposure.

To make allowance for reproducibility and leak corrections, a series of blank runs, i.e. without samples, and measurement of the volumes of steel balls of known volumes were made. The volumes of the steel balls were found to be reproducible to ± 0.02cc from a series of forty measurements using only the instantaneous solid volume readings. The blank runs also showed that the zero readings could vary between 0.11 ± 0.02cc; therefore all indicated solid volumes were corrected for zero readings by subtracting 0.11cc.

A series of prolonged runs performed on the steel balls of known volumes of 8.53 and 28.96 cc showed the leak features presented on Fig 2.10. It can be seen that the amount of leak tends to increase with the volume of the sample. The leak up to 10 hours was virtually the same for the blank run and the two steel balls, but significant differences result beyond 10 hours. It was therefore assumed that the leak depends on the position of the piston hence the volumes of the pastes were maintained within 12cc to enable the leak curve for the 8.53 cc steel ball to be used in correcting the indicated solid volumes. Hence the full correction for zero and leak was obtained by using equation 2.10.

$$V_{lz} = V_i - (V_z + V_l) \qquad (2.10)$$

where,

V_{lz} = corrected indicated volume

V_i = indicated volume

V_z = zero correction factor = 0.11cc

V_l = leak correction for 8.53cc steel ball (from fig 2.10

Typically for an indicated volume of 8cc at 40 hours exposure to helium, the corrected volume would be

$$8 - (0.11 + 0.18) * 7.71$$

which represents approximately 4% of the indicated solid volume and perhaps an insignificant difference provided the indicated solid volume monotonically reduced with time of exposure rather than increased as found in some cases.

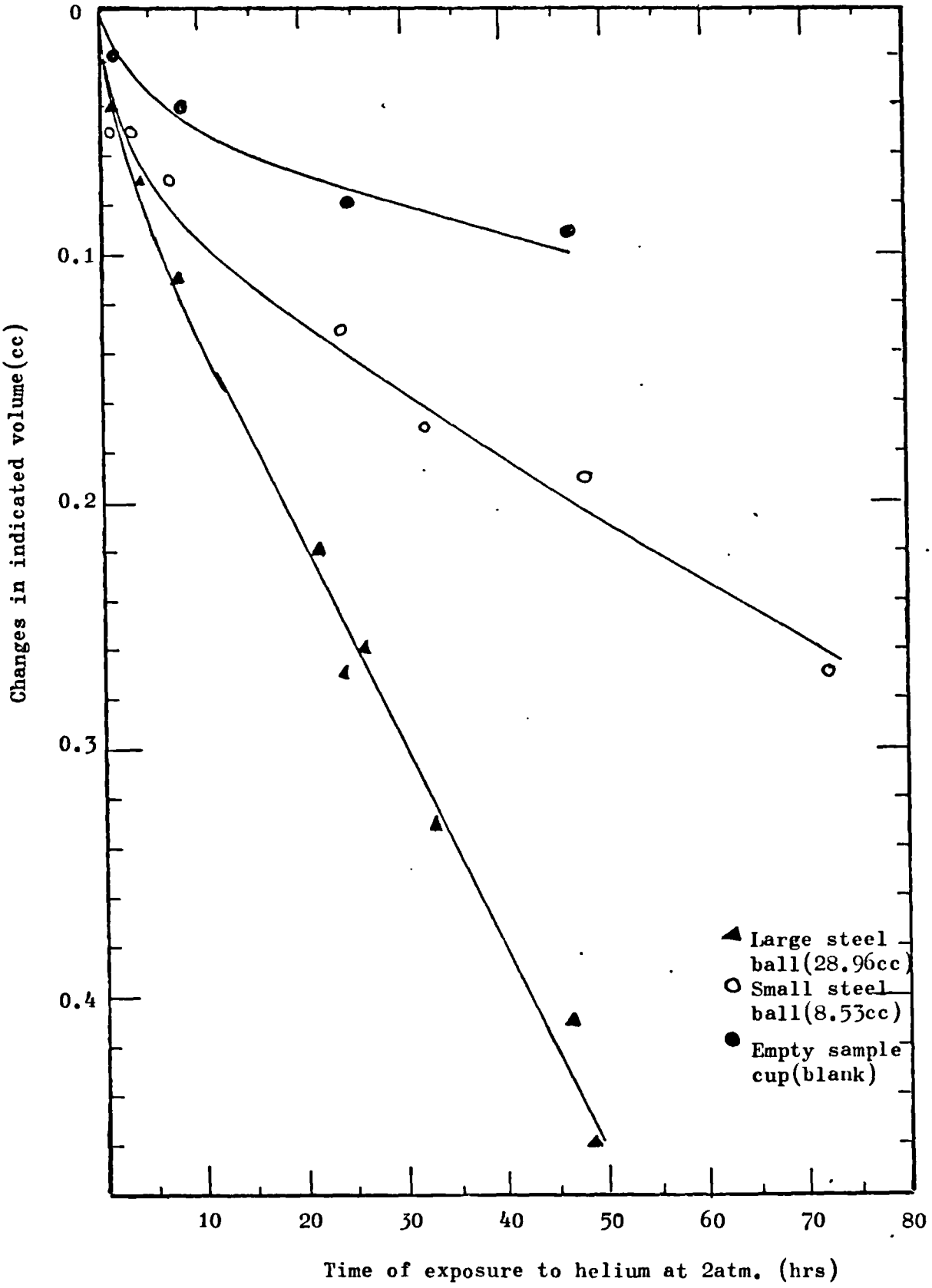

Fig. 2.10: The leak curves for the different steel balls for the helium comparison pycnometer.

2.6.4 Effect of moisture content on helium flow measurement of porosity.

Total porosity of hardened cement pastes is conventionally determined from the evaporable moisture contents at standard drying conditions, such as heating to 105°C or drying to a vapour pressure corresponding to 0.5 Hg at 23°C. It is usual to assume that the specific volume of the evaporable water is the same as free water i.e. 1.00cc/g. It is possible that this assumption may not be wholly appropriate as the water within the hydrates of hardened cement paste may be bound with different degrees of physical and chemical bonding forces in the different ranges of relative vapour pressures. The specific volume of the first 5.25% of water removed from pastes previously dried to 11% relative humidity for pastes have been estimated to be as low as 0.7886 - cc/g.[44,52] The preliminary experiments to be described were conducted to study.

(1) the nature of helium inflow into samples of different moisture contents.

(2) the evaluation of the densities of evaporable water in the range of relative humidities from 0% to 90%.

(3) the advantages of adopting the helium flow procedure in measuring porosity over conventional standard drying techniques.

Cylindrical specimens (diameter 2.54cm, w/c = 0.47 cured in water for 60 days) were sliced to thicknesses of between 0.5 to 0.6mm using a low speed diamond saw and ensuring that the specimens were kept continuously wet throughout. The disc specimens were grouped into six batches of approximately 20g per batch. The initial surface dry weights were measured on a chemical balance. The samples were transferred to six separate dessicators containing saturated salt solutions corresponding to relative humidities of 11,33,43,57,75 and 90% respectively at room temperature of 22°C. The desiccators were evacuated and the specimens allowed to dry to equilibrium weights at the respective humidities. The weights of the samples were periodically measured. A minimum of 21 days was necessary for equilibrium weights to be reached. The drying curves are shown on Fig 2.11. It can be seen that a substantial amount of the moisture loss for all the samples at the different relative humidities occured within the first 2 days of exposure and as expected more moisture is lost at lower humidities.

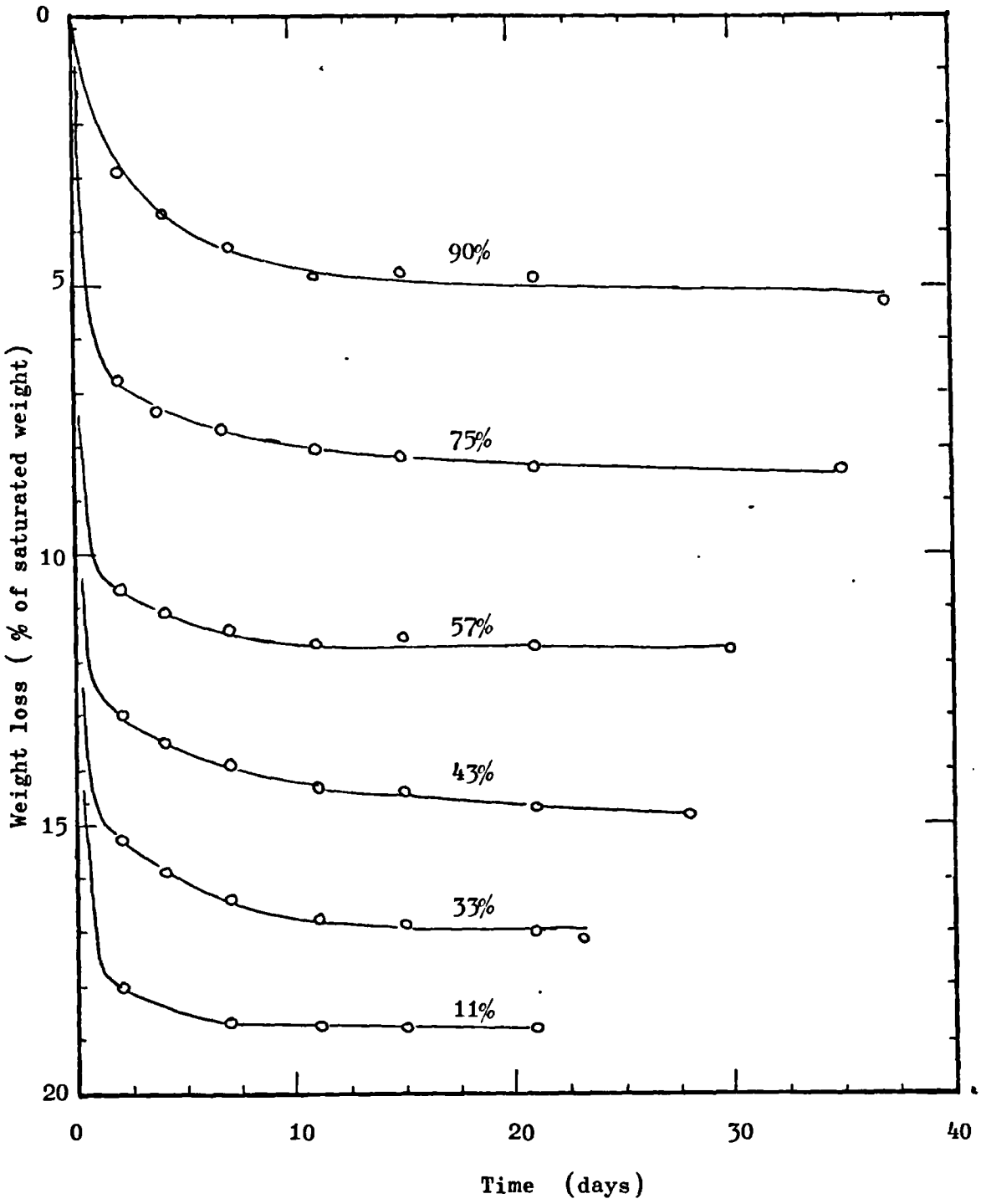

Fig 2.11: Drying curves for hardened cement paste samples conditioned at different relative humidities.

The helium flow runs were made on each of the six batches of samples at the equilibrium moisture contents reached on drying. The samples conditioned at 11% relative humidity were further dried to a state corresponding to the d-dried state (0% RH) by continously evacuating through a dry ice trap at - 78°C and by applying a vacuum of 0.005 torr for five days. The helium flow runs were performed for the d-dried pastes after transferring the samples to the sample cup in a moisture and carbon dioxide free glove box.

The curves for the observed amounts of helium flow into the samples of different moisture contents as a function of the time of exposure to helium at two atmospheres are given on fig 2.12 a. The vertical axis represents the change in the indicated solid volume per kg of sample. It can be seen that the indicated solid volume reduces with time for samples conditioned to 33% RH and lower relative humidities, whereas the indicated solid volume increases initially for samples conditioned to humidities above 33%. This initial increase is considered to be due to an increase in the vapour pressure of the sample cup on isolating the measuring and the reference cylinders because of loss of moisture from the moist specimens. After the initial increase in indicated solid volumes for the moist samples there is a reduction probably due to either the flow of helium into the pores of the sample or leak. Fig 2.12b represents the correction of the helium flow curve for leak using the leak curve for the 8.53 cc steel ball (fig 2.10). It can be seen that when the leak correction is applied, there is virtually no change in the indicated solid volumes after the initial rise for the moist samples (43% RH and greater). The sample at 33% RH indicates no substantial change in the indicated solid volume up to 40 hours exposure, whereas the 11% RH and d-dried pastes indicate large reductions in indicated solid volumes in the first 5 hours of exposure to helium. Since it is physically impossible for the indicated solid volumes of samples to rise after exposure to helium, the instantaneous solid volumes for the moist samples were used in the calculation of porosity after subtracting the zero error reading of 0.11cc. For the samples conditioned to relative humidities below 43% RH, which showed a reduction in indicated solid volume with time, the final 40 hr indicated solid volumes were used for calculating porosity after correcting for zero and leak as outlined in section 2.6.3.

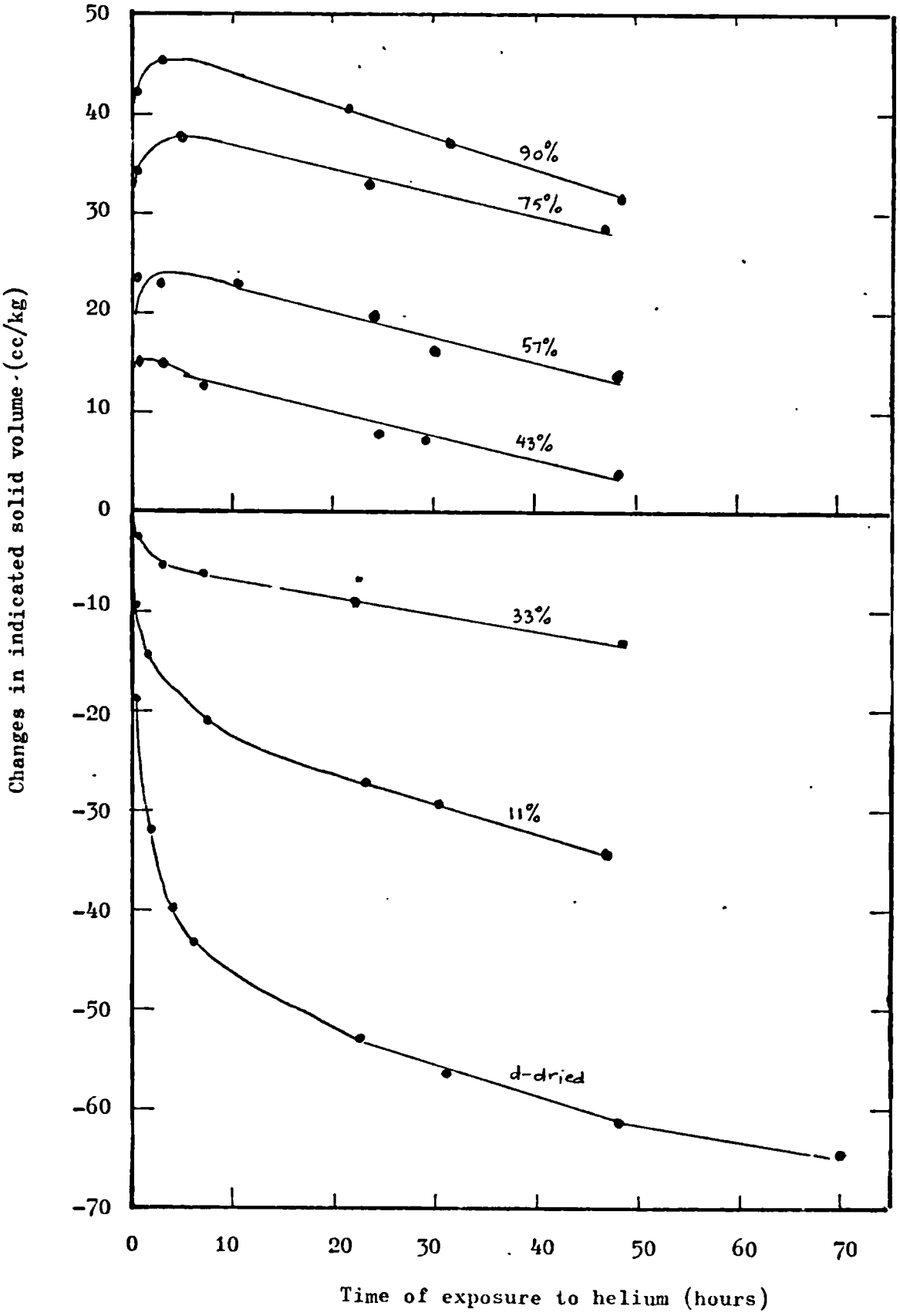

Fig 2.12a: The helium flow curves for samples conditioned at different

The apparent volumes of the samples were determined by taking several measurements of the thicknesses of the discs. The weights of the samples before and after the helium flow runs were measured to find the weight_loss during the helium flow measurements.

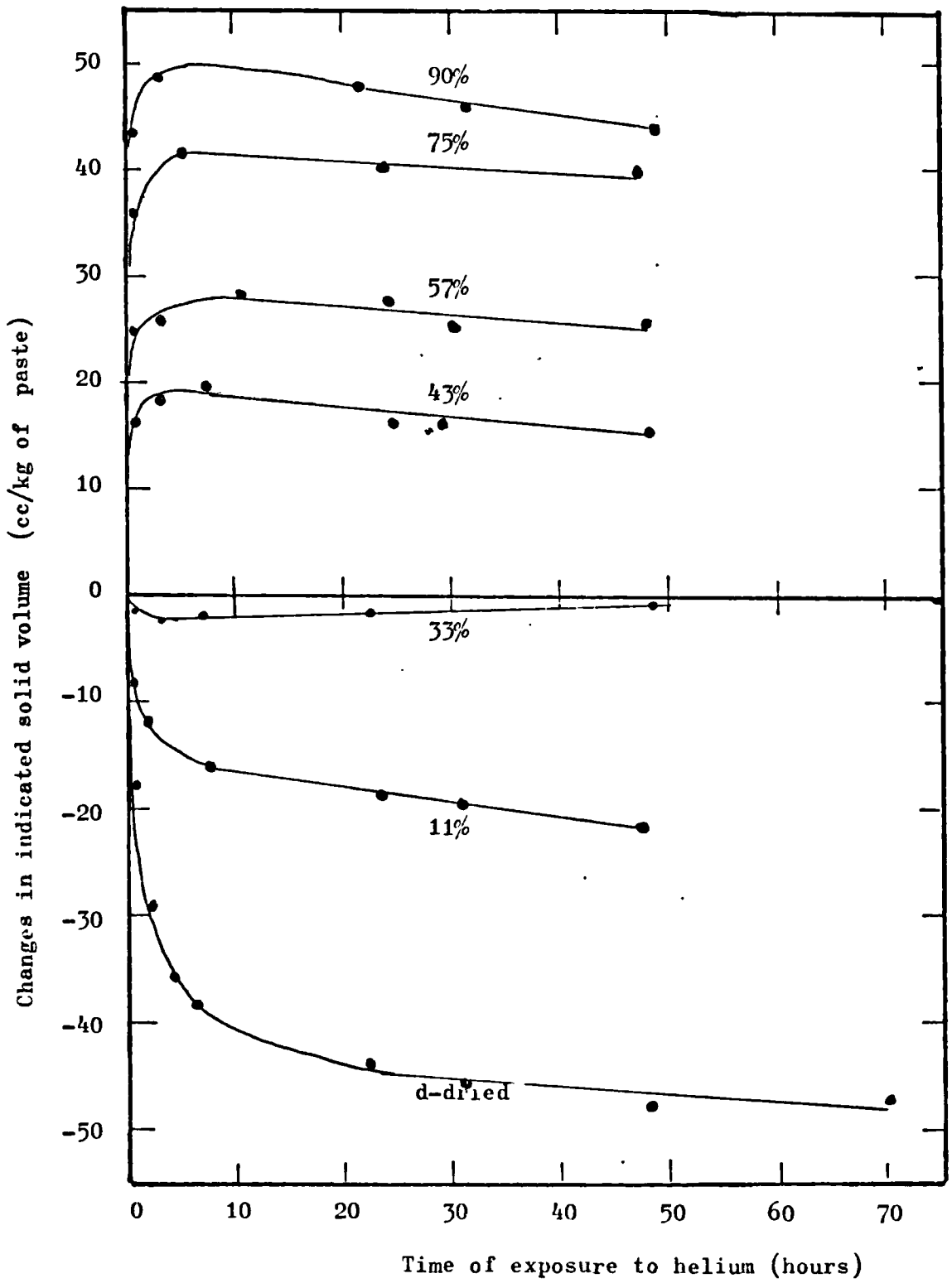

Fig 2.12b: The helium flow curves for samples conditioned at different relative humidities(with leak corrections applied)

The results for the changes in weight during the runs are presented in table 2.3 column 6. It can be seen that the weight losses were less than ± 2% of the initial weights prior to a run, hence it is concluded that no significant changes in the moisture contents of the samples occurred during the exposure to helium.

The percentage weight loss from saturation to equilibrium weight at each RH are shown in column 2 of Table 2.3. The desorption isotherm for the data is illustrated on Fig 2.13. From the isotherm, there is no obvious reason why the total porosity should be measured at 11% RH instead of the d-dried state (0%RH). It is however noted that the knee produced between 33% RH and 0% RH could be associated with a different type of water loss in comparison with that lost above 33% RH.

The total porosities calculated from the evaporable water (assuming density of 1.00g/cc) are given in column 3 of table 2.3. The instantaneous porosities obtained from the instantateous indicated solid volumes are presented in column 4 of Table 2.3. It can be seen that the instantaneous porosities tend to be greater than that from the evaporable water calculation at RH above 33% but below this RH, the instantaneous porosities are less than that from the evaporable water contents. The reasons for this could be that

(1) At low RH, the helium penetration is incomplete (this is shown in fig 2.12a)

(2) At high RH, the instantaneous indicated solid volumes are unreliable because of possible vapour pressure development in the sample cup. This is explained by the increase in indicated solid volumes with time (fig 2.12a

The porosities calculated from the indicated solid volumes at 40 hours exposure to helium are given in column 5 of table 2.3. Leak and zero correction were applied to the solid volumes before calculation (see section 2.6.3) for samples dried to 33% RH and below, otherwise, only zero correction were applied, as previously explained. The results indicate that the total porosities at low RH (below 33%) are closer to those from the evaporable water loss calculation (col 3) than at higher RH. A comparison is made for the porosities at different RH by the two methods in Fig 2.14 and it can be seen that the best agreement between the porosities occur at d-dried (0%) and 33% RH. Again, it is concluded that there is no obvious reason why the porosities should be measured at 11% RH instead of 0% (d-dried) or 33% RH.

TABLE 2.3 Pore volumes measured by helium penetration as a function of moisture contents of hcp

			Pore volumes (cc/cc of pastes)				
RH %	wt loss from saturation % of wet wt	Evaporable water	Instantaneous	Corrected for leak and zero reading	wt loss after rest (%)	Estimated density of pore water g/cc	Ps g/cc
d-d	23.6	44.4	36.9	44.6	0.2	1.46	1.88
11	18.8	35.3	34.5	38.9	0.1	0.52	1.88
33	17.0	31.9	32.3	33.3	- 0.3	1.57	1.87
43	14.9	27.8	30.6	31.6	- 0.4	1.26	1.88
57	11.7	22.0	25.6	26.6	- 0.6	1.39	1.88
75	8.4	15.7	21.7	22.7	- 1.0	1.35	1.86
90	5.3	9.8	18.1	19.2	- 1.4		1.85
Col.	1	2	3	4	5	6	7	8

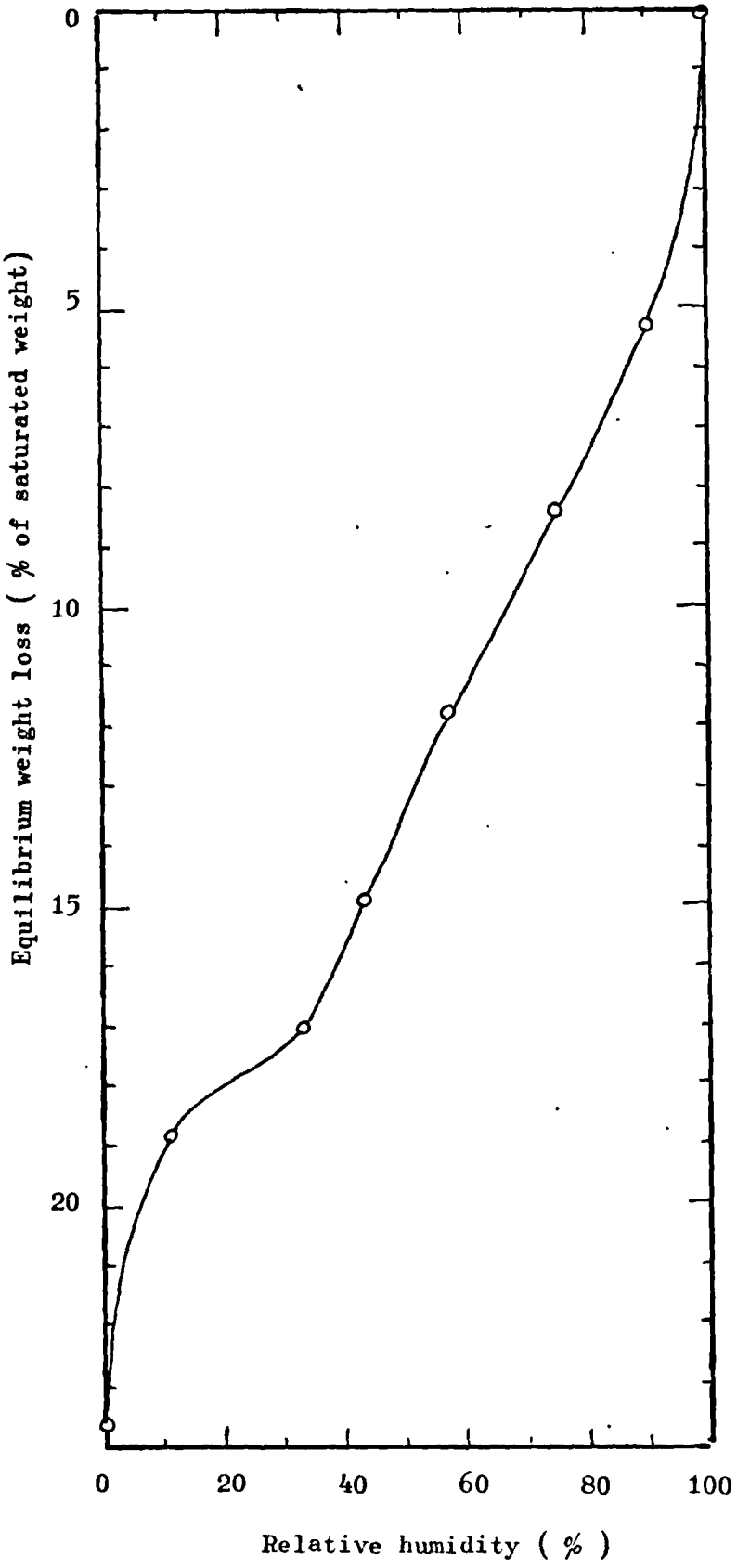

Fig 2.13: Desorption isotherm for hcp (w/c ratio 0.47 at 2mnths)

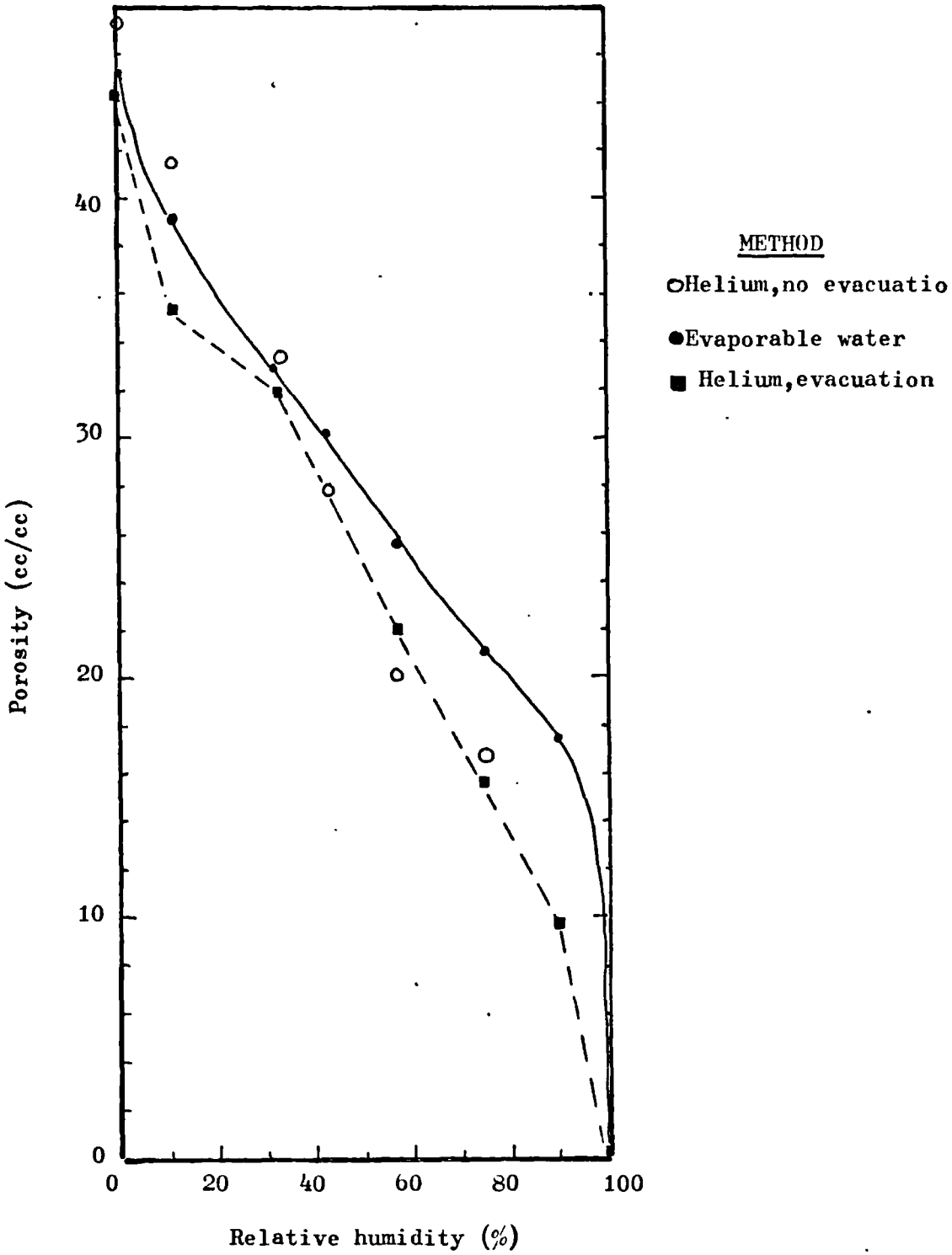

Fig 2.14: Porosity as a function of relative humidity at which samples were conditioned to equilibrium moisture contents.

Fig 2.15, illustrates the relationship between the weight loss on drying to equilibrium, the measured total porosity (col 5, table - 2.3) and the porosity calculated from the evaporable water loss (col.3 table 2.3). The results indicate that for a given weight loss, the porosity measured by helium is consistently greater than that from the evaporable water contents. To estimate the density of pore water from the porosity-weight loss curve for the helium flow method, it can be assumed that for a weight loss, ΔW corresponding to a porosity change of $\Delta \varepsilon$ between successive RH conditions is given by

$$\frac{\Delta W}{\Delta \varepsilon} = \frac{W_{pw}}{W_s} \Big/ \frac{V_{pw}}{V_a} = \frac{W_{pw}}{V_{pw}} \cdot \frac{V_a}{W_s} = \rho_{pw}/\rho_s$$

where

W_{pw} = weight of pore water lost on drying

W_s = saturated weight of sample

V_{pw} = volume of pore space vacated by water

Va = apparent volume of sample.

ρ_{pw} = density of pore water.

ρ_s = saturated density of sample.

The results of the values of the pore water densities calculated for successive changes in moisture contents at each stage of drying are presented in column 7, table 2.3. The saturated density of the pastes were to determined from the surface dry weights and the apparent volumes and found to be 1.86 $\pm$ 0.2g/cc (col 8 table 2.3). The density values for the pore water estimated by the foregoing method can be seen to be greater than 1.2 g/cc at all the ranges of relative humidity with the exception of 33%-11% where the value is unreasonably below that of free water (row 2 column 7). The pore water density in the high humidity range would be expected to be closer to that of free water than at low humidities but it appears that this is not the case. It is therefore concluded that this method of estimating pore water density is unreliable. The reasons could be due to

(1) Pore space vacated by water reduces in volume

(2) Pore space vacated by water is not completely filled with helium

(3) The accuracy of the instrument is inadequate for measuring pore water density.

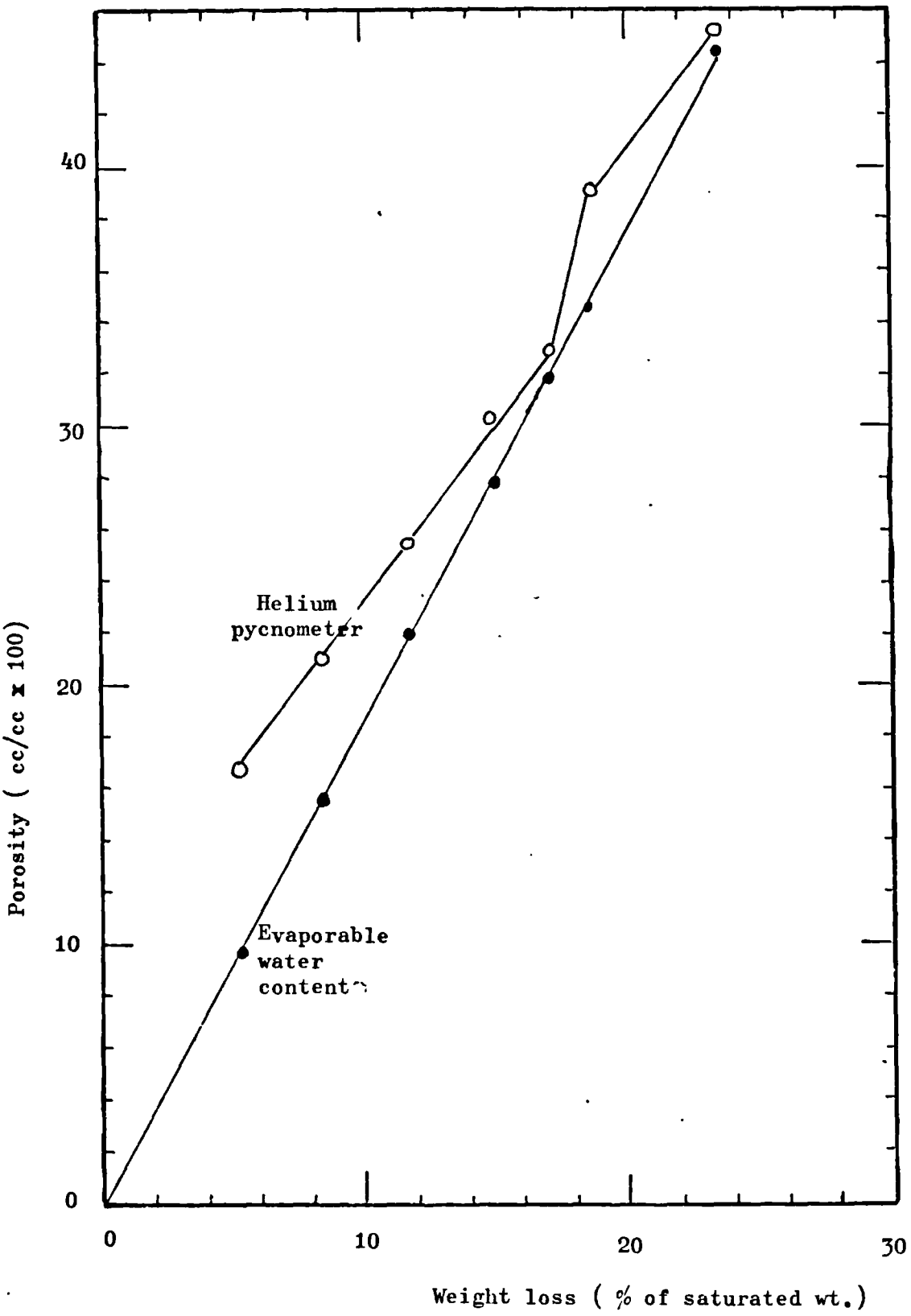

Fig 2.15: Porosity as a function of drying weight loss

The final decision from these tests was therefore to supplement the porosity measurements by simple oven-drying with helium penetration.

2.7 Analysis of results

The numerical treatments of the permeability and pore structure data obtained from the measurements are given in this section with the reasons for adopting any particular form of analysis.

2.7.1 Calculation of permeability coefficients

The length (l_s), and the two end diameters (d_1 and d_2) of each sample were measured with a vernier caliper. The coefficient of permeability was calculated by assuming that the slight taper of the specimen did not complicate the calculation based on cylinder of diameter $\frac{1}{2}(d_1 + d_2)$. The reason for this decision can be found from the following theoretical and experimental considerations.

Let us assume that the equivalent cylinder required to have the same permeability as a tapered specimen of length, l_s and large end radius R_o is of length l_s and radius R_1. This is shown on fig 2.15b

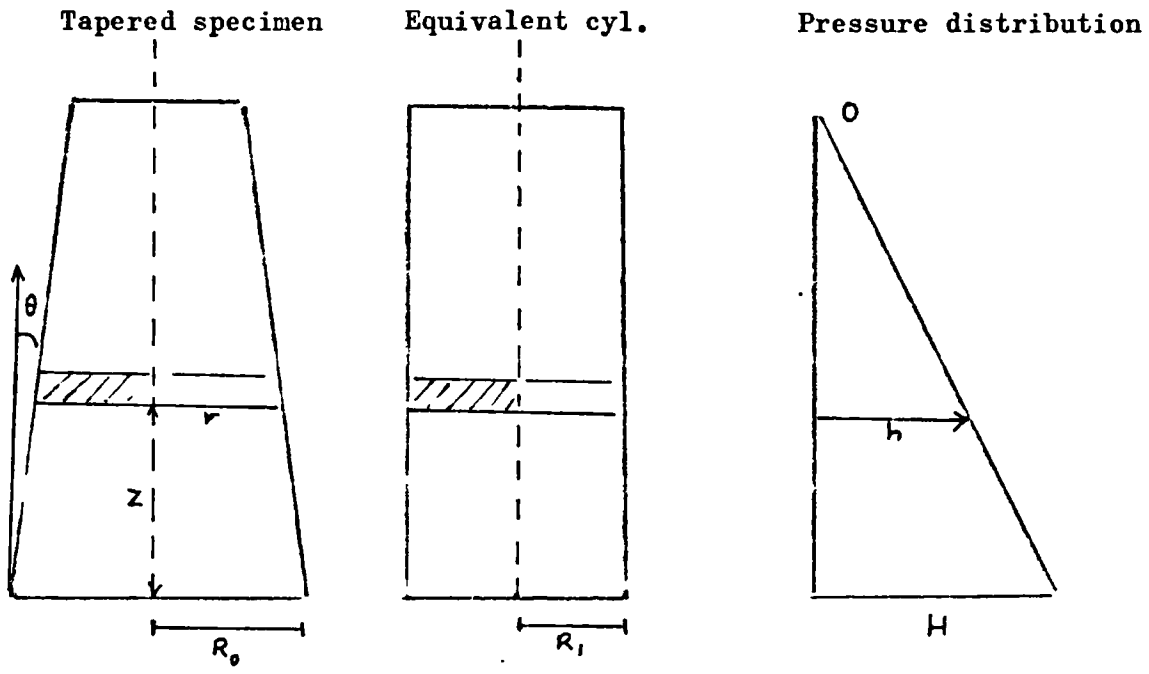

Fig 2.15b The equivalent cylindrical specimen of a tapered specimen.

Assuming that the flow is completly saturated and steady, then the Darcy equation for an element of material at a position z from the large end of the tapered specimen and of radius r is given by

$$Q_z/\pi r^2 = -K_T (dh/dz)_z \qquad (2.11)$$

where Q_z = flow through the element at z

K_T = permeability of the element

$(dh/dz)_z$ = hydraulic gradient across the element

For an angle of taper θ in the direction shown on fig 2.15, the radius of the element can be related to the large end radius by

$$r = R_o - z \tan \theta \qquad (2.12)$$

hence $$dz = - dr/ \tan \theta \qquad (2.13)$$

where R_o = radius of large end of tapered sample Replacing dz in equation 2.11 using the relationship of eq. 2.13 rearranging and integrating gives

$$-Q_z/\pi \tan \theta \int_{R_o}^{R_o - z\tan\theta} dr/r^2 = -K_T \int_H^h dh \qquad (2.14)$$

where Q_z and K_T are assumed to be constants along the length of the sample.

On evaluating the integrals of eq. 2.14 the permeability of the specimen of length z is given by

$$K_T = Q_z/\pi (H-h)R_o^2 \; (z/ (1 - z \tan \theta/ R_o)) \qquad (2.15)$$

For an equivalent cylinder of radius R_1 the permeability coefficient for the same flow rate Q_z is given by

$$K_c = Q_z \, z/(\pi R_1^2 (H - h)) \qquad (2.16)$$

If the permeability of the cylindrical specimen, K_c, is to be the same as the tapered specimen K_T, then comparing equations 2.15 and 2.16 gives

$$R_1^2 = R_o^2 (1 - z \tan \theta/R_o) . \qquad (2.17)$$

But ztan θ is the difference between the large end radius and the radius at position z_1 ie. the amount of taper, ΔR_o hence equation 2.17 can be written in terms of the only the radii of the tapered specimen and the equivalent cylinder as

$$R_1 = R_o (1 - \Delta R_o/R_o)^{\frac{1}{2}} \qquad (2.18)$$

where R_1 = radius of the cylinder equivalent to the tapered specimen

R_o = radius of the large end of the tapered specimen

ΔR_o = difference between the radius of the small and large ends of the tapered specimen.

The average radius of the tapered specimen can be written as

$$R_a = R_o (1 - \Delta R_o/2R_o) \qquad (2.19)$$

hence the average radius of the tapered specimen is related to the radius of the equivalent cylinder by

$$R_a/R_1 = (1 - \Delta R_o/2R_o) / (1 - \Delta R_o/R_o)^{\frac{1}{2}} \qquad (2.20)$$

and since for a given flow rate, the calculated permeability is inversely proportional to the square of the radius of the specimen (eq. 2.16), the ratio of the permeability calculated assuming an average radius to that assuming the equivalent radius is given by

$$K_a/K_T = (1 - \Delta R_o/R_o) / (1 - \Delta R_o/2R_o)^2 \qquad (2.21)$$

The typical ratios given by equation 2.21 assuming that the large end radius of the tapered specimen is 15mm are given in table 2.4 for different lengths of the tapered sample used in the tests in this work.

TABLE 2.4 Ratios of the true permeability of a tapered specimen to that of a cylinder with the mean radius of the tapered specimen

R_o = 15mm

length (mm)	taper ΔR_o (mm)	R_1/R_a	K_T/K_a
70	5	0.833	1.440
56	4	0.867	1.331
42	3	0.900	1.235
28	2	0.933	1.148
14	1	0.967	1.070
7	0.5	0.983	1.034

It can be seen from table 2.4 that if the large end diameter is kept constant and the length of the sample varied, the maximum difference between the permeability calculated using the average radius of the tapered specimen instead of the equivalent radius deduced from the theoretical considerations is of the order of 44% at full specimen length of 70 mm and the error reduces progressively to less than 10% at a length of 14mm. In the actual tests, the lengths of the specimens were within 10-20mm and the radii of the smaller ends were typically 11mm. For a typical 20mm long sample with large end diameter of 12mm hence a taper of 1mm, the theoretical ratio of the permeability calculated using the equivalent and average radius is given by

$$K_T/K_a = (1 - 1/24)^2/(1 - 1/12) = 1.002 \quad - (2.22)$$

indicating a difference of less than 1%. The theoretical analysis assumed constant permeability along the length of the specimens. It has been indicated in section 2.3 (fig 2.1) that porosity gradients develop along the lengths of the specimens, which might invalidate the assumption of constant permeability along the length of the specimen. Pastes were tested with different lengths to study the effect of the length of the specimens on permeability. Table 2.5 is presented to indicate the measured dimensions of the specimens, and the permeability coefficients calculated with the average radius are also compared with that using the equivalent radius.

TABLE 2.5 Effect of length of specimen on permeability

Sample	Length (mm)	$2R_o$	ΔR_o	K_a m/s	K_T/K_a
1.0/7d	26.5	26	1.5	0.99	1.004
	30	26	1.5	1.07	1.004
	31	26	2.0	1.11	1.007
	32	27	2.0	1.17	1.006
	34	28	2.5	1.31	1.010
	34	28	2.5	1.06	1.010
	40	28	2.3	1.43 $\times 10^{-8}$	1.008
0.59/7d					
	20	27	1.0	1.20	1.001
	20	27	1.0	1.18	1.001
	20	27	1.0	1.52	1.001
	21	27	1.0	1.26 $\times 10^{-11}$	1.001

It can be seen that the two methods of calculation (col.5) give permeability ratios not exceeding 1.01 for both cases. There is, however, a trend of increasing ratio of K_T/K_a with increasing length of sample for the 1.0/7 day paste but the differences are not substantial when compared with the possible errors involved in measuring the exact diameters of the specimens. It was decided in any case, to cut the specimens to lengths between 10mm and 20mm and to use the average radius in calculating the coefficient of permeability. It was considered that if larger and longer specimens were to be used, the effect of the taper could affect the scatter of permeability results regardless of the method adopted for calculating permeability.

The equation used for all the calculations of permeability was therefore

$$K = 2.3708 \times 10^{-7} \frac{l_s \, v_c \, C_d^2}{d_a \quad P} \quad m/s \qquad (2.23)$$

where,

l_s = length of specimen (mm)
d_a = average diameter of specimen (mm)
v_c = steady state flow velocity in capillary tube (cm/s)
P = applied pressure (psi)
K = sample permeability coefficient (m/s)
C_d = diameter of capillary tube (mm)

The constant in equation 2.23 allows for the mixed but practically relevant units of the parameters defined above.

2.7.2 Analysis of pore size distributions

As outlined in the review, it was necessary in this investigation to obtain a simple definition of the threshold diameters found from the pore size distributions by mercury intrusion porosimetry. The total volume of mercury intruded was therefore divided into 40 equal volumes and the pressures at which each volume step intrudes the sample were found from the pressure-volume data. This method of analysis enables a greater resolution of the differential pore size distributions to be found at the pore sizes at which a substantial amount of mercury flows into samples. Typical plots of the pressure-volume data are given on figs 2.16 and 2.17 as obtained directly from the strip chart recorder. The vertical axis represents the volume penetrated and the horizontal axis, the pressure at which penetration occurs. The pressure scales have two ranges; 0-200kg/cm^2 on the lower portion of the plot and 200-2000 kg/cm^2 on the upper portion of the plot. The threshold regions on the plots are marked T.R. These regions correspond approximately to the initial inflections of the pressure-volume functions. Clearly to obtain a smooth curve from the data either equal pressure or equal volume steps can be used but since the threshold diameter can only be calculated from the pressure, the use of equal pressure steps would tend to fix a position for the threshold diameter rather than making it follow the natural position of the inflection. The point of inflection corresponds to the maximum slope of the pressure-volume curve and is used here to define the threshold diameter to be described later.

2.7.2.1 Cumulative pore size distribution

The principle of the measurement of pore sizes by mercury intrusion is based on the Washburn equation for cylindrical pores, which summarily states that the pore radius is inversely proportional to the applied pressure, thus

$$r = -2\gamma \cos\theta / P \qquad (2.24)$$

where

γ = surface tension of mercury

r = pore radius

p = applied pressure

θ = contact angle between mercury and the solid surface.

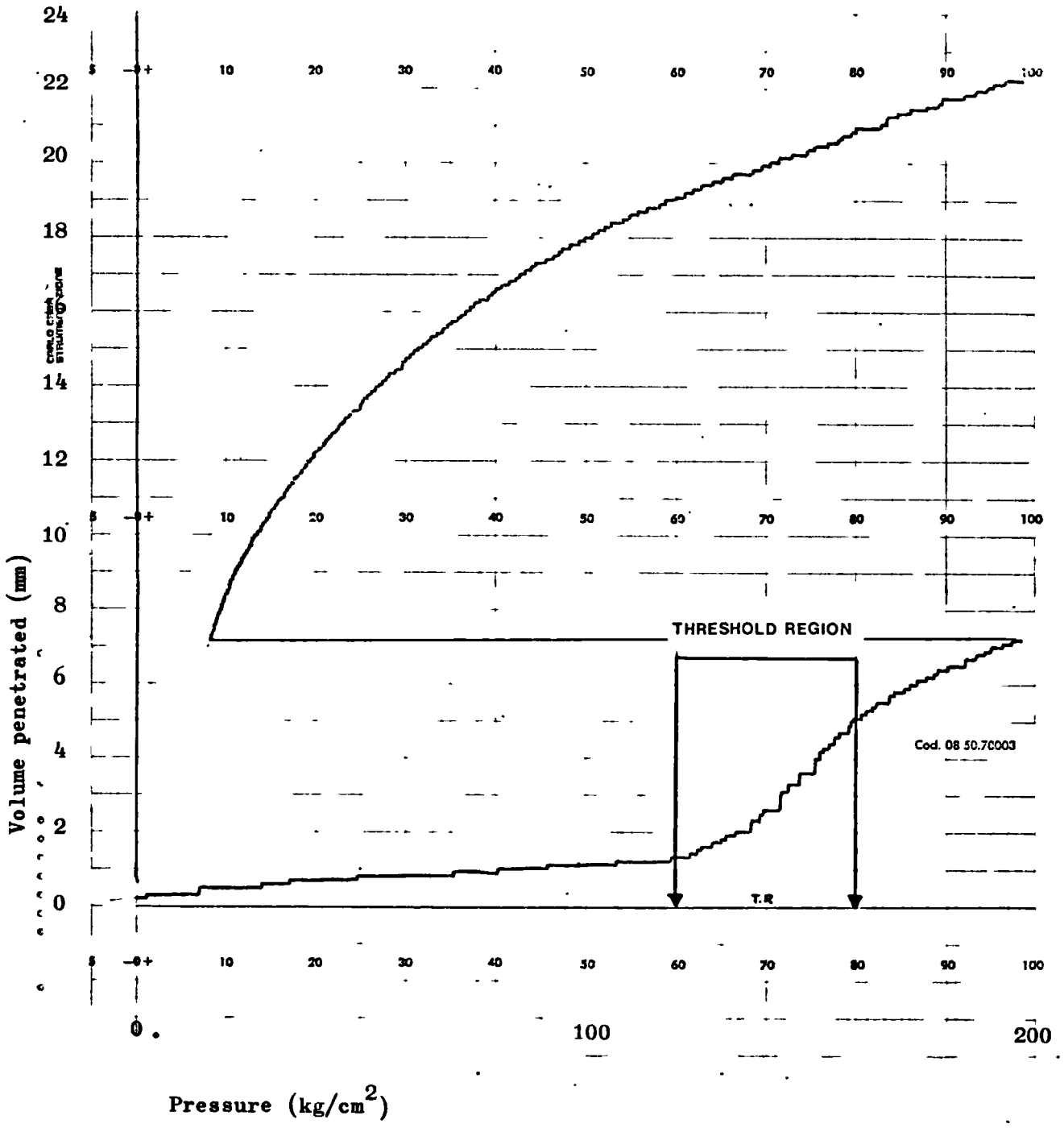

Fig 2.16: A typical pressure-volume plot from strip chart recorder. (x 0.2) hcp w/c 0.35,7days hydrated, weight = 0.92g

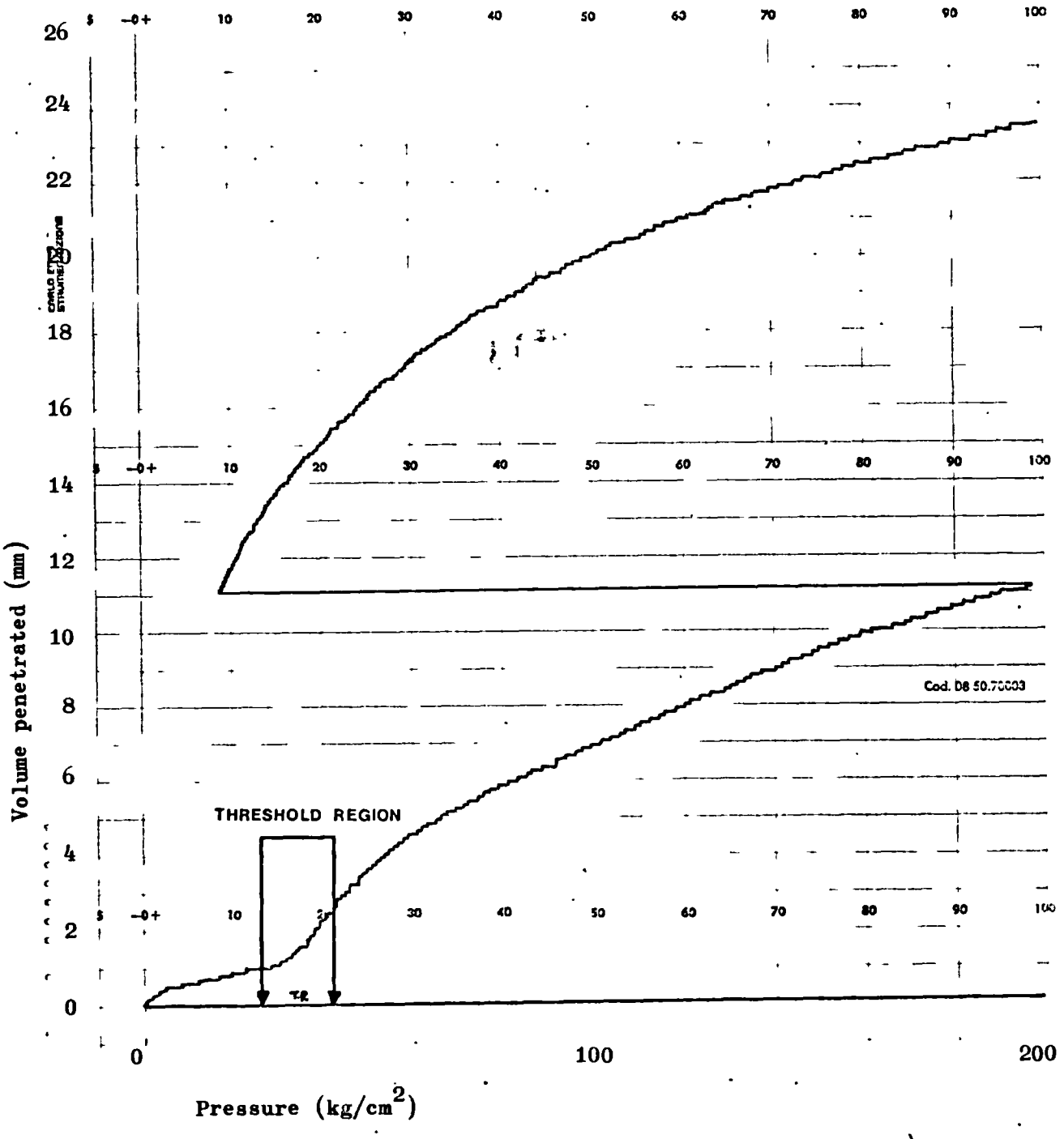

Fig 2.17: A typical pressure-volume plot from strip chart recoder. (x 0.2) hcp w/c 0.47, 7days hydrated, weight 0.58g

The relationship between the pore volume, V_p, intruded below a given pore radius (r), is the cumulative pore volume distribution, which in principle, is a transformation of the pressure-volume curves (figs 2.16 and 2.17) to a reciprocal pressure-volume curve. The pore radius was calculated from equation 2.24 for any tallied pressure corresponding to equal volume penetration steps by assuming the surface tension of mercury to be 0.48 N/m and a contact angle of 140^{o}. On substitution of these values in equation 2.24 and converting pressure from kg/cm^2 to N/m^2 by multiplying by the factor 9.7838×10^4 gives

$$r = 75\ 165\ /P \qquad (2.25)$$

where r is directly in Angstrom units. A further simplification was made by using a rounded down constant of 75 000 in equation 2.25. Contact angle of oven dried pastes has been measured and found to be 117^{o} in reference 28, and if this value is used, the pore radii would have to be multiplied by 0.58 to facilitate direct comparison. It is not certain whether the contact angle for mercury varies with pressure, hence the numerical values of pore radii can only be regarded as relative rather than absolute. The volume of mercury per gram of sample penetrating the specimens at a given pressure was corrected for the compressibility of mercury using equation 2.9, hence

$$\mathcal{E}_c(P) = \frac{A_d}{W_s} (H(P) - 0.00024\ P) \qquad (2.26)$$

where

$\mathcal{E}_c(P)$ = pore volume penetrating sample at pressure P corrected for mercury compressibility (cc/g)

A_d = cross sectional area of dilatometer (cm^2)

W_s = weight of sample (g)

$H(P)$ = total change in level of mercury in dilatometer (cm) at a pressure P

P = applied pressure (kg/cm^2)

The total intruded pore volume is found at 2000 kg/cm^2, the maximum applied pressure. The cumulative distribution is given as the difference between the total intruded pore volume and the pore volume intruded at given pressure as a function of log r.

A typical plot of a cumulative pore size distribution is given on fig 2.18 where the threshold region is marked. Again, these regions represent the initial inflections on the plot and approximately show the ranges of pore sizes likely to include the threshold diameter. Further definitions of other parameters of the distributions will be given in the next section.

2.7.2.2 Differential pore size distributions

The differential pore size distributions were plotted using the method suggested by Orr[74]. On this basis, for a given pore volume, dV, residing in pores of radii between r and r+dr, the distribution function is given by

$$dV = M(r)\, dr \qquad (2.28)$$

Differentiating the Washburn equation (2.24) with respect to pressure and pore radius, gives (on assuming that the contact angle and surface tension of mercury are constant)

$$P\, dr + r\, dP = 0 \qquad (2.29)$$

Combining equations 2.29 and 2.28 gives

$$M(r) = \frac{P}{r}\frac{dV}{dP} = \frac{dV}{dr} \qquad (2.30)$$

where

M(r) = frequency of pores of radius r on an equal radius interval distribution curve.

V = pore volume

r = pore radius.

P = applied pressure.

Because there is a wide range of pore sizes in hardened cement paste, it is convenient to plot the distributions on logarithmic pore radius basis, hence the frequency function must be transformed from an equal radius basis to an equal logarithmic pore radius basis. Using the identity

$$d\log r = 2.303\, dr/r \qquad (2.31)$$

dV/dr can be transformed to dV/dlogr by multiplying equation 2.30 by r/2.303.

Hence,

$$M(r)\frac{r}{2.303} = M^*(r) = \frac{P}{2.303}\frac{dV}{dP} = \frac{dV}{d\ \log r} \qquad (2.32)$$

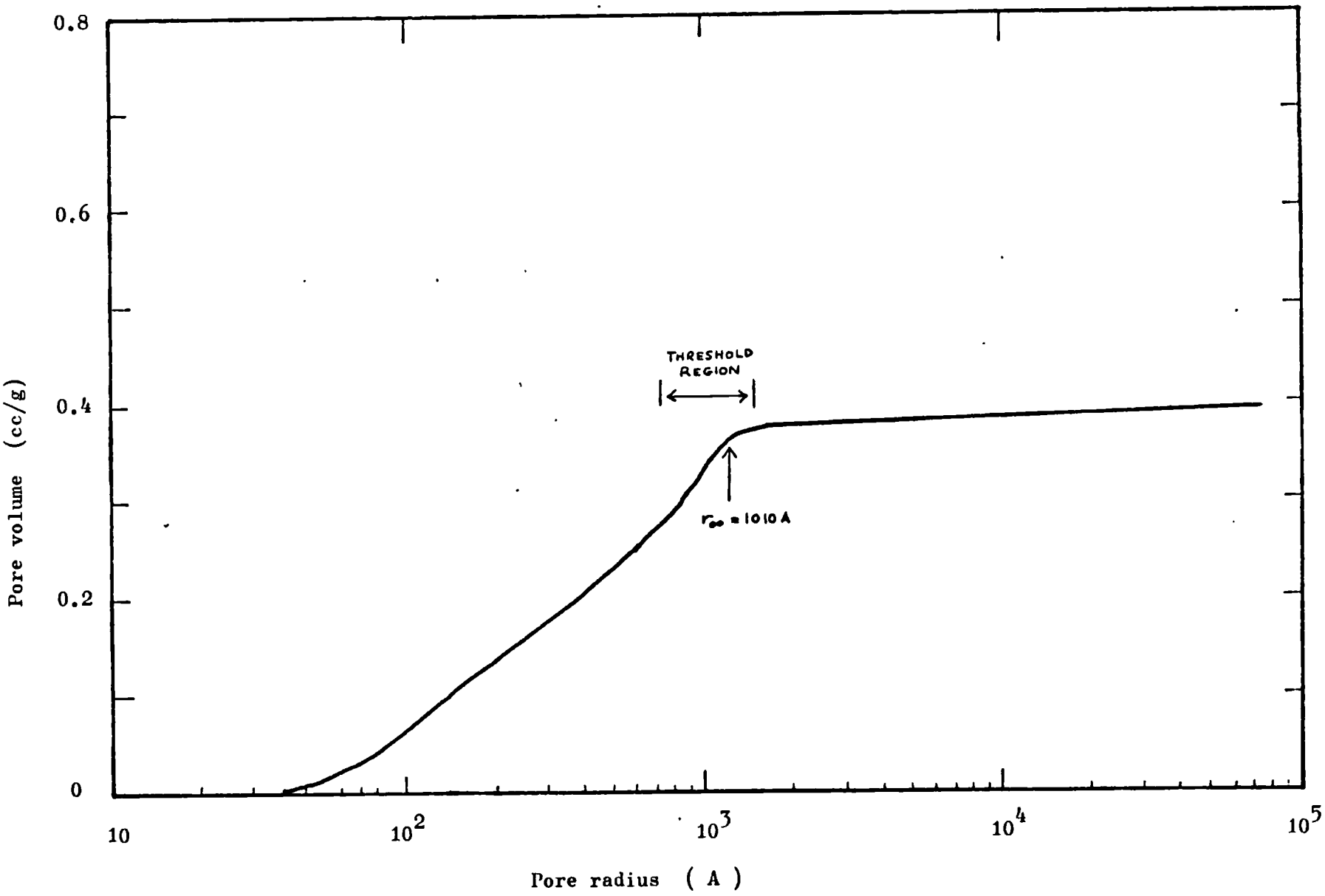

Fig 2.18: A typical cumulative pore size distribution of hardened cement paste(w/c 0.47/28day) showing the relationship between the threshold range and the primary continuous pore radius(r)

The actual pressure-volume plots from the strip chart recorder (see fig 2.17) are not smooth functions and contain a series of steps because the design of the porosimeter is based on applying the pressure in step increments followed by pauses to enable the metallic rod-mercury electrical contact to be reestablished to detect the amount of penetration. The broad outlines of the plots however indicate approximate smooth curves as can be seen on figs 2.16 and 2.17. By taking equal penetrated volume steps and finding the pressures corresponding to each volume increment, it was possible to define the primary continuous pore radius as the radius corresponding to the maximum value of dV/dP in equation 2.32. The mode or most frequent pore radius is given by the maximum value of the function $\hat{M}^{*}(r)$ as in equation 2.32. The differential distributions obtained with equation 2.32 tended to include the noise caused by the step changes in the pressure-volume data hence it was necessary to smoothen out the plots for clarity of presentation. An example of a typical unsmoothened and the smoothened plot is given on fig 2.19 and the positions of the mode pore radius and the primary continuous pore radius as obtained from the analysis of the data using a computer programme.

It is thought that in physical terms, the definition of the primary continuous pore radius corresponds to the maximum spacing between the links between the crystalline products of hydration and also indicates the pore sizes at which mercury tends to flow into the specimens for small changes in the applied pressure. It would correspond approximately to the description of the threshold diameter given by Winslow and Diamond[28] but to avoid confusion in definitions it is being called the primary continuous pore radius.

2.7.2.3 Surface area and hydraulic radii

The surface area and hydraulic radii may be estimated from the pressure-volume data by assuming a cylindrical pore model as usual. The curved surface area of a cylinder containing a volume of mercury dV_i is given by

$$S_i = 2 \frac{dV_i}{r_i} \qquad (2.33)$$

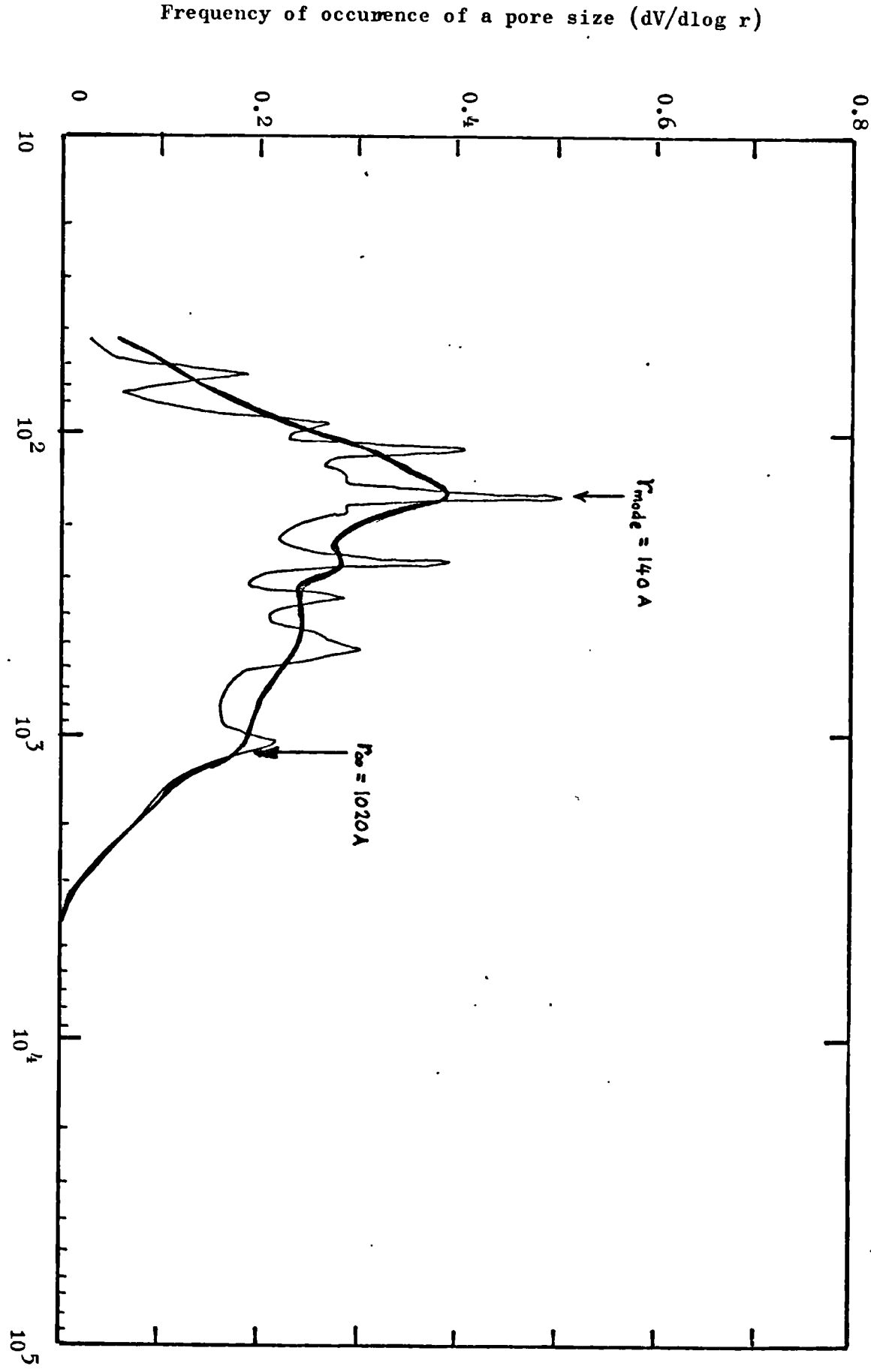

Fig 2.19: A typical differential pore size distribution curve showing the unsmothened and the smoothened curve and the positions of the mode pore radius and the primary continuous pore radius.

If it is assumed that there are several such cylindrical pores interconnected within the porous network then the contributions to the total surface area of the solid phases can be summed for all the volume steps dV_i thus the total surface area is given by

$$S_t = \sum_{i=1}^{n} 2 \cdot \frac{dV_i}{r_i} \qquad (2.34)$$

where

S_t = total measurable surface area

n = number of volume steps used

The hydraulic radius of the pore system is simply the ratio of the total intruded pore volume and the surface area.

Hence

$$r_h = \frac{\mathcal{E}_c(2000)}{S_t} \qquad (2.35)$$

where $\mathcal{E}_c(2000)$ = total intruded pore volume at 2000 kg/cm^2

The parameters that can be evaluated from a single porosimeter test offer different means of describing the pore structure of pastes and mortars and the relationships these parameters bear with permeability is the subject of chapter 3.

CHAPTER 3

RESULTS OF THE EXPERIMENTS

In this chapter, the results of measurements of the important variables of the structure of hardened cement pastes thought to have significant effects on saturated permeability are presented and interrelated. The variables affecting permeability of mortars are also presented and briefly discussed. The purpose here is to draw on fundamental definitions of the parameters of pore structure, and, from the measurements, identify those that are essential in relation to saturated permeability.

3.1 Permeability of hardened cement pastes.

3.1.1 Effect of water/cement ratio

Fundamentally water/cement ratio controls the spacing of unhydrated cement grains in the set structure and has therefore significant effects on the properties of hardened cement pastes. The effect of water/cement on the permeability of hardened cement pastes hydrated in water for 28 days prior to steady state permeability measurements is presented in Table 3.1. The individual values of permeability and dry densities are given for the test samples. The coefficients of variation of both dry densities and saturated permeabilities are also presented for each w/c ratio.

It is shown in Table 3.1 that the dry densities are within $\pm$0.1g/cc for each w/c ratio; the coefficients of variation are less than 2%; thus it may be reasonable to suggest that the samples are representative with respect to water/cement ratio. Examination of the permeability data reveals that barely the order of magnitude is retained at each w/c ratio. The coefficients of variation for the permeability data varies greatly and in excess of 100% in some cases. The results are presented in Fig 3.1 to illustrate the degree of scatter of permeability. It can be seen from the vertical lines drawn through the minimum and maximum values obtained from the measurements that the scatter is extremely large. The overlap of the results at the lower w/c ratios can be seen to be considerable, and might suggest that the scatter is partly due to the rather low rates of flow observed to be of the order of 0.01cc hour during the measurements despite the large hydraulic gradients of some 70,000 imposed on the specimens.

TABLE 3.1 Saturated permeability (K m/s) and dry densities (d g/cc) of hardened cement pastes hydrated in water for 28 days

w/c	0.23		0.35		0.47		0.59		0.71		0.83		1.00	
	K	d	K	d	K	d	K	d	K	d	K	d	K	d
	10^{-14}		10^{-14}		10^{-14}		10^{-13}		10^{-12}		10^{-11}		10^{-10}	
	0.89	2.04	1.69	1.83	2.03	1.52	0.95	1.39	1.60	1.20	2.76	1.12	1.01	1.05
	1.17	2.08	2.22	-	9.27	1.58	1.37	1.36	1.34	1.19	2.83	1.11	1.32	1.03
	1.18	2.07	4.74	1.82	4.11	1.58	1.45	1.35	4.42	1.24	-	-	1.80	1.04
	2.40	2.08	6.92	-	3.73	1.56	1.20	1.36	0.10	-				
	6.01	2.01	7.27	1.84	5.73	1.54	1.35	1.36						
	6.83	2.05			0.32	1.57	1.53	1.35						
					1.05	1.54								
					0.99	1.51								
Mean K	3.08	10^{-14}	4.57	10^{-14}	5.69	10^{-14}	1.31	10^{-13}	1.59	10^{-12}	2.80	10^{-11}	1.38	10^{-10}
C.O.V.	78.6	1.22	50.5	0.45	108.6	1.61	14.5	0.99	84.7	0.99	-	-	-	-

C.O.V. is the coefficient of variation (%)

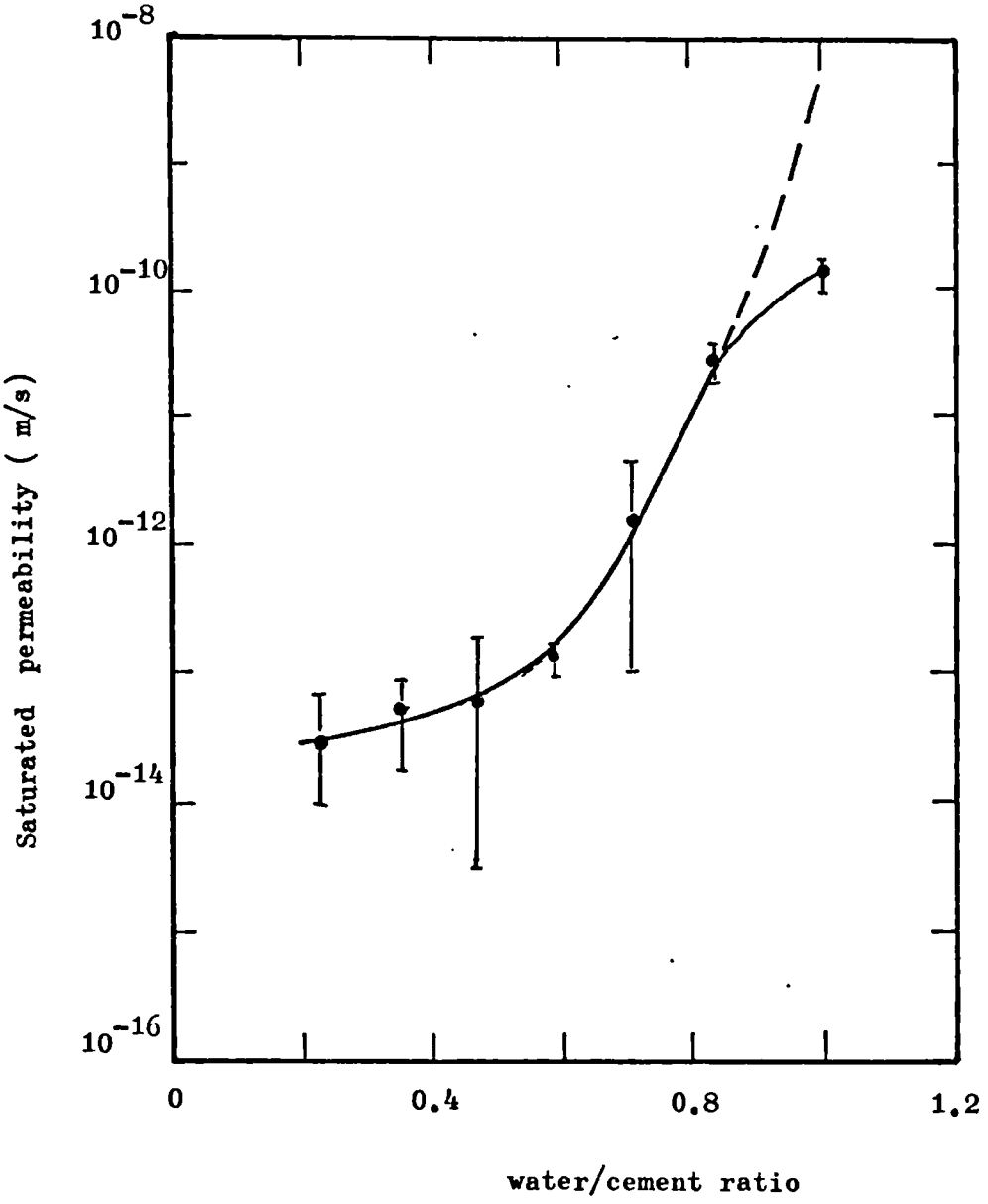

Fig 3.1: Effect of water/cement ratio on permeability of hardened cement pastes hydrated in water for 28 days.

The smaller variation in dry densities in comparison with the rather large variation in permeability for any w/c ratio would seem to indicate the sensitivity of permeability to minor variations of specimens due to minor inconsistencies in compaction and other factors influencing sample preparations and homogeneity. Variations due to room temperature changes are not considered to be significant since the tests were performed in an air-conditioned temperature controlled laboratory.

On the basis of the mean permeabilities shown in Fig 3.1, it can be seen that permeability increases approximately exponentially with increasing water/cement ratio. Table 3.1 indicates that the mean permeabilities of pastes with w/c ratios less than or equal 0.47 hydrated for 28 days are within the order of magnitude of 10^{-14}m/s, whereas the large increases in permeability result for pastes with w/c ratio above 0.47. This is a significant arbitrary limit of w/c ratio for permeability to start increasing rapidly and should be of great practical significance in the control of permeability in the design of mixes.

For the 1.0/28 day paste (henceforth 1.0/28 day paste refers to hcp with w/c of 1.0 hydrated for 28 days in water) the measured permeability deviates slightly below the expected trend of the smooth curve drawn through the mean values, and continued as a broken line on Fig 3.1. It is considered that this apparent reduction in permeability is due to bleeding of the pastes. A surface subsidience of approximately 10mm was found at the time of set. As previously explained with regard to the induced porosity gradients caused by the shape of the moulds (Sect 2.3 and Fig 2.1) bleeding would tend to reduce the intergranular spacing or the effective water/cement ratio which might tend to reduce permeability. If the moulds were cylindrical, there might have been an increase in permeability due to the development of specific continuous bleeding channels as suggested by the authors of reference 92.

In view of the rather large scatter obtained in Fig 3.1 it is apparent that w/c alone does not adequately and accurately indicate permeability as minor variations in sample preparations are likely to produce large differences in permeability. This suggests that more fundamental variables of the structure of the pastes need be sought to relate to the permeability of hardened cement pastes.

3.1.2 Effect of hydration

Table 3.2 illustrates the variation of mean permeability for pastes of different w/c ratios hydrated continuously in water up to 20 months. For clarity of presentation, the number of tests instead of the range of values are indicated. It must be borne in mind that the scatter is not dissimilar to that in table 3.1. The results for pastes of 0.23, 0.47, 0.71 and 1.0 w/c ratios are illustrated in Fig 3.2. It is found that for w/c greater than or equal to 0.47, hydration reduces permeability significantly by a factor of at least 10^4 from 3 days to 28 days initial curing after which the reduction is relatively low. This was not the case for the 1.0 paste where the reduction in permeability is still relatively significant up to 10 months curing.

The results of the 1.0 w/c paste indicates that given enough space, hydration continues relatively unhindred and does not result in a diminishing rate of change in permeability. Fig 3.2 also indicates that the 20 month samples were more permeable than the corresponding 10 month samples on a mean basis. The result, shown in broken line on Fig 3.2, is somewhat unexpected. Previous tests[22] indicated that long term curing leads to leaching of calcium hydroxide from the samples into the curing water which results in an increase in permeability. In this work no comparisons of the amounts of calcium hydroxide present in the pastes were made to verify this assertion but it was considered that whatever the cause may be it should be reflected by differences in pore structure measurements. This will be discussed further later.

The fact that attempts at measuring permeability for early age pastes of w/c 0.23 were unsuccessful leads to the suggestion that these pastes were probably both self-dessicated and highly impermeable even at the early age.

The results from table 3.2 clearly show the extent of the large range of values to the order of magnitude of 10^8 over which the permeability of hardened cement paste can vary depending on differences in w/c ratios and times of hydration. It is presented here to provide a fair indication of the kind of scales necessary in examining further results to be presented.

TABLE 3.2 Effect of hydration on permeability of hardened cement pastes

Saturated permeability (m/s)

Time of hydration (days)	3	No.of tests	7	No. of tests	28	No. of tests	10m	No. of tests	20m	No. of tests
w/c 0.23	U	-	*$2.93\ 10^{-13}$	7	$3.08\ 10^{-14}$	6	$2.62\ 10^{-15}$	2	$5.15\ 10^{-15}$	3
0.35	-	-	$8.04\ 10^{-13}$	3	$4.57\ 10^{-14}$	5	-	-	-	-
0.47	$3.41\ 10^{-10}$	3	$3.73\ 10^{-12}$	4	$5.69\ 10^{-14}$	8	$2.14\ 10^{-14}$	3	$7.8\ 10^{-14}$	3
0.59	$2.78\ 10^{-9}$	2	$6.93\ 10^{-11}$	7	$1.31\ 10^{-13}$	6	-	-	$1.09\ 10^{-12}$	4
0.71	$1.1\ 10^{-8}$	3	$3.6\ 10^{-10}$	8	$1.59\ 10^{-12}$	5	$4.41\ 10^{-13}$	2	$4.9\ 10^{-12}$	4
0.83	-		$2.6\ 10^{-9}$	5	$2.8\ 10^{-11}$	2	-		-	-
1.00	**$2.8\ 10^{-7}$	2	$1.1\ 10^{-8}$	8	$1.38\ 10^{-10}$	3	$5.13\ 10^{-12}$	3	-	-

* 14 days ** 2 days U - Unsucessful attempts at measurements

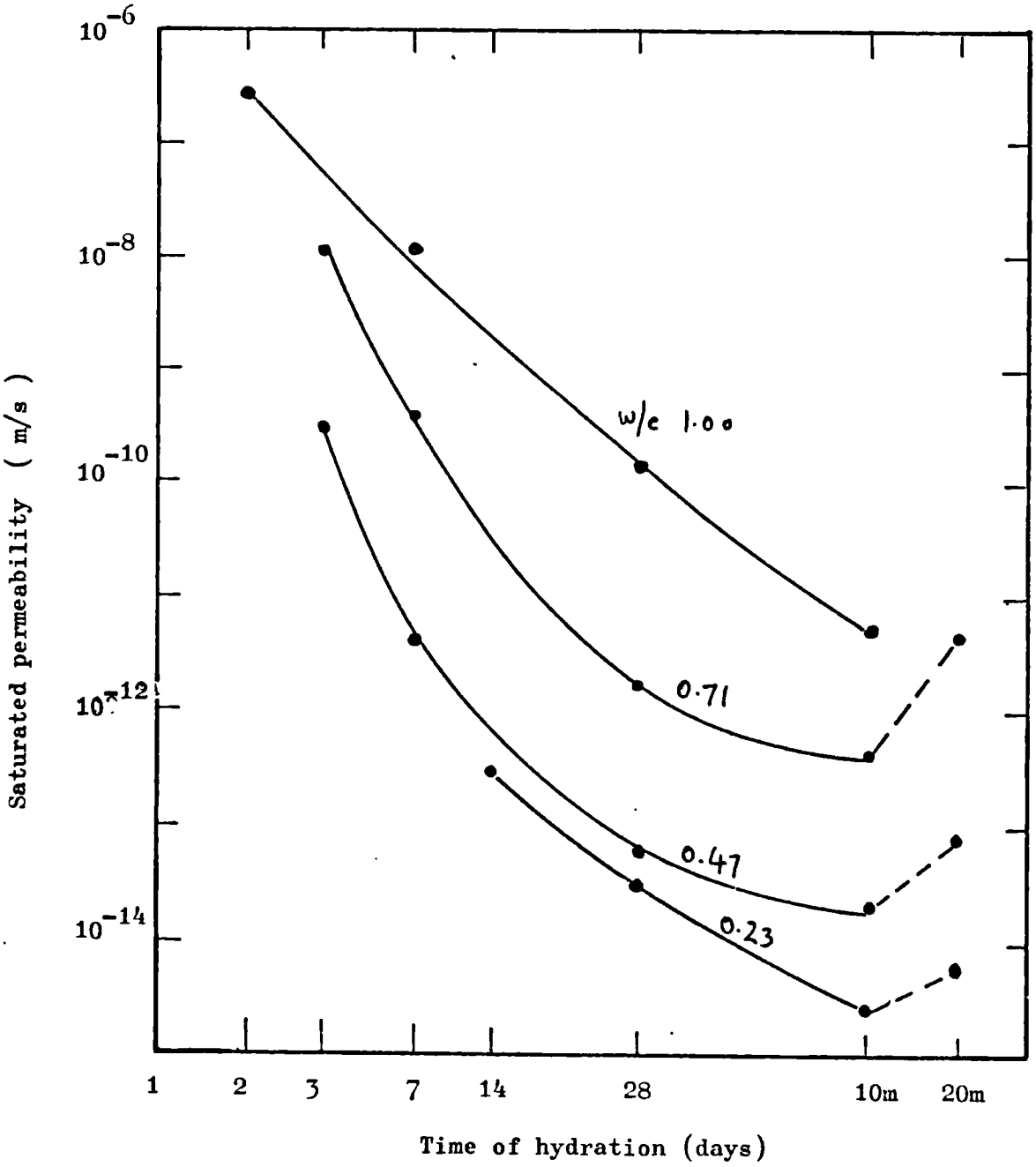

Fig 3.2: Effects of hydration on permeability of hardened cement pastes of different water/cement ratios.

The results from Table 3.2 and Fig. 3.2 can be summarised as follows:

(1) Hydration reduces permeability much more effectively than differences in w/c ratio in the early times of hydration. The greatest change occurs up to 28 days.

(2) The change in permeability after 28 days is relatively small and the rate depends on the initial w/c ratio.

(3) There is an apparent increase in permeability after 10 month hydration.

3.2 Pore structure of hardened cement paste.

3.2.1 Total porosity

The mean values of porosities obtained from the oven dried weight losses and the helium inflow techniques are presented in table 3.3. The helium inflow porosities are shown in paranthesis. The porosities are given as the total measurable pore volume per gram of oven dried weight of the samples.

TABLE 3.3 Variation of total porosity with w/c ratio and hydration

	Total porosity (cc/g) at 105°C (Helium Flow)				
Time of hydration (days)	3	7	28	10m	20m
w/c ratio 0.23	-	0.149 (0.109)	0.141 (0.089)	0.125 -	0.118 -
0.47	0.338 (-)	0.323 (0.263)	0.287 (0.224)	0.258 (-)	0.229 (-)
0.71	0.532 (0.479)	0.497 (0.461)	0.474 (0.393)	0.466 -	0.449 -
1.00	* 0.693 (0.669)	0.679 (0.607)	0.622 (0.534)	0.631 -	- -

*2 days

It can be seen that total porosity by both methods increases with w/c ratio and reduces with hydration as expected. The helium inflow method indicated less total pore volume than those obtained from the evaporable water contents at 105°C.

Fig 3.3 shows a plot of total porosity (cc/g) against logarithm of time of hydration. The plots indicate, within reasonable limits, that total porosity reduces linearly with logarithm of time of hydration. Two essentially different ways of varying total porosity, i.e. increase in water/cement ratio and hydration is demonstrated in Fig 3.3, and the mode in which these changes can affect permeability will be shown in section 3.3.1.

Although it is difficult to establish precisely when a sample can be said to be saturated and surface dry, a consistent procedure, as described in section 2.6.2 was adopted in this work to ensure that reasonable total porosities are measured as table 3.3 would suggest for the mean values of total porosities of the oven dried pastes. An advantage gained in the drying method is that most of the porosity measurements were made on samples previously tested at saturation for permeability.

The helium flow results and measurements were discontinued for the 10m and 20m samples because of the lower porosities obtained from these tests and also because of the erratic nature of helium inflows frequently observed. Some of the plots of the actual indicated specific volumes of the oven dried pastes are shown in fig 3.4. The double-time scale 0-5 hours and 5-30 hours is used for clarity of presentation. It can be seen that much of the inflow occurs in the first 5 hour periods for pastes with w/c ratio approximately 0.59 and less; a highly porous paste with w/c of 1.0 still has significant flow after 5 hours. These tests represent those that did not show an increase in indicated solid volumes after 24 hours exposure to helium. The increase in indicated solid volume after 24 hours of exposure of the samples to helium was a common feature, and in other cases, no change in solid volumes could be found after the 24 hour exposure. The nature of leaks of the pycnometer is far from simple and clear. It could be effectively used to indicate porosities on a relative basis for runs up to 5 hours.

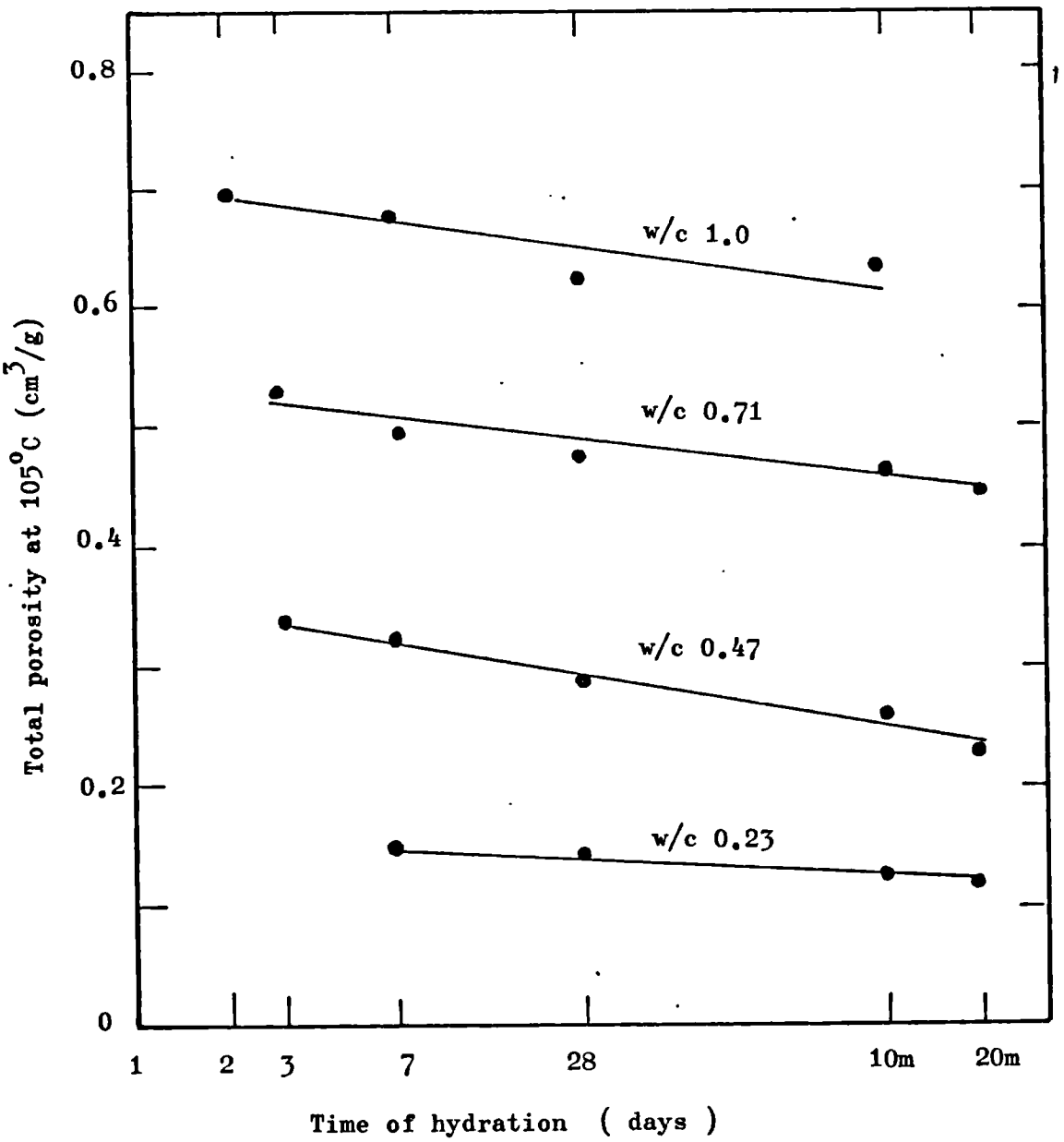

Fig 3.3: Effects of Water/Cement ratio and Time of hydration on the total porosity of hardened cement pastes.

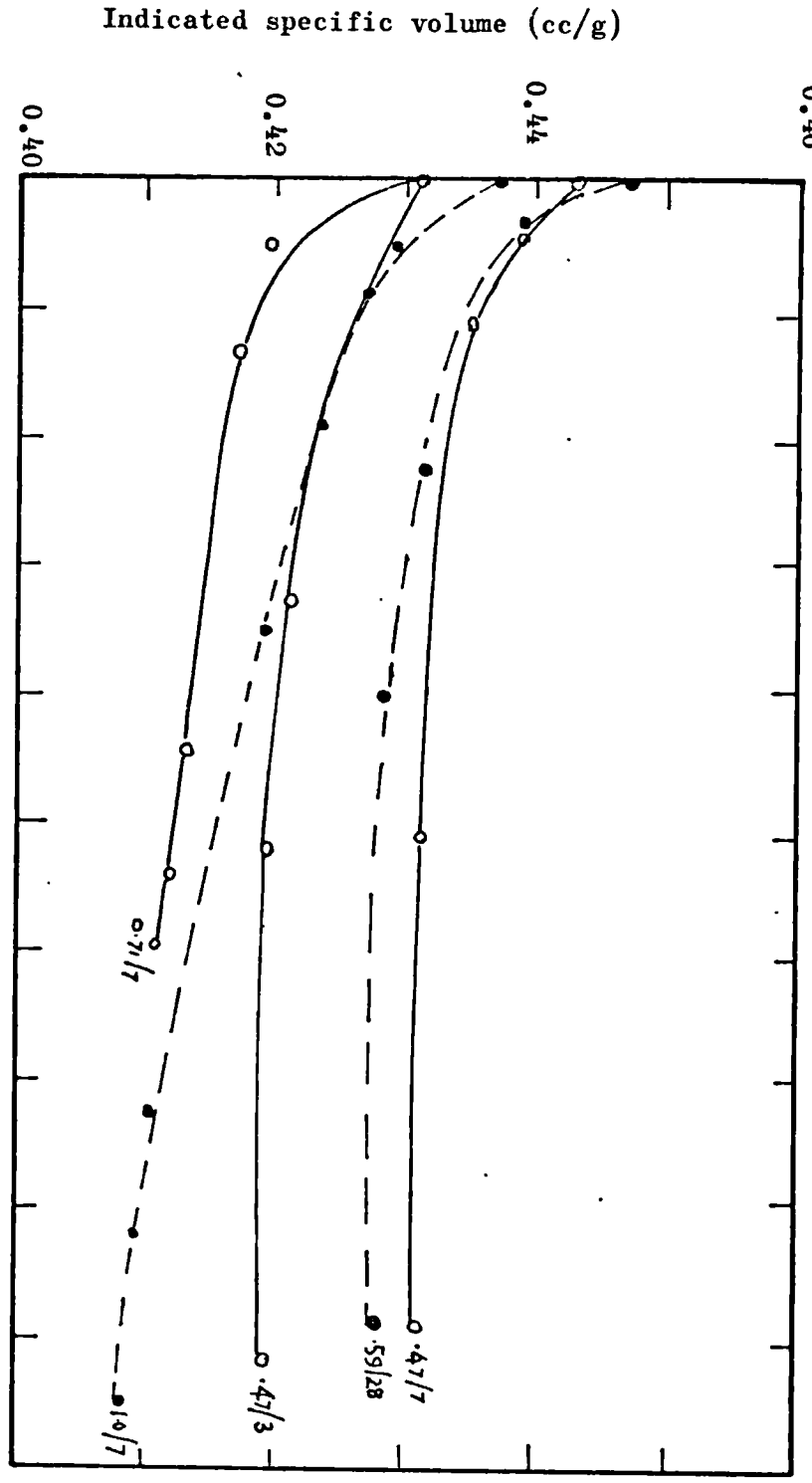

Fig 3.4: Helium inFlow vs. time curves for oven dried hcp samples.

** 47/3 represents hcp w/c = 0.47 hydrated for 3days in water

The conclusion from all this is that the measurement of total porosity by the simple oven drying procedure proved to be more successful in this work than the helium inflow method mainly because it was not subject to the uncertainties of leak corrections found with the pycnometer.

3.2.2 Pore size distributions

Pore size distributions were determined by mercury intrusion porosimetry for each sample tested for saturated permeability. Some 90 distributions were thus obtained for the hardened cement paste samples. The rather large number of determinations was absolutely essential mainly because with the kind of scatter demonstrated in section 3.1.1 one needs to look for trends in the study of permeability in order to identify the effects of variables of the structure on permeability. Due to the large amount of data accumulated, the analysis of the distribution were made using a computer programme. Each distribution was examined on a tektronix plotter to check the validity of the most important distribution parameter, identified here as the primary continuous pore radius (r_{∞}). The full discussion and interpretation of the significance of this parameter will be deferred till later sections. For the present purpose, it is essential to point out that the position of the parameter for hardened cement pastes was checked with the shape of the cumulative distribution functions to see if it did correspond to the threshold regions, as defined in section 2.7.3.1, and from the consistencies obtained, it was concluded that the definition of the primary continuous pore radius as corresponding to the mean pressure at the maximum value of the derivative of the pressure-volume data taken at equal volume steps was satisfactory for all the hardened cement paste samples examined.

Typical cumulative pore size distributions are presented in Fig 3.5a for pastes of different w/c ratios cured for 28 days in water. The distributions represent the pore volumes per gram of dry pastes existing below a given pore size as obtained from the measurements. The typical values of the primary continuous pore radius are shown on the curves.

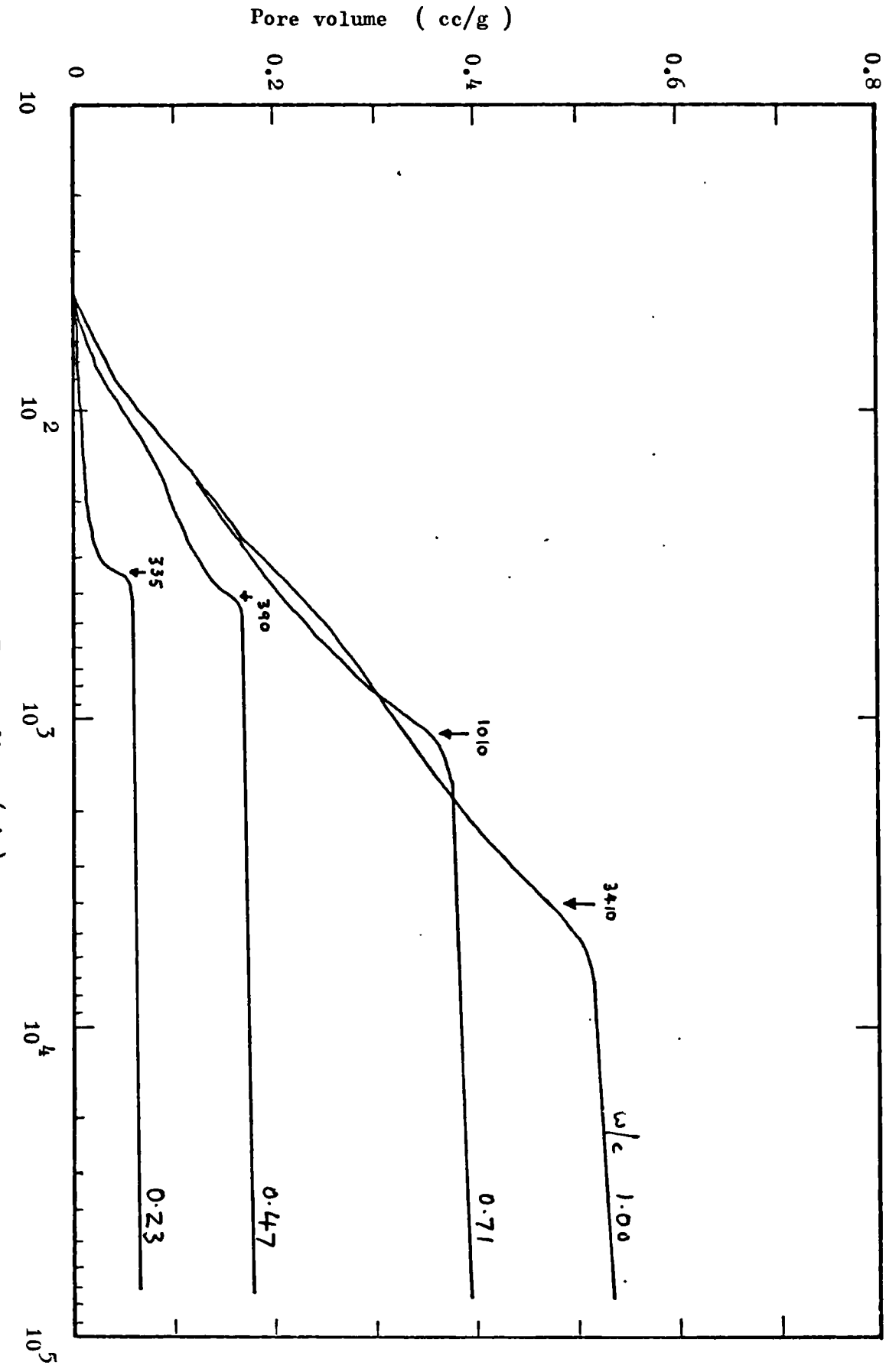

Fig 3.5a: Effect of water/cement ratio on the cumulative pore size distributions of hardened cement pastes hydrated in water for 28 days.

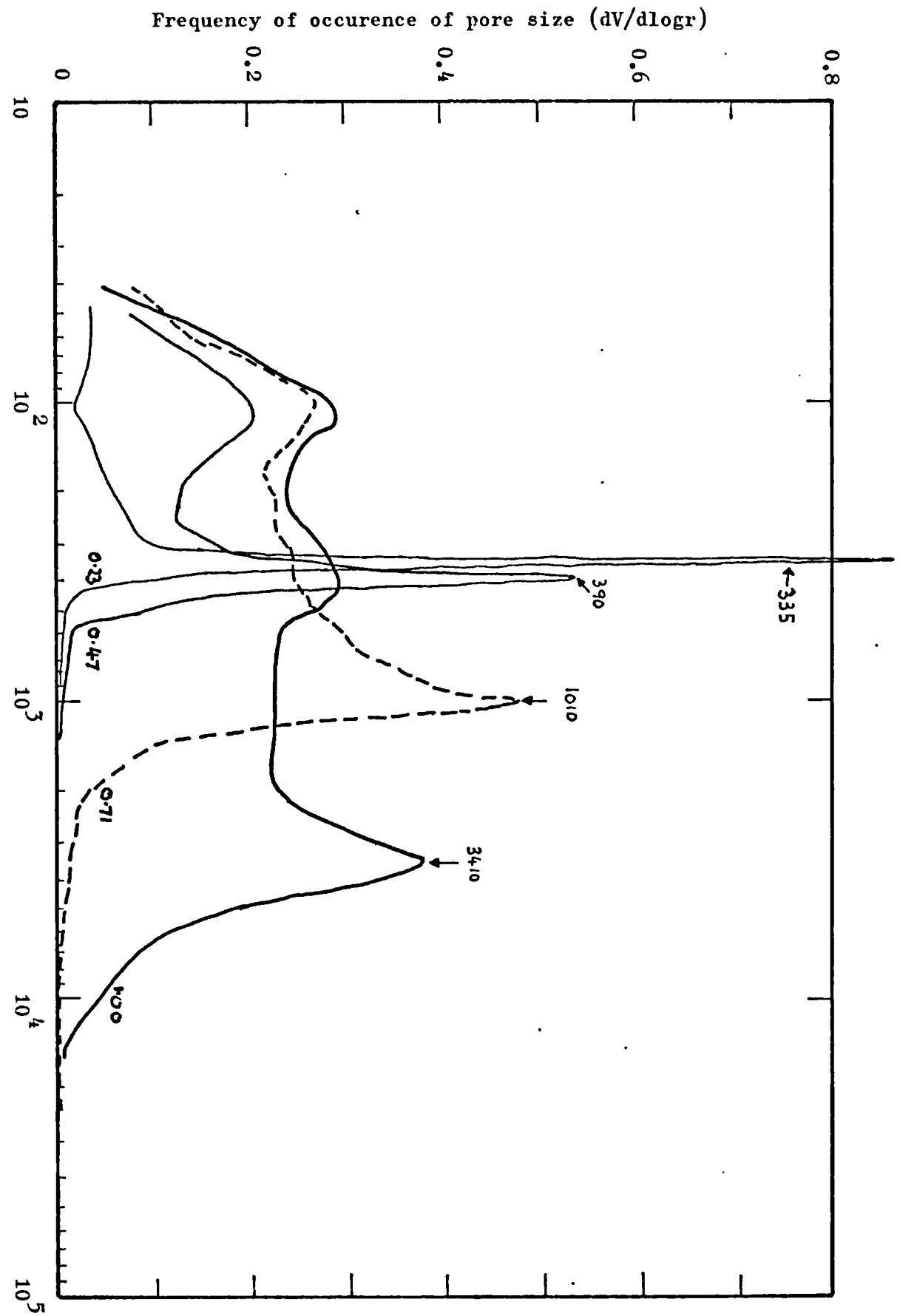

Fig 3.5b: Effect of water/cement ratio on the differential pore size distributions of hardened cement pastes hydrated in water for 28 days.

The cumulative distribution curves indicate well defined ranges of large pores sizes where there is very little mercury intrusion, and it can be seen that the range at which very little intrusion occurs varied with w/c ratio. The range is larger, the larger the w/c ratio. In essence, it appears that the range is mainly controlled by the inter granular spacing. The total intruded pore volume increases with w/c as expected. In order to obtain a clearer indication of the frequency of occurrence of different pore sizes in the spectrum, the differential pore size distrubutions are also shown in Fig 3.5b. This is a plot of the log r (pore radius) against dV/dlog r (see the basis of this approach in section 2.8.2.2)

The pore radii occurring most frequently in the spectrum, i.e. the mode pore radii are indicated on the plots. The mode pore radii are defined by the maximum value of the function dV/dlog r and is denoted r_{mode}. In the particular cases of the 28 day pastes cited on Fig 3.5b. the mode pore radii correspond exactly to the definition of the primary continuous pore radii.
Fig 3.5b shows that the mode pore radius and the primary continuous pore radius arrowed on the figure increases with increasing w/c ratio. In addition, the distributions also show that there are fairly well developed minor peaks - in the pore size vicinity of 100 A for pastes with w/c ratio greater than 0.23, whereas the 0.23 paste completely lacks this feature. This might seem to indicate that the development of the minor peaks depends on w/c ratio or space constraints and one might expect a critical w/c ratio at which the development of the broad shoulders commences.

3.2.3. Effect of hydration on the distribution of pores.

It is well accepted that the hydration products of cement and water occupy about twice the volume of the initial reactants[9,13]; hence continued hydration fills or bridges the initial water-filled space of the pastes with hydration products. Fig 3.6a is presented for the 0.71 pastes to illustrate the changes that occur to the cumulative pore size distribution curves as a result of continuous curing in water.

The first point is that the total intruded pore volume reduces with curing up to 10 months: at 20 months there appears to be a slight increase relative to the 10 month sample. Whether this change from the expected trend is real or due to sample preparational inconsistencies could not be established due to lack of time for a repeat conditioning of samples.

The second point is that the range of pore sizes at which very little intrusion occurs (i.e. the almost horizontal portions of the curves) increases with increasing time of hydration. This means that the pore sizes within the pastes are becoming finer with hydration.

The third and most important point concerns the regions of inflection following the horizontal portions of the distributions curves, called here the threshold regions in the spectrum of the pore sizes. It can be seen that for the 3,7, and 28 day pastes, the threshold regions are characterised by very steep slopes or sharp knees. This is taken as evidence to suggest that a substantial amount of pore volume exist in the threshold regions within a narrow range of pore sizes, which effectively means that the pore structure is highly continuous. In the actual measurements of the intrusion of mercury for these pastes, it was noticed that very minor increases in the pressure of the penetrating mercury caused a substantial amount of penetration.

It can be seen on fig 3.7a that as hydration continues beyond 28-days, the sharp knees exhibited by the early age specimens in the threshold regions become less steep but the horizontal portions of the curve remain more or less the same length. This is taken to suggest that the continuous pore volume reduces whilst the pore size at which mercury intrusion commences remain approximately the same. This aspect of the development of pore structure with hydration is very important from the point of view of both permeability and perhaps strength development of hardened cement pastes and will be further discussed in relation to the definition of the primary continuous pore radius.

The differential pore size distributions for the 0.71 pastes are shown in fig 3.7b., at different times of hydration.

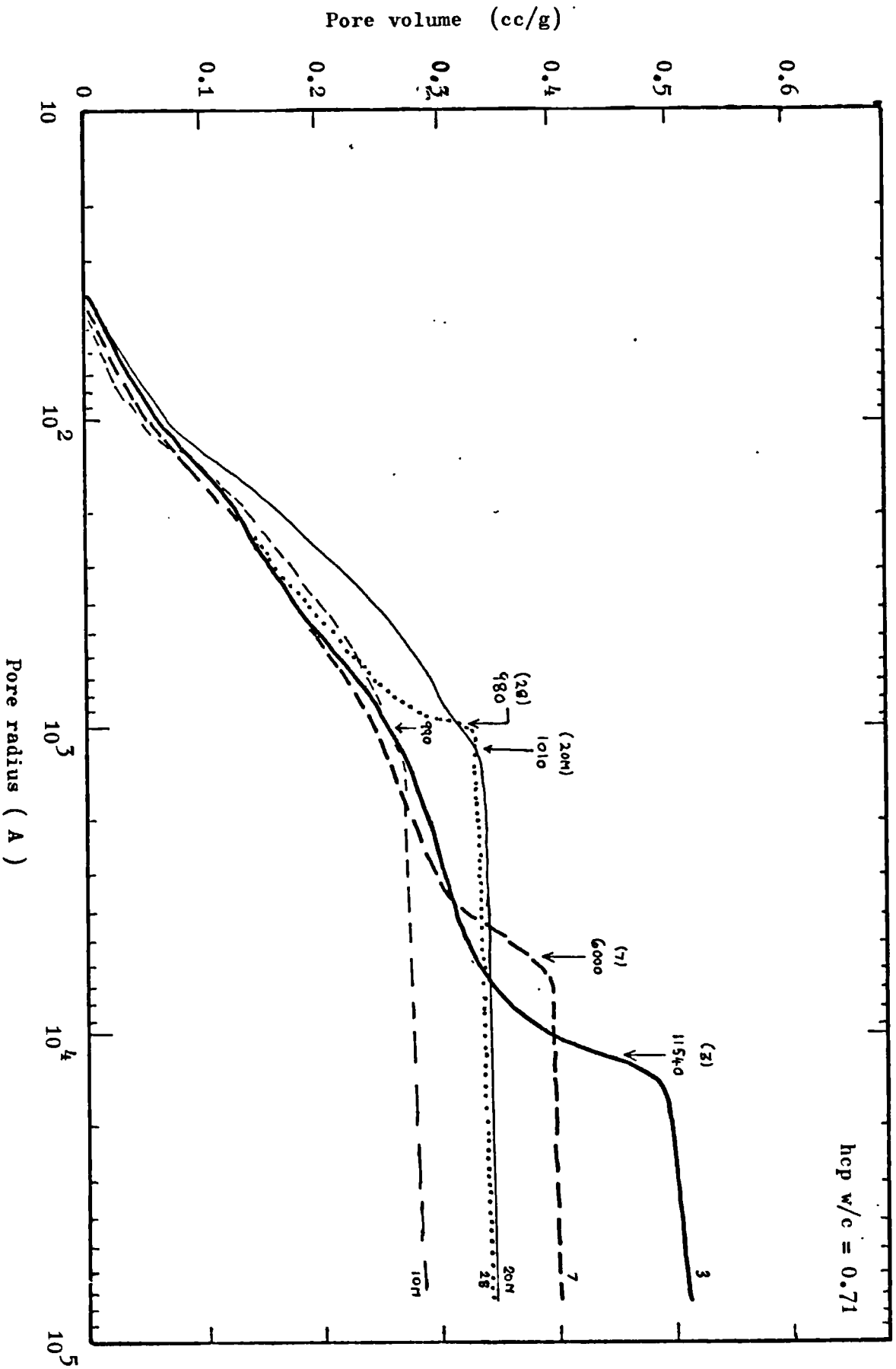

Fig 3.6a: Effect of time of hydration on the cumulative pore size distribution of hcp (w/c = 0.71)

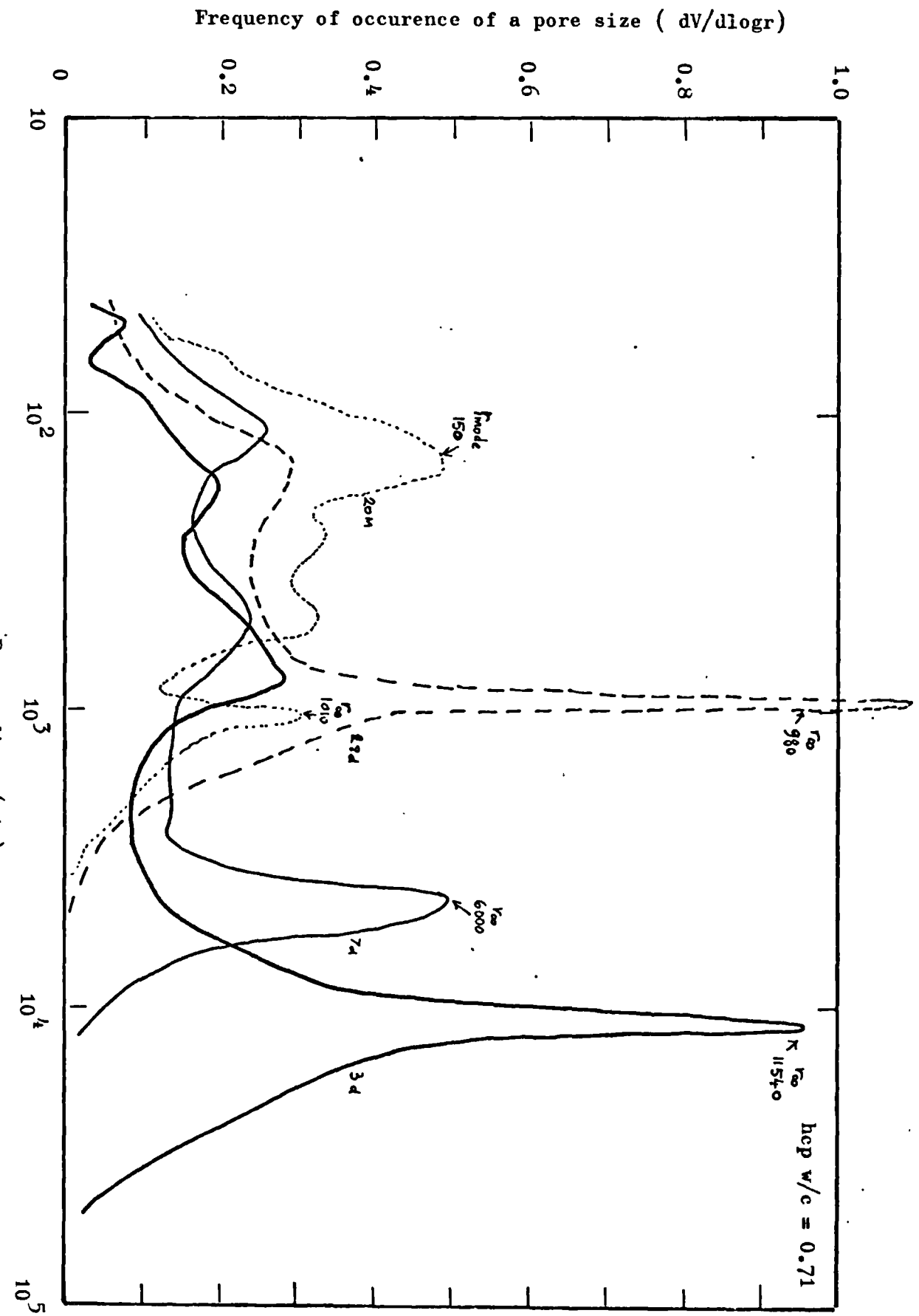

Fig 3.6b: Effect of time of hydration on the differential pore size distributions of hcp (w/c=0.71)

The values of the primary continuous pore radius and the mode pore radius are marked on the distribution curves. It can be seen that with the exception of the 20 month paste, r_{mode} coincides with the value of r_{∞}. It is also clear that the primary continuous pore radius reduces with hydration, at least up to 28 days curing after which it hardly changes.

Typical distributions for the 0.47 pastes are given in figs 3.6c and 3.6d. The typical values of the primary continuous pore radius are marked on both the cumulative and the differential distributions. Again it can be seen that r_{∞} reduces significantly from 3 days to 28 days from approximately 5170A to 350A. According to the definition of r_{∞} the 20 month paste has a slightly larger value of r_{∞} (407 A) than the 28 day paste. The value of r_{∞} depends very much on preparational procedures and although it can be seen that the very sharp knee shown on fig 3.6d for the 28 day paste is not so distinct for the 20 month sample, the general pattern indicates that the range of pore sizes for the 28 day paste is not significantly different in comparison with the earlier age specimens. The differential distribution (fig 3.6c) also illustrates the shift of the peaks associated with the primary continuous pore radii with continued curing to smaller sizes. The plot indicates that the 28 day peak associated with the primary continuous pore radius is particularly sharp whereas the 20 month peak is subdued and not easily distinguishable. In addition the minor peaks that developed at about 100 A pore radius as shown on fig 3.6 appear to be missing for the 20 month sample. This is in contrast to that found for the 0.71 paste at 20 month where the pattern developed to a major peak (see fig 3.6b). This suggests that the 100 A pattern thought to be a characteristic feature of the pore structure of hardened cement pastes[24,34] is probably not a particular feature of the pastes.

It may be concluded that the pores are simply becoming finer with hydration and less pore space or more, depending on the initial w/c ratio exist at 20 month with approximate pore radius of 100 A.

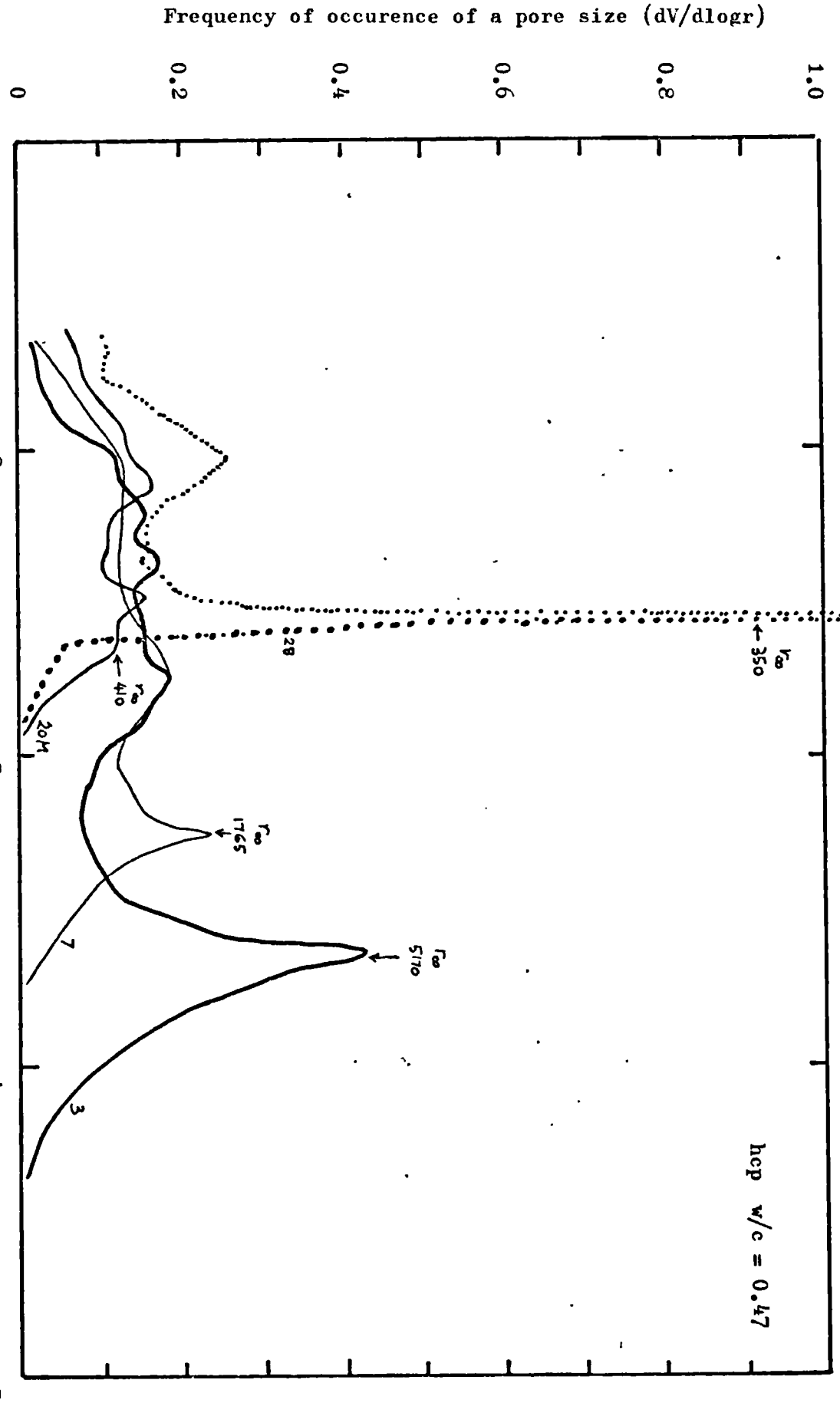

Fig. 3.6c : Differential pore size distributions of hcp(0.47 w/c) as a function of time of hydration

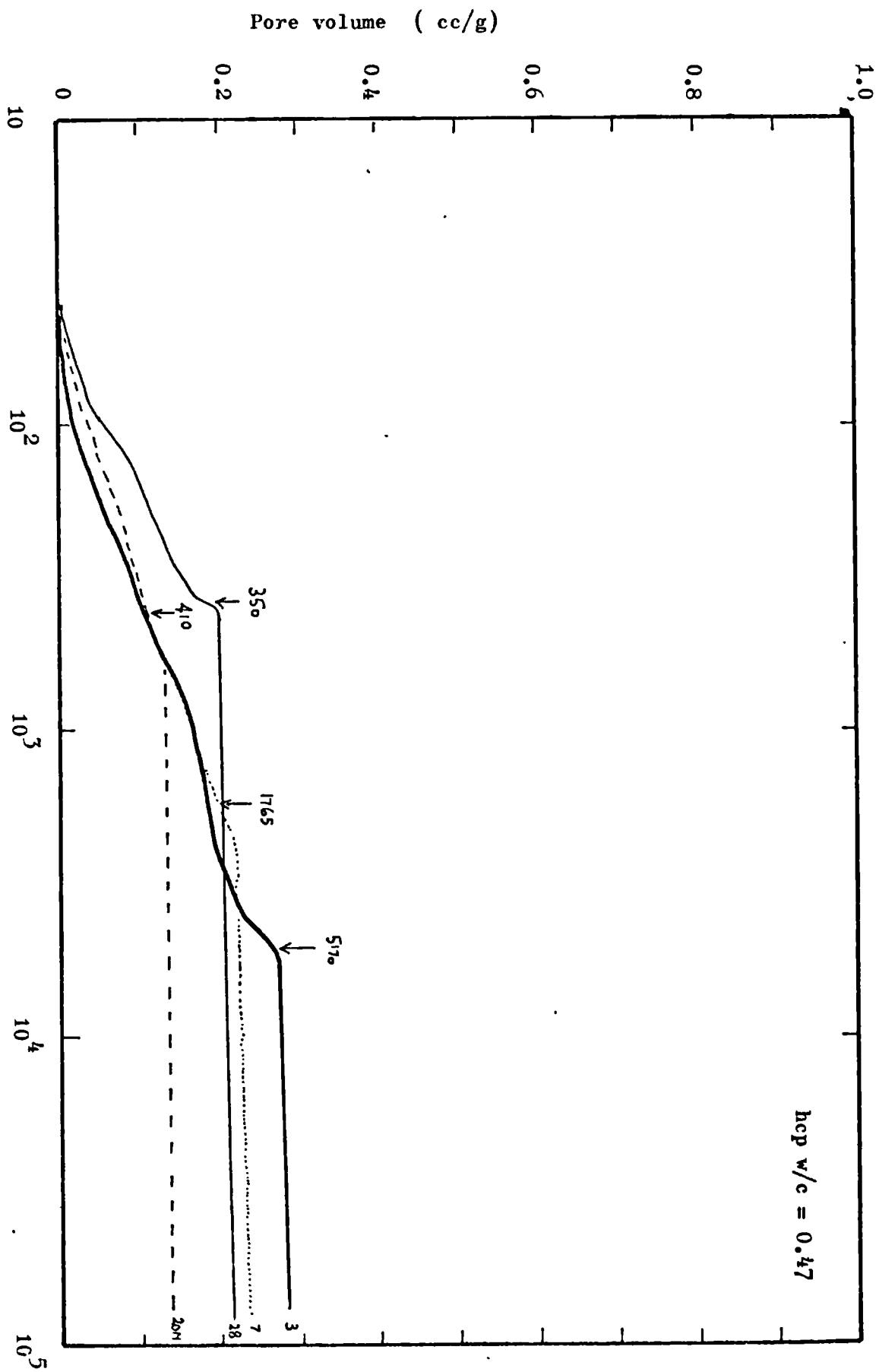

Fig 3.6d : Effect of time of hydration on the cumulative pore size distribution of hcp (w/c = 0.47)

3.2.4. The primary continuous pore radius

In the previous sections, typical pore size distributions were described mainly in a qualitative sense. The most important parameter of the pore structure of hardened cement paste mentioned, in the context of permeability, is the primary continuous pore radius. This was defined mathematically as the pore radius that corresponds to the mean pressure at which the derivative of the pressure-volume function is the maximum. In physical and practical terms this parameter indicates the pore radius at which the mercury actually begins to flow freely in to the samples. Examination of the pressure-volume data obtained from the graphs plotted in the course of the measurements showed that this feature was characteristic of all the hardened cement paste sample tested. The pressure corresponding to the onset of mercury penetration was found to depend on both the w/c ratio and the times of hydration.
As a result of the examination of the crack pattern on the fracture surface of the electron micrograph of the 0.25 w/c ratio paste, taken by Midgley and Pettifer shown on plate 1.1, it is the present authors strong belief that the primary continuous pore radius as defined here provides a simple measure of the pore sizes associated with the weakest links in the bonds of the hydration products of hardened cement pastes and must therefore bear a closer relationship with mechanical properties such as strength and elasticity as well as permeability of hardened cement pastes, than total porosity.

Table 3.4 is presented to show the mean values of the primary continuous pore radius obtained from the measurements for different w/c ratios at different times of hydration. The values are quoted to the nearest ten angstrom unit.

TABLE 3.4 Variation of the primary continuous pore radius with water/cement ratio and times of hydration

	Primary continuous pore radius(A)				
Time of Hydration(days)	3	7	28	10m	20m
w/c Ratio					
0.23	-	300	350	350	290
0.47	5170	1840	460	480	420
0.71	11540	6350	950	870	990
1.00	48220	13440	4190	1520	-

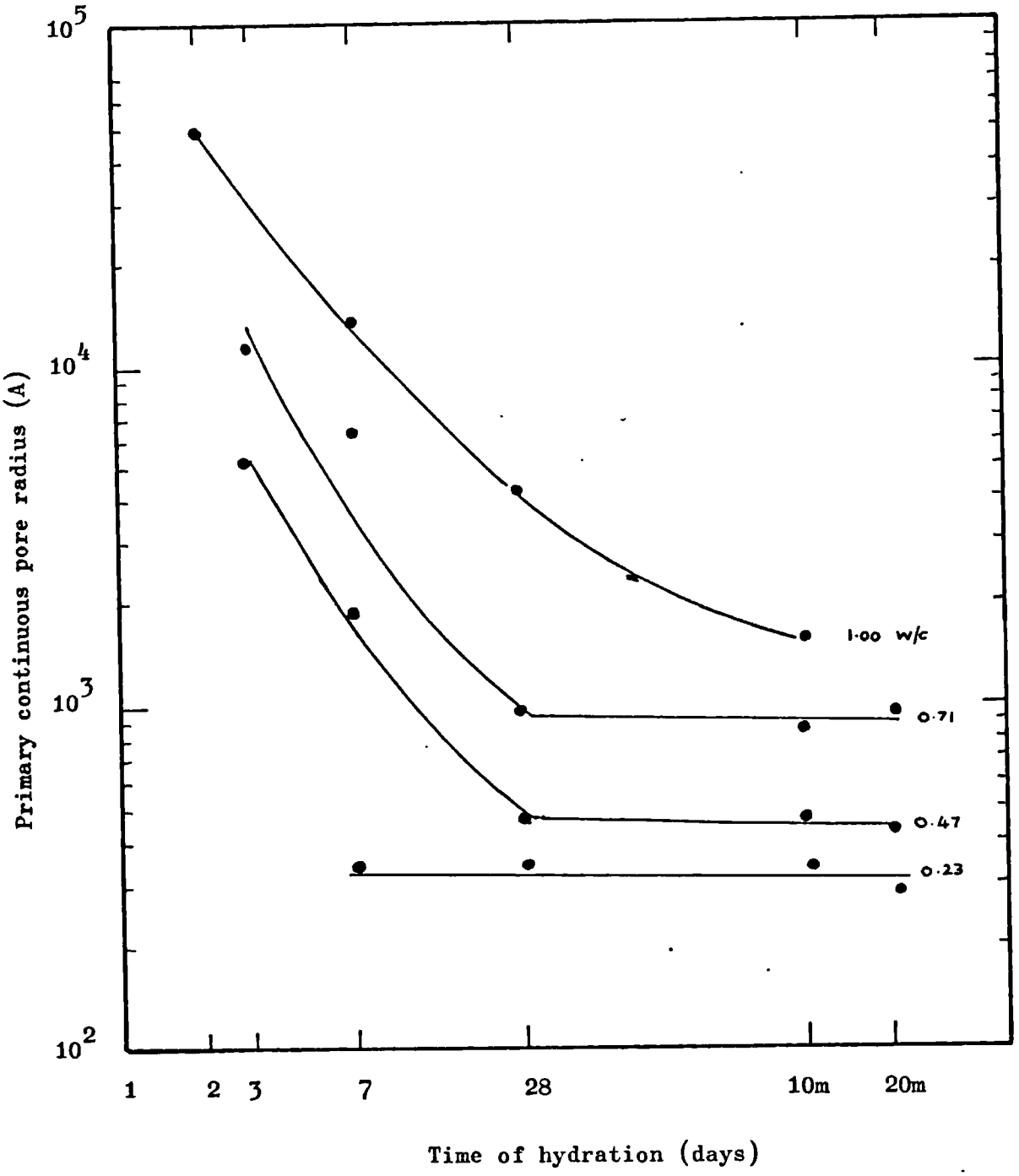

Fig 3.7 : Effect of water/cement ratio and time of hydration on the primary continuous pore radius of hardened cement paste.

The results are presented in fig 3.7 and it is found that the primary continuous pore radius reduces drastically for w/c ratios greater than 0.47 to more or less constant values after 28 days initial curing. The results for the 0.23 paste however shows that the primary continuous pore radius is more or less constant from 7 days to 20 months. It must however be mentioned that the values shown represent the average of between 3 to 8 specimens and indeed variations from specimen to specimen of the same conditioning occurred. In the case of the 1.0 paste it is found that the primary continuous pore radius continues to reduce significantly even after the initial 28 day curing. Adopting the idea that the primary continuous pore radius is mainly controlled by the intergranular spacing at the time of set, the variation of the primary continuous pore radius is consistent with the expected variation of capillary porosity with water/cement ratio and curing with the exception of the 0.23 paste. It is also interesting here to note the similarity in the shapes of the curves in Fig 3.7 to those of Fig 3.2 excepting the 0.23 paste and the 20 month permeabilities; this will be further discussed in section 3.3.2.

3.2.5 Surface areas from mercury intrusion data for hardened cement paste

The estimates of the surface area from the pore size distribution data has been outlined in section 2.8.2.3. Clearly the use of simplifying assumptions of the cylindrical pore model makes the computation of the surface areas rather very approximate, nevertheless, on a relative basis much information can be obtained from the results. The surface area of the pores (or the solid phases) of hardened cement paste or a porous substance is essential in relation to permeability in that it provides a measure of the extent of the surfaces which offer the retarding effect due to viscous drag on the flow of the fluid. In principle, the greater the surface area, the greater the retarding effect if it is assumed that the flow occurs wholly through the total porous network and is not confined to distinct flow channels.

Table 3.5 is presented to illustrate the effect of time of hydration and w/c ratio on the surface areas of hardened cement pastes computed in the manner outlined in section 2.8.2.3.

TABLE 3.5 Surface areas of hcps from mercury intrusion data in relation to w/c ratio and time of hydration

Surface area (m^2/g)

Time of hydration (days)	3	7	28	10m	20m
w/c					
0.23	-	8	7	4	4
0.47	16	23	27	21	21
0.71	24	30	40	37	42
1.00	11	34	43	44	-

The values are the average surface areas for each group of samples given to the nearest 1 m^2/g. The results indicate that the surface areas are much lower than typical values of 180-220 m^2/g obtained by water vapour sorption methods on fully hydrated pastes[9,13]. The only other available data on surface areas by mercury intrusion for hardened cement pastes, to the writer's knowledge, is that given by Bager and Sellevold[82]. They found a value of 39 m^2/g for 0.4/20 month paste of Danish 'Rapid' type cement paste. The maximum pressure exerted by their porosimeter was 3500 kg/cm^2 instead of the 2000 kg/cm^2 used here and in addition a contact angle of 117° instead of 141° was used in the calculation. Their surface area value is therefore clearly greater than the 0.47/20m paste given in table 3.5 but it is within the order of magnitude of the values found in table 3.5.

The results in table 3.5 are illustrated in fig 3.8 and it can be seen that the surface area increases with water/cement ratio at all stages of hydration. It is also found that the change in surface with time of hydration is not the same for the different water/cement ratio pastes. Broadly, it appears that the accessible surface area for the 0.23 paste reduces with time of hydration, whereas for the higher w/c ratio pastes, the surface area increases at least up to 28 days hydration and then decreases or remains steady thereafter, depending on the w/c ratio.

The surface area of hcps accessible to mercury may be important from the point of view of permeability and will be discussed in sections 3.3.3 and 4.3. In section 4.3, some interesting speculative deductions about the pore structure of hardened cement pastes below 37 A, the minimum intruded pore radius will be made using the surface area results in table 3.5 and the extent of the completeness of mercury intrusion.

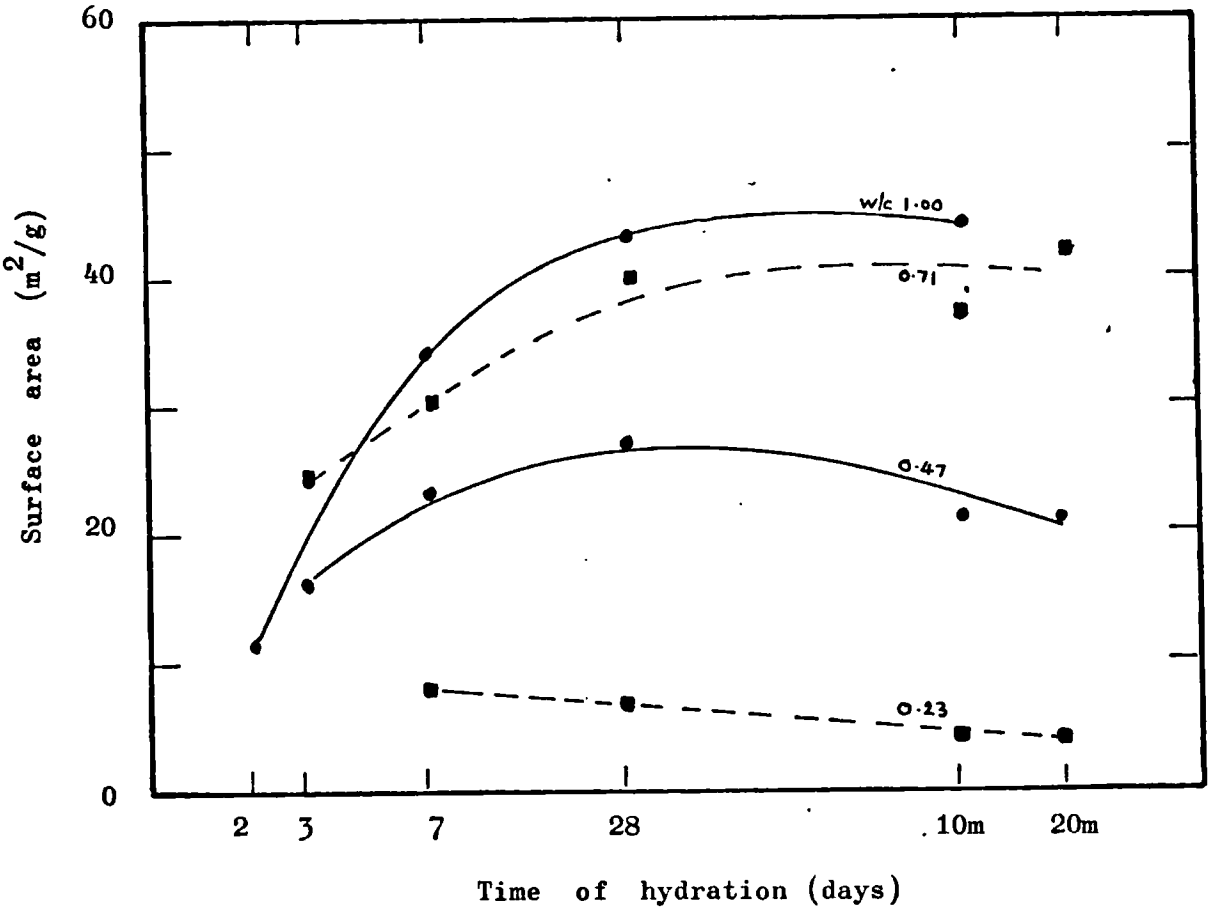

Fig. 3.8: Variations of surface area of hcp from mercury intrusion with water/cement ratio and time of hydration.

3.2.6 Hydraulic radii of hardened cement pastes

In the results presented so far, the pore size distributions of hardened cement pastes have been characterised by two important pore structure parameters, namely

(1) the primary continuous pore radius (r_{∞})
(2) the total porosity

The primary continuous pore radius represents a single-point measure of the distributions and although it has been shown to describe in a reasonable manner, the changes in pore structure resulting from both the changes in w/c ratio and hydration, it has, of course, the disadvantage that it does not account for the

(1) distributions of pores below and above itself
(2) nature and extent of surfaces of the solid phases formed as a result of hydration.

A useful and general measure which may partially account for the above limitations of the primary continuous pore radius is the hydraulic radius of the pore system. In the present context, it is being defined simply as the ratio of the pore volume to the surface area of the solid phases accessible to mercury at the maximum pressure of 2000kg/cm^2 used in the measurements in this work.

Hence, $$^{Hg}r_h = \varepsilon_{Hg}/S_{Hg}$$

where, $^{Hg}r_h$ = hydraulic radius accessible to mercury (10^{-6}A)

ε_{Hg} = pore volume accessible to mercury (cc/g)

S_{Hg} = surface area " " " (m^2/g)

The hydraulic radius is a measure of the average width or diameter of the pore system.

Mean values of hydraulic radii obtained from the measurements for pastes of different w/c ratios and times of hydration are given in table 3.6. The values are rounded to the nearest tenth of an angstrom unit.

Fig 3.9 illustrates the relationship for the different w/c ratios and times of hydration. It can be seen that the hydraulic radii of the pastes reduces with increasing times of hydration and increases with increasing water/cement ratio, for pastes with w/c ratio greater than 0.47. The 0.23 paste behaves differently for which it appears that the hydraulic radius is virtually independent of time of hydration.

TABLE 3.6 Hydraulic radii of hardened cement pastes

Hydraulic radii (A)

Time of Hydration (days)	3	7	28	10m	20m
w/c					
0.23	-	9680	9910	14420	10560
0.47	17510	12160	7360	7820	6320
0.71	21130	14670	9450	9020	8570
1.00	*66960	18800	12230	11810	-

*2 days

It is essential to point out that the changes in hydraulic radii found in table 3.6 occur over one order of magnitude, in contrast to the two orders of magnitude found for the primary continuous pore radii (see table 3.4), for the range of times of hydration and w/c ratio investigated here. This suggests, bearing in mind the large range of values of saturated permeability found in section 3.1.2, that the hydraulic radii of hardened cement pastes may not be as sensitive in relation to permeability as the primary continuous pore radius. It will nevertheless be correlated to permeability in section 3.3.4.

The values given in table 3.6 also effectively show that the hydraulic radius of hardened cement pastes is generally greater than 5000 A for the pore system above 37 A pore radius. The estimates of the maximum pore sizes within the weakest links of the hydration products, ie the primary continuous pore radii, given in table 3.4 suggested that the maximum pore sizes tend to be less than 5000 A for the pastes with w/c ratio at and below 0.47.

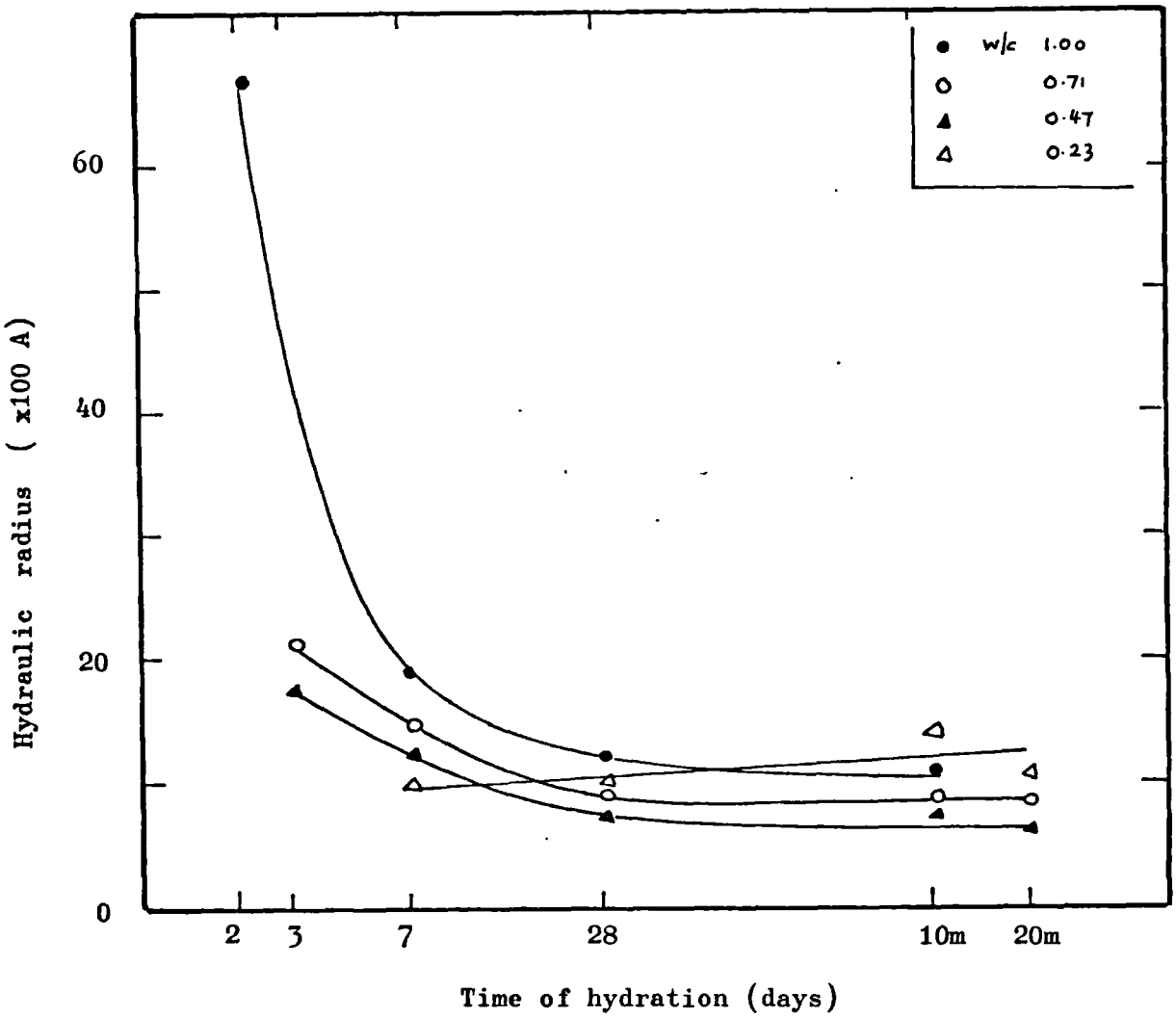

Fig 3.9: Effects of changes in w/c ratio and times of hydration on the hydraulic radius of hardened cement paste.

It may therefore be questioned as to the reasons for the rather larger average widths of the pores as indicated by the hydraulic radii in comparison with the maximum pore radii. The answer may lie in the lower estimates of the surface area of the pastes and will be discussed further in section 4.3.

3.2.7 Summary of the results on pore structure of hcp

(1) The changes in pore structure of hcp from the two effects of w/c ratio and times of hydration could be adequately represented by measurements of the evaporable water contents at 105°C and more accurately by use of a single-point measure of the pore size distribution function, namely the primary continuous pore radius.

(2) The surface areas indicated by mercury intrusion measurements were found to depend mainly on and increase with the initial water/cement ratio but no generally consistent pattern could be established for the effects of times of hydration on pastes of different w/c ratio.

(3) Hydraulic radius accessible to mercury at 2000 kg/cm^2 was introduced to account for the limitations of the single-point pore structure parameter (r_{∞}) obtained from the pore size distributions but it was found to be less sensitive to differences in w/c ratio and times of hydration.

3.3. The relationships between the pore structure of hardened cement pastes and saturated permeability.

In the previous sections, some variables representing the structure of hardened cement pastes were identified. The relationships between these variables and the effects of differences in w/c ratios and times of hydration were presented and discussed. It was shown that adequate descriptions of the combined effects of hydration and w/c ratios could be physically represented by the primary continuous pore radius. The sensitivity of variables such as hydraulic radius, total porosity and surface areas were also compared. It is the purpose of this section to interrelate these measured parameters of pore structure of the pastes to the measurements of saturated permeability, and to identify the simplest and most appropriate definition of the structure of hcp in relation to saturated permeability. Functional relationships that can be used to represent the data presented here will be given in Chapter 4. The emphasis in this section is therefore a critical assessment of the trends observed for the various parameters.

3.3.1 Total porosity and saturated permeability

Total porosity is expressed here on the basis of the total volume of pore space per unit bulk volume of the dry paste at 105°C. It is thus the product of the evaporable water content at 105°C (g/g of dry paste) and the apparent density of the dry paste measured as described in section 2.6.2. The porosity on a unit volume basis is preferred to that on a weight basis (as in table 3.3) because for flow problems one is mainly interested in the units of volumes rather than weight.

The results for the relationships between total porosities and saturated permeability are presented in fig 3.10 for a wide range of porosities and different times of hydration. It is found that the total porosity of hardened cement paste does not relate uniquely to saturated permeability. It can be seen that different functional relationships are necessary to describe porosity and permeability at any time of hydration. Generally, permeability is found to increase exponentially with increases in total porosity at any time of hydration. This is intuitively quite acceptable but great care must be taken in extrapolating this general feature to mortars as will be tentatively demonstrated in further results to be presented.

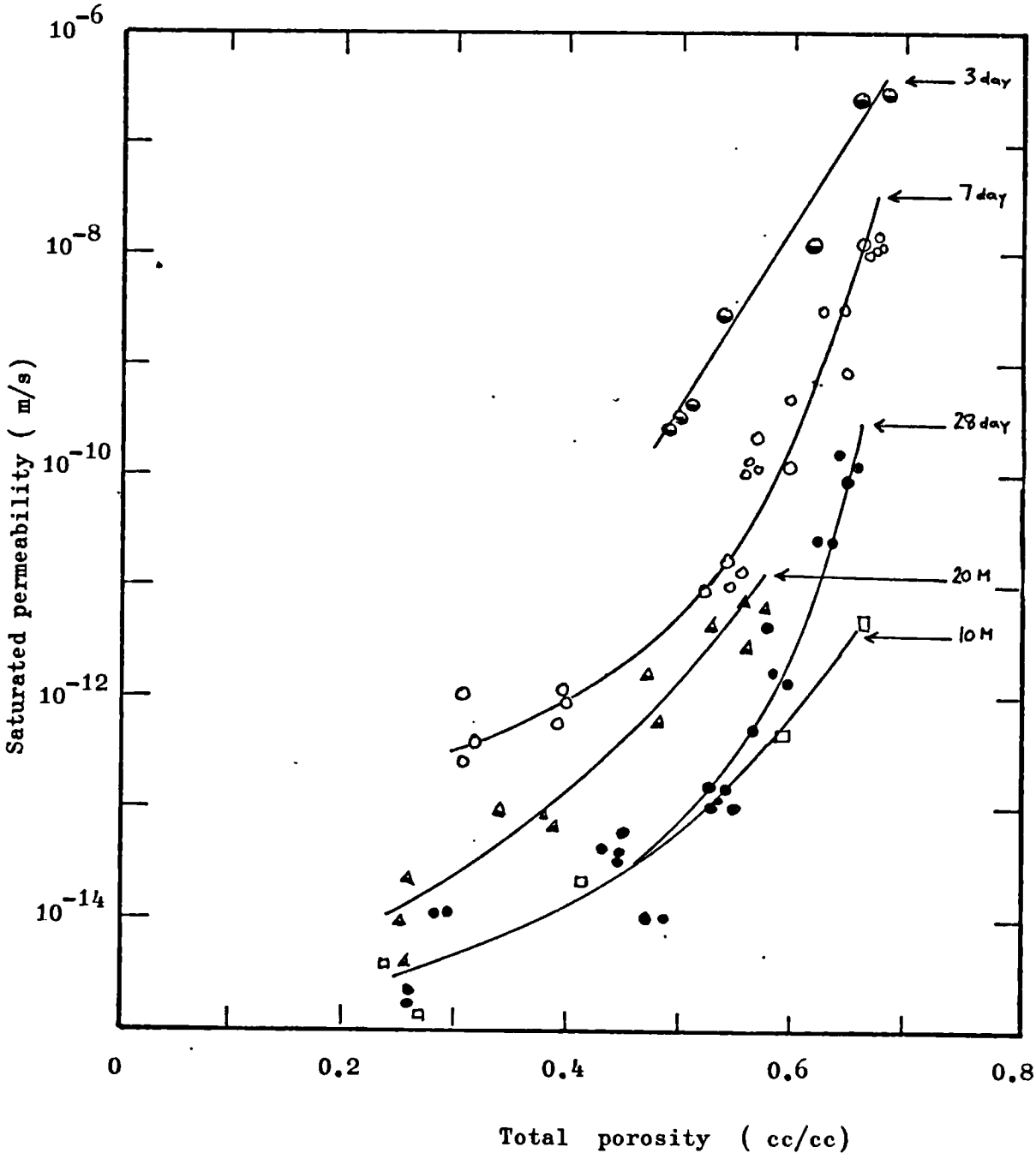

Fig. 3.10: The relationships between total porosity and saturated permeability of hardened cement paste

Approximate smooth curves are drawn for each time of hydration to show the manner in which differing times of hydration affect the total porosity function and it is quite clear that the relationships are unlikely to be simple exponential functions.

At high porosities (approx. 0.6 - 0.7) the results indicate that vast differences in permeability can be found for any particular value of total porosity. This suggests that at high porosities the probability of forming continuous chains of pores is so high that flow rates through hcps can vary enormously, depending on the degree of continuity of pores.

It is also clear that the 20 month porosity function does not follow the trend from 3 days to 10 months and again it can be seen that prolonged curing possibly results in an increase in permeability.

Fig 3.10 indicates that total porosity alone does not adequately and accurately predict permeability for different degrees of hydration. This essentially means that it is necessary to consider the pore size distributions.

3.3.2 Primary continuous pore radius and saturated permeability

The full mathematical description of a pore size distribution function, in the opinion of the writer, is elusive and unnecessarily complicated; therefore the single-point measure of the distributions defined in section 3.2.3 and called the primary continuous pore radius is being selected to represent the structure of the pastes. The primary continuous pore radius varied in a reasonable manner with changes in w/c ratio and times of hydration. It was also possible to observe a close resemblance of its variation with the variation of permeability with w/c ratio and hydration, apart from some anomalies at low w/c ratios and at 20 month curing. This nevertheless provided an encouragement to relate it to permeability.

The relationship between the primary continuous pore radius and the measured saturated permeabilities of the pastes is presented in fig 3.11. It is found that reasonably small scatter is achieved over the entire range of permeability and the primary continuous pore radius.

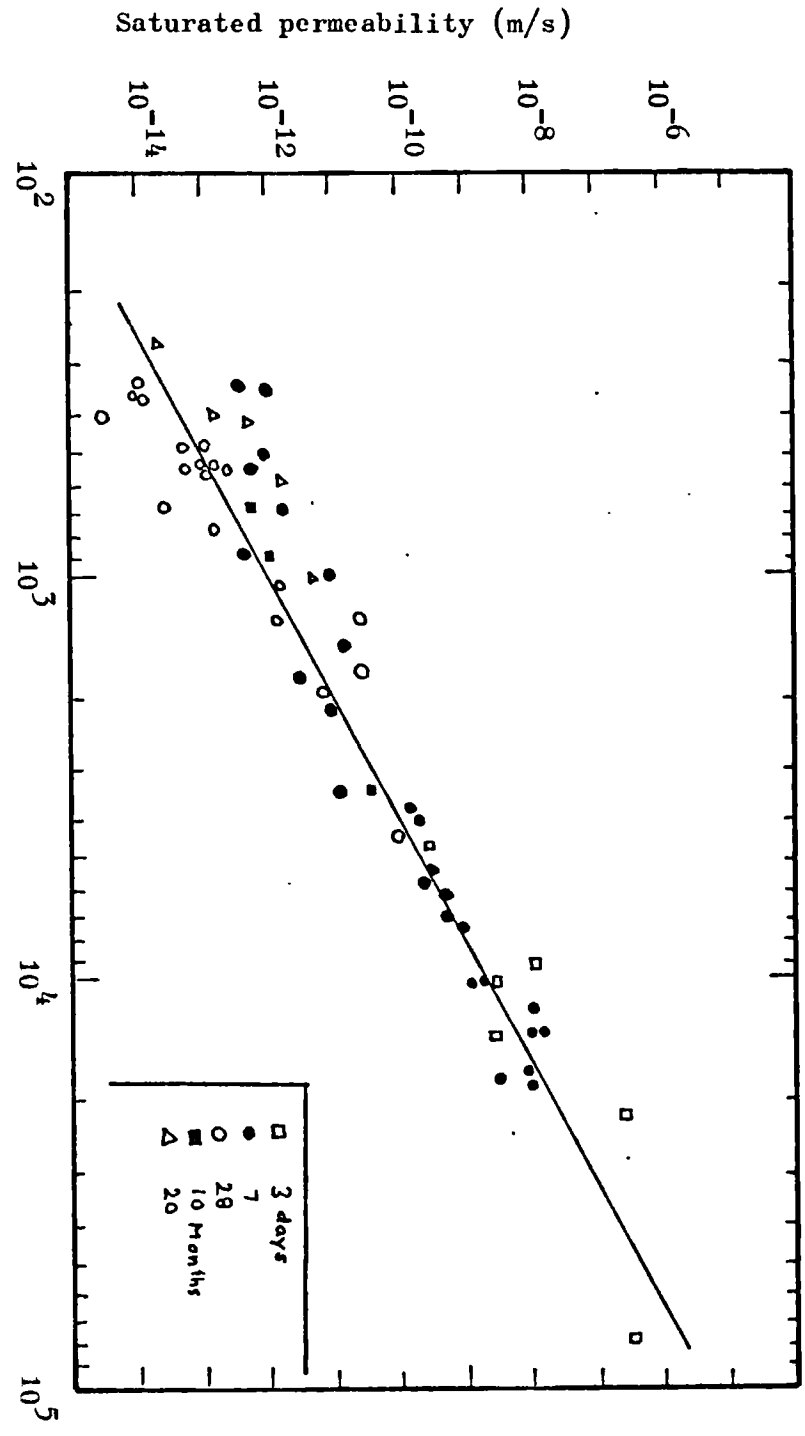

Fig. 3.11: The relationship between the primary continuous pore radius and saturated permeability of hardened cement paste.

In addition it is quite clear that a simple linear log-log relationship can be adequately used to represent the trend of the results for any time of hydration and w/c ratio. This definitely offers an improvement to the total porosity relationship which was found to be multivalued (fig 3.10). Clearly, the scatter progressively increases when the primary continuous pore radius becomes less than approximately 500 A, but this could be explained in terms of the limitations of the measurements or possibly more important, it could be due to the neglect of surface effect at such pore sizes. This possibility will be discussed further in section 4.3.

The important result from fig 3.11, however, is that the primary continuous pore radius provides a close relationship with saturated permeability of hardened cement pastes irrespective of its w/c - ratio or state of hydration, and for practical purposes is a possible permeability predictor of hardened cement paste. It is also intuitively satisfactory in that the flow takes place almost wholly through these large and continuous pores.

3.3.3 Mercury intrusion surface area and saturated permeability

The pore space of hardened cement paste admit the flow of water, whereas the surface area of the products of hydration detract from flow. There is ample evidence from fig 3.11 that the flow of water in hcp is mainly confined to the primary continuous pores, hence it is not inconceivable that the surface area resisting the flow is probably only a fraction of the total available surfaces of the solid phases. Mercury penetrates only a fraction of the total pore volume (see sec.4.3) hence only a fraction of the total surface area is measured. It is difficult to measure the actual fraction of the surfaces resisting the flow. In this section, the fractional surface measured by mercury intrusion is related to permeability. The relationship is presented in fig 3.12. The first and most important point to observe about the surface area relationship is that it is very complicated, and highly ambiguous. In the author's view, the trend lines from the relationship are those shown on the figure. The trends for the 28 day, 10 & 20 month pastes merge and suggest that permeability increases with an increase in the surface area accessible to mercury. The 7 day pastes indicate a similar trend, however, the 3 day pastes could be represented by any topologically admissible curve, including the one shown.

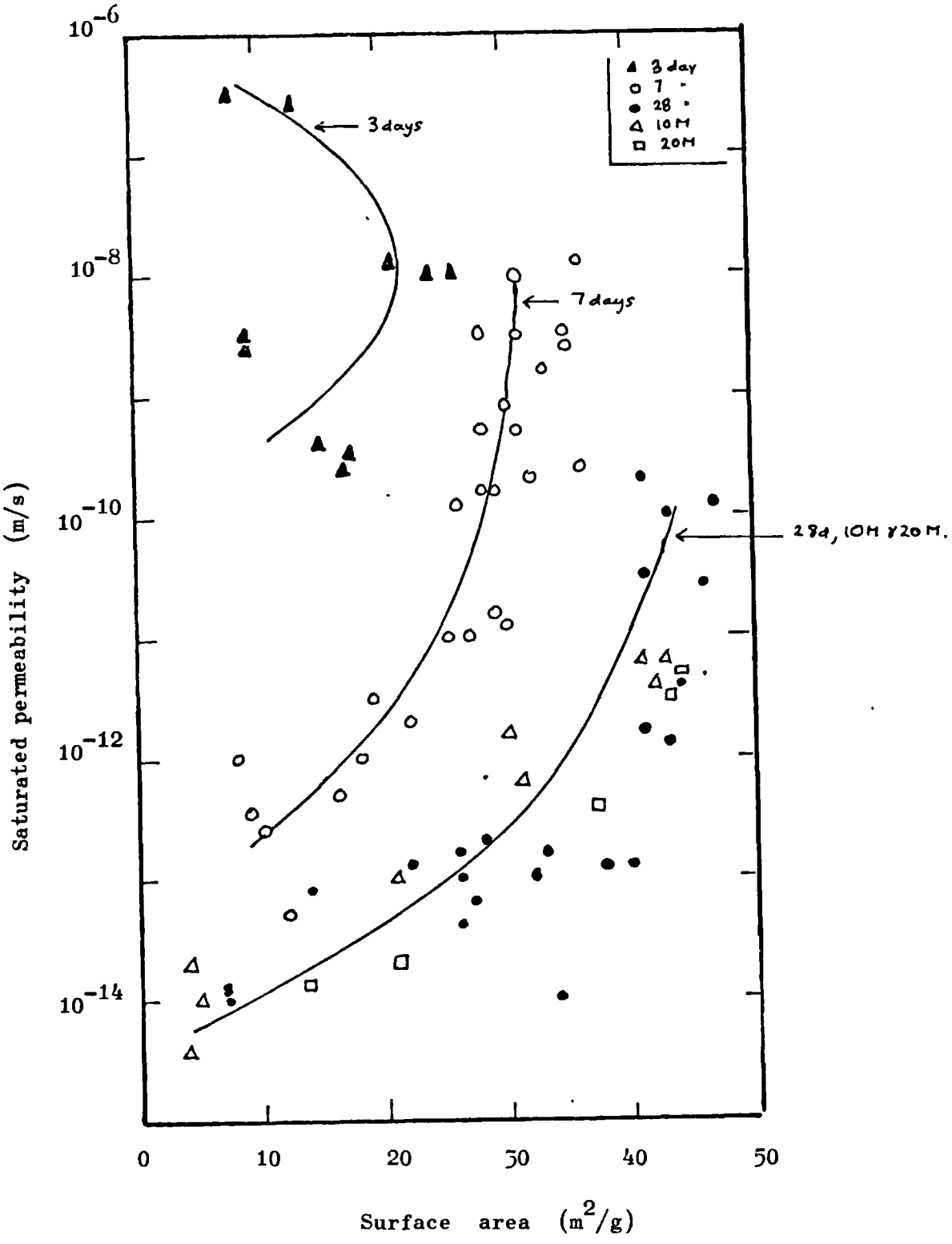

Fig 3.12: The relationship for the surface area and permeability of hardened cement paste.

In section 3.2.5 it was found that the surface area accessible to mercury increases with w/c ratio. It was also shown in sections 3.1.1 that permeability increases with w/c ratio, therefore the increase in surface area with increase in permeability shown for hcps cured for periods other than 3 days is not surprising but it is rather contrary to the acceptable hypothesis that surface area impedes the flow of water - a basic concept embodied in viscous drag theories of permeability[4,77,78]. This is further support for the fact that the measured surface area is not the total surface area, however, no deductions can be made as to the appropriate surface area resisting the flow in hardened cement pastes. All that can be deduced from fig 3.12 is that the surface area accessible to mercury is a multivalued function of saturated permeability and that permeability increases with an increase in surface area, expressed on a unit weight basis.

3.3.4 Hydraulic radius and permeability

The relationship between the hydraulic radius accessible to mercury and saturated permeability of hardened cement pastes is presented in Fig 3.13. It can be seen that a much broader and banded relationship exists between permeability and hydraulic radius in the range from approximately 5000 A to 25000 A where in fact a fair proportion of the pastes of different w/c ratios and times of hydration exist. Since the surface areas indicated by mercury intrusion is very unlikely to be the total surface area of the pastes, this might suggest that the true hydraulic radius is being grossly overestimated. It is therefore possible that the relationship between the hydraulic radius from mercury intrusion and permeability is not a true indicator of the dependence of the two parameters.

Nevertheless, it is quite clear from fig 3.13 that the use of hydraulic radius instead of the primary continuous pore radius did not improve the accuracy of prediction of permeability particularly in the range 5000 - 15000 A. Clearly a further parameter is needed, perhaps a porosity function, to improve the prediction of permeability from the combined functional. This again suggests that the primary continuous pore radius plays a special role in relation to permeability of the hardened cement pastes mainly because it varies over a much larger range of values than all the other parameters so far considered.

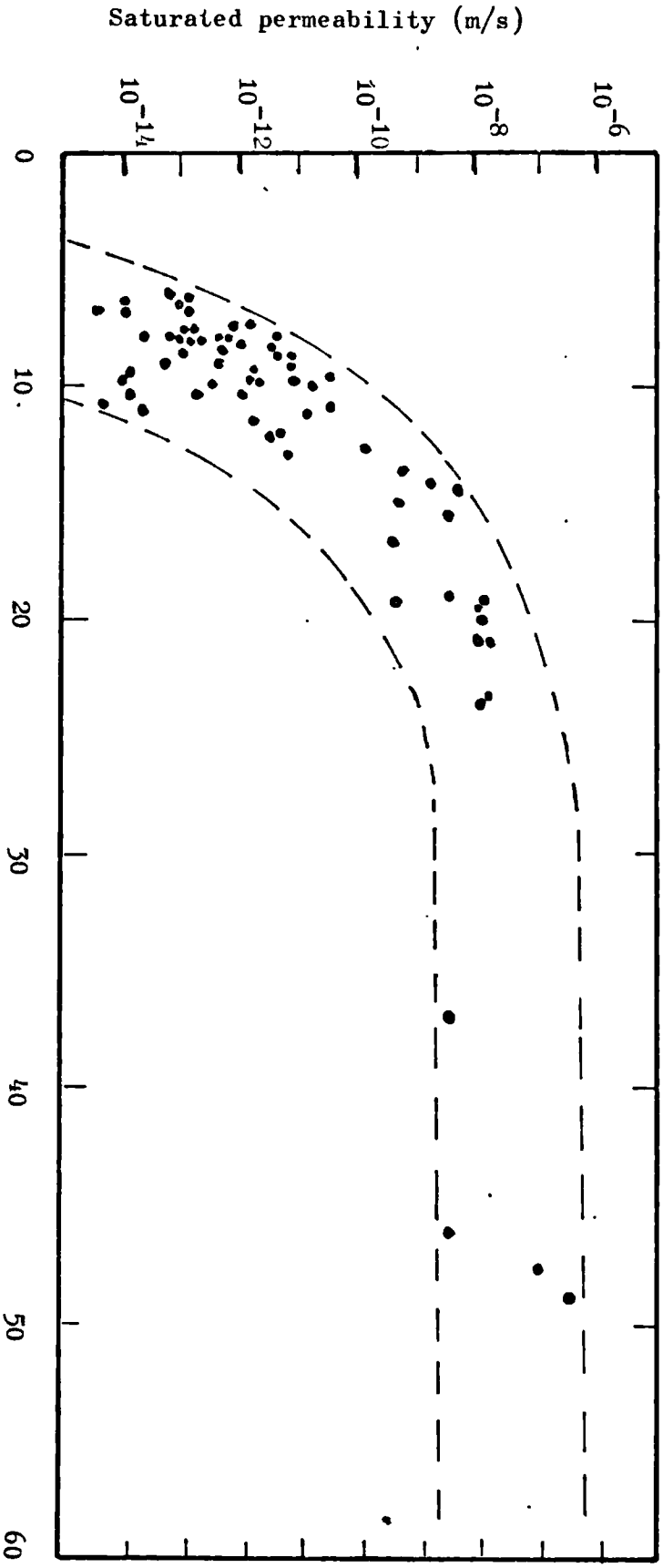

Fig. 3.13: Hydraulic radius in relation to saturated permeability of hcp

Considering the insensitivity of the hydraulic radius to w/c ratio and times of hydration obtained in fig 3.9, the apparent insensitivity of hydraulic radius to permeability of hardened cement pastes shown in fig 3.13 is not surprising.

It may be concluded that the introduction of hydraulic radius to account for the deficiency of the single point pore structure parameter, namely the primary continuous pore radius did not improve on the prediction of permeability, but produced highly ambiguous relationships at values below 15000 A where minor changes in hydraulic radius produce large variations in permeability. The insensitivity of hydraulic radius to permeability of the pastes could be taken to suggest that since from its basic definition, it includes a substantial proportion of the pores in which not much water flow occurs, it tends to underrate the relative magnitudes of the flow in the larger pores in the structure.

The reciprocal of the hydraulic radius can be taken to be the surface area per unit pore volume accessible to mercury. If this definition of surface area is used, then permeability would increase with a reduction in surface area; this would be in contrast to the relationship obtained in section 3.3.3. It could therefore be deduced that the basis of defining surface area per unit weight rather than unit volume is not wholly appropriate for permeability.

3.3.5 Summary of results on pore structure and permeability of hcp

(1) Permeability of hcp increases with increasing total porosity but the relationship is multivalued and depends on whether the mode of change in total porosity derives from changes in w/c ratio or hydration.

(2) The primary continuous pore radius, which is a measure of the maximum spacing between the network structure of the fine individual particles of hydration products could be uniquely related to permeability irrespective of whether the mode of change in pore structure results from different w/c ratio or hydration.

(3) Hydraulic radius of the pastes was found to be less sensitive to permeability than the primary continuous pore radius, but tends to increase with increasing permeability.

3.4 Permeability of mortars

Mortars were tested mainly to elucidate the effect of inclusion of particles in hardened cement paste on permeability and pore structure of the resulting composite. The bounds of the composite are therefore

(1) all hardened cement paste

(2) all aggregate

The results to be presented will be for two types of aggregate inclusions i.e lightweight and normal sand particles.

3.4.1 Effect of aggregate volume concentration

The effects of volume concentration of the aggregates were studied by varying the sand:cement ratio up to 3:1. The sand:cement ratios by weight were based on that of the normal sand. The lightweight aggregate, which was approximately 1.6 times less dense than the normal sand,was combined with the hcp to give an equivalent volume concentration as that of the normal sand. The results of the mean permeabilities at different volume concentrations of aggregate are given for the mortars in table 3.6.

TABLE 3.6 Effect of volume concentration on permeability of mortars hydrated in water for 28 days (w/c = 0.47)

sand:cement	aggregate vol.% conc **	Permeability 10^{-15} m/s: normal mortar	No. of tests	lightweight mortar	No.of tests
hcp	0	56.9	8	56.9	8
0.5:1	24	3.7	3	10.0	3
1:1	38	7.4	3	12.3	3
2:1	55	6.9	3	20.1	3
3:1	65	22.5	3	78.3	3

** The volume concentration of the aggregate was calculated from the relationship

$$V_a = (x/d_a) \,/\, (x/d_a + 1/d_{hcp}) \qquad (3.1)$$

where x = sand cement ratio by weight

d_a = dry density of aggregate (normal sand)

d_{hcp} = dry density of hardened cement paste

V_a = aggregate volume concentration (%)

The results indicate that normal sand mortar is less permeable than the hcp up to a sand:cement ratio of 3:1, whereas the lightweight mortar is only less permeable than the hcp up to a ratio of 2:1. It is also clear that there is an increase in permeability with increasing volume concentration for both types of mortar. The lightweight mortar is found to be barely about three times more permeable than the normal mortar. The results are illustrated on fig 3.14a and it can be seen that the rapid increase in permeability commences at a sand:cement ratios greater than 2:1. In the casting of mortars of higher sand:cement ratios than 3:1, it was found that a gapped and segregated structure forms which appeared to be obviously more permeable than perhaps even the pastes with w/c ratios above 0.71. This high permeability mortar was used to smoothen the hydraulic circuit as described in section 2.4.2.

The rather small differences in the permeability of the lightweight mortar in comparison with the normal mortar is surprising and will be further discussed in relation to pore structure. Also the fact that the addition of a small amount of aggregate seems to drastically reduce permeability in comparison with the neat paste, if real, would seem to indicate an important effect of the addition of aggregates to pastes because it would normally be expected that as the volume concentration of the aggregate approaches zero, the composite should tend to have the properties of the neat paste.

It should also be noted that the permeability of the mortars is of the extremely low order of magnitude of 10^{-15} m/s which is roughly in the range of that of the 0.23/10m-20m samples of hcp. Indeed the lowest permeability value obtained in the whole of this investigation was found for a normal mortar with a sand:cement ratio of 2:1. It was approximately 9×10^{-16} m/s - with this record low value and considering the hydraulic gradient imposed of some 70000, it is possible to suggest that the sample had virtually zero permeability.

3.4.2 Effect of sand particle size

One-size aggregate mortars prepared with a sand cement ratio of 2:1 were investigated. The results are presented in table 3.7 and illustrated on fig 3.14b. It can be seen that no significant changes in permeability result from using different particle sizes in the size range given and at the sand:cement ratio of 2:1. This implies that if any fissures form around the aggregate particles

INSERT

Insert on page 151 after line 24

The aggregates were laboratory dried, so that the effect of absorption of water from the paste by the dry aggregates could lead to the reduction of the local w/c ratio around the aggregate particles, resulting in an overall reduction in the effective w/c ratio, and hence the permeability.

Estimates of the possible changes in the effective w/c ratios based on the assumption that the aggregates absorb water from the paste and become fully saturated indicate changes from 0.47 to 0.43 and 0.47 to 0.32 for the normal and lightweight mortars respectively at the highest volume concentration of 65%.

Since,
(1) Complete saturation of aggregates is highly unlikely to occur
(2) The differences in permeability of pastes with w/c ratios below 0.47 are small (fig 3.1) in comparison with those caused by the effect of the addition of aggregates

it follows that
(1) The moisture condition of the aggregates will not produce a substantial influence on permeability of mortars at the low w/c ratio levels (less than 0.47)

(2) but could be significant at higher w/c ratio levels where minor differences in w/c ratios around the aggregate particles could result in relatively greater decrease in permeability of the paste-aggregate interfacial material. Such high w/c ratios were not used in the mortar tests in this thesis.

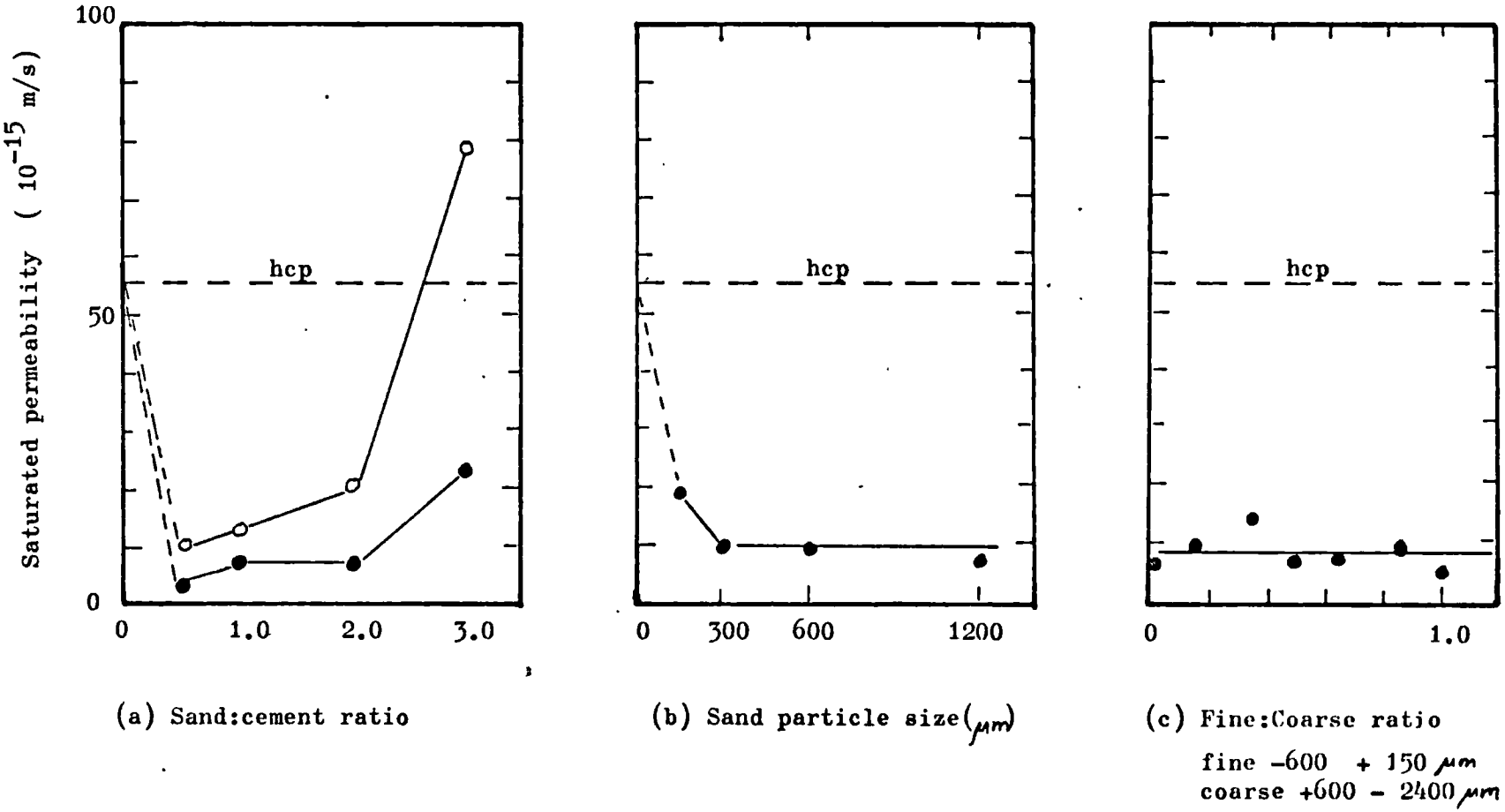

Fig. 3.14: Effects of particle sizes and sand:cement ratio on permeability of mortars (w/c 0.47/28 day)

of different sizes, they do not depend on particle size in the range used. Again it can be seen that the permeability of the one-size aggregate mortars is less than the hcp of the same w/c ratio.

TABLE 3.7 Effect of sand particles size on permeability of mortars (sand:cement 1:1 w/c = 0.47)

Particle size (μm)	Mean permeability (10^{-15}m/s)	No of tests
1200	7.1	2
600	9.7	3
300	9.9	3
150	19	2

3.4.3 Effect of different sand grading

Sand was graded by combining sand particles in the range -2400μm + 600μm with that in the range -600μm + 150μm at different proportions. The results of the permeability measurements are presented in table 3.8 and illustrated in fig 3.14c. Again it can be seen that the permeability is less than that for the corresponding hcp of the same w/c ratio but no significant differences in permeability results from the different combination of sand particles. This would seem to indicate that the mode of packing of the sand particles in the range investigated has practically no effect on the permeability at the sand:cement ratio of 2:1.

TABLE 3.8 Effect of grading of sand on permeability of mortars (sand:cement 2:1)

Ratio of -2400:-600μm	Permeability (10^{-15}m/s)
1.0	4.6
0.85	9.8
0.65	7.7
0.50	7.8
0.35	15
0.15	10
0.0	6.0

3.4.4. Summary of permeability of mortars

The results presented on the permeability of mortars can be summarised as follows

(1) Addition of both lightweight and normal sand to hcp initially reduce permeability.

(2) An increase in volume concentration of aggregate in mortars increases permeability.

(3) Sand grading and sand particle sizes have no significant effects on the permeability of mortars in the range of particle sizes used.

(4) Lightweight mortar is not substantially more permeable than normal mortar.

Points (2) and (4) suggest that predictions of permeability of mortars from a mathematical model probably need to account only for

(a) volume concentration

(b) permeability of hcp (and/or aggregates)

The fact that both lightweight and normal sand reduced permeability of mortars implies that the permeability of the aggregate is probably not a significant variable but this has not been measured: however it is possible to make deductions from the continuity of pores as obtained from the pore size distributions of the aggregates (see section 4.4)

3.5 Pore structure of mortars

The pore structure of mortars was studied to elucidate the third mode of change of pore structure by the inclusion of aggregate at different volume concentrations. Two modes of change i.e initial w/c ratio and hydration were studied for the hardened cement paste and it was shown in sections 3.2.1 and 3.3.1 that these modes of change affect total porosity differently and also relate to permeability in different forms, resulting in non-unique functional relationships between porosity and permeability. The mode of change associated with aggregate inclusion is presented in this section.

3.5.1 Total porosities and densities of mortars

The mean values of the total porosities of mortars measured by drying at 105°C at the conclusion of steady state permeability measurements are presented for mortars at different volume concentration of aggregates in table 3.9. The dry densities are also given and the corresponding values for the pastes of the same w/c ratio and the aggregates are compared. The aggregate porosities were measured by drying the particles retained on the 1200μ sieve at 105°C, resoaking in water for approximately ten days, then surface drying with damp tissue before determining the evaporable water contents at 105°C.

TABLE 3.9 Densities and porosities of mortars
(w/c = 0.47, 28 days curing)

Sand:cement	**Vol. conc. of aggregate (%)	Normal mortar density (g/cc)	Normal mortar porosity (cc/cc)	Lightweight mortar density (g/cc)	Lightweight mortar porosity (cc/cc)
hcp	0	1.55	0.456	1.55	0.456
0.5:1	24	1.87	0.336	1.76	0.389
1:1	38	1.88	0.273	1.68	0.371
2:1	55	2.09	0.235	1.69	0.350
3:1	65	2.13	0.221	1.67	0.358
aggregate	100	2.50	0.140	1.59	0.337

It is found from table 3.9 that the lightweight aggregate is less porous than hcp but more porous than the normal aggregate. Both aggregates are however less porous than the hcp. The results are presented on fig 3.15 to show the variation of porosity and densities with volume concentration. It can be seen that the addition of both types of aggregate to the hcp reduce the total porosity and increase density as the volume concentration increases. On the basis of the mean permeabilities presented in table 3.6 it was found that permeability of mortars increases with increasing volume concentration thus it appears here that the reduction in total porosity is not necessarily associated with a reduction in permeability of mortars. This is a highly significant feature of the relationship between total porosity and permeability associated with the mode of change of the pore structure caused by the inclusion of aggregate in pastes and will be further discussed.

** see equation 3.1 (section 3.4.1)

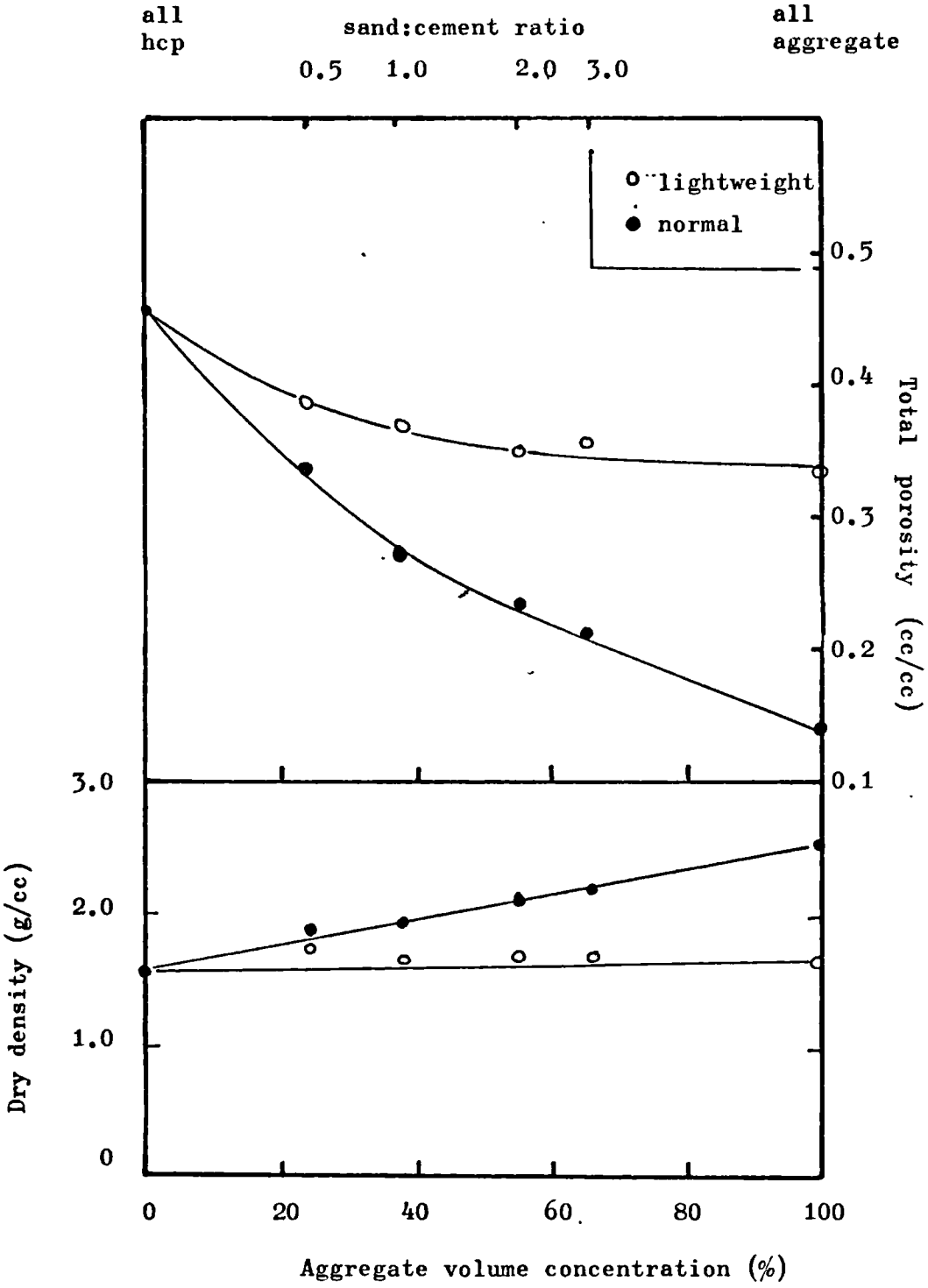

Fig. 3.15: Effect of aggregate volume concentration on densities and total porosities of mortars.

3.5.2 Pore size distribution of mortars

The changes in the pore size distributions of mortars resulting from the addition of the two types of aggregate to the pastes are examined in this section. Fig 3.16 is presented to show the relationship between the pore size distributions of the hardened cement paste and the aggregates. The distributions of the aggregate pore sizes were determined by using particles retained on the 1200μm sieve. It can be seen from fig 3.16 that the lightweight aggregate has a coarser pore structure than the normal aggregate. The total intruded pore volume can be seen to be greater for the lightweight aggregate than the normal aggregate. It can be seen that whereas much of the pore volume of the normal aggregate and the hcp occur in pore sizes below approximately 1000 A, the pore sizes within the lightweight aggregate are within the entire measurable range of pore sizes, and exhibit no threshold range of pore sizes. This characteristic of the lightweight aggregate pore structure might tend to indicate that the flow of water in the aggregate may not be concentrated within specific continuous channels as found for the case of the hcps. The influence of the addition of the aggregates to hcp are examined in the next section.

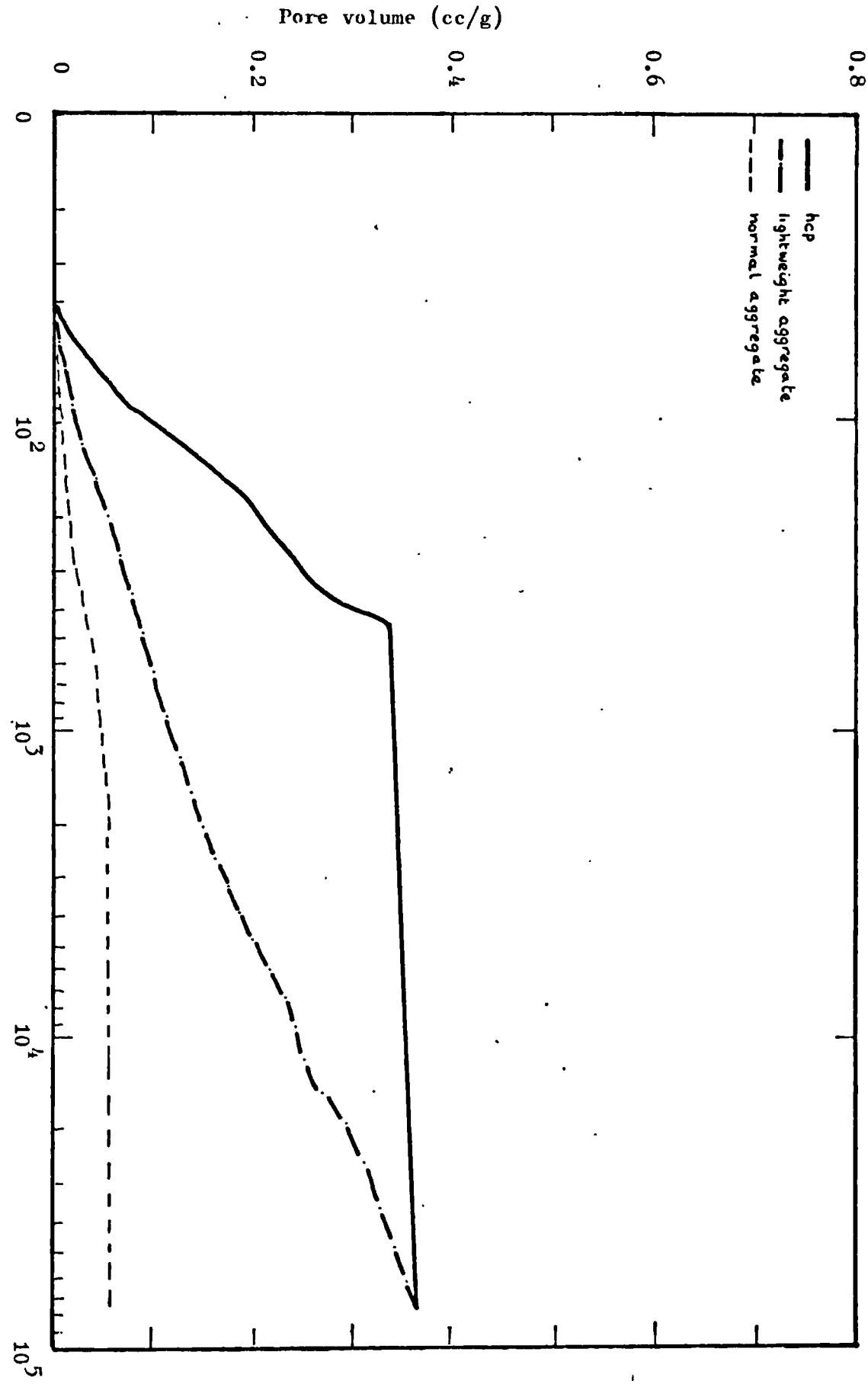

Fig. 3.16: Cumulative pore size distributions of the hardened cement paste, normal and lightweight aggregate.

3.5.2.1 Influence of volume concentration.

The distributions of pore sizes for the lightweight mortar are presented in fig 3.17 for typical samples of differenct volume concentrations. For the purpose of recognising the effect of the addition of the lightweight aggregate to hcp on the distributions, the results for the distribution of the aggregate pores and that of the hcp are also shown. It can be seen from fig 3.17 that the total intruded pore volume reduces with increasing volume concentration. The most distinct feature of the distribution concerns the threshold ranges of the mortars. The very sharp knee for r_∞ progressively flattens out as the volume concentration increases and generally shifts to the larger pore size range, until at a volume concentration corresponding to sand:cement ratio of 3:1 the knee is virtually non existent. The lightweight aggregate pore structure is shown to be coarser than that of the hcp but it does not have the characteristic range of pore sizes at which very little intrusion occurs as found for the hcp. The distribution curve is approximately a linear function of the logarithm of pore radius for the lightweight aggregate, and it is quite clear that with increasing volume concentration, the distribution curve for the mortars tend to that of the aggregate, that is the range of pore sizes increases and the curves tend to be linear. This implies that pore size distributions associated with the mode of change of the inclusion of aggregate could be regarded to comply with a simple addition law in a mathematical model of the composite, which is of great theoretical appeal. The progressive flattening out of the knee associated with the primary continuous pore radius with increasing volume concentration would also tend to indicate that this parameter which was successfully used to represent the modes of change of pore structure associated with both w/c ratio and hydration of pastes may not be particularly useful for mortars. An attempt will be made with the correlation between the various pore structure parameters later.

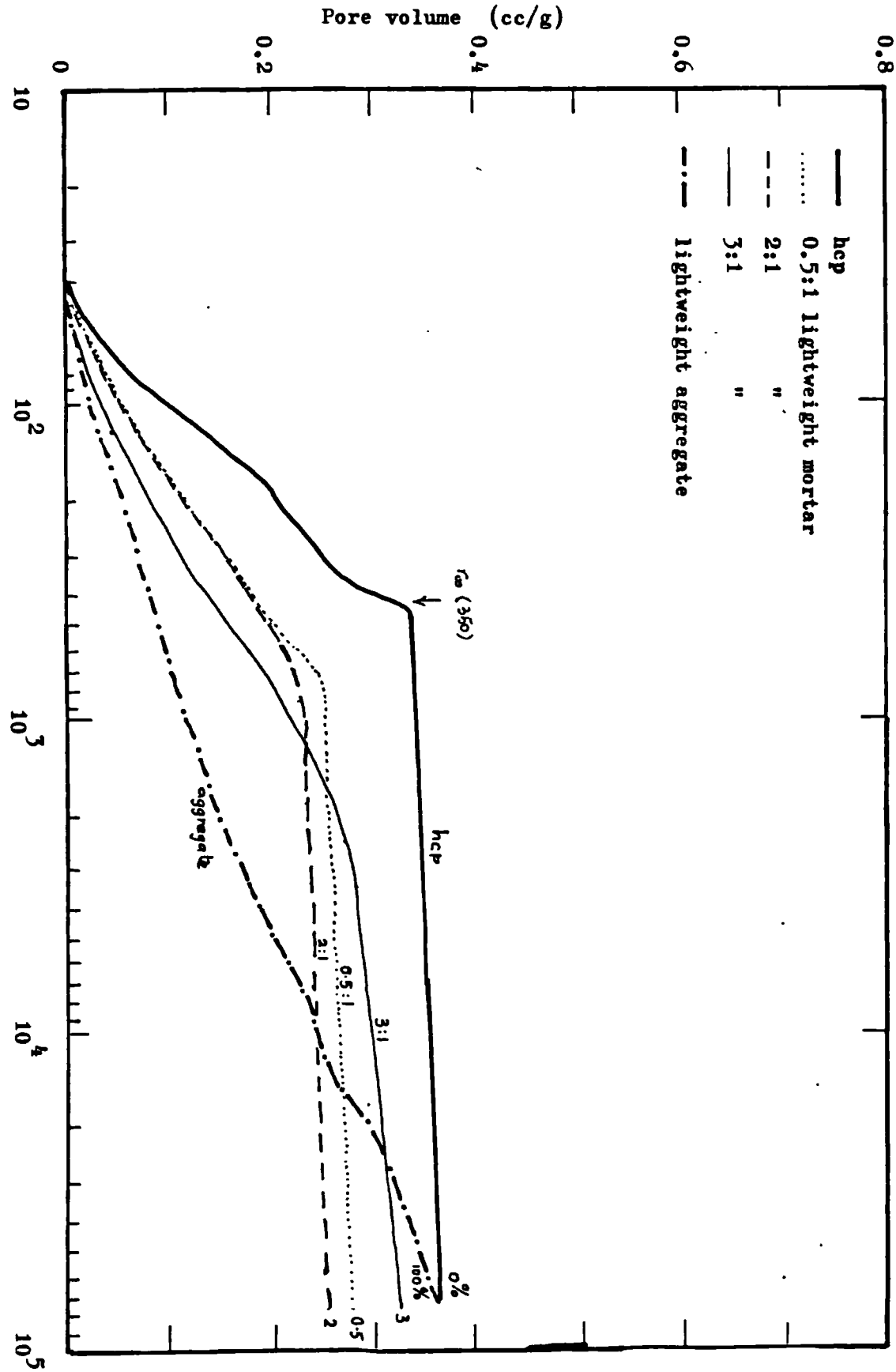

Fig 3.17: Effect of aggregate volume concentration on pore size distributions of lightweight mortar

3.5.2.2 Primary continuous pore radius and mode pore radius of mortars.

The same definitions of the primary continuous pore radius and mode pore radius given for the hardened cement pastes were applied to the pore size distributions of the mortars to investigate their appropriateness for the mode of change of pore structure associated with aggregate inclusions. The mean values for mortars obtained from the computer analysis of the distributions are given in table 3.10.

TABLE 3.10 Primary continuous pore radius and mode pore radius for mortars of different aggregate volume concentration

sand:cement	Agg. vol. conc. (%)	normal mortar		lightweight mortar	
		r_∞	r_{mode}	r_∞	r_{mode}
hcp	0	460	460	460	460
0.5:1	24	650	650	730	730
1:1	38	790	430	690	630
2:1	55	3060	580	710	530
3:1	65	75000	530	16970	430
aggregate	100	130	130	75000	75000

It can be seen that despite the relatively low value of the primary continuous pore radius for the normal aggregate in comparison with the hardened cement paste, the addition of normal aggregate to the paste tends to increase the primary continuous parameter of the mortar with increasing volume concentration. The mode pore radius is however not significantly affected by increasing volume concentration for both types of mortars and its variation with increasing volume concentration lacks order. It is highly probable that this is due to variable formation of fissures within the mortars. The most important point here is that despite the large variations in the primary continuous pore radius of mortars with increasing volume concentration of aggregates, the permeability values obtained in table 3.6 increases barely to one order of magnitude. If this nature of permeability variation is compared with that found for the hardened cement paste (section 3.3.2) then it can be seen that the functional relationship between the primary continuous pore radius and permeability of mortars cannot be the same as for hardened cement pastes. This is shown in fig 3.18.

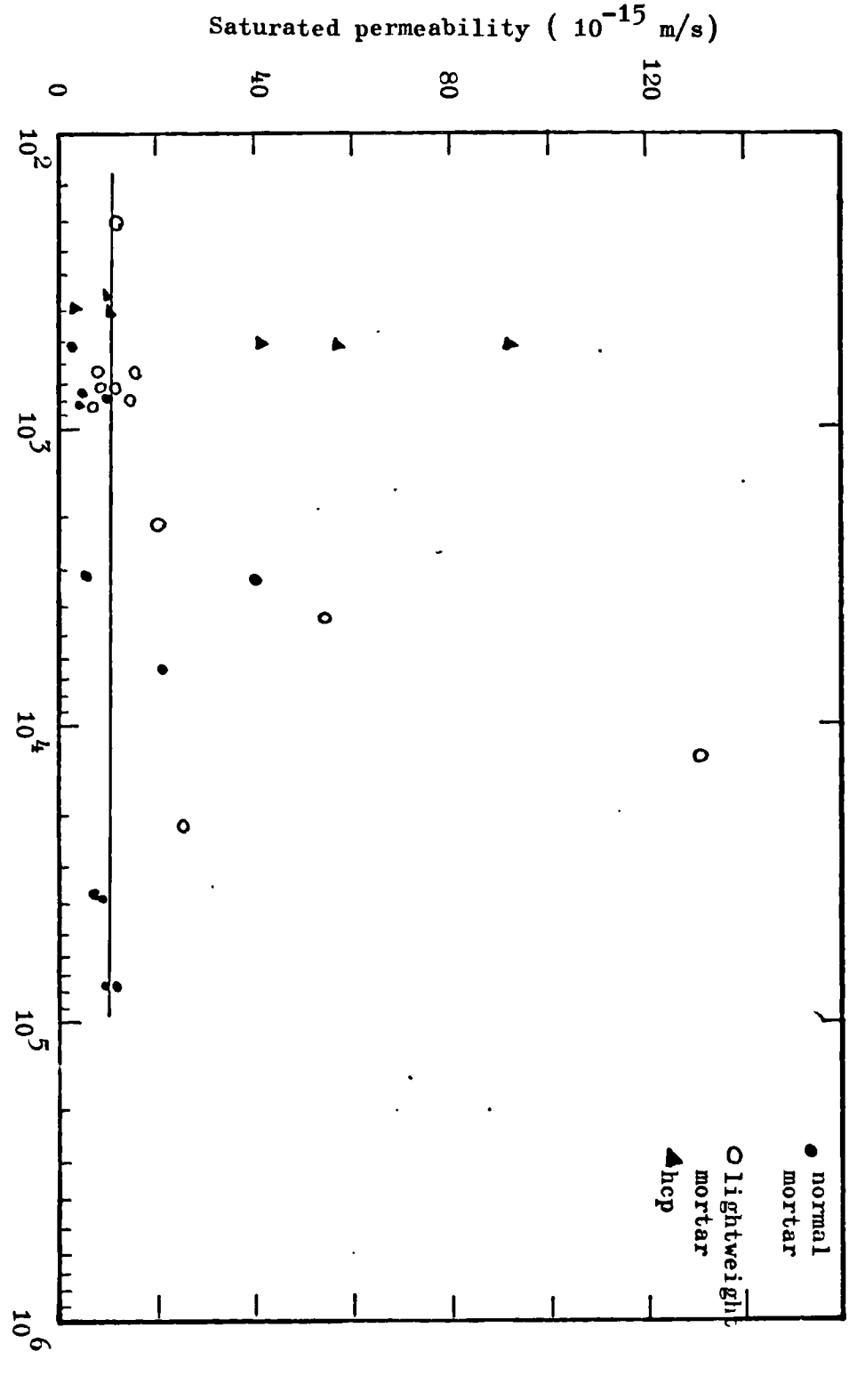

Fig 3.18: The relationship between the primary continuous pore radius and permeability of mortars.

3.5.2.3 Surface area and hydraulic radii of mortars

The surface areas and hydraulic radii accessible to mercury at 2000 kg/cm^2 are given for the mortars in table 3.11.

TABLE 3.11 Surface area and hydraulic radii of mortars

sand:cement	Agg. vol. conc. (%)	Normal mortar Surface (m^2/g)	r_h (A)	Lightweight mortar surface (m^2/g)	r_h (A)
hcp	0	27	7360	27	7360
0.5:1	24	10	12060	12	12460
1:1	38	6	13470	12	12770
2:1	55	4	17320	14	10310
3:1	65	4	17610	13	11810
aggregate	100	4	76	14	130

It can be seen that the surface areas of mortars are less than those of the hcp and remain practically constant as the volume concentration of the aggregate increases. On the basis of the mean permeabilities presented in table3.6, permeability increases with increasing volume concentration. The hydraulic radius of the normal mortar increases with increasing volume concentration whereas that of the lightweight mortar tends to reduce. The most important result from table 3.11 is that the hydraulic radii of the normal mortar are consistently greater than those of the lightweight mortar. But it was found from table 3.6 that the permeability of the normal mortar is less than that of the lightweight mortar. (?) and it is also known from fig 3.13 that the hydraulic radii of hcps generally tend to increase with increasing permeability.
The hydraulic radius is a measure of the average width of the pores so how is it possible that the larger average width of the pores of the normal mortar in comparison with that of the lightweight mortar does not represent a higher permeability of the normal mortar? It would appear that the mode of change of pore structure associated with aggregate inclusion does not uniquely relate to hydraulic radius.

3.5.3 Total porosity and permeability of mortars

The relationship between total porosity and permeability of mortars is presented in fig 3.18. It can be seen that in the range of porosity of 0.2-0.45, the permeability of both lightweight and normal mortar is generally less than 10^{-14} m/s. The trend lines indicated on fig 3.18 tentatively suggest that

(a) permeability increases as porosity reduces
(b) the permeability-porosity relationship for lightweight mortar is not the same as normal mortar.

The trend lines clearly need to be definitely established by more measurements. In section 3.5.1 it was found that the inclusion of aggregate of lower porosity than the hcp reduces porosity of mortar but increases permeability when considered on the basis of mean values, hence the trend lines suggested on fig 3.18 are not unreasonable. It should be possible to study this effect more closely by changing the water/cement ratio of the pastes.

3.5.4 Summary of pore structure and permeability of mortars.

With an increase in the volume concentration of aggregates of lower total porosity than the hardened cement paste

(1) The primary continuous pore radius was not as sensitive to the permeability of mortars as found for hcp.

(2) The hydraulic radius of normal mortar was greater than that of the lightweight mortar but permeability was not.

(3) Total porosity decreases but permeability increases.

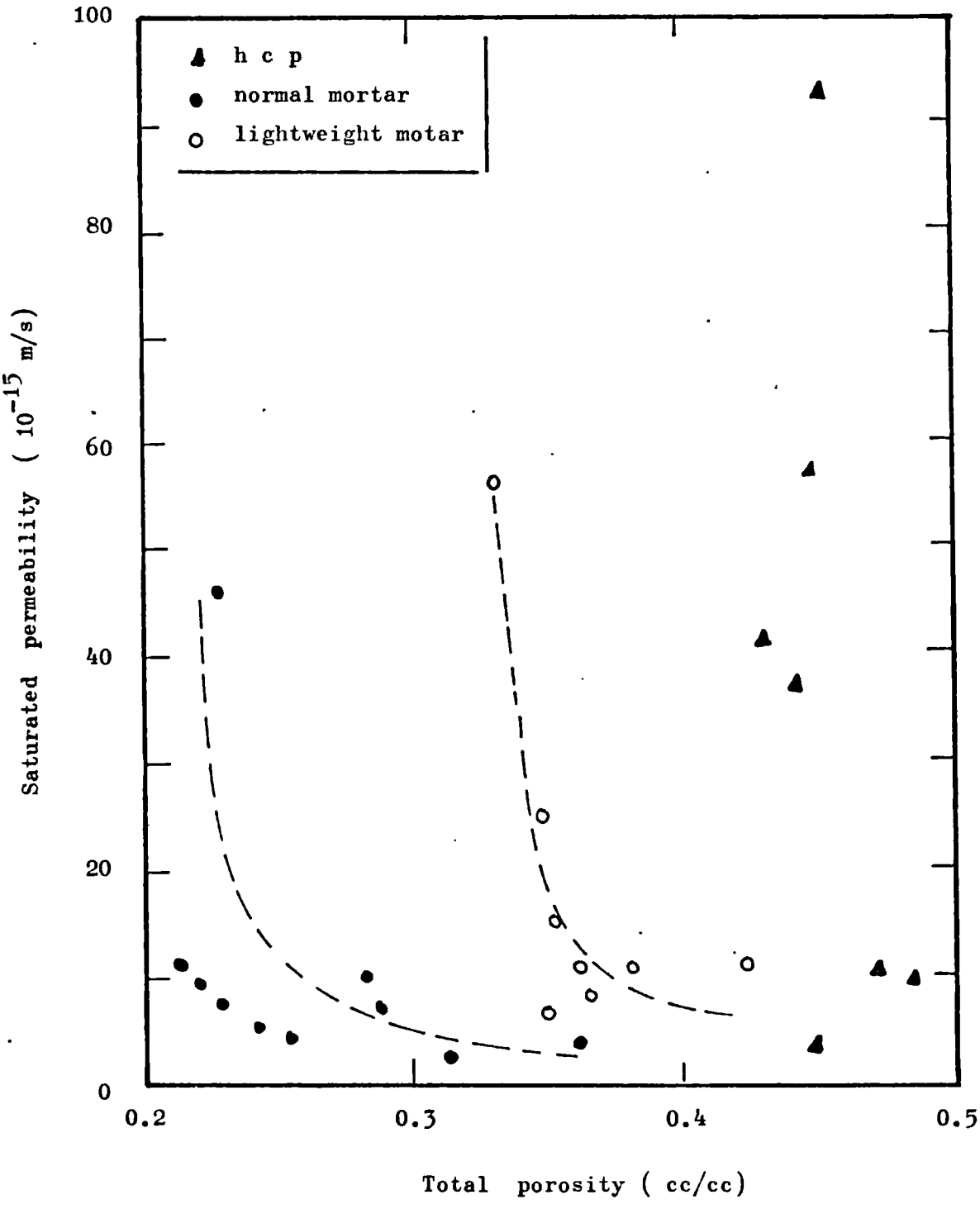

Fig. 3.19: The porosity-permeability relationship for mortars and hcp with a w/c ratio of 0.47,hydrated for 28 days in water.

CHAPTER 4

DISCUSSION OF RESULTS

The results in chapter 3 were discussed briefly while being presented. This chapter attempts to discuss the main implications of the results in greater depth. Functional relationships between the variables of the structure of hardened cement pastes and permeability are developed here and interpretations of the results made. Comparisons with previous results from published works are also made.

4.1 The significance of water/cement ratio and hydration

The contributions from Powers and Brownyard[9] provided much of currently accepted data on the differing effects of water/cement ratio and hydration on changes in permeability of hardened cement paste. The results presented in fig 3.1 and 3.2 generally confirm their conclusions regarding the increases in permeability with increasing w/c ratio and reductions in permeability associated with increased hydration. In addition, it has been found that permeability is highly sensitive to minor variations in sample homogeneity resulting from preparation of samples; therefore, predictions from w/c ratio is at best achieved in terms of the order of magnitude. This essential characteristic of the property of permeability of hardened cement pastes and concretes was first noted by Ruettgers and others[93] who suggested that permeability should be expressed as a logarithmic index as done for pH of solutions and clearly with the range of values obtained from table 3.2 approaching one hundred millions for permeability of pastes, this idea should be of great practical significance. Perhaps the method of measuring permeability suggested by Figg[100] could serve as a pseudo-pH meter.

The data summarised in table 3.2 for the variations of permeability of hardened cement paste prepared with different water/cement ratios and hydrated for different times could be fitted to the power law equation of the type stated in equation 4.1

$$K_{mean} = K_o\,(t)\,(w/c)^{b(t)} \qquad (4.1)$$

where,

K_{mean} = mean saturated permeability (m/s)

$b(t)$, $K_o(t)$ = empirical constants related to time of hydration in days

The values of the empirical constants are summarised in table 4.1 together with the correlation coefficients and ranges of validity of w/c ratios as determined from the measurements.

TABLE 4.1 Constants of regression for the relationship between water/cement ratio and time of hydration on permeability of hardened cement pastes.

Time of hydration (days)	$K_o(t)$	b(t)	correlation coefficient	w/c Range of validity
3	3.00×10^{-7}	8.82	0.999	0.47-1.00
7	5.62×10^{-9}	8.73	0.987	0.35-1.00
28	2.40×10^{-11}	5.76	0.875	0.23-1.00
10 months	2.88×10^{-12}	5.14	0.974	0.23-1.00
20 months	2.09×10^{-11}	5.92	0.967	0.23-0.71

It is found from table 4.1 that, with the exception of the 20 month samples the constants $K_0(t)$ and b(t) reduce with time of hydration; thus both parameters change in a manner consistent with the effect of curing on permeability. The correlation coefficients can also be seen to be reasonably high at all times of hydration but it should be noted that the equations were derived from mean permeability values, which according to the data presented in fig 3.1 and table 3.1 only represent variations of permeability to one order of magnitude for any water/cement ratio. Typical comparisons of the fit of data to the empirical equations are made in table 4.2.

TABLE 4.2 Comparison of accuracy of prediction of permeability from the constants of regression in table 4.1

Sample	Mean permeability (m/s)		$\frac{K_{actual}}{K_{predicted}}$
	Predicted	Actual	
.23/28	$5.1\ 10^{-15}$	$3.08\ 10^{-14}$	6.04
.47/28	$3.1\ 10^{-13}$	$5.69\ 10^{-14}$	0.18
.71/28	$3.3\ 10^{-12}$	$1.59\ 10^{-12}$	0.48
1.0/28	$2.4\ 10^{-11}$	$1.38\ 10^{-10}$	5.75

The variation of b(t) and $K_o(t)$ with time of hydration was found to lack order hence it was decided not to generalise the relationship between time of hydration, water/cement ratio and the mean permeability.

The results of the 20 month samples neither confirm the increase in permeability due to leaching of alkali reported in reference 22 nor establish that prolonged curing results in an increase in permeability because all these specimens were cast at different times and considering the nature of variability reported in section 3.1.1, it is not at all certain whether the observed differences are real. It must be pointed out that all the specimens tested at each time of hydration showed some degree of leaching of calcium hydroxide which were found to render the capillary flow tubes stained with dried crystals on drying. Large deposits of calcium hydroxide crystals were often found on the surfaces of the water-cured samples at the conclusion of the curing periods. It was generally thought that because of the rather high pressures used in these tests, osmotic pressure due to calcium hydroxide contents of the pastes would be insignificant and therefore not affect the flow rates. In any case, it is not certain whether for the purposes of assessing permeability, soluble hydration products such as calcium hydroxide need be considered as part of the solid phase or pores. The extra complication found at longer times of hydration suggests that this particular aspect needs reconsideration for future work, as it must bear an influence on practical situations where steady and long term percolation may occur in structures.

It may be concluded that

(1) Curing in water reduces permeability of hardened cement pastes at least up to 10 months due to hydration but there is an uncertainty about the opposing effects of hydration and possible loss of calcium hydroxide on permeability at later stages of curing.

(2) An increase in water/cement ratio definitely results in an increase in permeability at all stages of curing.

(3) The relationship between w/c ratio and permeability is banded to approximately one order of magnitude mainly because of the difficulty in accurately reproducing specimens of the same w/c ratio in the laboratory, and the large influence such minor variations have on permeability.

4.2 On the significance of total porosity, pore continuity and the primary continuous pore radius in relation to permeability

A porous material is permeable to fluids not because of its porosity but because of extent of the continuity of the pores within its structure. The concept of pore continuity is generally accepted [109,111,112] to be essential in relation to permeability, but until recently[28,32] no direct experimental definition and interpretation of pore structure data had been provided. Powers and Brownyard[9] made a distinction between capillary porosity and gel porosity of hardened cement pastes and on the basis of this division of the pore structure of the pastes found good correlations between the capillary porosity of pastes to that of permeability. Winslow and Diamond[28] concluded from their studies of pore size distributions and fracture surface of hcp that the pore structure of hcp consist of space between hydration products and is neither capillary nor gel porosity. They identified the threshold diameter of pastes and interpreted it to correspond to the minimum geometrically continuous pore diameter, and thus provided a means of identifying pore continuity in hardened cement pastes.

In the present investigation, the maximum value of dv/dp is used to locate the threshold diameter from the pressure-volume data and is called the primary continuous pore radius (see section 2.7.2.2) because

(1) It has been found to be primarily responsible for carrying the water flow in hcp (fig 3.11)
(2) It is thought to correspond to the maximum spacing between the weakest links in the bonds of hydration products (plate 1.1).
(3) It can be associated with the particular definition used in this thesis.

The results presented in table 3.4 and fig 3.6 generally show the nature of the variation of the primary continuous pore radius with hydration to be similar to that found for the threshold diameter[28] but differs in that nearly steady state values appear to occur after 28 days hydration for the intermediate w/c ratios instead of 7 days. At the low w/c level (0.23), no substantial variation in the primary continuous pore radius occurs from 7 days hydration, whereas at high w/c ratios (1.00), reductions occur even after 28 days initial curing. This suggests that the filling or bridging of the initial water filled space with hydration products is influenced by space limitations.

Thus although total porosity of the pastes can be seen to reduce with time of hydration for all the pastes (table 3.3) the primary continuous pore radius tends to steady state values indicating that the hydration products formed are relatively unable to reach and bridge the extreme zones between the intergranular spaces. This could possibly be explained by the induced porosity gradients in the intergranular space (plate 1.1) and the formation or growth of type 1V C-S-H gel (or reaction rim) according to the classification of Diamond[37].

It could be suggested that the decreasing rate of reduction in permeability after 28 days may be explained not necessarily in terms of the cessation of hydration, but rather in terms of the inaccessibility of the hydration products into the weakest and more porous interfacial zones formed at the time of set of the pastes. The same phenomenon could possible be extended to account for the diminishing rates of increase in strengths of pastes after 28 days initial hydration. Hence if the structure formed is initially porous enough as found for high w/c ratio pastes (1.00), substantial reduction in the spacings between the links of hydration products (i.e the primary continuous pore radius) would result (fig 3.6) after 28 days because there is enough space for the products to migrate to the main interfaces between cement granules from the surfaces of the granules.

Further support for the idea that the flow of water tends to occur almost wholly through the primary continuous pore radius was found during the experimentation. In many cases when the flow rates were reasonably high, it was possible to observe a sweaty appearance of droplets of water on the surfaces of the samples. The droplets were found to gradually grow in size with time, until the entire surfaces of the specimens were ponded or fully covered with water. Often, the size of the droplets were found to be larger for early age and high water/cement ratio pastes than for well cured and pastes with low water/cement ratios. It was concluded from these observations that the flow tends to develop initially in specific continuous channels.

The relationship obtained from fig 3.11 was fitted to a power law equation and could be represented by

$$K = 1.684\ r_{\infty}^{3.284}\ 10^{-22} \qquad (4.2)$$

where r_{∞} = primary continuous pore radius (A)

K = saturated permeability (m/s)

The correlation coefficient was found to be 0.9576 suggesting reasonable confidence for the simplicity and accuracy of the relationship between the primary continuos pore radius and saturated permeability of hardened cement pastes of different w/c ratios and times of hydration.

The relationship between total porosity and permeability in fig 3.10 were fitted to the power law functional of the form

$$K = K_{po}(t)\, \varepsilon^{c(t)} \qquad (4.3)$$

where,

K = saturated permeability (m/s)

$K_{po}(t)$, $c(t)$ are empirical constants related to time of hydration.

ε = total porosity

The constants are summarised in table 4.2

TABLE 4.2 Constants of regression for the relationship between total porosity, permeability and time of hydration for hcp

Time of hydration (days)	$K_{po}(t)$ (m/s)	$c(t)$	Correlation coefficient	Porosity range
3	$4.19\ 10^{-5}$	16.18	0.8811	0.49 - 0.68
7	$3.00\ 10^{-7}$	12.98	0.8323	0.30 - 0.68
28	$1.57\ 10^{-10}$	9.02	0.7031	0.28 - 0.66
10m	$2.25\ 10^{-11}$	6.44	0.9378	0.23 - 0.66
20m	$3.88\ 10^{-10}$	7.95	0.9661	0.25 - 0.58

It can be seen that $K_{po}(t)$ and $c(t)$ reduce with time of hydration in a similar manner to that obtained for w/c ratios in table 4.1. The values of $c(t)$ indicate the sensitivity of permeability to changes in total porosity at any time of hydration. Hence, as expected, at early times of hydration, when the pore structure is highly continuous, $c(t)$ is relatively high suggesting that minor differences in porosity will result in large variations in permeability. This was shown in fig. 3.10.

While discussing the concept of pore continuity, it may be pointed out that Powers, Copeland and Mann[26] deduced presently accepted ideas of the continuity or lack of continuity of the capillary pore system of hcp from considerations of the lack of fit of permeability data to a single semi-empirical equation of permeability and the concentration of particles in pastes.

Instead of that definition of pore continuity, the exponent of the relationship between total porosity and permeability could be used to reflect the degree of continuity of the pores at any stage of hydration.

The results from fig 3.6 on the variation of the primary continuous pore radius indicates that curing alone cannot produce a discontinuous paste with respect to the capillary pore system as the estimates of Powers, Copeland and Mann suggest[26] but what appears to occur is that a limiting continuous pore size is rapidly approached with increasing time of hydration. This evidence can be taken to suggest that the pore structure of hcp can be viewed as consisting of space within hydration products with an upper limit pore size corresponding approximately to the primary continuous pore radius which reflects the maximum spacing between the hydration products or the maximum capillary pore size. Similar conclusions have been reached by Winslow and Diamond[28] and later Diamond and Dolch[32] using different means of identifying this maximum pore size.

It may be concluded that

(1) The pore structure of hcp is continuous and bounded by the primary continuous pore radius which provides a simple measure of pore continuity and closely relates to permeability.

(2) The total porosity of hardened cement paste is not uniquely related to permeability but depends on the degree of pore continuity.

(3) The tendency for the primary continuous pore radius to attain steady state values suggests that the hydration products formed are relatively unable to bridge the continuous channels formed at the time of set probably due to the formation of type IV C-S-Hgel which inhibits the movement of the products.

4.3 Surface area, porosity and hydraulic radii in relation to permeability of hardened cement pastes

The surface area of the solid phases existing below 37 A pore radius, the minimum intruded pore size, will contribute substantially to the measured total surface area. Hence the unintruded pore volume could be more significant than the intruded pore volume, and an evaluation of the completeness of intrusion is necessary.

Assuming that the total porosity is given by the evaporable water content on drying at 105°C, the mean percentages of the total pore volume unintruded were calculated from the test results and are summarised in table 4.3. The absolute values of the unintruded pore volumes (cm^3/g) are also given.

TABLE 4.3 Unintruded pore volume of hcp below 37 A pore radius

Time of hydration (d)	3		7		28		10m		20m	
w/c ration	%	*abs	%	abs	%	abs	%	abs	%	abs
0.23	-	-	42	.06	52	.07	45	.06	61	.07
0.47	15	.05	30	.10	36	.10	36	.09	42	.10
0.71	13	.07	18	.09	19	.09	29	.14	20	.09
1.00	6	.04	12	.08	15	.09	17	.11	-	-

*abs = cc/g % of total pore volume

It can be seen that the percentage of pore volume below 37 A increases with time of hydration for any given w/c ratio which indicates that hydration increases the relative amounts of products packed in spaces less than 37 A. It can also be seen that at any time of hydration, the percentage of pore volime below 37 A decreases very strongly as the w/c ratio increases. The absolute unintruded pore volumes can be seen to be generally less than 0.1 cc/g and tend to increase with time of hydration. At the limiting cases of w/c ratio, the unintruded pore volume for the 0.23 paste is generally greater than 40% of the total pore volume whereas that of the 1.00 paste is less than 20%.

This can be interpreted to suggest that the surface area estimates for the high w/c ratio pastes (above 0.71) tend to be closer to the true values than the low water/cement ratio pastes because a greater proportion of the pore volume is intruded for the high water/cement ratio pastes. The results from table 3.5 indicated an increase in surface area with increases

in w/c ratio at any time of hydration which confirms the above interpretation in the sense that for each gram of paste, a greater proportion of the surfaces of the solid phases are measured for higher water/cement ratio pastes than for lower w/c ratio pastes.

It was shown in table 3.5 that the indicated surface areas from mercury intrusion are as low as 44 m^2/g for the highest mean value measured. It was also deduced from table 4.3 that the low surface areas could be due to the inaccessibility of mercury into pores less than 37 A radius. Much controversy exist on the correct value(s) of the surface areas of hardened cement pastes as outlined in the review in Chapter 1. It is thought that the relatively low surface areas indicated by nitrogen adsorption in comparison with water surface areas is due to the presence of ink-bottle pores in hcp which cannot be easily penetrated by nitrogen molecules because of the

(1) larger nitrogen molecule in comparison with water (3.5 cf 3 A)

(2) differences in temperature at which the experiments are carried out ($-179^{o}C$ cf $22^{o}C$ for water),

the nitrogen molecules do not possess sufficient thermal energy to overcome the barriers of the constrictions of the ink-bottle pores in reasonable time and at a reasonable speed.[27]

Water surface areas are found to be dependent on, and increase with, degree of hydration but virtually indépendent on w/c ratio[9,13] whereas nitrogen surface areas vary with w/c and degree of hydration. Whilst accepting the differences in the scales of the inaccessible pores for nitrogen in comparison with mercury, the dependence of surface area from mercury intrusion on water./cement ratio bears a weak resemblance to those obtained from nitrogen adsorption. Since it is well established that mercury intrusion does not measure the total pore volume of hcp[28,29,32] (and see table 4.3) it may be deduced that the problem of inaccessibility of nitrogen molecules into constricted pores is highly significant in relation to surface area determination. Many comparative measurements of the surface area by nitrogen adsorption and mercury intrusion would therefore provide useful indications on the nature of variations of surface area with w/c ratio or space constraints.

Very approximate estimates can be made for the pore structure of the unintruded pore volume (less than 37 A radius) to provide interesting speculations and conclusions and is attempted in table 4.4.

Considering the 10 month samples from tables 3.5 and 4.3 as an example. The surface areas accessible to mercury and absolute unintruded pore volumes for the different w/c ratios are given in columns 1 and 2 of table 4.4.

TABLE 4.4. Approximations of the surface area and hydraulic radii of the pore structure below 37 A pore radius of hardened cement paste.

	Measured pore properties		Derived pore properties		
col.	1	2	3	4	5
W/C	S_{Hg} (m^2/g)	ε_p (below 37 A) (cm^3/g)	$S_{H_2O} - S_{Hg}$ (m^2/g)	r_h(below 37A) (A)	$\bar{S}$ (m^2/g)
0.23	4	0.06	196	3	32
0.47	21	0.09	179	5	47
0.71	37	0.14	163	8	74
1.00	44	0.11	156	7	59

Firstly it could be assumed that the total surface area of hcp only depends on degree of hydration but not on water/cement ratio and a value of 200 m^2/g[13] adopted. The surface area of the solid phases existing in pores below 37 A is then given by the difference between 200 m^2/g and the surface measured by mercury intrusion. This is given in col. 3 which indicates that more solid phases exist below 37 A pore radius the lower the water/cement ratio. The hydraulic radii of the pores below 37 A can be estimated from the ratio of the unintruded pore volume (col.2) and the derived surface area (col.3). This is shown in col.4, where it can be seen that the hydraulic radii of pores below 37 A increase with w/c ratio (as found for the pores above 37 A, table 3.6).

Next, it could be assumed that the hydraulic radius of the pores below 37 A is independent of water/cement ratio and assume a value of 19A (half of 37 A) The surface area of the solid phases below 37 A can be estimated from the ratio of the unintruded pore volume (col.2) and the assumed hydraulic radius. This is given in col.5, where it can be seen that the surface area of the solid phases below 37 A vary with w/c ratio and tend to increase with w/c ratio, suggesting that on this assumption, less products of hydration are packed in spaces less than 37 A pore radius, the lower the w/c ratio.

Finally, if it is assumed that both the hydraulic radii of pores below 37 A and the total surface area of the hcp vary with w/c ratio, then no deductions can be made from the available data.

However, the first assumption which leads to an increase in hydraulic radii of the pores below 37 A radius with increasing w/c ratio is highly likely to represent the true situation since it is physically compatible with the measured increases in the hydraulic radii of the pores above 37 A with increasing w/c ratio (table 3.6).

For the purposes of assessing permeability, however, there are strong indications from the results for the total porosities and the primary continuous pore radius. (Figs 3.10 and 3.11 respectively) that the flow of water in hardened cement paste is confined to distinct continuous channels. This indicates that the total and absolute surface area of the hydration products may not offer the resistance to the flow, but the resistance would probably result from only a fraction of the products of hydration bounding the main continuous channels. The most important consequence of the above arguments is that in relation to permeability, all the parameters of pore structure such as porosity, surface area, and pore size must be defined to include only the effective pore space contributing to flow. This essential but difficult objective has been pursued vigorously by many previous workers in this area. Robson[109] postulated the 'Unit pore flow' hypothesis, which at the time (June 1965), was described as belonging to a 'new field of statistics, and is soluble only by subjective methods'. Ths hypothesis, involved a calculational procedure requiring repeated subdivision of the measured flow rates through hcp, mortars and concretes, and from this deducing average pore flow from a guessed number of pores. The unit pore flows were deduced from the number of pores and the average pore flows, and by use of 'new statistics' Robson deduced that permeability depends on the probability of continuous channels developing in mortars and concretes and is not a function of total porosity. Hancox[111] thought that the ineffective flow space was related to total porosity by $\varepsilon^{3.4}$ and was neither dependent on curing nor type of cement. The results on porosity and permeability presented in fig 3.10 suggest otherwise.

Using the general variables that affect permeability, such as porosity and surface area, hydraulic radius theories provide a useful means of defining permeability. A general form is given by[4]

$$K = C\, f(\varepsilon)\, r_h^2 \qquad (4.4)$$

where C = a constant related to tortuosity and degree of uniformity of the porous material.

$f(\varepsilon)$ = a porosity function

r_h = hydraulic radius (cm)

K = specific permeability (cm^2)

The results from the measurements are plotted in fig 4.1 using the most fundamental form of the porosity function,

$f(\varepsilon) = \varepsilon$ (total porosity from evaporable water at 105°C)

r_h = hydraulic radius of hcp measured down to 37 A pore radius(m)

K = saturated permeability (m/s)

A linear regression on log K and log $(\varepsilon r_h 2)$ results in the functional relationship

$$\log K = 38.449 + 4.077 \log (\varepsilon r_h^2) \qquad (4.5)$$

with a correlation coefficient of 0.8946 . The correlation coefficient is seen to be less than that obtained between the primary continuous pore radius and permeability (0.8946 cf 0.9576 - section 4.2). Thus it can be deduced that the inclusion of more general parameters did not improve predictions in comparison with that of the primary continuous pore radius.

The line for equation 4.5 is shown on fig 4.1, and it is immediately clear that the linear fit of log K on log (εr_h^2) grossly underestimates the permeability greater than approximately 10^{-13}m/s. It therefore appears that the hydraulic radius theories fail to describe permeability of hardened cement paste over the whole range of porosities examined. However, considering the approximations involved in the assumptions made in determining hydraulic radius from mercury intrusion data, it cannot be unequivocably concluded that the theory does not apply for hardened cement paste.

The discrepancy for the fit of data to equation 4.5 could be easily accounted for by the constant C related to tortuosity. The tortuosity factor for hardened cement paste is unlikely to be constant for any stage of hydration or w/c ratio because of the continuously varying pore size distribution as indicated in figs 3.6a - d. The relationship obtained in equation 4.5 is also based on the coefficient of permeability expressed in m/s and does not therefore allow for the effect of changes in the viscosity in small flow channels as the equation 4.4 assumes. It may therefore be suggested that the poor fit at low permeabilities (less than 10^{-13}m/s) could be due to lack of consideration for variations in fluid properties caused by the reduction in pore sizes.

Referring back to fig 3.11, it was shown that the primary continuous pore radii corresponding to permeability values of the order of less than 10^{-13}m/s were of the order of less than approximately 400 A.

If it is considered that the diameter of the water molecule is approximately 3 A[56], then it can be visualised that a maximum thickness of approximately 260 molecules of water occupy and flow through the primary continuous pore space, i.e. the maximum spacing between the links of the fine particles of the products of hydration, at the imposed hydraulic gradient of approximately 20,000.

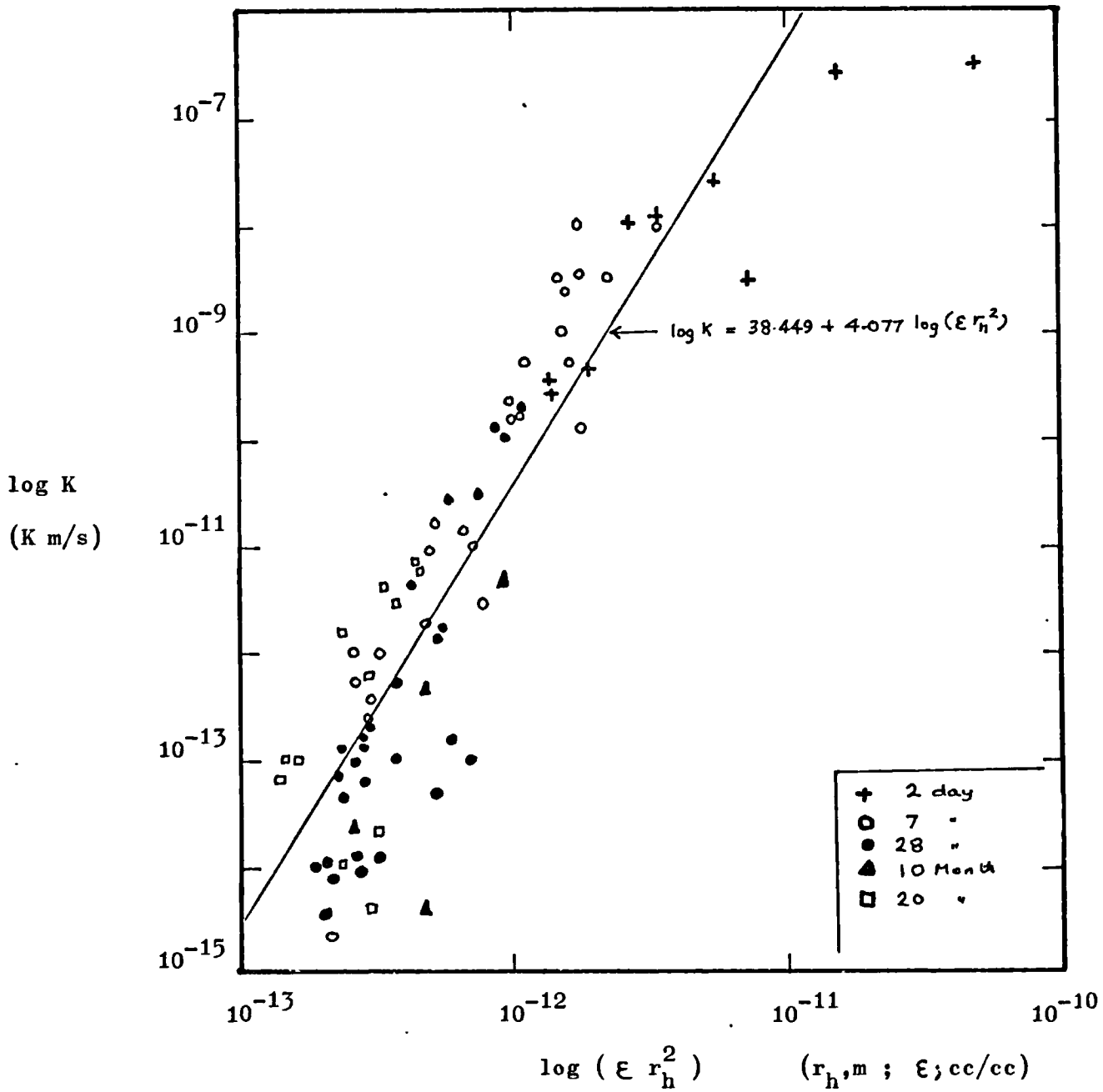

Fig. 4.1: A comparison of permeability data for hardened cement paste with hydraulic radius theories for permeability.

It is not inconceivable that, with so few molecules occupying the space from the surface to surface of the fine individual particles, the forces of attraction enamating from the surfaces are likely to alter the viscous properties of the fluid. In addition, the permeability coefficient of 10^{-13} m/s, represents an average velocity within the porous network of 10^{-3}A/s per unit hydraulic gradient; thus under a hydraulic gradient of 70,000, the bulk fluid velocity is of the order of 70 A/s, an extremely low creeping motion representing approximately 23 water-molecular diameters per second. Raising the order of vision to the practical laboratory conditions, at such a velocity, a particle starting from the base of the test sample of 10 mm thick, would require approximately 16 days to reach the top of the specimen by the most direct route.

Using the results from fig. 4.1, it can be seen that the linear relationship between log K and log (εr_h^2) results at approximately K greater than 10^{-13}m/s whereas a sharp downward deviation occurs below this value, where it appears that minor differences in log (εr_h^2) results in large drops in log K. This is taken as evidence that hydraulic radius theories do not describe the permeability of hardened cement pastes over the whole range of permeability measured. This evidence is valid only if the assumption that the hydraulic radius determined from mercury intrusion is the appropriate measure.

Three main conclusions can be drawn from fig 4.1 and the foregoing discussions.

The first conclusion is that although there is a general trend suggesting fair agreement between hydraulic radius theories and the permeability of hardened cement paste, there are also discrepancies at low permeabilities of the order of less than 10^{-13}m/s. The discrepancy at low permeability could be due to the limitations of the measurements as well as other factors such as the neglect of changes in the viscosity of water in small flow channels.
The second conclusion is that it cannot be unequivocably concluded that hydraulic radius theories fail to describe the permeability of hcp, because for such a conclusion to be reached, it must first be shown that the hydraulic radius measured by mercury intrusion is the appropriate parameter.
The third, final, and most important conclusion is that the inclusion of more general parameters, such as porosity and hydraulic radius did not improve on the prediction of permeability in comparison with that found for the primary continuous pore radius (fig 3.11). Hence, within the limitations of the measurements, it is clear that the primary continuous pore radius represents the most reliable single parameter in relation to permeability of hcp for the modes of change in pore structure associated with changes in w/c ratio and hydration.

4.4 Permeability of mortars in relation to pore continuity

It is thought that the addition of aggregate to hardened cement paste causes[102]

(1) a reduction in the number of flow channels per unit cross-sectional area and lengthens the flow paths - the effect being a reduction in permeability.

(2) the development of fissures around the aggregate particles - the effect being an increase in permeability.

No known studies were available in the literature to elucidate the relative importance of these two opposing effects on permeability of mortars or concrete. This is the third mode of change of pore structure in relation to permeability considered of interest in the present investigation.

Powers et al[92] reasoned that since, in general, the paste forms the continuous phase surrounding the aggregate particles, the permeability of mortars and concrete will in the main, depend on that of the paste, the permeability of the aggregate, and the relative proportions of the two. The effect of the grading of the aggregate on permeability of concrete is relatively more difficult to predict from straight forward reasoning since it involves a complex system of multiparticle arrangements in the continuous hcp phase.

The results on the effect of grading on permeability of mortar (fig. 3.14 and table 3.8) showed that for the grading of sand in the range of particle sizes below 2400 microns, there is practically no effect on permeability at a given volume concentration. No significant changes on the permeability of mortars were found for the effect of particle size on a one-size aggregate system (table 3,7 and fig 3.14 c), hence it may be concluded that the effect of particle arrangements on permeability of mortars in the range of particle sizes used has no significant effects on the composite behaviour and therefore can be ignored in the arguments and discussions to be presented on the third mode of change in pore structure and permeability. What therefore remains are

(a) paste permeability

(b) aggregate permeability

(c) relative proportion of paste to aggregate

(d) development of fissures.

The permeability of the pastes was extensively studied in chapter 3 where it was shown that although an increase in porosity generally results in an increase in permeability, the permeability of pastes is not a single-valued function of porosity but could be closely approximated by a single-valued function of the primary continuous pore radius, i.e, the maximum spacing between the fine individual particles of the products of hydration.

One of the greatest difficulties with the paste permeability was that the scatter of results, when considered on the basis of w/c ratio or hydration was substantially high (fig 3.1) hence in trying to relate the paste properties to the mortar properties (see for example fig 3.19) three groups of data can be identified for pastes of supposedly identical w/c ratio and degree of hydration - i.e. range less than 10 x 10^{-15}m/s, 30 - 60 x 10^{-15}m/s and greater than 90 x 10^{-15}m/s. It is possible to suggest that the lower permeability values represent the correct state of w/c ratio and same degree of hydration as the mortars, in which case the tentative trend lines shown would indicate that as more aggregate particles are added to the paste

(1) total porosity reduces - this is confirmed by fig 3.15

(2) permeability increases - this is confirmed by fig 3.14 a

On this rather subjective assumption, it could be tentatively postulated that the addition of the aggregate of lower porosity than the paste (but of unknown permeability) increases permeability when the volume concentration becomes greater than a given value or critical value as the effect of fissure development overides the effect of reduction in flow channels/flow path increase. Many more very carefully monitored tests are certainly needed here to confirm the above postulate but the most striking feature associated with this mode of change in pore structure in relation to permeability is the very fact that permeability increases although total porosity reduces.

Next, the lightweight mortar was only three times more permeable than the normal mortar of the same volume concentration. Within the large range of permeability values measured in this work and shown in tables 3.1 and 3.2, for different w/c ratios and times of hydration, a difference of three times can be considered to be negligible. Nevertheless, such a difference, all the factors affecting permeability being equal, must be caused by the differences in the permeability of the normal and lightweight aggregate. Since this could not be measured, is it possible to make deductions from the pore size distributions of the aggregate (fig 3.16) ? First, it might not perhaps be too erroneous to assume that because of the coarser and more porous nature of the lightweight aggregate in comparison with that of the normal aggregate (fig 3.16) the lightweight aggregate is probably more permeable than the normal aggregate. On this basis, the inclusion of the lightweight aggregate in paste may result in mortar of greater permeability than the normal mortar. This is barely confirmed by the results of fig 3.12.

Secondly, both aggregates had a lower porosity than the hcp (table 3.9), hence, the evidence obtained between total porosity of hcp (section 3.3.1) would suggest that the aggregates may be less permeable - than the hcp, in which case the addition of the aggregates should have reduced the permeability of the hcp; this is again found to be the case (fig 3.12), but the reduction does not proceed as the volume concentration increases, which may mean that

(1) either the aggregates are not less permeable than hcp

or (2) the factor associated with the development of fissures tends to increase permeability.

Neither (1) nor (2) can be proven by intuition, measurements would probably resolve the two possibilities.

Thirdly, the measured hydraulic radius of normal mortar was greater than that of the lightweight mortar, (table 3.11) hence it could be deduced intuitively that the permeability of the normal mortar should be greater than that of the lightweight mortar, but is is not (table 3.6).

Finally, it has been found that air entrainment reduces permeability [83,106] and this is often explained in terms of improved workability. In relation to pore structure, air entrainment results in an increase in porosity although this is apparently not accompanied by an increase in permeability. If the air-bubbles produced by entraining agents are considered as aggregates, then the permeability of these 'aggregates' would by definition - and incontestably correct - be infinite. It might then be considered that by the usual addition rule, air-entrainment ought to increase permeability, but it does not.

It may be suggested that

(1) The increase in permeability with increasing volume concentration of the aggregate, despite the reduction in total porosity is probably due to the development of fissures.

(2) The permeability of the aggregate, or more appropriately the porosity of the aggregate, does not substantially affect the permeability of the mortars tested.

and concluded that

(3) The grading of sand and sand particle size in a one-size aggregate mortar have practically no effect on permeability in the range of particle sizes used.

CHAPTER 5

CONCLUSIONS

The overall objective in this investigation was to study seperately the effects of hydration and water/cement ratio on the pore structure and the saturated permeability of hardened cement paste. The effect of the addition of both normal and lightweight aggregate to paste on the pore structure and hence the permeability of the resulting composite was also investigated. The main conclusions reached from the measurements made are first summarised in this chapter. Detailed conclusions are given together with recommendations for future research relating to the main findings in this work.

5.1 Main conclusions.

(1) The effect of an increase in water/cement ratio was found to be an increase total porosity. The effect of hydration was found to reduce total porosity but the changes in porosity resulting from these two seperate effects were found to affect permeability in quite different ways. Hence although permeability of hcp was found to increase with total porosity, the change in permeability was found to depend on whether the change in total porosity is caused by changes in w/c ratio or times of hydration, therefore, permeability was found to be a multivalued function of total porosity.

(2) The two seperate modes of change in total porosity (i.e w/c and hydration) could be adequately represented by the primary continuous pore radius, which is thought to correspond to the maximum spacing between the weakest links in the bonds of cement hydration products. Permeability was found to be closely and uniquely related to the primary continuous pore radius, (r_{∞}) thus indicating that r_{∞} is mainly responsible for carrying the water flow in hardened cement paste.

(3) The tests on mortars indicated that the addition of aggregate of lower total porosity than the hardened cement paste reduces total porosity but increases permeability as the volume concentration of the aggregate increases. Lightweight aggregate additions to the paste did not result in a substantial difference in permeability of the lightweight mortar in comparison with that of normal mortar. The application of the mathematical definition of the primary continuous pore radius to the pore size distributions of the mortars showed the parameter to be less sensitive to the permeability of mortars than that found for hardened cement paste.

5.2 Detailed conclusions

5.2.1 Pore structure of hardened cement paste

(1) The porosity measurements from the evaporable water contents at 105°C were found to be more reliable than the helium comparison pycnometer method. The helium porosity estimates were generally less than those found from the evaporable water contents.

(2) The total porosity of hcp reduced linearly with logarithm of time of hydration and increased with increasing w/c ratio.

(3) It was possible to identify a primary continuous pore radius (r_∞) from the pore size distributions, defined as the pore radius corresponding to the mean pressure at the maximum value of the derivative of the pressure-volume data, and physically representing the maximum spacing between the weakest links in the bonds of cement hydration products.

(4) r_∞ increased with w/c ratio and reduced to steady-state values with times of hydration beyond 28 days. It is thought that the attainment of steady state values is due to the formation of type IV C-S-H gel on the rims of the original cement grains which tends to prevent further migration of hydration products to fill or bridge the extreme interfacial zones between cement grains.

(5) The occurence of the primary continuous pore radius at all stages of hydration and w/c ratio suggest that the capillary pore structure of hcp is not rendered discontinuous by the growth of cement gel but instead a limiting maximum continuous pore size (r_∞) is rapidly approached with hydration.

(6) Hydraulic radius of hcp increased with w/c ratio and reduced with time of hydration but was not as sensitive as the primary continuous pore radius to differences in w/c and times of hydration.

(7) The surface area of the solid phases accessible to mercury increased with w/c ratio but the variation with time of hydration depends on w/c ratio. The surface area diminishes at low w/c ratios (0.23) and increases to seemingly constant values at high w/c ratios with increasing times of hydration.

It is thought that the surface areas estimates from mercury intrusion tend to be closer to the true values at high w/c than at low w/c ratios. The surface areas were in the range of 4–44 m^2/g for w/c between 0.23 and 1.00 at times of hydration up to 20 months.

5.2.2 Permeability and pore structure of hcp

(1) Despite coefficients of variations in dry-densities of pastes with the same water/cement ratio of less than 2%, permeability scatter was large (coefficients of variation exceeding 100%) for any w/c ratio which indicates the sensitivity of permeability to minor variations in specimen homogeneity.

(2) Permeability increased with increasing w/c ratio and reduced with time of hydration, but there were uncertainties about the opposing effects of hydration and leaching of alkalis in curing water on changes in permeability beyond 10 months hydration.

(3) The most reliable single parameter of pore structure in relation to permeability was found to be the primary continuous pore radius. The relationship could be represented by

$$K = 1.684\ r_{\infty}^{3.284} \times 10^{-22}$$

K = permeability (m/s)

r_{∞} = primary continuous pore radius (A)

(4) Total porosity of hcp could be related to permeability by

$$K = K_0(t)\ \varepsilon^{b(t)}$$

where both $K_0(t)$ and $b(t)$ depend on time of hydration.

(5) Hydraulic radius was introduced to account for the limitations of the primary continuous pore radius but was found to be less sensitive to permeability.

(6) Hydraulic radius theories of permeability were compared with the measurements for hcp and found to adequately describe the data, but not as accurately as that found for the primary continuous pore radius in relation to permeability.

(7) Discrepancies between hydraulic radius theories and permeability of hcp at low permeabilities (10^{-13}m/s) is thought to be due to surface effects on the viscosity of water in small flow channels as well as limitations of measurements, and other unknown factors.

5.2.3 Permeability and Pore structure of mortars

(1) Lightweight mortar was found to be not substantially more permeable than normal mortar of the same aggregate volume concentration.

(2) The effect of an increase in aggregate volume concentration was to increase permeability of mortar.

(3) The grading of sand retained on 2400 micron sieve has practically no effect on permeability of mortars.

(4) Different sand particle sizes in a one-size aggregate mortar have practically no effect on permeability of mortar.

(5) The hydraulic radius of normal mortar was greater than that of the lightweight mortar but permeability was not.

(6) The addition of both normal and lightweight aggregate to paste at an aggregate volume concentration of 24% reduced surface area to approximately half the value for hcp but with increasing volume concentration, the surface area remained virtually constant.

(7) Lightweight mortar indicated a higher surface area than normal mortar.

(8) The trends for the porosity-permeability relationships for mortar indicates that lightweight mortar may not have the same porosity relationship with permeability as normal mortar.

5.3 Practical implications of work

(1) The identification of the primary continuous pore radius as corresponding to the maximum spacing between the weakest links in the bonds of cement hydration products would suggest that the mercury porosimeter can indicate, on a comparative basis, the extent of deterioration of the hcp component in structural concrete. This could be checked simply by comparing the pore size distributions of core samples, and identifying the changes in the primary continuous pore radius.

(2) Development studies for improving the material could also be aided by attempting to find the processes of preparations that minimise the size and relative frequency of the primary continuous pore radius.

5.4 Recommendations for future work

(1) Further studies on the effects of aggregate addition to paste on permeability of mortars to obtain a closer fix on the porosity-permeability relationship for mortars.

(2) Measurements of compressive strengths and elastic constants of hcp in relation to the primary continuous pore radius or other pore size distribution parameters. The densities of the solid phases could be measured by the helium pycnometer.

(3) Further measurements to elucidate the effects of alkali loss and hydration on permeability for samples hydrated in water for long periods.

(4) Studies on the effect of grading on permeability of larger test samples of concrete.

(5) Studies of the effects of flow of ions at high pressures into hcp and mortars to simulate the conditions found on off-shore oil platforms.

REFERENCES

1. HELMUTH R, TURK D.
The reversible and irreversible drying shrinkage of hardened Portland Cement paste and Tricalcium Silicate paste.
Bulletin 215, Portland Cement Assoc., 1967.

2. FELDMAN R.
'Sorption and length-change scanning isotherms of methanol and water on hydrated Portland cement pastes'.
Proc. 5th Int. Symp. on the chem. of Cement, Tokyo, part 3 vol3 (1968) p.36-44, 53-66.

3. DUBININ MM.
Quarterly Review of chem soc. vol9, pl01 (1959)

4. A.E. SCHEIDEGGER.
The physics of Flow through porous media. 3rd edition (1974)
University of Toronto Press.

5. BRUNAUER S, MIKHAIL R SH BODOR EE.
'Some remarks about capillary condensation and pore structure analysis'
Journal of Colloid and Interface science, 25, 353-358 (1967)

6. WINSLOW DN, DIAMOND S
'Specific surface of hardened portland cement paste as determined by small angle x-ray scattering'
Jour. Amer. Ceramic Soc. Vol 57, No 5, p 192 May 1974

7. MIKHAIL RS, TURK DH, BRUNAUER S.
'Dimensions of the average pore, the number of pores and the surface areas of hardened cement pastes'.
Cem. and Con. Res. vol5, p433-442 (1975)

8. KARNAUKOV AP.
'Structure, classification and simulation of porous materials'
Pore structure and properties of materials, RILEM/IVPAC Praque 1973 vol I pA3-33.

9. POWERS TC, BROWNYARD TL.
'Studies of the physical properties of hardened Portland cement paste. (Nine parts)'. Proc. AC.I vol43 Oct. 1946 - April 1947.

10. BODOR EE. SKALNY J, BRUNAUER S, HAGYMASSY J, YUDENFRENND M.
'Pore structures of hydrated calcium silicates and Portland cement by nitrogen adsorption'
J. Colloid & Int Sci vol34, No.4 (1970)

11. CARMAN PC.
'Flow of gases through porous media'
Butterworths (1956)

12. BRUNAUER S, EMMETT P, TELLER E.
'Adsorption of gases in multi-molecular layers'
Jour. A. Chem. Soc. vol 10, No.2, p 309-319 (1938)

13. POWERS TC.
'The physical structure of Portland cement paste' in chapter 10 of
'The chemistry of cements' ed. H FW Taylor
Academic Press (1964)

14. COPELAND L, HAYES J.
'Porosity of hardened Portland cement pastes'
Jour. Am. Conc. Inst. vol52 p633-640 (1956)

15. HANSEN TC.
'Physical composition of hardened portland cement paste'
J. Am. Conc. Inst vol67 p404-407 (May 1970)

16. POWERS TC.
The nonevaporable water content of hardened portland cement paste: Its significance for concrete research and its determination'. ASTM. Bull. No.158 (1949) p68-76.

17. FARGERLUND G.
'Strength and porosity of concrete'
RILEM/IUPAC: Praque 1973 pD -173 Ed. Modry Vol2.

18. WINSLOW DN
'The validity of high pressure mercury porosimetry'
Jour. Colloid and Int. Sci Vol 67, No 1 p 42 - 47, (Oct 1978)

19. FAGERLAND G.
'Connections between porosity and mechanical properties of materials'
Teknista Hogskolan i Lund, Inst. for Byggnadskeknik.
Rap. 26. Lund 1972.

20. FAGERLUND G
'Elastic modulus of concrete'
RILEM/IUPAC, Prague 1973, pD129 - 149, Vol 2.

21. PARROT LD, ILLSTON JM
'Load-induced strains in hardened cement paste'
Jour. of the Engrn. Mech. Div.,ASCE, Vol 101, p13 - 24, (1975)

22. POWERS TC, MANN HM, COPELAND LE
'Flow of water in hardened cement paste'
Highway Res. Bd. Spec. Report No. 40, p308, July 1959.

23. POWERS TC
'Structure and physical properties of hardened cement pastes'
Jour. Amer. Ceramics Soc. Vol. 41,No 1. p 1 - 6, Jan. 1958

24. DANYUSHEVSKY VS, DJABAROV KA
'Interrelations between pore structure and properties of hydrated cement paste'
RILEM/IUPAC Prague 1973, Vol. 2, pD97

25. ILLSTON JM
'Aspects of the behaviour of the cement paste phase of composite materials with reference to practical problems of concrete technology'
Proc. Int. Conf. on Hydraulic Cement Pastes, Univ. of Sheffield .
p 232 - 247, (1976).

26. POWERS TC, COPELAND LE, MANN HM
'Capillary continuity or discontinuity in cement pastes'
Jour. PCA Res. & Dev. Lab. Vol 1, No 1, p 38 (Jan 1959)

27. MIKHAIL R Sh, COPELAND LE, BRUNAUER S
'Pore structure and surface areas of hardened portland cement pastes by nitrogen adsorption'
Can. Jour. of Chemistry, Vol 42, p 426, (1964)

28. WINSLOW DN, DIAMOND S
'A mercury porosimetry study of the evolution of porosity in portland cements'
Jour. of Materials, JMLSA, Vol 5, No 3, Sept. 1970, p 564 - 585

29. AUSKERN A, HORN W
'Capillary porosity in hardened cement paste'
Jour. of Testing and Evaluation, Vol 1, p 74 - 79, (1973)

30. DIAMOND S, DOLCH WL
'Generalised log-normal distribution of pore sizes in hydrated cement paste'
Jour. Colloid and Int. Science, Vol 38, No 1, p 234 - 244, (1972)

31. DIAMOND S
'Pore structure of hardened cement paste as influenced by hydration temperature'
RILEM/IUPAC, Prague 1973, Vol 1, p B73 - 88

32. SELLEVOLD EJ
'Mercury porosimetry of hardened cement paste cured or stored at 97°C'
Cem. and Conc. Res., Vol 4,No 3, p399 - 404, (1974)

33. VERBECK GJ, HELMUTH RH
'Structure and physical properties of cement paste'
Proc. of the 5th Int. Symp. on the Chemistry of Cement, Tokyo 1968
Session III -1, p 28.

34. DANYUSHEVSKI VS, DJABAROV KA
'Three types of pore in set cement'
Inorg. Materials. Vol 10, No 2, p 303 (1974)

35. MIDGLEY HG, PETTIFER K
'The effect of water-cement ratio on the microstructure of set portland cement'
Micron Vol 1, p428 - 432 (1970)

36. MIDGLEY HG
'Electron microscopy of set portland cement'
Structure,Solid Mech. and Engnr. Design. Proc. of Conf. at Univ. of Southampton. Session III, p 275, (1969)

37. DIAMOND S
'Cement paste microstructure - an overview at several levels'
'Hydraulic cement pastes: their structure and properties'
Proc. of conf. at Univ. of Sheffield, p 2, April 1976.

38. BRUNAUER S
'Tobermorite gel - the heart of concrete'
American Scientist, Vol 50, No 1, March 1962, p 210 - 229

39. GREGG J, SING KWS
'Adsorption, surface area and porosity'
Academic Press, London 1967

40. DIAMOND S
'A critical comparison of mercury porosimetry and capillary condensation pore size distributions of portland cement pastes'
Cem. and Conc. Res., Vol 1, p531 - 545, (1971)

41. SKALNY J, ODLER J
'Pore structure of calcium silicate hydrates'
Cem and Conc. Res. Vol 2, No 4, p387 - 400, (1972)

42. FELDMAN RF, SEREDA PJ
'A new model for hydrated portland cement and its practical implications'
Engineering Journal, Aug/sept 1970, Vol 53, No 8/9, p 53 - 59

43. FELDMAN RF, SEREDA PJ
'A model for hydrated portland cement paste as deduced from sorption length-change and mechanical properties'
Materials and Structures, RILEM, Vol 1, No 6, p 509 - 520, (1968)

44. FELDMAN RF
'Volume change, porosity and helium flow studies of hydrated portland cement'
RILEM/IUPAC Prague 1973, p C 101 - 116

45. KONDO R, DAIMON M
'Phase composition of hardened cement paste'
Proc. VI Int. Conf. on Chem of Cement, Moscow, (Sept 1974)

46. BRUNAUER S, ODLER I, YUDENFREUND M
'The new model of hardened portland cement paste'
Highway Res. Rec. No 328, p 89 (1970)

47. ROY D, GOUDA G
'Optimization of strength in cement pastes'
Cem and Conc Res. Vol 5, p 153 - 162 (1975)

48. ODLER I, HAGYMASSY J, BODOR E, YUDENFREUND M, BRUNAUER S
'Hardened portland cement pastes of low porosity, IV: Surface area and pore structure'
Cem. and Conc. Res. Vol 2, p 577 - 589 (1972)

49. MANNING D, HOPE B
'The effect of porosity on the compressive strength and elastic modulus of polymer impregnated concrete'
Cem. and Conc. Res. Vol 1, p 631 - 644 (1971)

50. FELDMAN RF
'The flow of helium into the interlayer spaces of hydrated portland cement pastes'
Cem and Conc Res. Vol 1, p 285 - 300 (1971)

51. FELDMAN RF
'Helium flow and density measurements of hydrated tricalcium silicate-water system'
Cem and Conc Res. Vol 2, No 1, p 123 - 136 (1972)

52. FELDMAN RF
'Density and porosity studies of hydrated portland cements'
Cement Technology Vol 3, p 5 - 14 (1972)

53. HAYNES J
'Determination of pore properties of constructional and other materials-General introduction and classification of methods'
Materials and Structures Vol 6, No 33 p 169 - 179 (1973)

54. DULLIEN AL, BATRA VK
'Determination of the structure of porous media'
Industrial and Engineering Chemistry Vol 62, No 10, Oct 1970 p 25 - 53

55. FELDMAN RF
'Helium flow characteristics of rewetted specimens of dried hydrated portland cement paste'
Cem. and Conc. Res. Vol 3, No 6, p 777 - 790 (1973)

56. KANTRO DL, BRUNAUER S, COPELAND LE
'BET Surface areas - methods and interpretations'
Chapter 12, Vol 1, Solid-gas interface ed. E Alison-Flood
Edward Arnold , London (1967)

57. KALOUSEK GL
Proc. ACI Vol 51, p 233 1954

58. FELDMAN RF
'Assessment of experimental evidence for models of hydrated portland cement'
Highway Research Rec. No 370 p 8 - 24 (1971)

59. BARRETT EP, JOYNER LG, HALENDA PP
'The determination of pore volume and area distribution in porous substances I. Computations from ntrogen isotherms'
Jour. Amer. Chem. Soc Vol 73, p 373, (Jan 1951)

60. DOLLIMORE D, HEAL GR
'An improved method for the calculation of pore size distributions from adsorption data'
Jour. Applied Chem., Vol 14, p 109, Mar 1964

61. ROBERTS BF
'A procedure for estimating pore volume and area distributions from sorption isotherms'
Jour. Colloid and Int. Sci, Vol 23, p 266 - 273 (1967)

62. LECLOUX A
' A general method of analysing the nitrogen adsorption isotherms to determine the porous texture of solids'
RILEM/IUPAC Vol IV, p C43

63. SETZER MJ, WITTMAN FH
'Modified method to calculate pore size distributions using sorption data'
RILEM/IUPAC Vol IV p C69

64. HAGYMASSY J, BRUNAUER S, MIKHAIL R Sh
'Pore structure analysis by water vapour adsorption 1: t-curves for water vapour'
Jour. Colloid and Int. Sci. Vol 29, No 3, p 485 (1969)

65. BRUNAUER S, MIKHAIL R Sh, BODOR EE
'Pore structure analysis without a pore shape model'
Jour. Colloid and Int. Sci Vol 24, p 451 - 463 (1967)

66. MIKHAIL R Sh, BRUNAUER S, BODOR EE
'Investigation of a complete pore structure analysis' I. Analysis of micropores'
Jour. Colloid and Int. Sci. Vol 26, p 45 - 53 (1968)

67. BRUNAUER S, SKALNY J
'Complete pore structure analysis'
RILEM/IUPAC Prague 1973 p C3 - 29

68. BERING BP, DUBINNIN MM, SERPINSKY VV
'On thermodynamics of adsorption in micropores'
Jour. Colloid and Int. Sci Vol 38, No 1, p 185 - 194 (1972)

69. DUBINNIN MM
'On the specific surface area of micropore containing adsorbents'
RILEM/IUPAC Vol 4, p C27, Prague 1973

70. DUBINNIN MM
'Methods of determination of pore structure: adsorption methods'
RILEM/IUPAC Vol 4 p C5, Prague 1973

71. DUBINNIN MM
'On the physical feasibility of Brunauer's micropore analysis method'
Journal Colloid and Int. Sci. Vol 46, No 3, p351 - 356 (March 1974)

72. LIABASTRE AA, ORR C
'An evaluation of pore structure by mercury penetration'
Jour. Colloid and Int Sci Vol 64, No 1, p 1 - 17 (1978)

73. ROOTCARE MM, PRENZLOW CF
'Surface areas from mercury porosimeter measurements'
Jour. Physical Chem. Vol 71, No 8, p 2733 - 2736 (1967)

74. ORR C
'Review of the mercury porosimeter technique'
Powder Technology Vol 3, p 117, (1969)

75. BRUNAUER S
'Discission of helium flow results'
Cem and Conc Res Vol 2 No 4, 1972, p 489 - 492
No 6, 1972, p 749 - 753

76. FELDMAN RF
'Reply to discussions by Brunauer'
Cem. and Conc. Res Vol 2 No 4, p 493 - 498 , (1972)

77. SLATTERY JC
'Momentum, energy and mass transfer in continua'
McGraw-Hill (1972)

78. BEAR J, BRAESTER C
'Fundamentals of transport phenomena in porous media'
Elsevier, Amsterdam (1972)

79. DERJAGUIN B, ZACHAVAERA N
Bulletin RILEM No 27 p 12 (1965)

80. HASKEL ENGINEERING - Applications Catalogue M-20
'Haskel air driven hydraulic pumps'

81. MIDGLEY HG
Private Communication

82. BAGER DH, SELLEVOLD EJ
Mercury porosimetry of hardened cement paste: The influence of particle size
Cem and Conc Res. Vol 5, p171 - 178, (1975)

83. MURATA J
'Studies on the permeability of concrete'
Bulletin RILEM No 29, p 47, Dec 1965

84. VALENTA O
'The permeability and durability of concrete in aggressive conditions'
Proc. Dixieme congres des grands barrages, Montreal 1970, p 103

85. COLEMAN JR, CORRIGAN GL
'Fineness and water/cement ratio in relation to volume and permeability of set cement'
Trans. AIME Vol 142, p 205 1941

86. NORTON PT, PLETTA DH
'The permeability of gravel concrete'
ACI Jour. Vol 27, p 1093 May 1931

87. WILEY B, COULSON D
'A simple test for water permeability of concrete'
ACI Jour. Sep/Oct 1937, Proc. Vol 34, p 65

88. PEARSON JC, ADAMS RF
'Low head permeability tests of mortar pots'
ACI Jour. Proc. Vol 35, p 285 - 288, (Feb 1939)

89. McMILLAN FR, LYSE INGE
'Some permeability studies of concrete'
ACI Jour. Proc Vol 26, p 101, (Dec 1929)

90. TOY HC
'The permeability of concrete'
ICE Selected Engineering papers No 20, (1924)

91. WASHA GA
'Comparison of the physical and mechanical properties of hand rodded and vibrated concrete made with different cements'
ACI Jour. Vol 36, No 31, p 617, (June 1940)

92. POWERS TC, COPELAND LE, HAYES JC, MANN HM
'Permeability of portland cement paste'
ACI Jour. Vol 26, No 3 , p 285 (Nov 1954)

93. RUETTGERS A, VIDAL EN, WING SP
'Permeability of mass concrete with particular reference to Boulder dam'
ACI Jour. Vol 31, p 382, (Mar/April 1935)

94. DUNAGAN WH
'Methods of measuring the passage of water through concrete'
Proc. ASTM, Vol 39, p 866, (1939)

95. Van der MEULEN G, Van DIJK J
'A permeability testing apparatus for concrete'
Mag. Conc. Res. Vol 21, No 67, p121 - 123 (1969)

96. OYEKA CC
'Pore structure and crude oil permeability of hardened cement paste and concrete' PhD Thesis Univ of Sheffield (1978)

97. PIHLAJAVAARA SE, PARROLL H
'On the correlation between permeability properties and strength of concrete'
Cem. and Conc. Res, Vol 5, p 321 - 328 (1975)

98. LEVITT M
'The ISAT A non-destructive test for the durability of concrete'
Brit. Jour. of Non- destructive testing Vol 13, No 4 p 12

99. LEVITT M
'Non-destructive testing of concrete by initial surface absorption method'
ICE Conf. on non-destructive testing of concrete and timber'
London 1970

100. FIGG JW
'Methods of measuring the air and water permeability of concrete'
Mag. Conc. Res. Vol 5, No 85, p 213 - 219 (1973)

101. TYLER IL, ERLIN B
'A proposed simple method for determining the permeability of concrete'
Jour. PCA Res. and Dev. Lab. Vol 3, No 3, Sept 1968 p 2 - 7

102. BRACS GUNAR, EMERY BALINT, ERCHARD DF
'Use of electrical resistance probes in tracing moisture permeation through concrete'
ACI Jour. Proc Vol 67, No 8, p 642, Aug 1970

103. WOODS H
Durability of concrete construction
ACI Monograph No 4 (1968)

104. HIGGINSON EC
'Effect of steam curing on the important properties of concrete'
ACI Jour. Vol 58, No 3, Sept 1961, p281

105. Recommended practice for atmospheric pressure steam curing of concrete
ACI Jour. Vol 66, Aug 1969, p 629

106. ACI COMITTEE 207
ACI Jour. Vol 67 , p 273, (April 1970)

107. DIKEON JT, KUKACHA LE, BACKSTROM TE, STEINBERG M
ACI Jour. Vol 66, p 829 (Oct 1969)

108. NEVILLE AM
Properties of concrete
Pitmans Publications

109. ROBSON RA
'Mobility of water in porous media of high surface area'
Bulletin RILEM No 27 p 65 (June 1965)

110. van BRAKEL J
'Pore space models for capillary liquid transport'
Powder Tech. Vol 11, p 205 (1975)

111. HANCOX NL
'An electrical measurement of the effective cross sectional area for conduction or flow processes in cement paste'
Mag. of Conc. Res. Vol 20, no 64, Sept 1968, p171 - 175

112, CHILDS EC, COLLIS-GEORGE N
'The permeability of porous materials'
Proc. Royal Soc of London Ser A 201, p 392 (1950)

113. HAPPEL J, BRENNER H
'Low Reynolds number hydrodyanamics'
Prentice-Hall (1965)

APPENDICES

APPENDIX 2.1

DETAILS OF CEMENT USED

Source: O.P.C from Rugby Chinnor

Chemical analysis of D 25

Compound Composition	Mass (%)
C_3S	64
C_2S	13
C_3A	6.8
C_4AF	7.3
$CaSO_4$	3.6

Full Chemical Analysis

SiO_2	21.86	(0.31% Insoluble)
Fe_2O_3	2.47	(0.07% ")
Al_2O_3	4.48	(0.40% ")
CaO	65.77	
MgO	1.08	
SO_3	2.13	
Loss	0.76	
Na_2O	0.15	
K_2O	0.66	
P_2O_5	0.15	
TiO_2	0.34	
Mn_2O_3	0.10	
	99.95	Total

Insoluble Residues	0.78%
Free lime	0.78%
Density	318 kg/m^3
Specific Surface	348 m^2/kg

APPENDIX 2.2

DETAILED DESIGN DRAWINGS OF THE PERMEAMETER

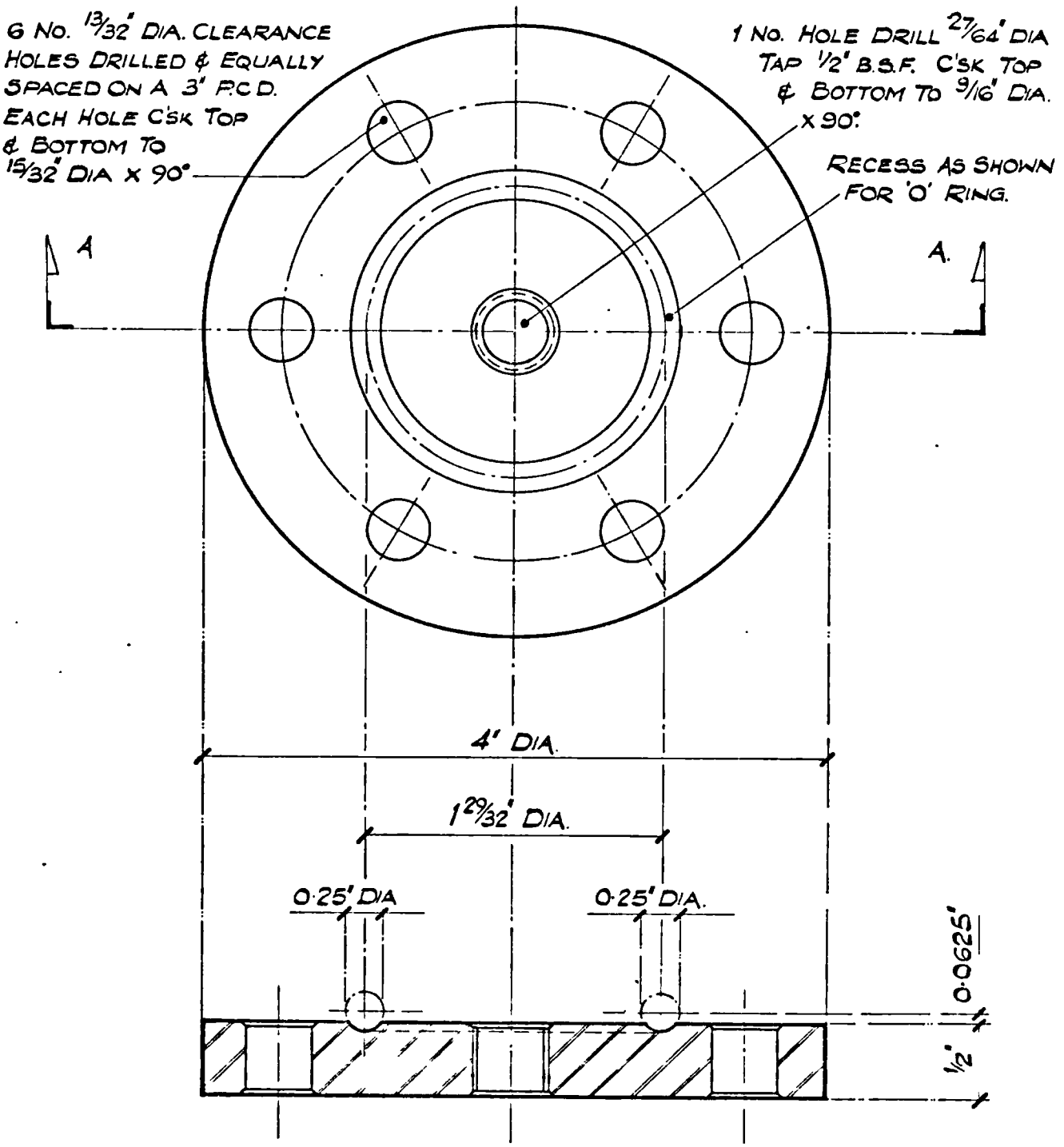

SECTION AA.

BASE PLATE.

PROJECTION – THIRD ANGLE

MATL. – E.N.8. STEEL.
SCALE – 1:1
▽▽ ALL OVER

drg no	H/1.

drawn by J.W. Gaffney.

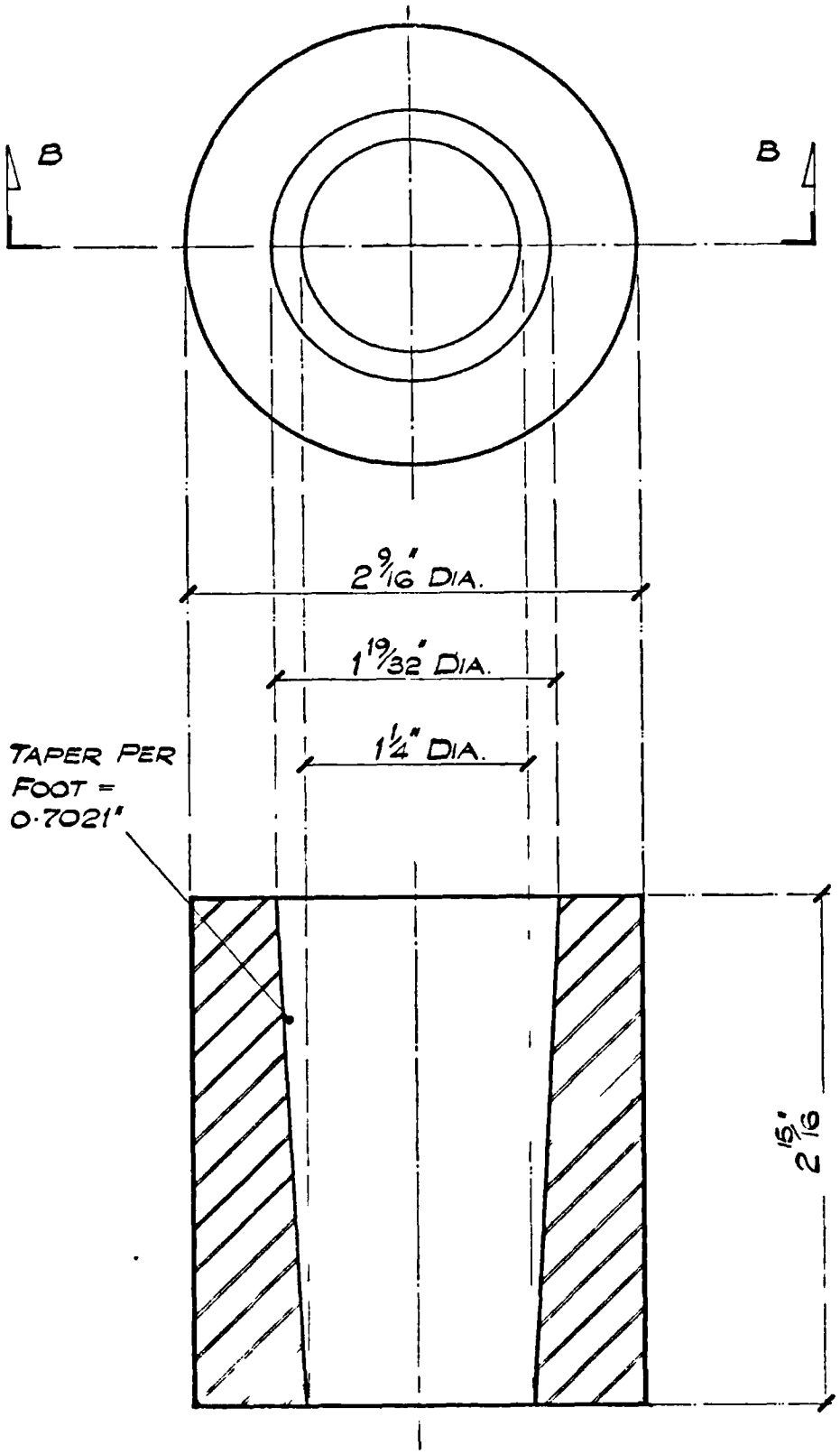

SECTION BB.

CHAMBER.

PROJECTION – THIRD ANGLE.

MAT'L – E.N.8. STEEL.
SCALE.– 1:1.
▽▽ ALL OVER.

drg no	H/2

drawn by J.N.Gatney.

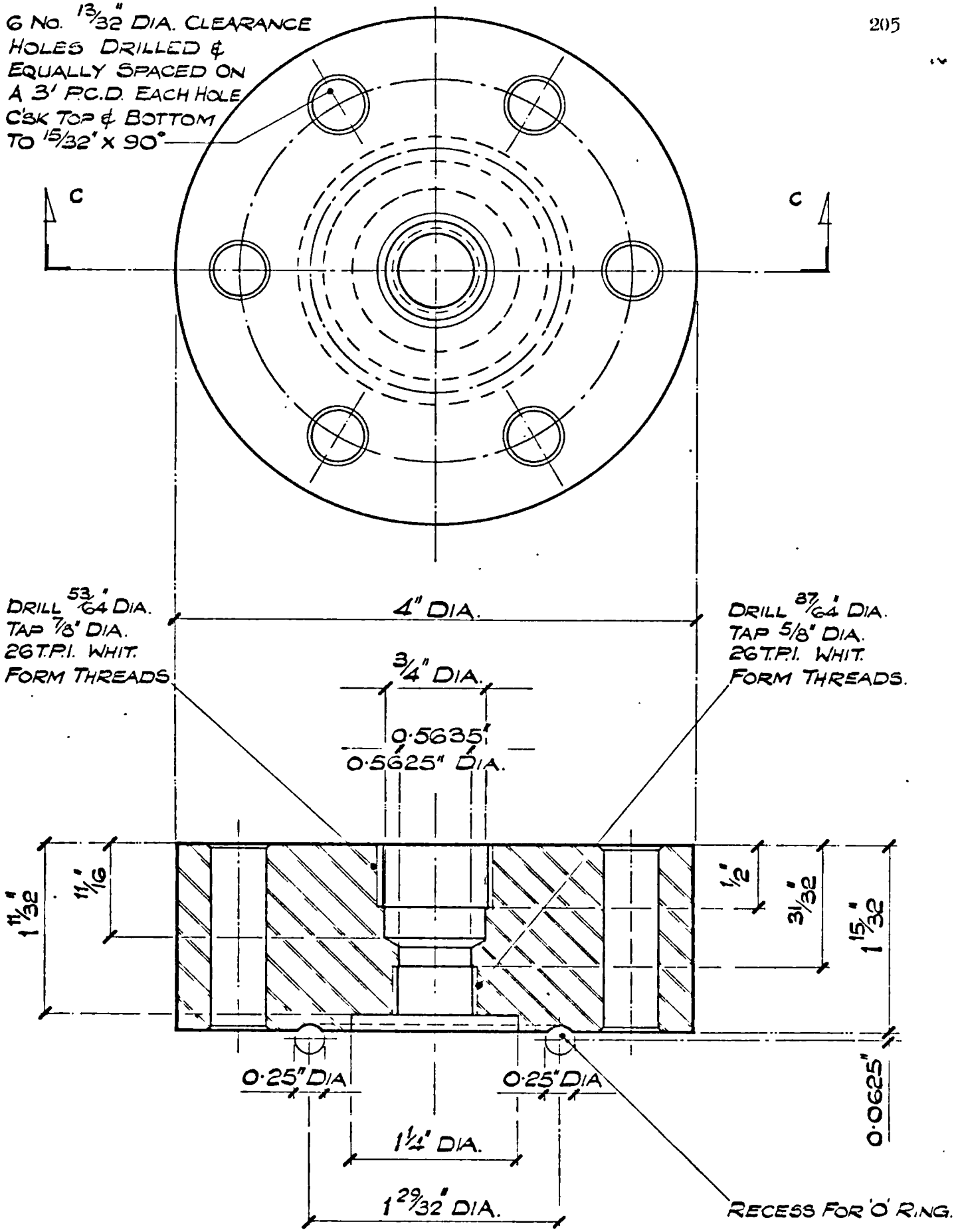

SECTION CC.

TOP PLATE.

PROJECTION – THIRD ANGLE

MAT'L – E.N 8. STEEL

SCALE – 1 : 1.

▽▽ ALL OVER.

rg no	H/3

drawn by J.W. Gaffney.

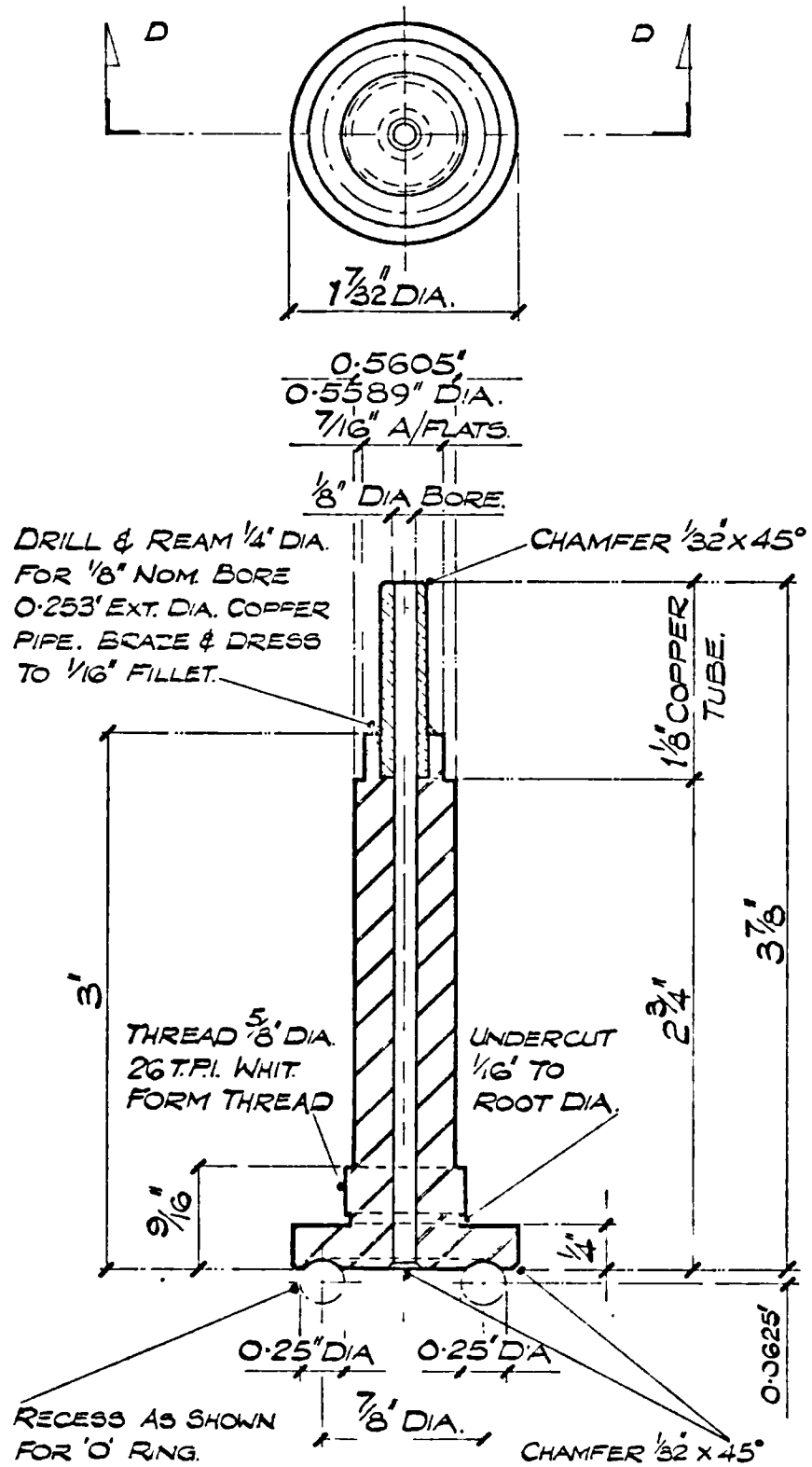

SECTION D D.

CENTRE SPIGOT.

PROJECTION – THIRD ANGLE.

MATL – E.N.8. STEEL.
COPPER TUBE.

SCALE – 1:1.

▽▽ ALL OVER.

rg no	H/4

drawn by J.N Gurney.

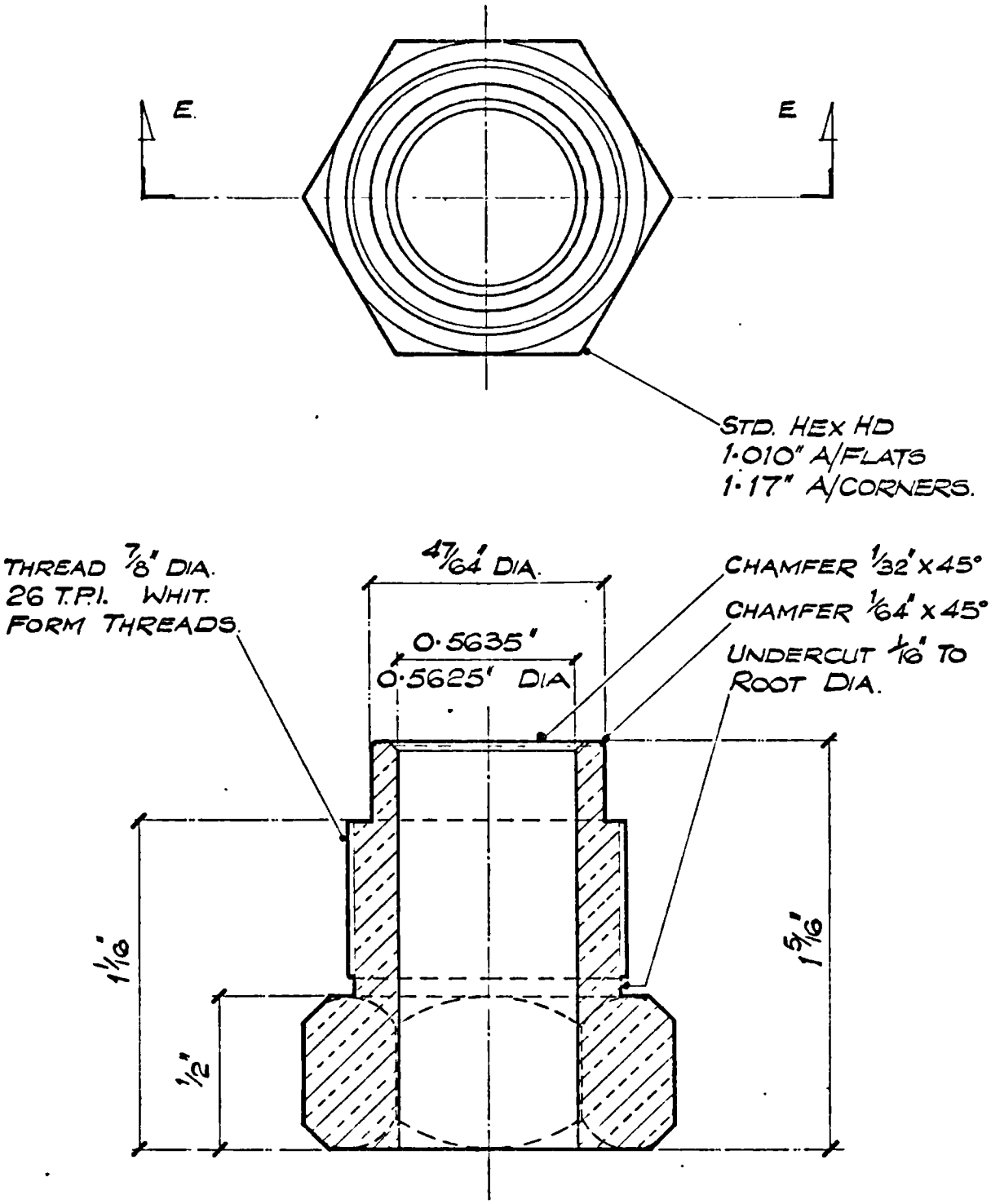

SECTION EE

HEXAGONAL BUSH.

PROJECTION – THIRD ANGLE

MAT'L – BRASS. S.A.E STD No 41.
SCALE. – TWICE FULL SIZE
▽▽ ALL OVER.

rg no	H/5

drawn by J.W. Gaffney

GENERAL ARRANGEMENT OF THE PERMEABILITY TEST UNIT

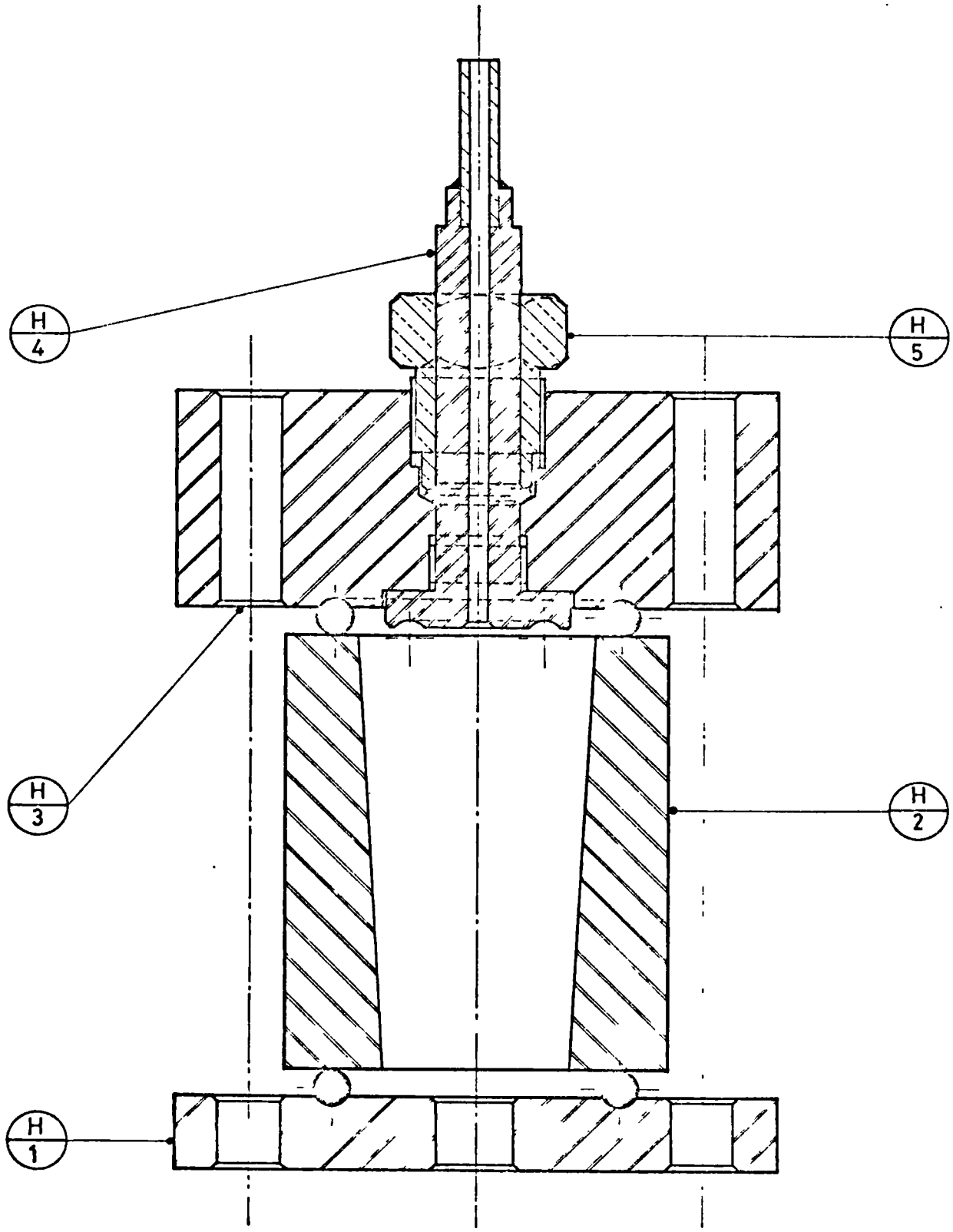

SCALE: FULL SIZE.

~ FILE FINISH.
▽ ROUGH MACHINE.
▽▽ FINISH MACHINE
▽▽▽ GRIND.

drg no. H/6

drawn by J.W.Gaffney